



Steel Hybrid Onshore Wind Towers Installed with Minimal Effort **(SHOWTIME)**

A large, abstract graphic of blue and white waves occupies the bottom half of the slide. It features several concentric, swirling patterns of lines that transition from dark blue to light blue against a white background.

EUR 30144 EN

Steel Hybrid Onshore Wind Towers Installed with Minimal Effort (SHOWTIME)

European Commission

Directorate-General for Research and Innovation

Directorate D – Clean Planet

Unit D.3 — Low Emission Future Industries

Contact Hervé Martin

E-mail rtd-steel-coal@ec.europa.eu

RTD-PUBLICATIONS@ec.europa.eu

European Commission

B-1049 Brussels

Manuscript completed in 2019.

This document has been prepared for the European Commission however it reflects the views only of the authors, and the Commission cannot be held responsible for any use which may be made of the information contained therein.

More information on the European Union is available on the internet (<http://europa.eu>).

Luxembourg: Publications Office of the European Union, 2020

PDF

ISBN 978-92-76-17333-5

ISSN 1831-9424

doi:10.2777/27429

KI-NA-30144-EN-N

© European Union, 2020.

Reuse is authorised provided the source is acknowledged. The reuse policy of European Commission documents is regulated by Decision 2011/833/EU (OJ L 330, 14.12.2011, p. 39).

For any use or reproduction of photos or other material that is not under the EU copyright, permission must be sought directly from the copyright holders.

All pictures, figures and graphs © University of Coimbra, RFCR-CT-2015-00021 SHOWTIME

Research Fund for Coal and Steel

Steel Hybrid Onshore Wind Towers Installed with Minimal Effort **(SHOWTIME)**

Carlos REBELO, M. MOHAMMADI, S. JOVASEVIC

University of Coimbra

Paço das Escolas, PT-3001 451 Coimbra, PORTUGAL

O. LAGERQVIST, E. KOLTSAKIS

LULEÅ UNIVERSITY OF TECHNOLOGY

Universitetsområdet, Porsön, SE-97187 Luleå, SVERIGE

M. FELDMANN, C. RICHTER

RHEINISCH-WESTFÄLISCHE TECHNISCHE HOCHSCHULE AACHEN

Templergraben 55, DE-52062 Aachen, DEUTSCHLAND

BANIOTOPoulos, M. GKANTOU

THE UNIVERSITY OF BIRMINGHAM

Edgbaston, GB- BIRMINGHAM B15 2TT, UNITED KINGDOM

D. HERRERO, M. PEREZ ALONSO

SIDENOR INVESTIGACIÓN Y DESARROLLO S.A.

Barrio Ugarte s/n, Apartado de Correos 152ES-48970 Basauri (Vizcaya), ESPAÑA

B. BURGAN, A. GIRAO-COELHO, A. CHEN

THE STEEL CONSTRUCTION INSTITUTE

Buckhurst Road, Silwood Park, GB Ascot (Berkshire) SL5 7QN, UNITED KINGDOM

A. MATOS SILVA

MARTIFER ENERGIA - EQUIPAMENTOS PARA ENERGIA, SA

Zona Industrial de Oliveira de Frades, PT-3684-001 Oliveira de Frades, PORTUGAL

S. GÜRES

FRIEDBERG PRODUKTIONSGESELLSCHAFT mbH

Achternbergstrasse, 38a, DE-45884 Gelsenkirchen, DEUTSCHLAND

Grant Agreement RSFR-CT-2015-00021

1/07/2012 – 30/06/2018

Final Report

Table of contents

FINAL SUMMARY	5
1 Predesign of hybrid truss-tubular tower	15
1.1 Load calculation.....	15
1.2 Transition segment between Lattice and Tubular structure.....	22
1.3 Hybrid tower study cases conceptual design and structural predesign	25
1.4 Conclusions.....	33
2 Erection process	35
2.1 Detailing of the construction process of a chosen case study from WP1	35
2.2 Production of a scale prototype of the tower	40
2.3 Experimental tests on scale prototype	46
2.4 Risk assessment and analysis of construction procedure.....	56
2.5 Conclusions.....	57
3 Bolt material testing and selection for onshore and near-shore application.....	59
3.1 Selection and manufacturing of steels for bolts	59
3.2 Metallurgical and mechanical characterization of the chosen steels	61
3.3 Testing of fatigue strength of specimens (steels for bolts)	65
3.4 Fatigue testing of corroded double shear pre-stressed connections	71
3.5 Selection of the most adequate steel grade for bolts manufacturing.....	78
3.6 Conclusions.....	79
4 Detailed design of in-situ bolted connections	81
4.1 Profiles with closed and semi-closed polygonal cross-section.....	81
4.2 Experimental testing on connections.....	86
4.3 Compression tests on pylons	91
4.4 FE models validation and parametric study.....	102
4.5 Conclusions.....	108
5 Life cycle assessment and design recommendations	110
5.1 Worked design examples of hybrid steel-steel wind towers	110
5.2 Life-cycle assessment and life-cycle cost analysis of onshore installation	115
5.3 Design and installation of onshore hybrid steel wind towers: principles and details.....	124
5.4 Conclusions.....	129
6 Coordination, management and dissemination	130
6.1 Coordination	130
6.2 Expert's workshop	130
7 Impact of the results and conclusions	132
List of Figures	136
List of Tables	140
List of acronyms and abbreviations	141
References	142

FINAL SUMMARY

INTRODUCTION

The aim of this project is to optimize the construction process and the hybrid lattice-tubular tower geometry in order to ensure that steel towers to support wind turbines. Innovative aspects are the development of an erection process for the upper tubular part that dispenses with the need for large cranes, the new type of cross section of truss bars, allowing for longer elements and efficient in-situ connection, the use of bolted connections, the development of a transition segment that provides an efficient connection between the lattice and tubular parts of the tower, and the performance of tower with respect to cost and life cycle performance.

PARTNERSHIP

The research group includes both European academic institutions and companies, i.e. four universities, a R&D institute, a steel producer, a bolt supplier and a steel structures manufacturer.

PROJECT OBJECTIVES, STRUCTURE AND MAIN RESULTS

The main objective of this project is to develop a new hybrid steel solution for multi-megawatt wind turbine towers, using a steel lattice structure for uplifting, in construction phase, and finally for supporting a steel tubular upper part. The project shall provide an integrated view on the feasibility of the hybrid steel tower, optimizing the performance of the whole structure with the aim of developing a new system of assembly and erection of hybrid lattice-tubular steel wind towers higher than 120 meters.

The optimization of the lattice tower part using innovative solutions for truss elements and assembly joints and considering the possible use of high strength steel is investigated in WP1 and WP4. Feasibility demonstration of the erection solution by manufacturing and assembling a down scale prototype is investigated in WP2. Development of a new type of steel for improving fatigue resistant bolts is performed in WP3. Aggregation of results and life cycle assessment is developed in WP5. WP6 is dedicated to coordination and dissemination. The work was carried-out and structured according to the work-packages illustrated in Figure 0-1.

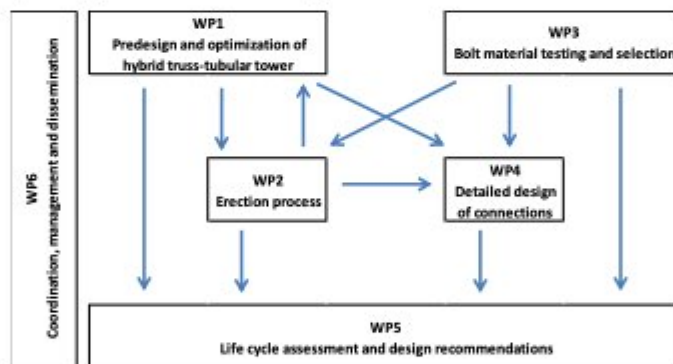


Figure 0-1: Structure of the work-packages developed in the project

WP1 - Predesign and optimization of hybrid truss-tubular tower

Development of the concept for the hybrid tower in WP1, establishing optimal proportions and geometry of the lattice and tubular parts, considering transport and crane size constraints; calculation of complete load sets for structural assessment of the optimizing the tower shape, the lattice/tubular proportion and the transition elements. A minimum number of 24 case studies were predesigned and three of them used for further analysis in the project; The interaction between WP1 and WP2 was necessary in order to establish the relation between relevant case studies used in WP1 and the geometry for the small-scale prototype built and tested in WP2.

In **task 1.1** a set of load tables was developed to be used in the predesign of the study cases foreseen in task 1.3. In the ultimate limit state, the critical design load cases were identified, and the design load tables were provided in two primary and the final stages. The complete load tables are provided for both Design Load Cases DLC1.1 and DLC1.3 established in standard IEC61400-1. Concerning fatigue assessment, the number of cycles and the range of loads and normal stress were obtained for the fore-aft and side-side overturning moment corresponding DLC1.3.

In **Task 1.2** three different concepts for the transition piece proposed by the different partners involved were compared. After a parametric study and design of the transition piece considering the

erection mechanism and use of HSS, two alternatives are proposed for the transition piece design and manufacturing for the scale prototype to be developed in WP2.

In **Task 1.3** results showed viability of the hybrid supporting structure and the final three study cases were selected for further analysis in WP5. The work in this task provides a parametric study concerning the design of the lattice part of hybrid wind turbine towers ranging from 120m to 220m height using two different design methodologies. The main difference between the two methods is the basic assumptions in the first step of analysis. The first method is based on a parametric analysis of a number of study cases where the geometry of the lattice structure is assessed based on the least number of connections and the lowest weight assuming that no secondary bracing is allowed. The analysis converges to class II cross sections. The second method targets the upper bound of class III cross section, which leads to less mass, however, the geometry of the lattice structure might need secondary and horizontal bracing systems, which may put some additional difficulties in the erection process.

The final result was the definition of three different solutions for the tower accomplishing Milestone M1. The three structures target the height of 185 meters, i.e. 120m for lattice part and 65m for tubular part. The main characteristics of the three study cases are: (1) 6-legged tower using K bracings, no secondary bracing and 30m equivalent footprint diameter; (2) the same as (1) but with secondary bracing and (3) 4-legged tower using V bracings and secondary bracing.

WP2 – Erection process

Development of an effective erection procedure in WP2 including design, construction and testing of a scale prototype for the lattice-tubular structure, development of finite element models and simulation of erection procedures, testing the sliding mechanism erection procedure under different loading conditions and fatigue assessment of the transition segment that facilitates an efficient in-situ connection between the lattice and tubular parts of the tower.

In **Task 2.1** a state-of-the-art solution for erection was found in collaboration with all partners and industrial experts invited to participate in project meetings. This solution is described in detail in deliverables D1.2 and D2.1. The feasibility test was performed on the 1/4 scaled transition piece including part of the lattice and the tubular tower. The scaling was done by defining a scale policy based on the similitude law of geometry dimensionless parameter explained in D2.1.

In **task 2.2** The scale prototype design, fabrication and erection execution test were performed, and the feasibility of 1/4 scale prototype was validated and reported in Deliverable D2.2.

In **Task 2.3** numerical investigation on fatigue details in transition piece was performed and reported in Deliverable D2.3. In **Task 2.4** the risk assessment was performed, concerning all the risks involved in the construction process and reported in Deliverable D2.4.

The fabrication and lifting execution were successful, and conclusions concerning the fabrication and assembling of the cold formed truss elements and the transition segment were obtained. In this scale prototype, the plate thickness used in the transition piece was 20 mm and there was some difficulty to keep the precision during the cold forming process of the transition piece components, specially the parts with consecutive rolling and bending. This caused some problems in assembly, which were problematic in the erection process tolerances. Moreover, the stabilizers should be stiffer to restrict more effectively the tilt angle during elevation. Nevertheless, the difficulties were overcome, the foreseen erection tests were successfully run and Milestones M2 and M3 have been accomplished.

WP3 – Bolt material testing and selection for onshore and near-shore application

Development of a very high strength steel for bolts in WP3, to be used in preloaded bolts to fit new requirements posed by high fatigue loading in multi-megawatt turbine towers including production of test specimens of the steel, production of bolts for testing, metallurgical and mechanical characterization of steel and bolts and fatigue testing of double lap bolted connections under normal and aggressive environments.

In **Task 3.1** two steel grades based on a new manufacturing process were chosen: 32CrB4 EQ and 30MnNiB4 EQ. After a complete characterization in **Task 3.2**, it was concluded that all the requirements established by the standard ISO 898-1:2015 were easily fulfilled. Furthermore, the grade 30MnNiB4 EQ exhibited a very high toughness at low temperatures. Once the corresponding fatigue tests were carried out in **Task 3.3**, it was observed that the fatigue limit of the conventional 32CrB4 was improved in a 13% by 32CrB4 EQ and in a 7% by 30MnNiB4 EQ. This fatigue improvement would diminish the bolt risk of failure, leading thus to a safer wind tower operation. From fatigue tests performed in **Task 3.4** on double shear pre-stressed connections the expected performance of the bolts can be concluded, both in corroded and non-corroded specimens, although no direct failure

in bolt region was achieved. Bolts have been produced and delivered to partners accomplishing Milestone M4.

WP4 – Detailed design of in-situ bolted connections

Numerical and experimental study in WP4, concerning new type of polygonal cold-formed closed and semi-closed cross-sections and respective connections, including experimental tests and FE model calibration and parametric study.

In **Task 4.1** the stability behaviour of built-up welded and bolted semi-closed cold-formed elements using different types of cross-sections is investigated numerically: (a) closed polygonal cross-sections built of cold formed and welded plates and (b) semi-closed cross-section built of plates cold-formed into lipped polygon sectors, bolted together along the length of the member. For closed cross-sections the ultimate resistance of the members with imperfections show good agreement with the design curve (c) from EN1993-1-1. The results show that an optimal cross-section would lie at the edge of class 3 to class 4. For semi-closed cross-sections the results showed that the failure mode of such columns is strongly influenced by the distortional buckling of the individual sectors. The main outcome was that for bolt spacing between 3 and 5 times the profile, diameter distortional buckling is apparent. It was observed that for bolt distances below 1.2 times the diameter, the column failed purely under overall buckling.

In **Task 4.2** four sets of tests on a total of 12 specimens of gusset plate bolted connections were performed, where the pylon section was varied (Welded and Bolted) and the pylon-to-diagonal angle was varied (90° and 45°). Tests B90, W90 and B45 demonstrated a global and local behaviour in line with the predictions in the preliminary numerical study. Failure modes were: i) buckling of gusset plate in the compression zone, and gusset plate net section failure in tension zone; ii) buckling of brace in the compression zone, and brace net section failure in tension zone; iii) out of plane buckling of gusset plate; respectively. For W45 configuration brace bearing in tension zone was observed instead of the expected failure of brace block tearing.

In **Task 4.3** three groups of laboratory experiments were performed. Steel grades up to S700 were used in the Group A of experiments (9 specimens) to validate the findings of the parametric FE models developed in Task 4.1. Group B (3 welded specimens, closed polygonal cross sections) and Group C (4 bolted specimens, semi-closed cross sections) consisted of two diagonals connected to pylon and were used to assess the joint rotation. Results show a distinct difference between the rotation stiffness of the joint in the bolted and the welded pylon in the later stages of the experiments. However, the initial rotational stiffness values are quite close in all cases. A gusset plate failure mechanism *inside* the pylon element emerged. Should this failure mode not be prevented (by way of appropriately reinforcing the gusset plate *inside* the pylon element), no reduction of the buckling length of the bracing trusses' bars of the tower is recommended. However, if the gusset-plate buckling issue is remedied appropriately the provisions for effective buckling length given in EN1993-3-1, Annex G.2 can be applied.

Task 4.4 refers to the development of FE models of the tested joints, which have been developed and validated against the test results. The validated numerical models were then used in a parametric study to examine the influence of various parameters (e.g. gusset plate thickness and brace-to-pylon angle) on the stiffness and resistance of the joints. The parametric study using the validated FE model showed that the joint used in the lattice structure can be treated as semi-rigid for moment transmission. the largest ultimate moment capacity occurs when the brace-to-pylon angle is around 75° while the highest initial stiffness can be archived at 45° . Increasing the gusset plate thickness will increase the moment resistance capacity of the joint, eventually transferring the failure mode to buckling of the brace and moderately increasing the initial stiffness.

WP5 – Life cycle assessment and design recommendations

Life cycle assessment of best-performing case studies is done in WP5, including cost evaluation and design recommendations. The life cycle performance of 185 m hybrid towers has been assessed by computing environmental impact parameters and payback time. These results are compared with those of the LCA performed for 150 m tubular towers (steel only; concrete only; steel and concrete named as hybrid) with 5 MW wind turbines.

In **Task 5.1** worked examples and cost estimates for the wind tower case studies were developed (Deliverable D5.1). In **Task 5.2** the life cycle assessment of a 185 m tall hybrid wind turbine tower was performed (Deliverable D5.2) In **Task 5.3** a report was produced giving the principles and details which address the design and installation of onshore hybrid steel wind towers (Deliverable D5.3).

The results show that the hybrid towers, even though taller, present comparable results with the conventional tubular towers. The energy payback time is similar to the 150 meters steel tubular

tower and is about 40% higher when the 150 meters steel-concrete solution is used for comparison. Assuming average unit prices for material, transportation, cranes and lifting equipment and estimated manhours for the complete process of manufacturing, assembling and maintenance, the total cost estimates for the two different solutions were calculated and no significant difference between them was found. Considering the cost of Rotor Nacelle Assembly based on average values including installation, operation and maintenance cost, the estimation of the cost for the whole tower comprises approximately 25% of the total cost. This represents about 600€/kW of a total of 2300€/kW. Considering 25 years and energy production of 10GWh/year, the estimated value of 0,046€/kWh compares fairly well with the cost of onshore wind energy in 2017.

DEVELOPMENT OF THE CONCEPT FOR THE HYBRID TOWER

As part of WP1 (Tasks 1.1 and 1.3), a parametric study on tall wind supporting structure (>120 m) was undertaken. The design of any supporting structure required detail load analysis (Task 1.1) for ultimate limit and fatigue checks, and also the structural integrity such as tower-blade tip clearance and the modal analysis. Task 1.1 and related Deliverable D1.1 contain a description of the complete aeroelastic model for the NREL 5 MW Rotor Nacelle Assembly (RNA).

The load cases for the design and certification of the onshore wind turbine structure are based on the IEC 61400-1 recommendations, which defines the design and installation depending on the external site conditions. The wind turbine classification is based on wind speed and on the turbulence intensity at 15 m/s wind speed. The A (II) class is considered in this study, which means a turbulence intensity $I_{ref} = 0.16$ and a reference wind speed $V_{ref} = 42.5$ m/s measured at hub height

From the complete set of design load cases (DLCs) foreseen in IEC 61400-1 the relevant load cases for tower design were identified and selected for the simulations are given in Table 0.1. These load cases correspond to different wind conditions. The wind regime for load and safety considerations is divided into the Normal Wind Conditions, which will occur frequently during normal operation of a wind turbine, and the Extreme Wind Conditions, which include wind shear events, as well as peak wind speeds due to storms and rapid changes in wind speed and direction. Wind speed is defined on the basis of the V_{ref} for 1-year or 50-year recurrence period. Wind models associated to operational condition (DLCs 1.1, 1.2, 1.3, 2.4, 3.1, 4.1 and 4.2) and to parked condition (DLCs 6.1 and 6.4) of the wind turbine. Table 0-1 provides an overview of these load cases.

Table 0-1: Design Load Cases for Tower Design

Wind turbine Situation	DLC	Wind Conditions	Analysis Type
Operation	1.1	Normal Turbulent Model (NTM)	Ultimate Limit States
	1.2	Normal Turbulent Model (NTM)	Fatigue Limit State
	1.3	Extreme Turbulent Model (ETM)	Ultimate Limit States
	2.4	NTM and fault occurrence	Fatigue Limit State
	3.1	Start up with Normal Wind Conditions	Fatigue Limit State
	4.1	Shut down with Normal Wind Conditions	Fatigue Limit State
	4.2	Extreme Operating Gust (EOG)	Ultimate Limit States
	6.1	EWM 50-year recurrence period	Ultimate Limit States
Parked	6.4	NTM ($V_{hub} < 0.7V_{ref}$)	Fatigue Limit State

TurbSim software from NREL was used to simulate turbulent wind speed datasets generated with a grid resolution of 31 x 31 over the rotor swept area, which already include the wind speed variation along the height (wind shear).

The aeroelastic models of the case studies were developed and analysed in ASHES software after initial validation of results obtained using the state-of-art FAST software. The complete load tables for Ultimate Limit States design are provided in detail for the shortest and tallest towers and for the final selected 185 m tall supporting structure. Furthermore, the fatigue design load table is provided for 185 m tall supporting structure.

A comparison between three different hub heights using 220 m, 185 m and 120 m hybrid (H) tower and 120 m and 90 m tubular (T) tower was carried out. The geometry of the hybrid towers (see Figure 0-2-a) is similar except that the H220 has 120-meter lattice and 100-meter tubular tower, H185 has 120-meter lattice and 65-meter tubular and H120 has 60-meter lattice and 60-meter of tubular tower. As example, Figure 0-2 (b) and (c) show the fore-aft and overturning moment at the TP level and at the ground respectively. DLC 1.1 simulations are used for this comparison.

A total of 24 different case studies were established for parametric investigation considering tower heights 120 and 220 meters, lattice structure with 4 or 6 legs and different height-to-spread ratios. In the design process (see task 1.3 and Deliverable 1.3) at least three iterations were needed,

alternating between load calculation using the aeroelastic tool and the structural design, in order to achieve a stable solution, since the loads are affected by the changes in the structural stiffness. Two different approaches for design were adopted according to the possibility of existing secondary bracing in the system. In the design process tubular elements, steel S355 and buckling curve c (EN1993-1-1) were considered for sake of final geometry definition. Three typical solutions were selected as the most suitable for analysis, with the total height of 185 meters (120 meters lattice, 60 meters tubular and 5 meters transition), in a 6-legged geometry using K-bracing (with/without secondary braces) and 4-legged geometry using V-bracing (with secondary braces). From these, the 6-legged solution without secondary bracing was identified as the most suitable to comply with the solution developed for the erection procedure.

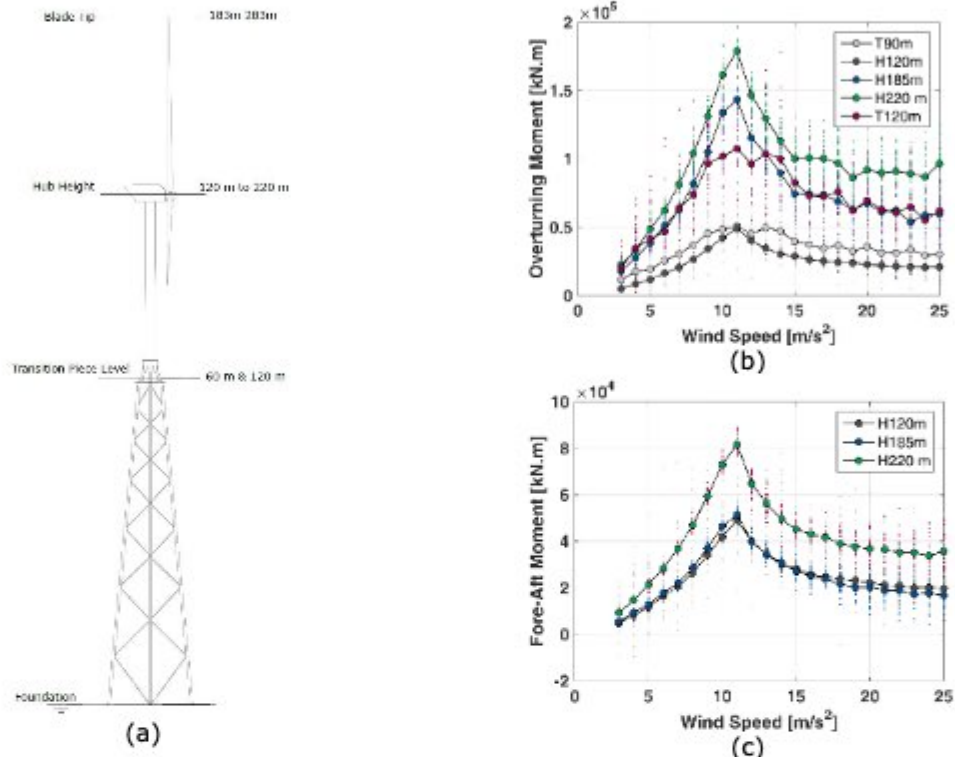


Figure 0-2: Schematic dimensions of hybrid supporting structure reference designs (a); overturning moment (b) and fore-aft moment on transition piece level (c)

The development of two alternative solutions for the transition piece taking into account the mechanical design requirements and material properties was performed for both 4-legged and 6 legged geometries. Possible use of bolted and welded connections of the transition piece to the lattice part, the need for integration of the lifting system and possible use of steel grades S460 and S690 were the guiding aspects. Moreover, the size limits for road transportation were a major constraint for the adopted solutions illustrated in Figure 0-3 and detailed in the Task 1.2 and Deliverable 1.2.

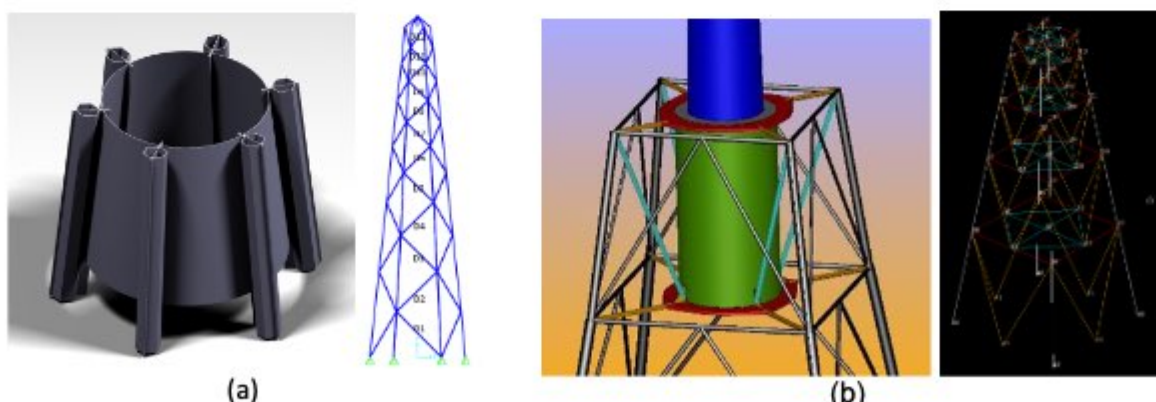


Figure 0-3: The schematic of transition piece for 6-legged (a) and 4-legged (b) tower geometries

DEVELOPMENT OF AN EFFECTIVE ERECTION PROCEDURE

The detailing of the erection process was studied including the transition piece referring to the chosen case study and regarding the downscale prototype. This chapter deals mainly with the study of the alternatives for the erection process and the downscale policy (Task2.1), design, construction and feasibility tests on the 10 meters tall scale prototype (Task2.1 and Deliverable 2.1). Task 2.2 included the production of the scaled prototype and the feasibility tests. Detailing and structural analysis of a 10 meters high small-scale prototype of the tower was performed (deliverable D2.2), consisting of a scale model of the hybrid tower studied in Task 1.3.

A state-of-the-art solution for the assembling sequence was developed in collaboration with external industrial experts (Figure 0-4). It is completely described in deliverables D1.2 and D2.1 and consists in three main phases. First, the tubular parts are assembled inside the lattice structure and the transition piece is mounted on top of the lattice structure. This phase ends with the stabilization of the tube in vertical position and preparation of the strand-jackets positioned on the platform of the transition element. The second phase is the erection of the tube to a position that allows the nacelle and the rotor to be mounted on top of it. Last phase uses the jackets to pull the moving part up to the final position.

The feasibility test is performed on the 1:4 scaled transition piece (Figure 0-5-a) including part of the lattice and part of the tubular tower (Figure 0-5-b). The scaling was done by defining a scale policy based on the similitude law of geometry dimensionless parameter which is completely explained in deliverable D2.1. The prototype was designed and fabricated considering EN 1090-2 requirements. Moreover, partners used BIM method to organize the design, fabrication and execution planning and reduce the misunderstanding and errors.

Although the production process could be successfully performed, some improvements can be identified for future developments. Cold form process could not provide full accuracy for the transition piece component as the most complex structure. Especially, the parts with consecutive rolling and bending had lower precision. Rolling direction versus bending direction is important otherwise, it cannot meet the tolerances. In this scale prototype, the thickness of the transition piece was 20 mm and some difficulties arose to keep the precision when performing the bending on the plate. The low precision of cold form parts caused some problems during assembly and erection process. However, potential of cold form is clearly identified as potential. For instance, dedicated plant for truss legs in a process of continuous roll forming can help maturation of the truss elements fabrication, e.g. new machines and technologies have to appear in an evolution of the purlin fabrication using thick plates.

The erection process, mainly the pull-up phase, was successfully tested by several runs of the feasibility test. Two main indicators were considered. First is the general behaviour, response of the lifting equipment and the feasibility of the tubular tower movement through the transition piece. The second indicator were the transient forces on the stabilizers and on the tubular shell during execution. The test executes three different scenarios, first is the lifting of the tubular tower as the initial stage. Initial stage aims to simulate the tubular tower initial lifting until the stage it arrives to the transition part (TP). Next, the lifting of the tubular tower continues after TP with an extra mass attached to the lever arm. The extra mass is supposed to change the centre of gravity (CoG) in the same way as the rotor nacelle assembly (RNA) will change. Therefore, the lifting and TP should resist a bending moment. The stabilizers are designed inside the TP to facilitate the lifting of the tube by avoiding swinging, guiding the tube through the TP, and also avoid collision between the TP shell and the tube after RNA mounting and induced moment by changes in CoG. The last scenario is lowering process of the tube which is done in between two liftings. The last scenario is trying to simulate unmounting and disassembling of the tubular tower. The erection process is performed with Hebetec equipment, which includes 4 HA-10 strand jacks, capacity 100 kN each incl. CP-10 and EV-1 (necessary for lowering process), 1 Hydraulic pumping unit with controls, 4 strand bundles L-20m and Electric-hydraulic installation. Strain and displacement measurement points were included in the tubular segment and the transition piece to monitoring the effects of the elevation procedure.

To assess fatigue behaviour of the TP in the selected 185 meters case study, two different solutions were considered, bolted solution and a welded solution using S355 and S690. The fatigue detail shown in Figure 0.5-c was investigated using finite element model generated in the ABAQUS software. A mesh convergence study was done for the transition piece which is modelled using tri-dimensional solid element. The fatigue loads obtained from the aero-servo- dynamic analysis were used to check fatigue life. The analysis was performed using FE-safe software with following procedure: 1. The stress tensors are multiplied by the time history of the applied loading, to produce a time history of each of the six components stress tensor; 2. The time histories of the in-plane principal stresses are calculated; 3. The time histories of the three principal strains are calculated from the stresses; 4. A multiaxial cyclic plasticity model is used to convert the elastic stress-strain

histories into elastic-plastic stress-strain histories; 5. A "critical plane" method is used to identify the most damaging plane by calculating the damage on planes at 10° intervals between 0° and 180° in the surface of the component; 6. For each of the critical planes, strains are resolved onto the three shear planes; 7. The time history of the damage parameter (which in this case, using the Brown-Miller algorithm, is the shear and normal strain) is cycle counted; 8. Individual fatigue cycles are identified using a "Rain-flow" cycle algorithm, the fatigue damage for each cycle is calculated, and the total damage is summed; 9. The plane with the shortest life defines the plane of crack initiation and fatigue life is computed, which has been checked to be longer than minimum design life of 25 years.

The focus on the risk assessment concerning the risks involved in the construction process, including both structural and mechanical equipment risks, was performed in Task 2.4 and Deliverable D2.4.

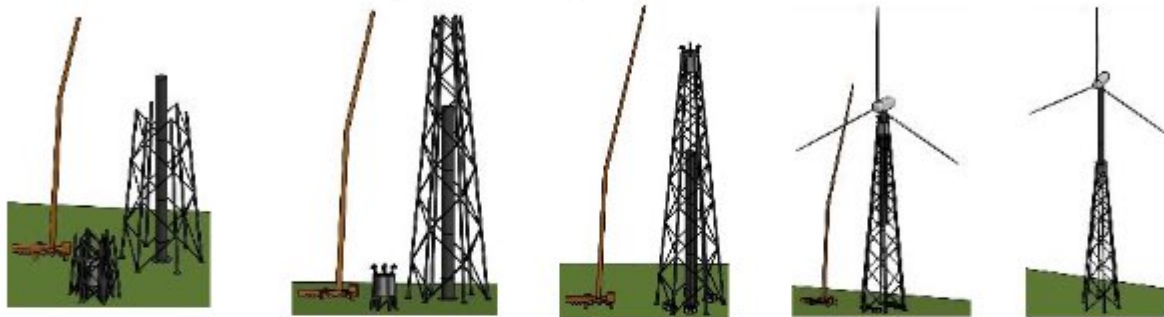


Figure 0-4: Erection sequence

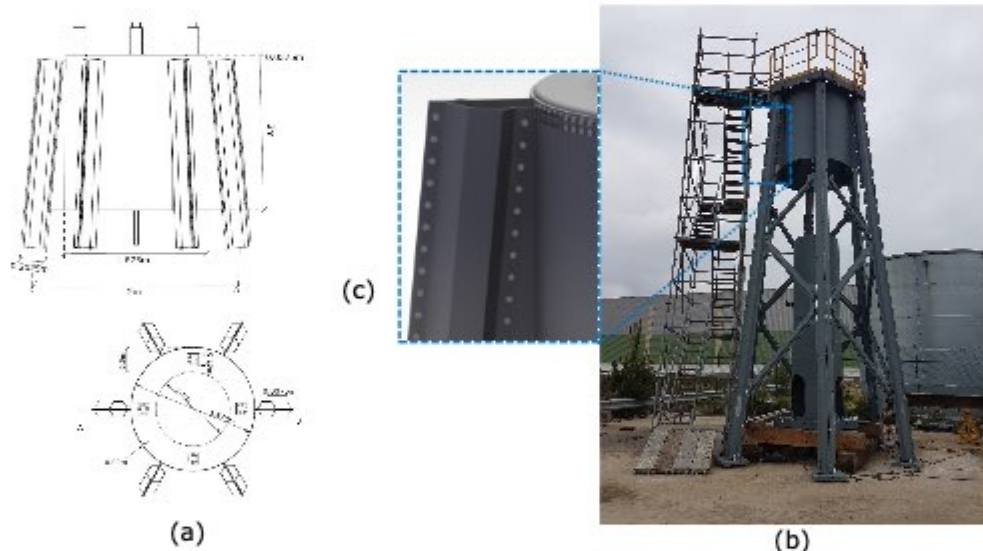


Figure 0-5: Down-scaled transition piece (a) prototype ready for erection test (b) and detail for fatigue assessment (c).

DEVELOPMENT OF VERY HIGH STRENGTH STEEL FOR BOLTS

This work-package deals with the steel manufacturing, the complete characterization of the steels to be used in the bolts and the bolted connections testing. Two steel grades were manufactured with the technology developed by Sidenor. The steel manufacturing process allows a maximization of the steel mechanical properties and fatigue performance by fulfilling all the requirements established in the standard using low-alloyed steels in large diameter bars.

The most suitable steel grades were chosen in order to improve the mechanical properties and the fatigue performance of the steels conventionally used for the bolts manufacturing. These grades were the 32CrB4 and 30MnNiB4, both of them manufactured following the EXTREME technology (EQ) developed by Sidenor. Metallurgical characterization results were compared with ISO898-1:2015 for class 10.9 bolts. Both steel (32CrB4 EQ and 30MnNiB4 EQ) fulfilled all the requirements specified in the standard ISO 898-1:2015 regarding UTS, hardness, toughness and microstructure.

The hardness and UTS values of the 32CrB4 were higher than the 30MnNiB4 ones. However, and as it is logical given the inversely proportional relationship between the UTS and the toughness, the

30MnNiB4 presented higher toughness values at low temperature. The ductile-brittle transition temperature was about -45 °C for the 32CrB4 and -60 °C for the 30MnNiB4.

After a complete characterization, it was concluded that all the requirements established by the standard ISO 898-1:2015 were easily fulfilled. Furthermore, the grade 30MnNiB4 EQ exhibited a very high toughness at low temperatures. Both steel grades (32CrB4 and 30MnNiB4) were manufactured in 500 mm length and 30 mm diameter bars (Task 3.1, Deliverable D3.1).

Task 3.2 focused on the complete characterization including fatigue tests of the steels used in the bolts manufacturing and the tests on the bolts (deliverable D3.2). Fatigue test on both steel grades concluded important improvements of the fatigue performance in comparison with conventional 32CrB4. The fatigue limit of the 32CrB4 EQ resulted to be a 13% higher than the one of the conventional 32CrB4, while in the case of the 30MnNiB4 EQ, the fatigue limit was improved in a 7% with regards to the same reference steel. This fatigue improvement would diminish the bolt risk of failure, leading thus to a safer wind tower operation. In order to check if this improvement of the fatigue performance of the bolts could be also applicable to the whole connection, fatigue tests were performed on double shear pre-stressed connections.

Fatigue testing on double shear connections allow to conclude that bolt performance is as expected. Most of the failures were initiated in different regions of the plates, most probably due to undetected imperfections in the plates' edges. Furthermore, only small differences were observed between corroded and non-corroded connections. These fatigue test did not provide direct information on the bolt performance, since the rupture was in the connected plates. Concerning the corroded specimens, the bolts kept the same behaviour and the rupture was again in the connected plates.

In conclusion, both steel grades considered along the project could be suitable for bolts with diameters up to $\emptyset < 36\text{mm}$. Looking at the characterization carried out in this WP it can be concluded that both grades, 32CrB4 EQ and 30MnNiB4 EQ, reach easily the required properties by class 10.9 of ISO 898-1:2005. Furthermore, both grades with EXTREME quality exceed the fatigue limit of the standard 32CrB4. The current trend of increasing tower dimensions involves higher diameter bolts at the same time. In that sense, if bigger fasteners $\emptyset > 36\text{mm}$ want to be manufactured the 30MnNiB4 EQ represents a competitive and suitable alternative. 30MnNiB4 EQ presents higher hardenability than 32CrB4 EQ so the martensite requirements are more easily achieved for large diameters. Furthermore, the price of 30MnNiB4 EQ its lower in comparison with other alternative high alloyed grades (i.e. 30CrNiMo8).

STABILITY BEHAVIOUR OF ELEMENTS AND DESIGN OF CONNECTIONS

Experimental and numerical investigation on the cold-formed elements with closed (built-up, welded) and semi-closed (built-up, bolted) cross-sections and respective connections has been performed.

Compressed members with polygonal cross-section

In the scope of task 4.1 and task 4.3 numerical investigation and experimental testing were performed in order to clarify the failure (geometric instability) mechanisms of the Regular Polygonal Cross-sections used in the truss elements.

A new type of polygonal built-up members was proposed for the lattice part of hybrid steel wind turbine tower, which are composed of cold formed pieces connected together with preloaded bolts creating polygonal (hexagonal and nonagonal) cross-section. The results of the initial numerical study showed that the failure mode of such columns is strongly influenced by the distortional buckling of the three individual sectors. Distortion of the single sector cross section occurred between two consecutive bolts. Significant interaction with flexural overall buckling was also observed, especially for the higher slender cases. For this type semi-closed built-up column composed of folded plates, there is no expression in Eurocode for the critical distortional buckling load. The main outcome of the initial parametric study was that for bolt spacing between 3 and 5 times the profile diameter, distortional buckling is apparent. In further analysis, it was observed that for bolt distances below 1.2 times the diameter, the column failed purely under overall buckling. Above that spacing, distortional buckling of the individual sectors occurred in combination with the overall buckling.

In the case of welded cross-sections, the resistance of is calculated according to EN 3-1-1 and EN 3-1-5. For the resistance calculation, classification is performed for plated cross-sections, under the assumption that the creases effectively provide simply supported boundary conditions for the faces of the polygon. This assumption is valid for a small number of sides but becomes invalid as the number of sides increase. The results of the experiments allow to draw following conclusions:

- Columns made of regular convex polygonal cross-sections can be grouped in two categories based on how strongly they are attracted towards either a plate-like or a shell-like failure.

- Two regions of the search space (plate failure governed and spillover failure governed) were identified via the FEM analyses and were verified through the experiments.
- The provisions of EN 1993-1-5 and EN 1993-1-6 were checked and found to be suitable for calculating the design resistance within each of the two regions.
- An empirical formula was developed for the boundary between the two identified regions. The proposed formula returns the number of vertices, n_v , for an input of facet plate slenderness, p_c , yield strength, f_y and imperfection amplitude U_0 and suggests which of the two Eurocodes should be applied.
- By comparing between models with and without initial imperfections, columns were proved to be highly sensitive.
- The eigenmode-affine imperfection pattern was proved improper in certain cases, for which the double-spillover imperfection pattern yielded lower resistance.

Single-sided brace-to-pylon connections

In the scope of task 4.2 and task 4.4 experimental and numerical parametric investigations were developed. The joint set-up for testing was with pylon to diagonal angle of 90° and 45°. Three specimens for each parameter (B90, W90, B45 and W45) were tested (12 experiments in total). Tests B90, W90 and B45 demonstrated a global and local behavior in line with the predictions. According to preliminary numerical study predicted failure modes were: i) buckling of gusset plate in the compression zone, and gusset plate net section failure in tension zone; ii) buckling of brace in the compression zone, and brace net section failure in tension zone; iii) out of plane buckling of gusset plate; respectively. The same failure modes were observed in the experiments. Test on W45 configuration gave a failure different than predicted. According to the preliminary numerical study expected failure mode was brace block tearing. In the experiments brace bearing in tension zone was observed.

Parametric finite element models of bolted and welded joints were validated and calibrated against test results. It was shown that the response of the FE models were in excellent agreement with the test results when appropriate imperfections and material properties are used.

The parametric study using the validated FE model showed that:

- The joint used in the lattice structure can be treated as semi-rigid for moment transmission
- The largest ultimate moment capacity occurs when the brace-to-pylon angle is around 75° while the highest initial stiffness can be achieved at 45°
- Increasing the gusset plate thickness will increase the moment resistance capacity of the joint, eventually transferring the failure mode to buckling of the brace and moderately increasing the initial stiffness

The validated FE model can be used in further study to investigate the joint behaviour in various conditions and assist better design of the connections in lattice structure.

Double-sided brace-to-pylon connections

In the scope of task 4.3 a group of experiments on specimens composed of pylon and two branches of the diagonal (double-sided connections) were tested applying opposite direction vertical forces (one upwards the other downwards) on diagonals.

A gusset plate failure mechanism emerged: that was buckling if the gusset plate *inside* the pylon element due, obviously to the compression stress field of the branches. Should this failure mode not be prevented (by way of appropriately reinforcing the gusset plate *inside* the pylon element), no reduction of the buckling length of the bracing trusses' bars of the tower is recommended. However, if the gusset-plate buckling issue is remedied appropriately the provisions of EN1993-3-1, Annex G.2 can be applied.

LIFE CYCLE ASSESSMENT AND DESIGN RECOMMENDATIONS

This WP was focused on examining the possibilities to reduce the overall cost of the hybrid tower by optimising the production and construction process while maintaining the required level of structural reliability and sustainability.

The study cases presented within Task 5.1 (Deliverable 5.1) consist of three variants for the 185 meters tall structure with 120 m lattice structure (bottom part) and a 65 m tubular tower (upper part). The tubular part has a diameter ranging from 4500 mm at the base to 3500 mm at the top with 26 mm plate thickness. The lattice part comprises S355 cold-formed polygonal sections. In task 5.3 a report was produced giving the principles and details which address the design and installation of onshore hybrid steel wind towers covering the following aspects: (i) Design principles for the lattice

structure, (ii) Concept design of the transition piece and (iii) Fundamentals of the innovative tower erection system (Deliverable D5.3).

The study cases addressed above, including construction stage and foundations, were the basis for the life cycle assessment concerning environmental impacts and costs (Task 5.2 and Deliverable D5.2). A NREL 5 MW baseline wind turbine with a total mass of 350 ton has been considered. The tower and transition piece details for each geometry is summarized in Figure 0-6. Focus has been placed on three impact parameters (abiotic depletion, global warming potential and acidification potential) and on the energy payback time (months/year), which shows how long the wind energy system has to operate in order to generate the amount of energy that was used during its life cycle assuming 2000 operational hours leading to a total annual production of 10 GWh.

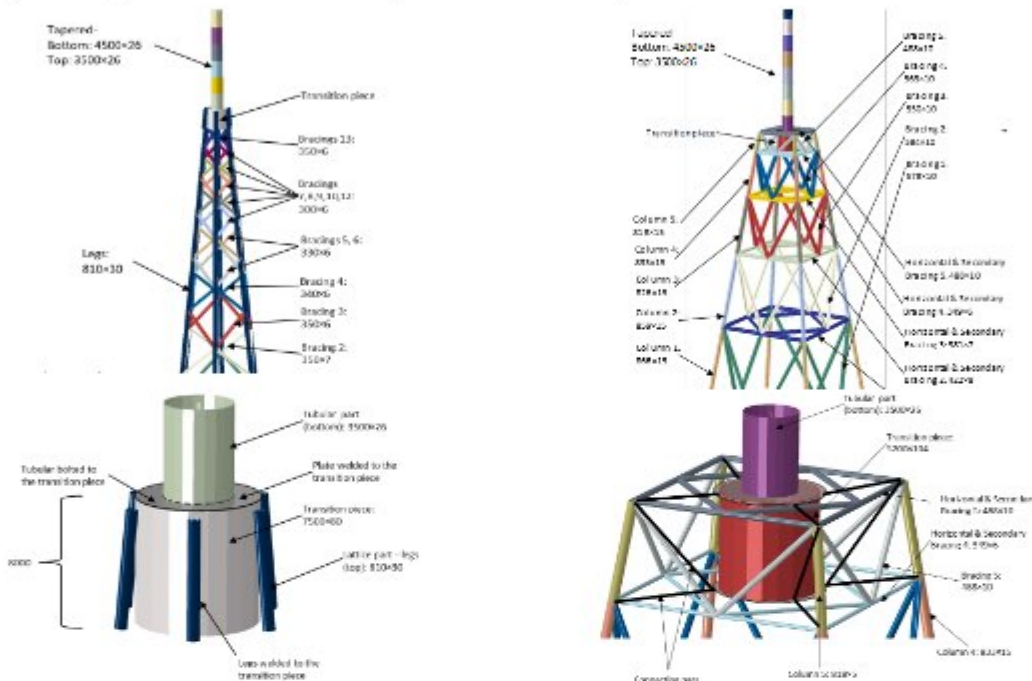


Figure 0-6: The 185 meters tall worked examples for 6-legs (a) and 4-legs (b) with TPs

These results are compared with those of the LCA performed for 150 m tubular towers (steel only; concrete only; steel and concrete named as hybrid) with 5 MW wind turbines. The results show that the hybrid towers, even though taller, present comparable results with the conventional tubular towers. The energy payback time is similar to the 150 meters steel tubular tower and is about 40% higher when the 150 meters steel-concrete solution is used for comparison.

Assuming average unit prices for material, transportation, cranes and lifting equipment and estimated manhours for the complete process of manufacturing, assembling and maintenance, the total cost estimates for the two different solutions were calculated and no significant difference between them was found. Considering the cost of Rotor Nacelle Assembly based on average values the cost for the whole tower comprises approximately 25% of the total cost. This represents about 600€/kW of a total of 2300€/kW. Considering the production over 25 years and 10GWh/year, the estimated value of 0,046€/kWh compares fairly well with the cost of onshore wind energy in 2017¹¹.

COORDINATION AND DISSEMINATION OF RESULTS

In WP6, the coordination work was undertaken with general meetings, participation of invited external experts from companies and the organization of a final workshop. During the full-day workshop results of the project in view of possible practical application were presented by the project partners. Additionally, invited experts from two companies directly interested in the project outcomes presented possible future developments, i.e., Salzgitter Mannesmann Renewables, that offers lattice solutions for wind towers presented possible developments concerning the hybrid lattice-tubular concept, and HEBETEC Engineering Ltd, that was involved in the erection process presented the state-of-art solutions for computerized elevation of heavy structural parts. This workshop counted on the presence of designers and a wind turbine producer. Deliverable D6.4 gives the detailed program, presentations and list of participants.

¹¹ https://www.irena.org/-/media/Files/IRENA/Agency/Publication/2018/Jan/IRENA_2017_Power_Costs_2018.pdf

1 Predesign of hybrid truss-tubular tower

Currently, onshore steel wind turbine towers, assembled on-site from a series of prefabricated ring segments are the most used solution. Some of the reasons that led the European market to use steel tubular towers, rather than lattice towers, were valid for heights up to 100 meters. Speed of construction using pre-fabricated steel tubes equipped with all the internals of the towers and transported across the country on public roads were the main reasons for the competitiveness of this solution. However, these reasons are not valid for towers higher than about 120 meters, which are limited by the maximum tube diameter of the pieces that can be transported on public roads. New concepts are therefore required to optimize the cost of taller steel towers and it is recognized by the steel industry that alternative solutions must be found to maintain the competitiveness of steel in this sector.

One alternative technique, which takes advantage of modular building of steel tubular towers, has already been investigated in other RFCS projects. Those projects investigated solutions that are mainly based on the use of tubular towers with circular or polygonal cross-sections, assembled on site using transverse and longitudinal bolted slip-resistant (friction type) connections. A lattice type tower offers several advantages. However, the costs of lattice construction may be adversely influenced by an increase in work on site due to the number of bars and connections involved and the maintenance requirements of bolted connections subjected to fatigue loading. Also, torsional stiffness of a whole lattice tower can be lower than that of an equivalent tubular tower suffering from excessive vibration in consequence of resonance of load excitation frequencies in the range of the torsional eigenfrequency. When using a hybrid structure composed by lattice and tubular tower these drawbacks can be avoided.

As part of Work package 1 (Tasks 1.1 and 1.3), a parametric study on tall wind supporting structure (>120 m) was foreseen. The design of any supporting structure requires detailed load analysis (Task 1.1) for ultimate limit state and fatigue limit state structural checks and also the structural integrity such as tower-blade tip clearance and avoiding of resonance during steady state wind turbine operation. Task 1.1 and related Deliverable D1.1 contain a description of the complete aeroelastic model for the designed supporting structure for the NREL 5 MW RNA. The aeroelastic model is studied in ASHES software [58]. The complete ultimate limit load tables were provided in detail for the shortest and tallest towers and also the final selected supporting structure with 185 m total height.

The work developed in Task 1.2 is the background for deliverable D.1.2, which focuses on the development of two alternative conceptual solutions for the transition piece taking into account the mechanical design requirements and material properties. In this case, the bolted and welded connections of the transition piece to the lattice part, the need for integration of the lifting system and possible use of high strength steel (S690) are the guiding aspects. Moreover, the size limits for road transportation are constraints for the proposed modularized solution.

In Task 1.3 the project proposal established 24 different case studies to develop the hybrid tower with 120-, 160-, 180- and 220-meters height. The different proportions of lattice/tubular part and different height to spread ratio were redefined for the parametric studies. Moreover, different number of legs for lattice structure are proposed to be investigated which can be found more in detail in Deliverable D1.3. In the design process performed there were several iterations alternating between load calculation using an aeroelastic tool (Task 1.1) and the structural design. This process was performed at least three times for all different structures, until the structural layup was changed and the aeroelastic setup was adjusted.

WP1 was concluded and the related deliverables (D1.1, D1.2 and D1.3) and Milestone 1 (M1) were accomplished.

1.1 Load calculation

1.1.1 General remarks and definitions

Figure 1-1 shows the coordinate system used for input and output parameters. Moreover, the x-axis pointing in the nominal (0°) wind flow direction, y axis pointing to the left when looking to the wind flow and z axis pointing down from the centre which means the compression is consider as a positive force.

To date only one onshore wind turbine properties have been published open source and are available for research, which is the NREL 5MW baseline wind turbine used here for the analysis. The controller, power electronics, generator, blades and other parts properties mentioned in Table 1-1 are NREL baseline turbine default [42] including the Rotor Nacelle Assembly (RNA) mass properties.

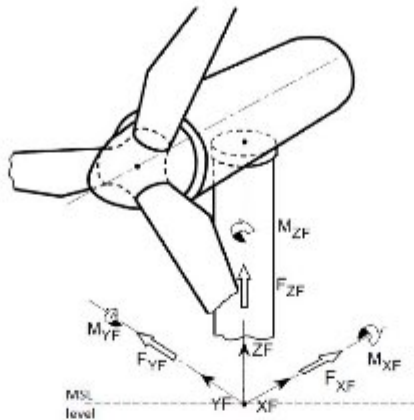


Figure 1-1: The Global coordinate system (GL 2010)

Table 1-1: NREL 5MW Gross Properties.

Properties	Value
Rated power	5MW
Rotor Orientation, Configuration	Upwind, 3 Blades
Control	Variable Speed, Collective Pitch
Drive Train	High Speed, Multiple-stage Gearbox
Rotor, Hub Diameter	126m, 3m
Cut-In, Rated, Cut-Out Wind Speed	3 m/s, 11.4m/s, 25m/s
Cut-In, Rated Rotor Speed	6.9 rpm, 12.1rpm
Rated Tip Speed	80m/s
Overhang, Shaft Tilt, Pre-cone	5m, 5°, 2.5°
Rotor Mass	110 ton
Nacelle Mass	240 ton
TOTAL RNA Mass	350 ton

The hybrid supporting structure consists of three main components. The tubular tower, the lattice structure and the transition piece which is a connection between the tubular tower and the supporting structure. Figure 1-2 shows the schematic dimensions of the wind turbine towers studied in this project. The full description of the tower and the supporting structures can be found in deliverable 1.3.

The dimensions of the tubular tower were designed based on EN1993-1-6 [11]. The tubular tower's height varied between 60 m and 100 m. Additional 5 m is considered for the transition piece. Considering that the rotor blade radius is 61.5 m including the hub, this will avoid any possible blade tip collision with the lattice structure. The base diameter of the tubular tower is 4.5 m and the top diameter is 3.5 m. The dimensions for the 220 m tubular tower are given in Table 1-2.

Table 1-2: The dimensions of 100 m tubular tower for 220 m hybrid tower.

	Diameter (m)	Thickness(mm)
Base	4500	34
Top	4000	34

1.1.2 Design Load Cases

The load cases for the design and certification of the onshore wind turbine structure are given in IEC 61400-1 standard. The approach in this project is based on the IEC 61400-1 recommendations, as will be described in detail in the following sections.

The wind turbine design and installation are depended on the external site conditions. The wind turbine classification is based on wind speed and the turbulence deviation. Table 1-3 shows the wind turbines' classes and the respective parameters, where A, B, C are for higher, medium, lower turbulence characteristics. Moreover, I_{ref} is turbulence intensity at 15 m/s wind speed. As the wind turbine is onshore wind turbine and it is high rise structure, the A (II) class is considered in this study. The turbulence intensity is 0.16 and the reference wind speed (V_{ref}) is equal to 42.5 m/s.

The most crucial load cases for normal operational condition and parked were selected for the simulation. All the wind models for the simulations are provided by TurbSim software from NREL [49]. Turbulent wind datasets generated with a grid resolution of 31 x 31 are simulated. These datasets already include wind shear and may be used directly.

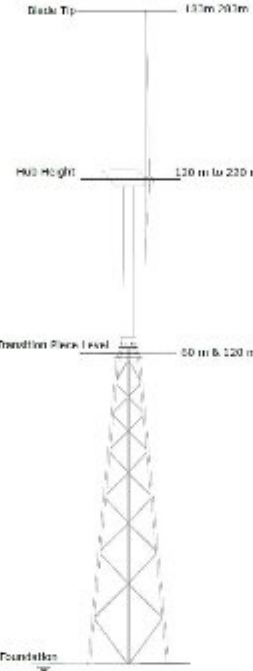


Figure 1-2: Schematic dimensions of hybrid supporting structure reference designs.

Table 1-3: Basic parameters for wind turbine classes acc. IEC 61400-1

Wind Turbine Class	I	II	III	S
V_{ref}	50	42.5	37.5	Values specified by the designers
A	$I_{ref} (-)$	0.16		
B	$I_{ref} (-)$	0.14		
C	$I_{ref} (-)$	0.12		

1.1.2.1 Modal Analysis

Modal analysis is performed in absence of wind according to the Table 1-4. In all the calculations concerning wind effect on the rotor initial conditions for the simulations must be established. The parameter Ω is the rotor speed, Φ is the pitch angle of the blades and Θ the tilt angle of the nacelle.

Table 1-4: Detail Load Case for Modal Analysis.

Load Case	Enable DOF	Wind Conditions	Analysis Type	Initial Condition
0.1	Tower Support Structure	No Air	Eigen analysis, no gravity or damping, natural frequency and mode shapes	$\Omega = 0 \text{ rpm}$ $\Phi = 0 \text{ deg}$ $\Theta = 0 \text{ deg}$

Table 1-5: Detail Load Case for ULS Design.

Load Case	Enable DOF	Wind Conditions	Analysis Type	Initial Conditions
1.1 & 1.3	All	NTW & ETM	Time series solution, Ultimate Strength	$\Omega = 12.1 \text{ rpm}$ $\Phi = 0 \text{ deg}$ $\Theta = 0 \text{ deg}$
6.1	All	EWM 50-year recurrence period	Time series solution, Ultimate Strength	$\Omega = 0 \text{ rpm}$ $\Phi = 90 \text{ deg}$ $\Theta = 0 \text{ deg}$
4.2	All	EOG	Time series solution, Ultimate Strength	$\Omega = 12.1 \text{ rpm}$ $\Phi = 0 \text{ deg}$ $\Theta = 0 \text{ deg}$

Table 1-6: Detail Load Case for Fatigue state Design.

Load Case	Enable DOF	Wind Conditions	Analysis Type	Initial Conditions
1.2	All	NTM	Fatigue	$\Omega = 12.1 \text{ rpm}$ $\Phi = 0 \text{ deg}$ $\Theta = 0 \text{ deg}$
2.4	All	NTM	Fatigue	Fault occurrence
3.1	All	NWP- Normal Start up	Fatigue	$\Omega = 6.9 \text{ rpm}$ $\Phi = 0 \text{ deg}$ $\Theta = 0 \text{ deg}$
4.1	All	NWP- Normal Shut down	Fatigue	$\Omega = 0 \text{ rpm}$ $\Phi = 90 \text{ deg}$ $\Theta = 0 \text{ deg}$
6.4	All	NTM ($V_{\text{hub}} < 0.7 V_{\text{ref}}$)	Fatigue	$\Omega = 0 \text{ rpm}$ $\Phi = 90 \text{ deg}$ $\Theta = 0 \text{ deg}$

1.1.2.2 Ultimate Limit State and Fatigue Limit State

In the load cases for ultimate limit state (ULS) and fatigue limit state (FLS) analysis, a land base turbine under turbulent wind loads is investigated. In order to provide the loads for the different hub height, the different wind models are simulated. The loads on the structure are provided at the different level of the tubular tower. The load cases are illustrated in Table 1-5 and Table 1-6.

For each analysis, the partial safety factor shall be considered. IEC 61400-1 specifies several factors for different normal, abnormal, transport and erection situation. As the ULS analysis is for the normal power production and the fault occurrence is not considered, therefore, only normal safety factor equal to 1.35 will be used in the analysis. The partial safety factor of 1.0 shall be used in all normal and abnormal condition.

1.1.2.3 Output Parameters

To design the lattice part and the tubular part, it is crucial to have the forces and the moments on the tower top and tubular section base. The ASHES² as a servo-hydro-aeroelastic software is used to analyse the system in different operating condition. The signals of the sensors in the structure ought to be recorded in the global coordinate system.

In Figure 1-3 the possible positions of each element or node sensor is illustrated. In the case of tubular part, sections can be divided to the arbitrary number of elements and for the lattice structure, each element is defined as a connection between two nodes.

The sensors on elements will record force, moment, and stress and sensors on nodes records displacement, velocity and acceleration. A sensor is located on the blade tip which records the blade

² <http://www.simis.io>

tip displacement to check the tower-blade tip clearance. Moreover, the ground reaction forces are measured to provide enough information for the foundation design and sizing.

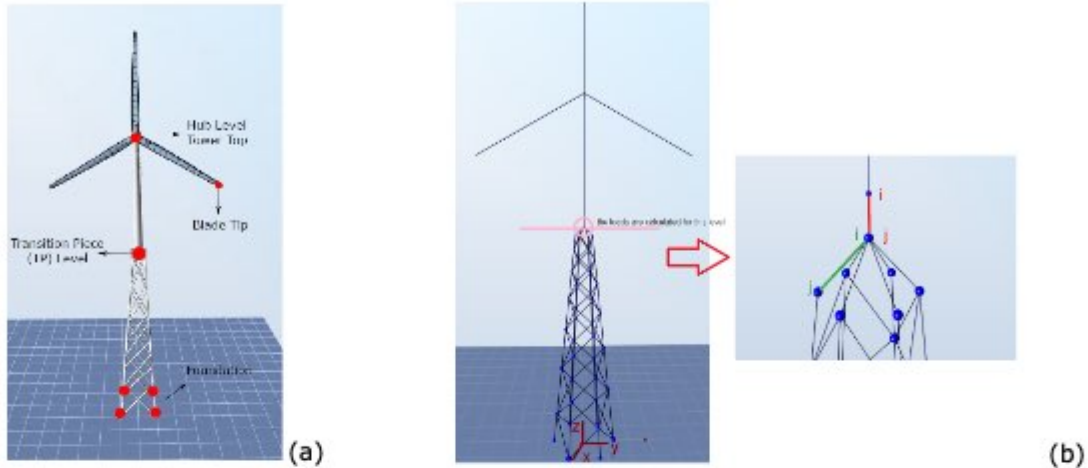


Figure 1-3: Sensor positions in the structure (a) and model as a beam element model.

In the Table 1-7 and Table 1-8 the forces and the moments are defined and fully explained for the Transition piece and top respectively. However, the subscript of base is used to transition piece forces and moments.

Table 1-7: Output parameters at wind turbine Transition piece.

Name	Definition
Fxb	Transition piece fore-aft shear force
Fyb	Transition piece side to side shear force
Fzb	Transition piece axial force
Mxb	Transition piece roll (side to side) moment (the moment caused by side to side forces)
Myb	Transition piece pitching (fore-aft) moment (the moment caused by force-aft forces)
Mzb	Transition piece yaw (torsional) moment

Table 1-8: Output parameters at wind turbine tower top.

Name	Definition
Fxt	Tower-top / yaw bearing fore-aft (non-rotating) shear force
Fyt	Tower-top/yaw bearing side-to-side (nonrotating) shear force
Fzt	Tower top/ yaw bearing axial force
Mxt	Nonrotating tower-top / yaw bearing roll moment
Myt	Nonrotating tower-top / yaw bearing pitch moment
Mzt	Tower-top / yaw bearing yaw moment

Table 1-9: Case studies and the corresponding load Tables provided in D1.1.

Case Study	Tubular tower height	Lattice height	Primary loads	Final loads
120m	60m	60m	D1.1-Table 3-1 D1.1-Table 3-2 D1.1-Table 3-3	D1.1-Appendix A
160m	100m	60m	D1.1-Table 3-4 D1.1-Table 3-5 D1.1-Table 3-6	----
180m	60m	120m	D1.1-Table 3-7 D1.1-Table 3-8 D1.1-Table 3-9	D1.1-Appendix A
220m	100m	120m	D1.1-Table 3-10 D1.1-Table 3-11 D1.1-Table 3-12	D1.1-Appendix A

In Table 1-9 the dimensions of the towers are given for which the loads were calculated and reported in deliverable D1.1. Since loads depend on the structural stiffness, the preliminary load were calculated based on simplified geometry for all case studies.

1.1.3 Aero-servo-elastic load results for Hybrid Towers

The load prediction is necessary for the structure to be designed for maximum loads (ULS) and for the fatigue (FLS). The design criteria were considered based IEC 61400-1 standard. The structure design procedure is explained in deliverable 1.3. Since aero-servo-dynamic loads depend on structural response, an iterative approach was performed until both structural design and aeroelastic design are satisfied. Hereafter, the aeroelastic results obtained from ASHES aero-servo-elastic software [58] are discussed. First of all, the statistical analyses are addressed. Then the ULS loads are discussed and the primary and final load Tables are provided. Finally, fatigue loads and spectrums for the selected structure.

In order to verify the controller performance and investigate the aeroelastic behavior of the tower, a wind step is simulated. Figure 1-4 presents wind steps (red line), pitch angles (orange line), and rotor power (blue line), respectively. It can be seen that the controller performs accurately and start the pitch angle right after the rated wind speed of 11 m/s. In the next step, the statistics for DLC1.1 are investigated. The scatter of all values from each simulation in DLC1.1 including the mean values are shown inFigure 1-5, where the circle symbol illustrates the mean value and the dots different response values.

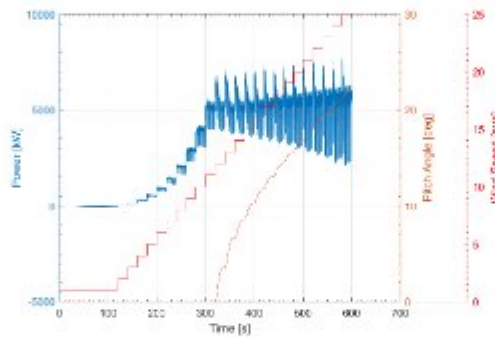


Figure 1-4: A wind step case, red line: wind speed, orange line: pitch angle, and blue line: generator power.

It can be seen in Figure 1-4 that with increasing the wind speed, the deviation in rotor power increases, however, the dark blue area shows concentration of the samples around 5MW as maximum power and also it can be verified by generator power mean values shown in Figure 1-5.

Tower fore-aft force and bending moment are shown in Figure 1-6. The effect of pitch controller and decreasing the loads on structure are obviously observed. Moreover, the hub height displacement remains stable after few minutes of operation and it is less than 10 cm of fluctuation.

1.1.3.1 Ultimate load analysis

The load carrying components of the wind turbine structures include the tubular tower, lattice structure, and the transition piece should be verified with the ULS and fatigue strength of the structural members to demonstrate the structural integrity of a wind turbine with the appropriate safety level. The ultimate loads were simulated in order to verify the hybrid tower design. The IEC 61400-1 standard recommends that the extreme values of the loading from DLC1.1 are determined using the statistical extrapolation for the 50-year recurrence period. Moreover, it requires a partial safety factor of 1.35. The ultimate loads at hub height and transition piece level are reported for designing the tubular tower and lattice structure respectively. Figure 1-6 shows the fore-aft and side-side maximum bending moment for the tower bottom and top in simulated load cases. All values illustrated are the maximum of the absolute values from each load case. From the results it is seen that DLC1.3 is a design load case for the tower top fore-aft, side-side and tower bottom fore-aft, however, DLC 6.1 is the design load case for tower bottom side-side.

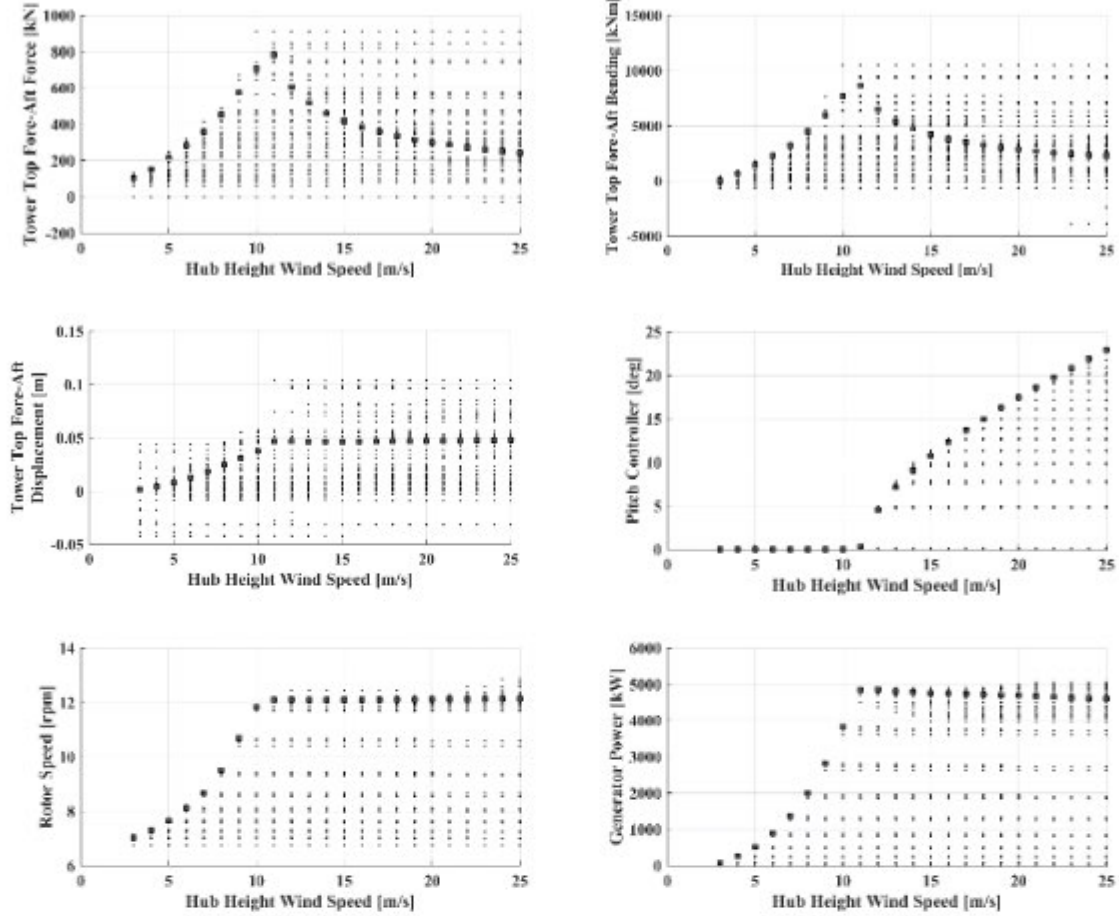


Figure 1-5: The main characteristics of the wind turbine dynamic response from DLC 1.1.

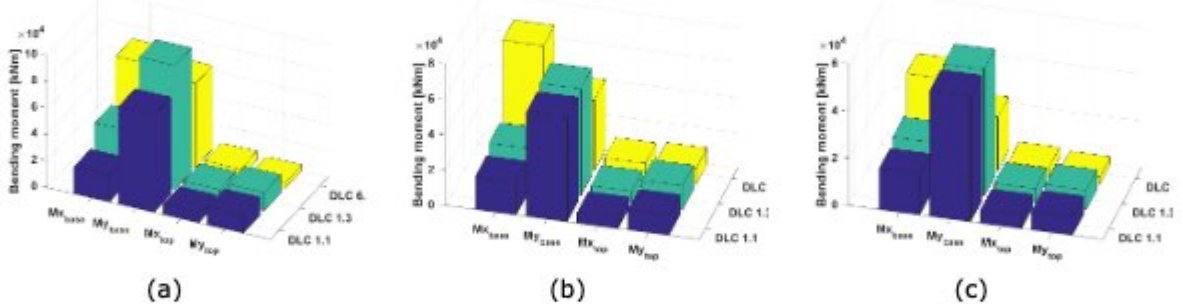


Figure 1-6: The fore-aft and side-side bending moment at tower top and at transition level for (a) 120+100 m, (b) 120+65 m, and (c) 60+60 m supporting structure (lattice-tubular).

Figure 1-6 (a), (b), and (c) show that DLC1.3 is a design load case for the lattice top fore-aft bending moment. However, DLC6.1 is a design load case for the side-side moment. In order to verify the structural design of the lattice structure and tubular tower, the maximum and the cross-sectional loads are required with which the strength and buckling analysis are performed based on EN1993-1-3 [20] and EN1993-1-6 [11]. In deliverable D1.1 Appendix A the final obtained load envelopes of three different DLC1.1, DLC1.3, and DLC6.1 for structures with 120m, 185m, and 220m are listed. The load envelopes are the maximum of all forces and moments including the thrust at tower top and the tower top moment, which occurred simultaneously when the maximum and the minimum tower top thrust occurred, should be reported.

1.1.3.2 Fatigue load analysis

The IEC 61400-1 standard [40] suggests DLC for simulating fatigue loads and the equivalent fatigue life time. In this report, the life time equivalent fatigue loads for the tower was investigated and only DLC1.2 which is most frequent design load case was considered for the calculation [50].

Corresponding DLC1.2, 10-min time domain simulation was performed for all cut-in to cut-out wind speed. In Table 1-10 the wind speeds are divided into six different operational mode based on IEA recommendation [46].

Table 1-10: Wind Turbine Mode of Operation.

Mode	Wind speed (m/s)
3	≤ 9
4	$9 < V \leq 11$
5	$11 < V \leq 13$
6	$13 < V \leq 15$
7	$15 < V \leq 17$
8	≥ 17

After defining the typical operational conditions, the rainflow counting method should be applied on all the time series [46]. In order to estimate the number of hours of each wind interval, the Weibull distribution function is used. Generally, Weibull function provide the number of hours of each wind speed occurrence by multiplying the probability to 20 years equivalent hours. Figure 1-7 shows the number of cycles of Fore-Aft bending and side-side bending at the tubular tower base.

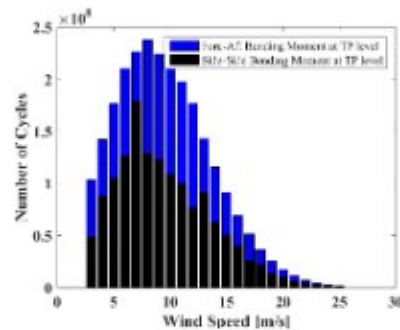


Figure 1-7: The number of cycles per wind speed.

The number of cycles versus the value of normal stress, fore-aft bending and side-side bending moment at the base of the tubular tower are shown in Figure 1-8. It can be observed that the mode 8 has the highest share on the number of cycles and also the amplitude as the wind fluctuation is bigger in higher wind speeds. The mean and amplitude of 10-min time series of each wind speed is provided in deliverable 1.1 (Appendix B).

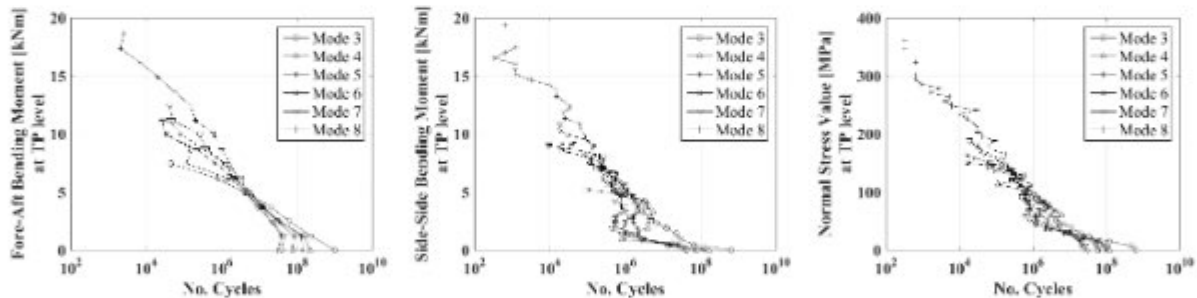


Figure 1-8: Load spectra for different modes of operation.

1.2 Transition segment between Lattice and Tubular structure

1.2.1 Erection process and transient loads

Two variants of an erection processes are described in deliverable D.1.2. The variants differ in relation to the assembly of lattice and tubular part. In both variants, a mobile crane and strand jacks are used. The actual lifting process of the tubular tower is the same in both variants. In the variant 'Erection process with alternating erection of tubular and lattice part' the lattice tower is mounted on site in several pieces first and the pieces are put together by a mobile crane afterwards. The tubular part is assembled simultaneously inside the lattice structure. At the top of the transition piece a support area for the strand jacks is necessary. In this support area holes have to be arranged beneath the strand jacks. In the inside of the transition piece has to be enough free space for the strands and

also for the hydraulic pressure rollers or springs. The top plate has to be large enough to carry the strand guidance also. The transition piece serves also as connection element to the lattice tower. In the bottom plate of the tubular tower, which closes the transition piece afterwards, holes have to be arranged as well. These holes are for the strand jacks at the bottom. The detailed load calculation is provided in D1.2.

1.2.2 Concepts of transition piece

1.2.2.1 Concept 1

Concept 1 for a Transition Piece (TP) Design is based on the idea that the TP may be completely independent of the lattice part of the tower and least dependent of the tubular part. In this way, this non-classical structural piece can be industrially mass-produced and applied to each individual tower design on the basis of the performance needs (loads to be transferred from the tubular to the lattice part). Following the parametric investigations of the lattice part (Deliverable 1.3), the top width of the lattice part B_{top} was found to be one of the important parameters that affect the final amount of steel required. Weight minimizing values of B_{top} were found in the range of 12-16m. A uniform TP connecting directly to both to the tubular and the lattice part of the tower would be un-economical and very difficult to hoist up to its final position.

As the tower actually is a vertical cantilever, the essence of the function of the TP is to transform the bending moment that is imparted to it by the tubular part into equivalent bending in the lattice part, i.e. pair of forces in the legs of the tower. The design fulfills this function by the following concept:

- (a) the base bending moment of the tubular part M_{tub} is first transformed into a pair of horizontal forces (F_1, F_2) by way using a cylindrical extension (T_{ext}) of the tube as shown in Figure 1-9 which is rigidly connected to the diaphragm plates C1 and C2 at its top and bottom respectively. In this way M_{tub} can be converted to a pair of horizontal forces F_1 and F_2 respectively.
- (b) The diaphragms (C1 and C2) are subsequently attached to the truss girders ABCD and A'B'C'D' as shown in Figure 1-10.
- (c) Finally the truss girders ABCD and A'B'C'D' extending outwards from the cylindrical extension T_{ext} are attached to the legs of the lattice tower. In the end, vertical forces F_{V1} and F_{V2} develop that ensure the equilibrium of the transition piece. These forces are transferred directly to the legs of the lattice tower.
- (d) In addition, the cylindrical extension T_{ext} may be arranged in the interior of the lattice tower top module i.e. may continue lower than the actual termination of the tubular part (shown in green). In that way node A of the girder is connected to node LA of the lattice part, node B of the girder to node LB of the lattice part etc.

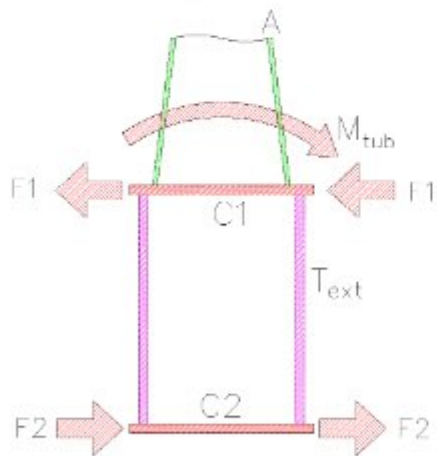


Figure 1-9: Section of the lower tubular part and TP

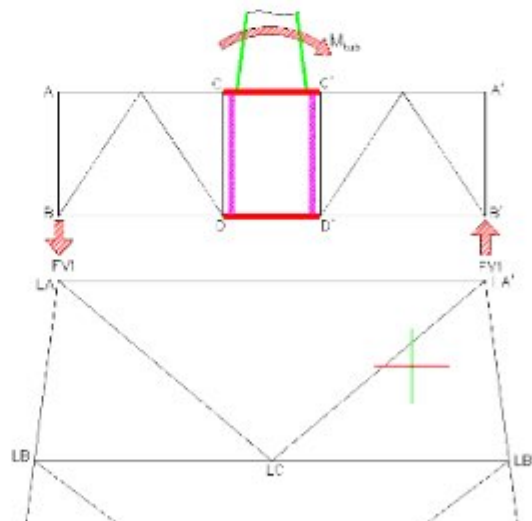


Figure 1-10: The diaphragms subsequently attached to the truss girders ABCD and A'B'C'D'

The resulting arrangement is schematically depicted in Figure 1-11. The design of this transition piece for the 185m tower (120/65) is given in Deliverable 1.2.

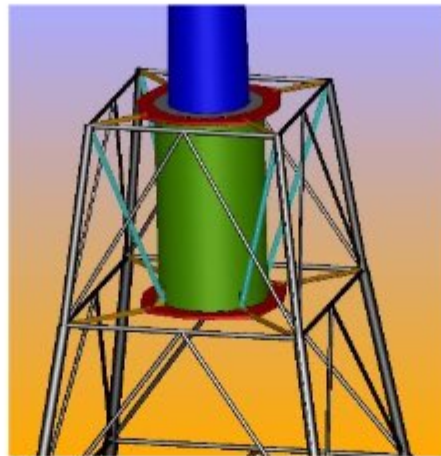


Figure 1-11: schematic representation of the Concept 1 transition piece concept.

1.2.2.2 Concept 2

Concept 2 results from merging two independent developments during the project and is used in WP2 as the basis for downscaling. It assumes the use of steel grade S690 in the TP divided into six segments and bolted connections. The geometry of the new proposed conical shell TP is illustrated in Figure 1-12(a) and the main components are shown in Figure 1-12(b). The upper plate is the support for the lifting equipment and the diameter is slightly more than 8 m. The lower plate is an intermediate plate which holds the last segment of the tubular part. Furthermore, the chords which are basically the lattice columns are integrated into the body in the initial concept.

The last segment of the tubular tower has two exterior flanges. The upper plate and the lower plates are connected to the tubular segment through these flanges. Moreover, plates are connected to the transition piece through bolted flanges as well. As it is shown in Figure 1-13, the strand jacks are sat on the upper plates and the slings are passed through the holes on the upper plates and they are connected to the lower plate which is connected to the last tubular segment before the lifting gets started. The shells can be manufactured in six separate shells which are bended at the end edges and connected to the intermediate plate in the lattice's columns. The detail of two connections are also shown in Figure 1-13.

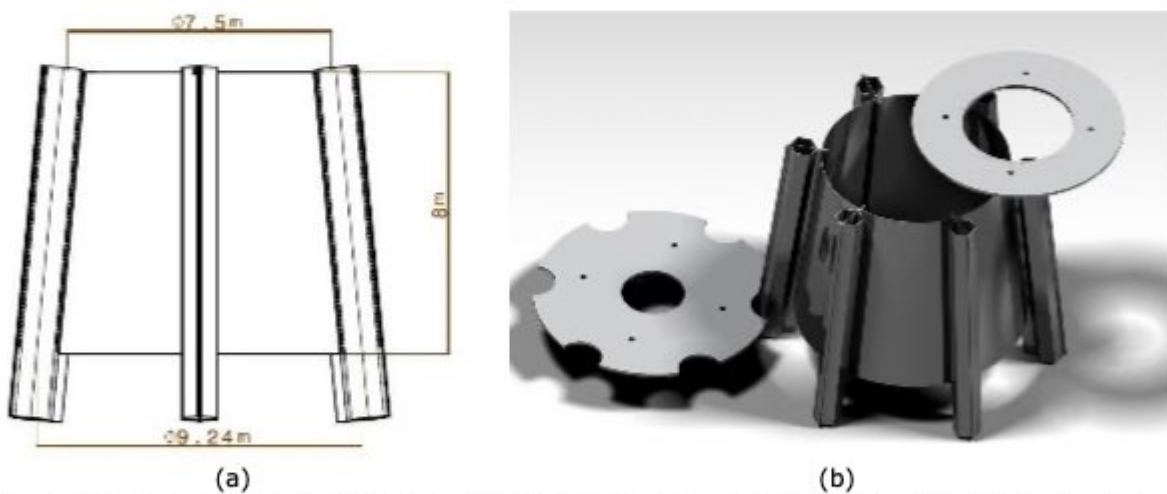


Figure 1-12: (a) Dimensions of the Cylindrical Shell, (b) The transition piece main components

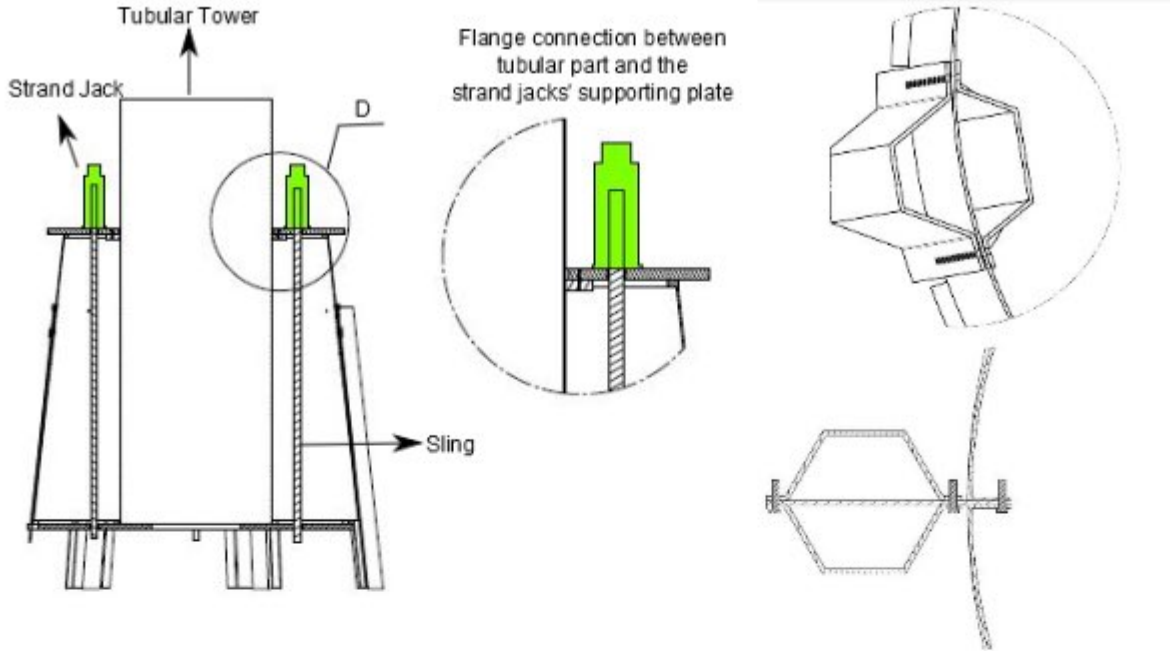


Figure 1-13: The schematic view of transition piece and the detail view of the connections

1.3 Hybrid tower study cases conceptual design and structural predesign

1.3.1 Introduction

The project proposal establishes 24 different study cases to develop the hybrid tower between 120- and 220-meters height. The different proportions of lattice/tubular (L/T) part and different height to tower base spread ratio (H/S) is defined for the parametric studies (Table 1-11). Moreover, different number of legs (4 and 6) for lattice structure are considered. The main objective is to propose three different configurations, which are best suited to be used in further detailed analysis in subsequent WPs, especially dealing with detailed design of members/connections and with life cycle assessment and design recommendations.

Table 1-11: Study cases for parametric investigation of lattice structure

Tower Height (m)	120 L/T=60/60	160 L/T=60/100	180 L/T=120/60	220 L/T=120/100
No. Legs		4 and 6		
Height/Spread ratio		3/1; 4/1; 5/1		

1.3.2 Design Procedures

In order to obtain the most suitable lattice topology two different approaches were used. Following simplifications were assumed in this phase: the loads on the top of the lattice tower were fixed and the elements were designed as tubular elements. The first approach is based on a parametric study that optimizes the geometry of the lattice structure based on discrete number of study cases with the target of obtaining the least number of connections and the lowest weight assuming that no secondary bracing is used. The analysis converges to class II cross sections. The second method is based on structural optimization criteria, targeting the upper bound of class III cross section, which leads to less mass. However, the geometry of the lattice structure might need secondary and horizontal bracing systems, which may pose additional difficulties in the assembling and erection process. First methodology uses software SAP2000 to design the structures and obtain the steel weight, the number of connections and bolts associated to each typology. For the second methodology a MATHEMATICA code was developed to minimize the steel weight. Both methodologies follow EN1993-1-3 [20] for the design of the elements and EN1993-1-8 [17] for connections.

1.3.3 Parametric study

The decision for a parametric approach to obtain the most suitable geometry is supported by the complexity of the external variables that are constraints to the problem. The first constraint is the dimensions and weight of the transition piece, which conditions the top section of the lattice. It was assumed 8 m to have enough space for transition piece assembly and the wind turbine self-rising mechanism. The second constraint is the load definition, which is dependent on the structural response. Fixed values for horizontal forces and for the TP weight were assumed to obtain suitable geometry and afterwards, load-design iterations were performed only for those geometries. The third constraint is the avoidance of resonance of the dynamic loads in the eigenfrequencies. This was also only verified for those geometries chosen.

The parametric study starts with geometry definition. In order to select the bracing configuration and obtaining minimum number of connections, 2D models were analyzed (Figure 1-14). Four solutions for geometry of the braces were considered. For each case, the angle of the brace from horizontal plane was varied between 30° and 50° with the increment of 5° . Weight and number of the connections for each typology was determined and compared. Based on 4-legged lattice structure results, two solutions for the 6-legged structures with X-bracing and k-bracing were considered. The K-bracing configuration is selected to be investigated in 6-legged structures. This type of bracing is not possible for 4-legged structures because it leads to extremely long braces.

Then, the 3D models were studied for height over spread ratios of 1/1 to 6/1. In first stage, the lattice structure was considered with constant cross-section for the braces along the height. In the next stage, geometry was optimized and the cross-sections for the braces were varied along the height. The structural analysis and design were performed with SAP2000 software for loading applied in main directions shown in Figure 1-15. The amount of steel is plotted against the number of connections in Figure 1-16(a)(b) and against the estimated number of M30 bolts in Figure 1-16(c)(d), both for 220- and 120-meters tower. K-braces are used for the 6-legged structures and X-braces for 4-legged structures, both with 45° angle for bracing system.

Whatever the configuration adopted the minimum mass of the structure is obtained for H/S ration between 3/1 and 5/1, however at cost of increasing number of connections. The number of the bolts was estimated from the slip resistance of preloaded bolts necessary to sustain the design force in the elements. It can be observed that the number of the bolts as well as the weight of the lattice structure are decreasing with the increase of the H/S ratio up to 5/1 and 4/1 for 4-legged and 6-legged structure respectively. The lattice structure with H/S ratios of 3/1, 4/1 and 5/1 are chosen for further analysis. Table 1-12 shows the maximum length for the bracing system.

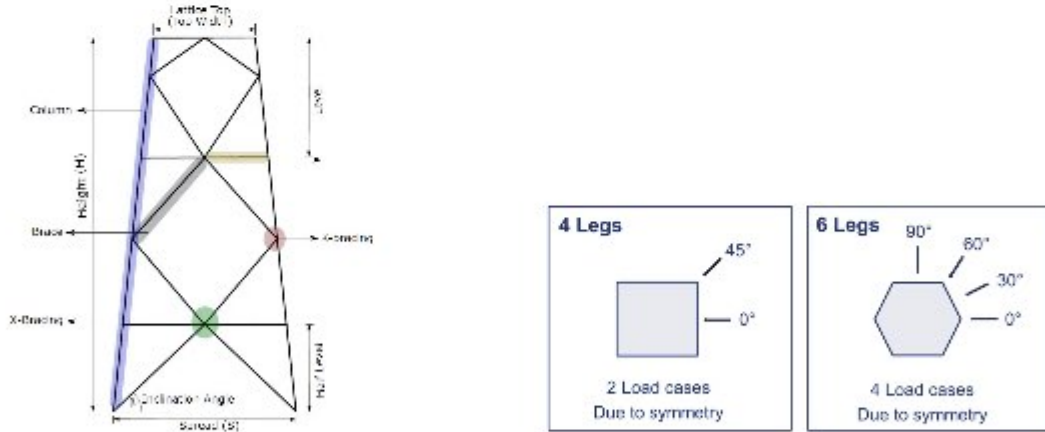


Figure 1-14: Schematic of 2D lattice structure

Figure 1-15: Wind load direction on structure

Next, the tubular tower and the transition piece are added to the selected lattice structures. Three iterations are performed in the process of load calculation and design. The 6-legged and H/S=4/1 is proposed for 60m and 120m lattice structure to proceed with design. The tubular part was modified according to the third iteration of the loads. The calculated geometry of the tubular part is shown in Table 1-13. The 50 tonnes transition piece is considered.

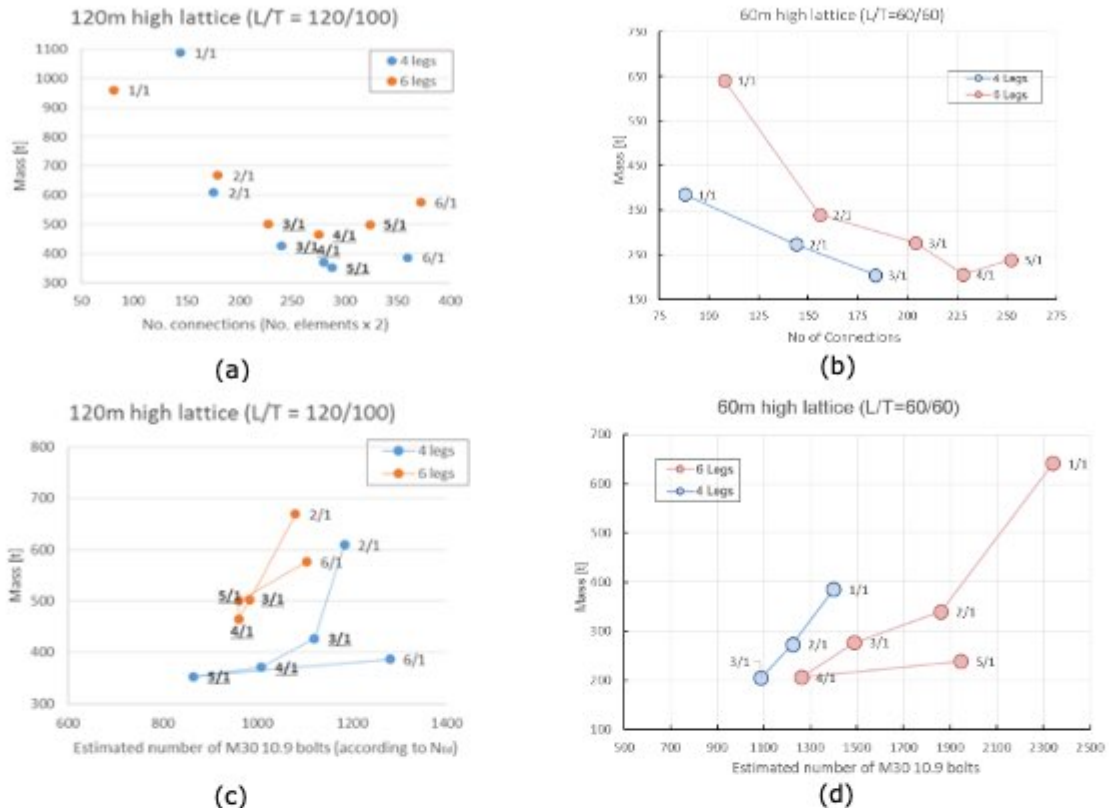


Figure 1-16: The steel mass against number of connections (a) and (b), and against the estimated number of bolts for (c) and (d) for 120- and 60-meters lattice structures

Table 1-14 and Table 1-15 show the set of cross sections which were re-designed with the new load Tables for 120m lattice and 60m lattice respectively. There was an important reduction in cross section's diameter particularly in column in the iteration process. The column diameter decreased from 1350mm to 930mm which is around 30% for 120m lattice and from 711mm to 323.9mm which is around 45.5% reduction. This reduction happens for all the members' diameter and thickness.

Table 1-16 shows the maximum displacement at tower top. As it can be seen, the maximum top displacement is in the range of 2 meters which is quite realistic. Figure 1-17 shows the first mode shapes and eigenfrequencies of the designed 220m and 120m towers, which allow to avoid resonance with the rotor operation. The maximum and minimum reaction forces are presented in Table 1-17 for the ground joints.

Table 1-12: Maximum element length [m] of bracing system

H/S	4 legs	6 legs
4/1	27.3	23.3
5/1	22.4	18.8
6/1	14.1	15.0

Table 1-13: Geometry of Tubular part

	Diameter (m)		Thickness(mm)	
	100m	60m	100m	60m
Base	4500	4500	34	26
Top	4000	3500	34	26

Table 1-14: 120m lattice cross sections

Section Name	Diameter [mm]	Thickness [mm]
Column	930	32
D01	350	10
D02	350	10
D03	320	10
D04	320	10
D05	300	10
D06	300	10
D07	290	10
D08	290	10
D09	280	10
D10	280	10
D11	270	10
D12	350	10

Table 1-15: 60m lattice cross sections

Section Name	Diameter [mm]	Thickness [mm]
Column	324	25
D01	245	5
D02	219	5
D03	219	5
D04	219	5
D05	219	5
D06	219	5
D07	219	5
D08	193	5
D09	245	5

Table 1-16: Maximum displacements at the top of the towers

	120-meters tower	220-meters tower
u_{\max} [mm]	1135	2225

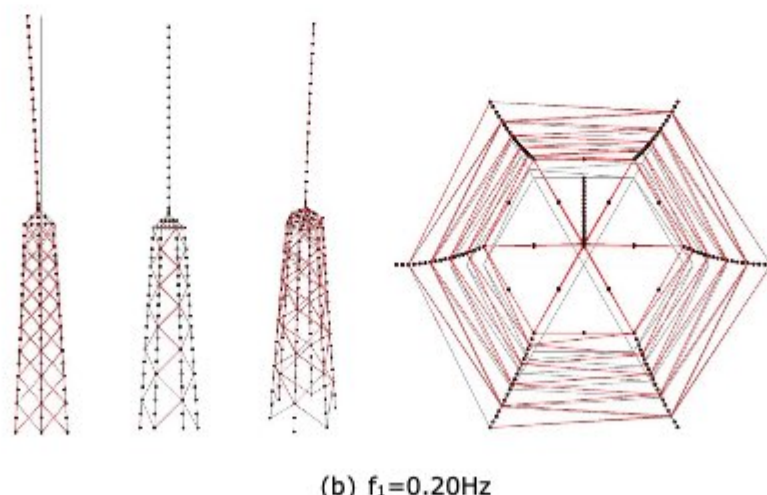
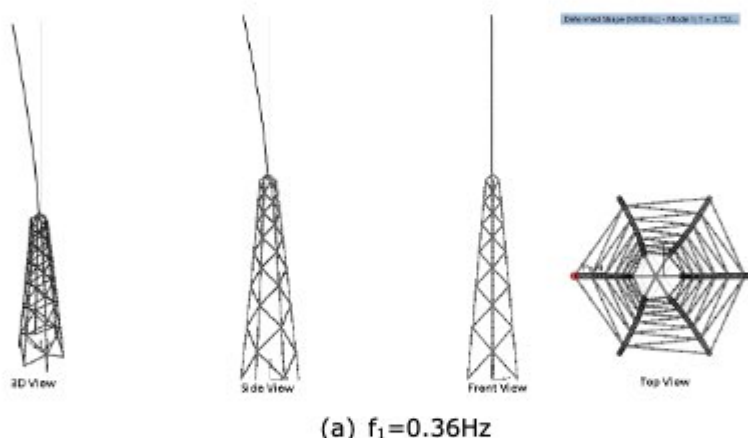


Figure 1-17: The Mode Shapes of (a) 120m, and (b) 220m tower and respective first natural frequencies

Table 1-17: Maximum reaction forces in ground joints

Joint	Type	F3	F1
		[KN]	[KN]
		220m tower	120m tower
2	Max	10391	1598
2	Min	-179	-3421
4	Max	7631	4983
4	Min	-1234	-1874
6	Max	7117	7127
6	Min	-1699	-5
8	Max	7859	6496
8	Min	-2206	1087
10	Max	9458	4524
10	Min	70	-1959
12	Max	9455	2865
12	Min	899	-4552

1.3.4 Structural optimization

The problem of the design of a cross section to be used in a certain member calls for the choice of a cylindrical cross section (i.e. Diameter (D), Thickness (t)) that will result to a $N_{b,Rd}$ equal to the design axial force N_{Ed} (according to EN1993-1-1 [18]). The problem of finding the most economical cross section can be solved by keeping the D/t ratio to the limiting value of Class-III cross sections i.e. $90\epsilon^2$ where $\epsilon = (235/f_y)^{0.5}$ (according to EN1993-1-1 Table 5.2, Sheet 3).

As the whole issue of structural optimization was treated by way of developing a specialized Mathematica code, a dedicated routine was written for this task.

The way this code works is the following: the buckling resistance $N_{b,Rd}$ of a member with:

- (a) an axial load equal to N_{dsrn} ;
- (b) a buckling length equal to L_{geo} ;
- (c) a D/t ratio equal to D_{tra} ;
- (d) a material modulus E_{you} and a yield strength f_y ;
- (e) buckling imperfection coefficient $alpha$;

Will be given by the expression

$$\frac{0.186882D_{out}^2}{0.5(\frac{0.00137486L_{buk}^2}{D_{out}^2} + 0.49(0.0370791\sqrt{\frac{1}{D_{out}^2}L_{buk}} - 0.2) + 1) + \sqrt{0.25(\frac{0.00137486L_{buk}^2}{D_{out}^2} + 0.49(0.0370791\sqrt{\frac{1}{D_{out}^2}L_{buk}} - 0.2) + 1)^2 - \frac{0.00137486L_{buk}^2}{D_{out}^2}}}}$$

If D_{tra} is set to, f_y to 35.5kN/cm², E_{you} to 21000kN/cm² and $alpha$ to 0.49.

The corresponding $N_{b,Rd}$ expression for S460 reads

$$\frac{0.313624D_{out}^2}{0.5(\frac{0.00178327L_{buk}^2}{D_{out}^2} + 0.49(0.0422288\sqrt{\frac{1}{D_{out}^2}L_{buk}} - 0.2) + 1) + \sqrt{0.25(\frac{0.00178327L_{buk}^2}{D_{out}^2} + 0.49(0.0422288\sqrt{\frac{1}{D_{out}^2}L_{buk}} - 0.2) + 1)^2 - \frac{0.00178327L_{buk}^2}{D_{out}^2}}}}$$

We can observe that in the last two $N_{b,Rd}$ expressions there exist two variables:

- the outer diameter of the tube
- the buckling length

As the buckling length is usually given, one can use the library function "FindRoot" of Mathematica:

$$xxx = \text{FindRoot}[N_{\text{brd}} == N_{\text{dsgn}}, \{D_{\text{out}}, 1.\}];$$

to obtain the value of the outer diameter that fulfills the task (i.e. to resist a design load value N_{dsgn} for a buckling length L_{geo} and observing the prescribed D/t ratio). The thickness values (in mm) are rounded to the next integer value for the purpose of weight calculation of the tower.

In the Figure 1-18, the influence of choosing varying D/t ratios for the same problem (buckling length 10m, Design Load 4000kN, steel grades S355 (blue), S460 (orange)). On the vertical axis there is given the weight of the resulting strut.

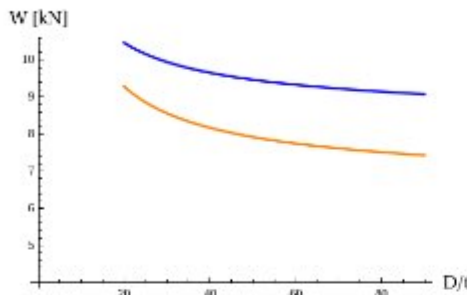


Figure 1-18: Weight of a strut as a function of D/t

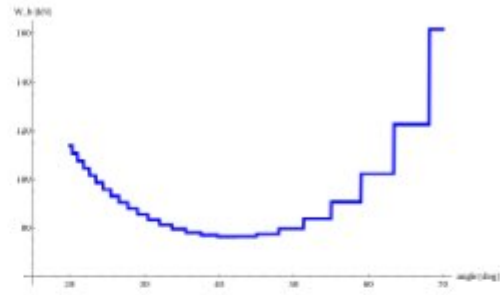


Figure 1-19: Face brace total weight as a function of V-diagonals angle to the horizontal

1.3.4.1 Optimization of the Face Bracing Trusses (FBT)

Here the optimal choice of a face bracing system is discussed. First the designer is faced the choice with a number of basic bracing trusses geometries:

- (a) X braces
- (b) V braces
- (c) inverted V braces

As the form of the tower is conical, option (c) appears to be the most favorable as it keeps the total length of the diagonals lesser than that of option (b); option (a) can be perceived as a combination of (b) and (c) and therefore is subject to the aforementioned argument. The V braces are therefore considered as the most favorable option.

The angle of the V diagonals is now left as the only parameter that affects the total weight of the bracing system. To investigate its effect, the following piece of code was written. In it, the face of a tower of total height H_{tot} and of constant width B_{brc} with a top horizontal shear H_{frc} is considered. The angles of the V diagonals to the horizontal are varied between 20 and 70 degrees (variable P_{brc}), the steel grade is S355 (variable f_y) and the D/t ratio of the struts is set to 90 (variable DTR).

The resulting weight of the brace is plotted with respect to their angle to the horizontal in the Figure 1-19. It can easily be seen that keeping the V-brace diagonals angle between 40 to 45 degrees results to a minimal total weight of the bracing for the face.

This is the result of two antagonizing factors:

- small V brace diagonals inclination angles (i.e. diagonals close to the horizontal) decrease struts' length and diminish their axial force
- small V brace inclination angles result to a large number of V braces needed to cover the full height of the tower

The stepwise nature of the plotted total weight function owes to the fact that the number of V braces that fit to the tower's height is integer; therefore varying the inclination angle in steps of 0.05 degree (as the code above attempts to do) results to the same number of V braces over the height of the tower thus ending up with the same total weight.

One might argue that a large number of V braces also reduces the buckling length of the legs. The practice followed here is to reduce the legs' buckling length by means of using secondary bracing (which is a lighter option) instead of affecting the density of the primary V bracing.

It may be mentioned here that, for a square cross-section towers, the governing loading situation arises when the horizontal shear loads are applied in a direction normal to a face.

1.3.4.2 Optimal Design of the Legs

The normal force that develops in the legs of a tower of square cross section can be derived by equilibrium considerations as the structure is statically determinate.

For the case of a square cross-section tower of height, the governing situation for the legs appears when the top shear acts in the direction of the diagonal of the tower. In that case the axial force in the legs is

$$N_{\alpha=45}(z) = \frac{M(z)}{b(z)\sqrt{2}} \times \frac{1}{\cos(\pi/2 - \phi_d)}$$

Where $M(z) = M_{top} + (H-z) \times F_{top}^H$ i.e. the bending moment of a vertical cantilever acted upon by a moment M_{top} and a horizontal force F_{top}^H at its top, and

$$b(z) = \frac{B_{top} - B_{base}}{2} \times \frac{z}{H} + B_{base}$$

The angle of the leg to the horizontal plane is given by

$$\phi_d = \tan^{-1} \frac{\sqrt{2}H}{B_{base} - B_{top}}$$

Keeping the axial force constant in the legs requires that the base width of the square has the value

$$B_{base} = B_{top} \frac{M_{top} + H \times F_{top}^H}{M_{top}}$$

This means that choosing a value of the square side B_{top} as an independent design parameter, there is a value of the base cross section side, given by B_{base} that keeps the axial force in the legs constant. Reducing the lever arm (i.e. designing a tower with a narrower base) obviously results to an increase of the legs' axial stresses towards the base.

1.3.4.3 Optimal Design of the Tower - Strategy

Having demonstrated that there is an optimal face brace geometry (the V brace) and an optimal V brace angle (the 40 - 45 degree range), what remains is to determine the top and bottom dimension of the tower cross section. Since there is a characteristic value of B_{base} the search space of the problem is defined by the independent variables.

- B_{top} and
- $\mu = B_{top} / B_{base}$

Which, to the author's view gives a better understanding of how far, a given design is away from the theoretically "optimal" base width. Of course, this does not guarantee that result of the design will indeed be of minimal weight as the cross section of the legs is determined by the buckling checks of EN1993-1-1 which is a highly non-linear procedure. In addition, the result of a buckling check is to a great extend controlled by the buckling length which, as said before, is controlled by the introduction of secondary bracing.

Let us now come to the strategy of the minimal weight investigation as followed in the present work. Two major factors appear to be at play:

- closing the distance between the legs reduces the weight of the face braces but increases the axial force
- increasing the distance between the legs reduces the axial force in the legs but increases the total length (and slenderness) of the V braces

Therefore, a two-dimensional search was deemed necessary in order to assess the variation of the total tower weight with respect to the two parameters B_{top} and μ mentioned above.

In addition to that, a policy concerning the automatic introduction of secondary bracing was implemented in the Mathematica optimization script. Additional secondary bracing is introduced in a "leg part" if the ratio between the maximum and the minimum leg cross sections calculated, exceeds an upper limit (set to 1.2 or 20% in the numerical investigation that was performed).

An initial number of bracing points can be specified which may increase to ensure cross section parity between the various leg parts. As a "leg part" is understood the length of a leg along the height of a V brace truss. The technique works well as it tends to introduce additional braces to the lower leg

parts where, due to the flare of the tower and the constant V brace angle policy, the leg buckling lengths are substantially longer.

The self-weight of the steel part of the tower turns out to be a significant part of the loading. The search program takes it into account by means of a successive iterations scheme (loads from previous iteration / new cross sections calculation - repeated until convergence).

Also, the top V brace of the tower is fixed to a height equal to $(2/3)(H/10)$ in order to accommodate the transition piece.

1.3.4.4 Parametric Study - numerical investigation matrix

For the investigation of the structural parameters for which a minimal weight design is sought, the load data as supplied in [57] were used. For each case a minimal weight solution for the steel grades S355 and S460 was calculated. The initial (minimal) number of secondary braces was set to 2, 2, 2, 1 for the V braces starting from the ground level respectively. The search algorithm can only increase these.

Table 1-18: Ranges of independent parameters values as used in the parametric investigation

Group	Parameter	Range of values							
H=60m	B_{top} [cm]	600.	700	800	900	1000	1100	1200	
	μ	1.00	0.9	0.8	0.7	0.75	0.65	0.6	0.55
H=120m	B_{top} [cm]	700	800	900	1000	1100	1200	1300	1400
	μ	1.00	0.9	0.8	0.75	0.7	0.65	0.6	0.55

1.3.4.5 Parametric Study - Overview of Results

The extreme values of the resulting total weight for the tower material is given in Table 1-19.

Table 1-19: Minimum and maximum total weights found

Data set	S355		S460	
	min	max	min	max
Table 09	83.5	131.7	74.2	106.8
Table 10	163.9	286.7	139.2	232.8
Table 11	54.2	76.1	49.4	66.4
Table 12	132.6	244.4	111.7	199.2
Table 13	174.9	331.0	145.1	268.2
Table 14	85.3	146.9	74.8	122.9
Table 15	183.8	256.8	165.9	226.5
Table 16	324.1	476.8	275.5	404.1
Table 17	138.5	184.9	131.1	153.2
Table 18	251.4	434.6	229.0	374.7
Table 19	335.7	598.4	294.6	502.4
Table 20	178.2	270.0	167.5	237.7

1.4 Conclusions

The proposal for three study cases of hybrid towers is defined as a Milestone for this WP1. From the several supporting structure with different heights investigated and designed, three scenarios are selected, the detail design and sketches are provided in Appendix D of Deliverable D1.3. The 185m is selected as the tower height. To the initial height of 180m extra 5m was added to the tubular tower to avoid the blade collision with the transition piece substation.

Table 1-20: Three selected solutions

Analysis Method	Legs	Height	Lattice/Tubular	Bracing
1 parametric	6	185m	120m/65m	K-Bracing without secondary braces
2 optimization	6	185m	120m/65m	K-Bracing with secondary braces
3 optimization	4	185m	120m/65m	V-Bracing with secondary braces

2 Erection process

Work package two (WP2) deals mainly with the development of the erection process and the design and construction of the scaled prototype, which is tested for showing feasibility of manufacturing and erection concepts developed and introduced in task 1.2. The following objectives were established within the proposal:

- Computational simulation of erection procedure by developing and analysing finite element models for the construction phases;
- Evaluation of specific transient loading during the construction and erection phases;
- Design and construction of the prototype;
- Development of an experimental set-up and performing a feasibility study and load tests of the sliding mechanism on the scale prototype;
- Monitoring of scale prototype during feasibility test.
- Risk assessment of the construction process.
- Study on fatigue details of the transition piece proposed in task 1.2

2.1 Detailing of the construction process of a chosen case study from WP1

2.1.1 Introduction

Task 2.1 includes the detailing of the erection process and the transition piece referring to the chosen case study from M1 and regarding the prototype in task 2.2. Therefore, the following work was developed:

- Study of state-of-the-art technologies for erection process to find the best solution for hybrid steel wind turbines;
- Detailed analyses of erection process and precise determination of erection process, which could be used with very high wind turbines and will be used with the scaled prototype;
- Evaluation and consideration of specific transient loading during the construction and erection phases;
- Scaling down the hybrid steel tower for wind turbine with development of an experimental set-up for feasibility study.

There are some common design assumptions between the partners and there are some assumptions which are taken by partners individually. Design assumptions are important as the outcome assessment and possible further discussion is highly dependent on the initial and boundary conditions of the analysis.

The common assumptions relate to geometry and topology of the supporting structure and the simulated aerodynamic and inertia loads in transition piece level.

Therefore, according to D1.3 and M1 the following tower properties are chosen:

- 5MW NREL reference wind turbine
- 6-legged lattice structure
- Polygon cold-form cross section of legs
- Height of Lattice part 120m
- Height of Tubular Part 65 meters (slightly larger than the blade used in calculations 63 meters)
- Lattice height to spread ration of 4/1 without secondary bracings
- Constant diameter for tubular part with 4.3 m

Moreover, detail design load cases are considered based on D1.1. The other details and individual design assumptions as e.g. cross sections of legs and truss segments, type of bracing, details of connections and transition piece were defined in Deliverable D1.3.

2.1.2 Tower assembling procedure

The draft of an erection process was discussed among partners and with the company that offers in the market the solution Donges Steeltec. Thereby the lattice tower is mounted on site in several pieces first and the pieces are put together by a mobile crane afterwards. For the hybrid tower, the

tubular parts are assembled on the ground in the inside of the lattice tower additional. In the final state a transition piece which is located at the top of the lattice tower connects the lattice and the tubular part. During the assembly process, the transition piece also serves as a supporting area for four strand jacks which lift the tubular part from the ground to its final position. To prevent an overturning during the assembly of the tubular parts on the ground and also during the lifting, the tubular tower should be fixed by strand jacks from the bottom also. Therefore, a pedestal with four strand jacks is installed to the foundation. Additionally, hydraulic pressure rollers or springs are installed on the inside of the transition piece as a horizontal support and guidance during the lifting of the tubular tower. These horizontal holding devices have to be positioned in at least two height levels to enable a release of the device in one level when the flange of the last tubular segment passes by.

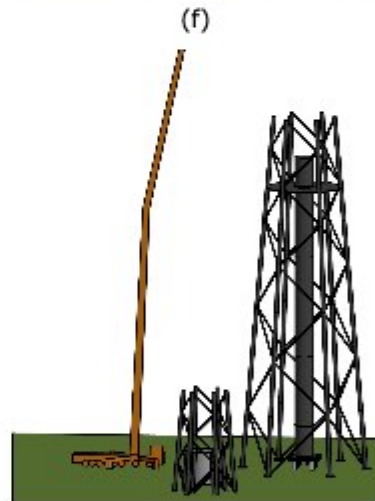
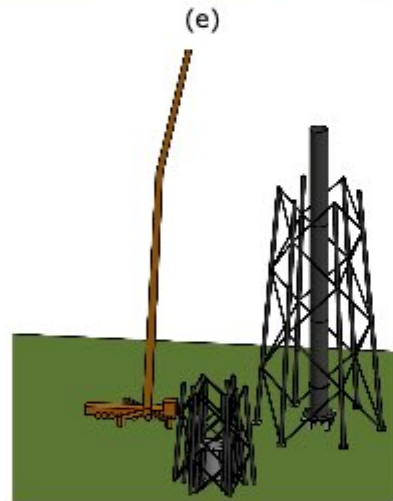
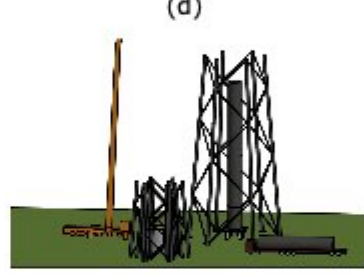
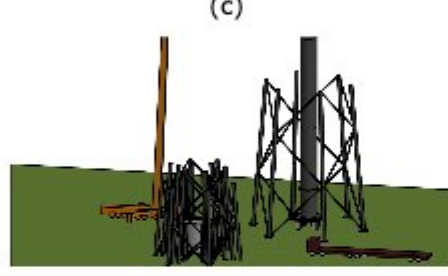
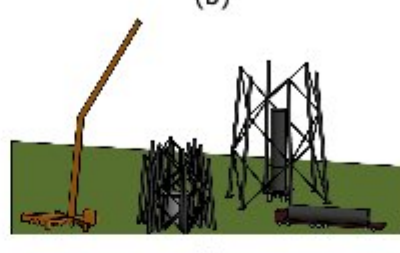
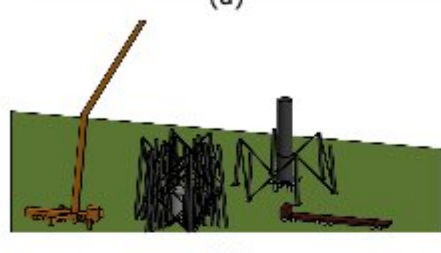
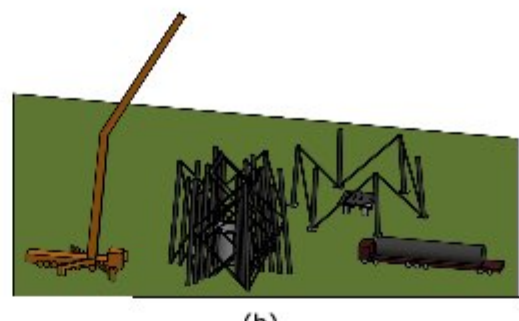
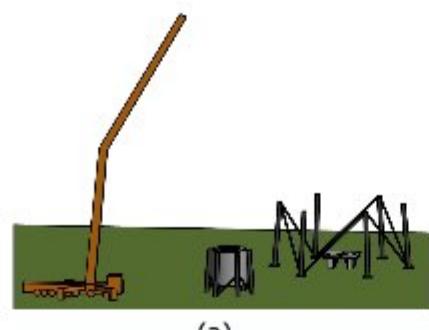
About 880 t has to be lifted. Therefore, four strand jacks H-300 of the company HebeTec [34] are chosen. As an example: the weight is composed of the tubular tower (306 t), the bottom plate (50 t), the flange (5 t), nacelle with rotor and blades (404 t), eight end-anchorages (0,456 t) and the estimated weight of the strands ($4 \times 26t = 120$ t). The assembling process is detailed in Deliverable D2.1 and reproduced in Figure 2-1 (a) to (n) and strands pedestal in Figure 2-1 (o) to (p).

The 120 m high lattice tower is separated into six units. First of all, unit one of the lattice is mounted and fixed to the foundation by means of a mobile crane. Besides the final construction side last unit at highest position of the lattice tower is set up and the transition piece is fixed to this last unit, cf. Figure 2-1 (a). Afterwards, the other sections of the lattice part are assembled one above the other next to the real construction site. The tubular tower should be erected in the inside of the lattice tower. Therefore, a foundation and the pedestal have to be built. To prevent an overturning of the tower during the assembly of the different parts, the tower should be fixed from the bottom by strand jacks. Therefore, the above-mentioned pedestal is fixed to the foundation, cf. Figure 2-1 (p).

Regarding additional stiffening, it could be useful to install four additional strand jacks beneath a plate. This plate is supported by a circumferential downstand beam. Four columns transfer the loads to the foundation. The plate of the pedestal needs holes for the strands. A bottom plate for the tubular tower has to be positioned on the pedestal. The strands are fixed to the bottom plate by end-anchorages. So, the bottom plate of the tubular tower also needs holes for the strands. The strand jacks attach the bottom plate to the pedestal during the setup of the tubular tower. Near to the pedestal strand carousels with the strands are positioned.

Then the alternating assembly can be started. The lower segment of the tubular tower is transported to the construction side and is lifted inside the first lattice unit, cf. Figure 2-1 (b). It is fixed to the bottom plate and a flange is welded to the tubular segment in a certain distance to the bottom plate. Then the second lattice unit is lifted by mobile crane and is mounted to the first unit. Alternating lattice and tubular segments are lifted and fixed until unit three of lattice and the third and last part of tubular are in its position (cf. Figure 2-1-c-g). After that all lattice parts, except the last one, are mounted to the lattice tower (cf. Figure 2-1 h). Then a stabilization plate is installed at the highest tubular part, so that it is at the middle height of the lattice tower (cf. Figure 2-1 h). Before the last unit is lifted, the strand jacks and strand guidance are installed to the transition piece, cf. Figure 2-1 i). After the last unit is connected to the lattice tower, the strands are arranged to the strand jacks and guidance and led down to the ground (cf. Figure 2-1 j). The strands are connected to the bottom plate. Here also end-anchorages are used. A strand carrousel is established on the ground into the inner hexagon of the lattice to wind up the strands when they reach the ground. After that the tubular part is lifted until it reaches the top of the transition piece, cf. Figure 2-1 k), so that the nacelle and the rotor with the blades could be put on top (cf. Figure 2-1 l). After that the whole tubular part including all equipment on top could be lifted to final position (cf. Figure 2-1 m and n).

This erection procedure is also discussed with the company HebeTec, from which the strand jacks and equipment will be used for the prototype.



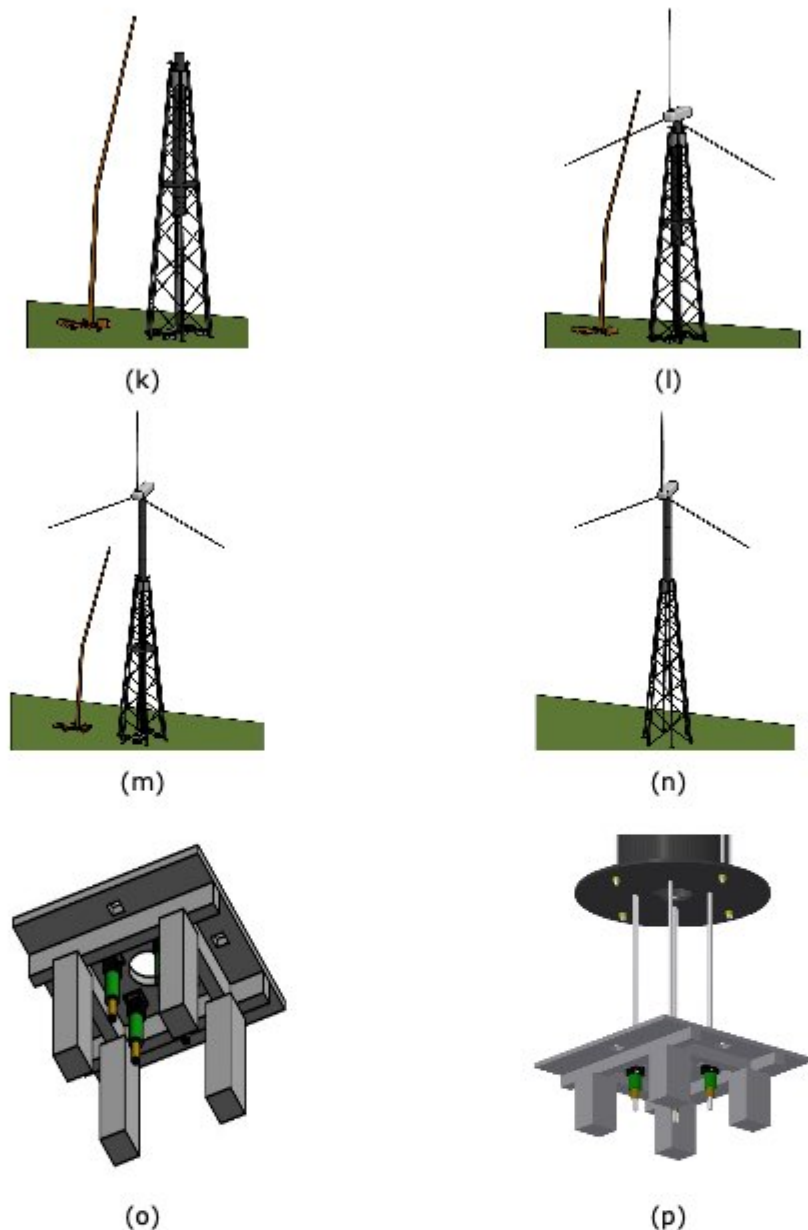


Figure 2-1: Assembling sequence (a)-(n) and strands pedestal, bottom plate (o)-(p)

2.1.3 FE calculations of the construction process at the relevant stages

Regarding the detailing of construction process of the chosen case study: 6-Legs, height of lattice part 120m, height of tubular Part 65 meters, lattice to spread ratio of 4/1 without secondary bracing, the program AutoCad was used to detail the construction process and then export the geometry to ANSYS workbench for structural modelling. The static loading was calculated within WP1. The specific transient loading, which is mainly the wind loading, is also calculated and taken into account. The relevant stages, which were investigated, are:

- S1: final position (cf. Figure 2-2 a)
- S2: shortly before tubular part achieves transition piece (cf. Figure 2-2 b);
- S3: nacelle and blades are put on top of tubular part (cf. Figure 2-2 c);
- S4: nacelle and blades are erected and shortly before final connection (cf. Figure 2-2 d).

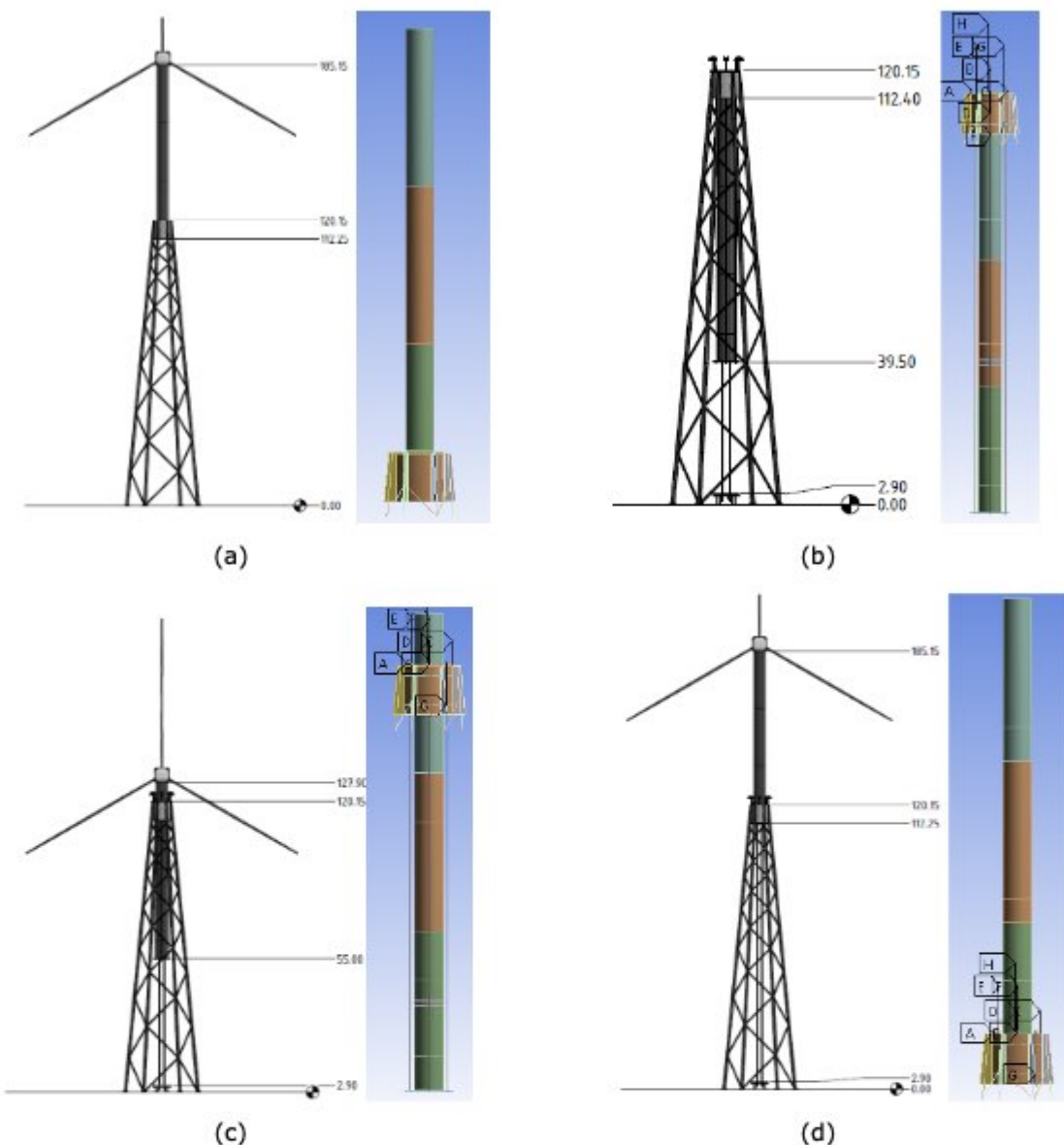


Figure 2-2: Critical stages for erection process

Regarding a theoretically predesign of a full-scaled transition piece, these FE simulations were performed. At first the four stages were investigated to find out, which stage is the critical one for which component of the transition piece. The investigated components and the corresponding critical stages are the following:

- S1: final position
 - Critical for components:
 - Shell of transition piece
 - Shell of tubular part
 - Upper and lower flange for connection of transition piece and tubular part
- S2: shortly before tubular part achieves transition piece
 - Critical for components:
 - Bottom plate
- S3: nacelle and blades are put on top of tubular part
 - Critical for components:
 - Not critical for any component
- S4: nacelle and blades are erected and shortly before final connection
 - Critical for components:
 - Top plate

2.2 Production of a scale prototype of the tower

2.2.1 Introduction

Task 2.2 includes the production of the scaled prototype and the following sub-tasks:

- The erection process (including the control system) is scaled down for feasibility test of scaled prototype.
- The scaled prototype is designed.
- The scaled prototype is fabricated.

First step is the “scaling down” of the 185 meters wind tower. Since the main objective is the feasibility of production of the transition piece, the decision was to scale down a small part of the lattice structure, which should be enough to install a small part of the tubular part. Therefore, the transition piece would be the most interesting part to follow a scale down policy. For the erection process itself, the smallest strand jack from HebeTec would be used, because the scaled prototype of the tubular part to be lifted has a weight of around 30 tonnes, which has to be divided by four strand jacks. This leads to a needed load capacity of 85 kN for each jack. Further details are given in deliverable D2.1.

The erection mechanism includes four strand jacks on top of the transition piece which is supported by the lattice structure. Four parallel slings from strand jacks with 0° angle with vertical axis lift up the tubular tower through the transition piece.

The down-scale prototype was decided to be not more than 4 m in overall. The feasibility test should consist of lattice structure, transition piece, lifting equipment, and the tubular segments. For the ease of downscaling and stay in the correct geometrical constraints, only the last level of the lattice structure was down scaled. The lattice structure and the transition piece have 4m height together and tubular segment/s can have 4 m height as it will be lifted up through the lattice and transition piece. The lattice and transition piece will be supported in height by pre-built structure.

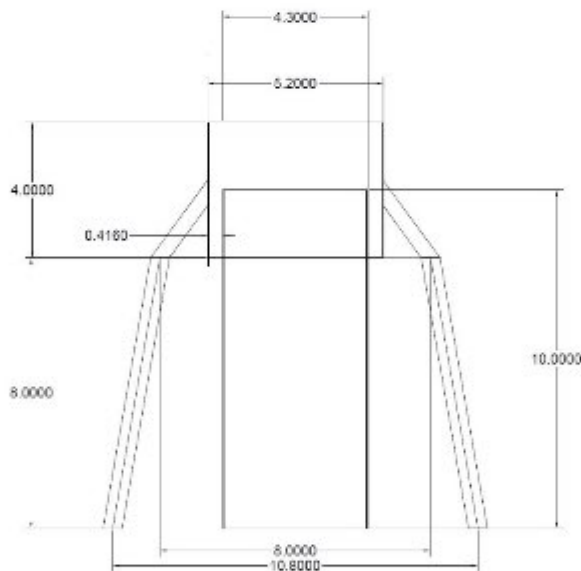


Figure 2-3: The schematic of tower parts for downscaling

The lattice structure has height of 120 m, the base spread of 30 m, the top spread of 8 m. The transition piece chord circumstance area is 8 m and the shell diameter is 7.5 m with thickness of 52 mm. If the last level of the transition piece was considered for the feasibility test, the base spread would be 10.82 m. Furthermore, the tubular segment diameter is 4.3 m with the thickness of 34 mm.

2.2.2 Scaling and design of prototype

The scaling of the RWTH-UC concept is done based on the discussed scaling policy for different components. The scaling can be applied on the transition piece and the lattice structure which are designed for the operational and lifting loads. The scale prototype can resist the scaled load. It doesn't mean that the scale loads can be considered for any wind turbine with the scale factor.

The down scaling by the factor of 4 is performed on the Concept 2 transition piece [55] and the last level of the 185m wind turbine tower proposed [56]. The original and scaled down dimensions are given in Table 2-1.

The general arrangement and dimensions of the scaled prototype is shown in Figure 2-4. The last level of lattice structure is fixed on the stationary crane showed previously.

Table 2-1: The full scale and down scaled dimensions of the transition piece

Component	Real Scale [mm]	Down Scaled [mm]	Down Scaling Factor
Lattice Structure Column (h-D-t)	16000 - 810 - 30	4000 - 202 - 7.5	4
Lattice Structure K-brace (D-t)	350 - 6	87.5 - 1.5	4
Transition Piece Shell (h-D-t)	8000 - 7500 - 80	2000 - 1875 - 20	4
Tubular Tower Shell (D-t)	4400 - 34	1100 - 8.5	4
Lower and Upper Plate (t)	150	37.5	4
Gusset Plate (t)	40	10	4

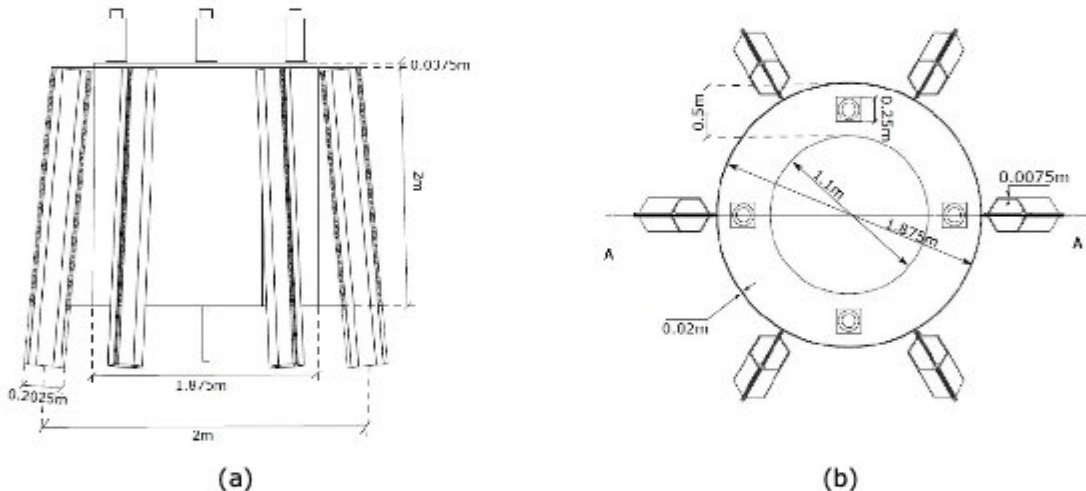


Figure 2-4: The dimensions for TP prototype, (a) front view, (b) top view

Moreover, the strand jack and slings configurations are as it is discussed in D2.1. The only difference is using smaller jack as is defined in previous section. The arrangement of the jacks on the scale prototype is shown in Figure 2-4(b).

2.2.3 Fabrication of prototype

EN 1090-2 [16] was used in order to certify the execution of the fabrication, erection of the steel structure. All requirements were taken into account for the materials, fabrication and erection process, anti-corrosion methods, tolerances and the quality assurance and control. According to the standard and considering no flaw in design and calculations, the execution class were assumed to be in EXC3 and EXC4.

The Building Information Modelling is used from design to the execution stage. BIM covers budget, manpower, schedules and conflicts of information in the project. The scale prototype is designed in 3D by UC and then it is transferred to Martifer to convert into Tekkla software model and further into the fabrication sketches. The difference between the 3D model and Tekkla model is more in the assembly tolerances, bill of material, manufacturing details such as welding, cutting, rolling and etc. Moreover, Martifer designed a space for labour work on top the scale prototype during the erection to control the hydraulic jacks' condition. Figure 2-5 (a) shows the first model and Figure 2-5 (b)

shows the Tekkla model. The main and the only difference in the models is the work station on top of the TP.

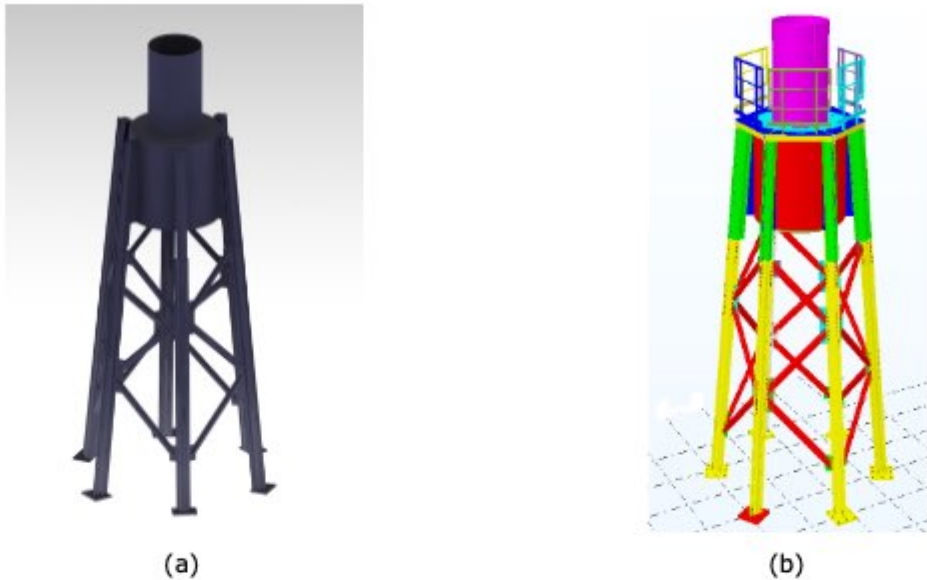


Figure 2-5: (a) The initial 3D model, (b) Fabrication ready model in Tekkla

Figure 2-6 (a) shows the detail of work station connection to the prototype Figure 2-6 (b) shows the detail of TP connection to the lattice structure. The work station is designed as the six separate piece which are connected to the chords and the TP shells. Moreover, an intermediate continuous gusset plate connects the TP chord and the lattice structure columns together.

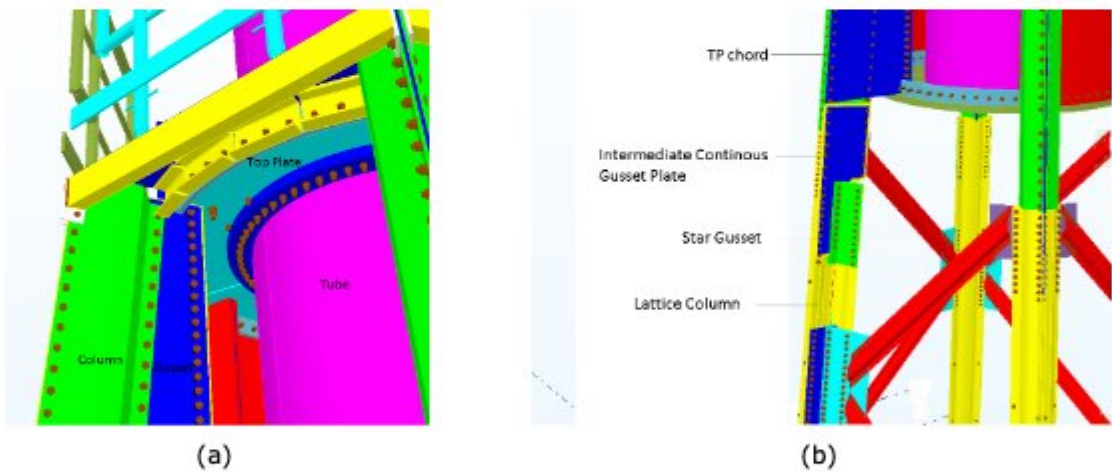


Figure 2-6: The fabrication details in the Tekkla model, (a) the working station space detail and (b) the connection between transition piece and the lattice structure

The fabrication details including dimensions, welding, tolerances and the bill of material are presented in appendices. Moreover, M16 bolts from 10.9 class are used and the corresponding preload are applied.

The other important detail in which is very important for the erection procedure is the stabilizer in the TP. In order to control the possible tilting of the tower and the ease of the tube erection, eight different position inside the transition piece is considered for the stabilizers. Moreover, the load capacity of the stabilizers was calculated based on the exerted mass as the RNA representative and the point load calculations for the mentioned stabilizers position.

The other important point in the design of the stabilizer was the total possible height and the displacement capacity of the stabilizer. The space between the tube shell and the TP shell can be considered as the permitted height (349 mm) and the tolerance between the top plate and the tube (20 mm) should be the maximum limit for the displacement capacity of the stabilizer.

The designed stabilizer system is an elastomeric mount and a roller wheel assembled on top. The elastomeric mount is used as a generator damper in the nacelle and the roller wheel can be found in the heavy-duty transportation in the industry. Figure 2-7 shows the elastomeric mount and the roller assembly which is going to be used as stabilizer system in the erection process. The maximum height of the whole assembly is 309 mm and the displacement capacity is 5 mm to 20 mm. The surface of the wheel is made out of rubber to have appropriate friction between roller and the tube in order to avoid any damage to the tube.



Figure 2-7: The transition piece stabilizer system

Both lattice structure and the transition piece segments are fabricated using cold form process and only the tubular tower is manufactured using hot rolling process. The cold form process includes dies and punches. Figure 2-8(a) and (b) show the cold form rolling and press brake schematics.



Figure 2-8: Schematic of cold form processes

In real application dip-galvanized process would provide a thin layer of zinc as coating for the columns and braces. The zinc coating induced by dip galvanize process enhance the corrosive behaviour of the components in the environmental conditions. For the feasibility test simple painting was provided.

The lattice structure has a straightforward manufacturing process. The lattice's columns and braces are manufactured using press brake machines and bending of the plates then the bolts' holes are cut through the plates. The transition piece segments are fabricated using cold form rolling and short tip of each plate that is designed as a connection point to the gusset plate, is formed by press brake machines. Figure 2-9Figure 2-9(a) shows the post treating of the column section and the holes by an operator and Figure 2-9(b) shows the transition piece segments.



Figure 2-9: The manufactured column and post treating procedure

Figure 2-10 shows the braces of the scaled lattice structure. The hot-dip galvanized coating is clear which is due to stand during the environmental corrosive condition for the whole lifetime.



Figure 2-10: The braces of the scaled lattice structure

The tubular tower is manufactured by rolling procedure and the both edges are longitudinally welded. The tower is made from two separate segments and then they are welded horizontally. The tubular segment is supposed to be connected to a lower plate. The lower plate and the top plate, both have 90° bended tip. They are manufactured in four arcs and welded together. However, the edges are designed to be bended, they bended sides are manufactured separately and welded to the each corresponding arc. Figure 2-11 show the fabrication sketches for tubular segment and the top plate.

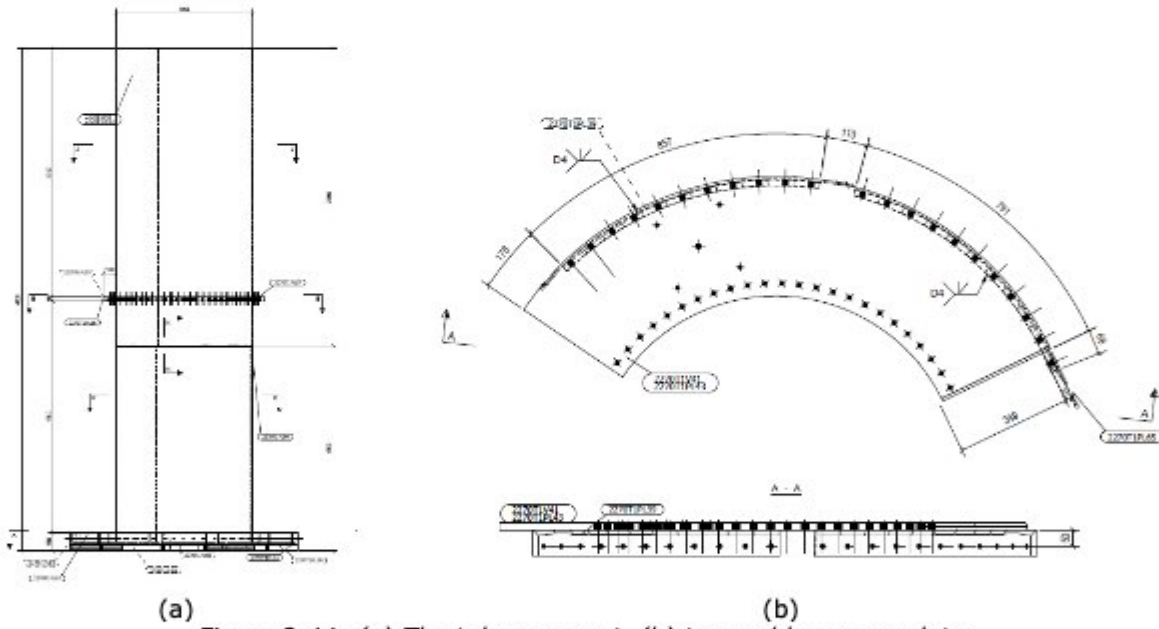


Figure 2-11: (a) The tube segment, (b) top and lower arc plates

The final lattice structure, transition piece and the tubular segment are painted to be waterproof and reduce the corrosion level. All components are assembled and located on site. The lattice structure is assembled first and the tube is located inside the lattice structure. Finally, the transition piece is lifted and mounted on the lattice structure.



(a)



(b)

Figure 2-12: the tower components assembled before on site

Figure 2-13 shows the final test arrangement on site with the stair access of the workers to the transition piece level which is supposed to be a temporary elevator in the real scale tower.



Figure 2-13: The assembled scaled prototype

2.3 Experimental tests on scale prototype

Task 2.3 and deliverables D2.2 and D2.3 include the tests on the scaled prototype and the following sub-tasks:

- The scaled prototype is assembled and the feasibility of the erection process is performed.
- The structural behaviour is monitored while performing static tests using centric and eccentric load.
- Numerical analyses are validated.
- Numerical calculations are performed to investigate the fatigue behaviour of the transition piece.

2.3.1 Overview of feasibility test

The feasibility test is performed on the 1/4 scaled transition piece including the last level of the lattice and the tubular tower. The scaling was done by defining a scale policy based on the similitude law of geometry dimensionless parameter which is explained in Deliverable D2.1. The transition piece includes three main components, the tubular tower segment with lower plate, upper plate and the cold form curve plates as a transition piece (TP) shell. The curve plates are connected to the lattice columns through the gusset plates. The upper plate is connected to the TP shell and it is a space to place the strand jacks for lifting.

The test executes three different scenarios, first is the lifting of the tubular tower as the initial stage. Initial stage aims to simulate the tubular tower initial lifting until the stage it arrives to the TP. Next, the lifting of the tubular tower continues after TP with an extra mass attached to the lever arm. The extra mass is supposed to change the centre of gravity (CoG) in the same way as the rotor nacelle assembly (RNA) will change. Therefore, the lifting and TP should resist a bending moment. The stabilizers are designed inside the TP to facilitate the lifting of the tube by avoiding swinging, guiding the tube through the TP, and also avoid collision between the TP shell and the tube after RNA mounting and induced moment by changes in CoG. The last scenario is lowering process of the tube which is done in between two liftings. The last scenario is trying to simulate unmounting and disassembling of the tubular tower. Figure 2-14 shows the procedure of the three scenarios.

The erection process is performed by the company Hebetec, supervised by RWTH. Therefore, Hebetec transported all the necessary equipment from Switzerland to Martifer, which includes:

- 4 HA-10 strand jacks, capacity 100 kN each incl. CP-10 and EV-1 (necessary for lowering process)
- 1 Hydraulic pumping unit with controls
- 4 strand bundles L-20m
- Electric-hydraulic installation.

Two supervisors performed the lifting, one to control the system from the ground and one, who will be present on the TP to control the strand jacks and the process. They provided the project team with the relevant information concerning their measured ways, loading velocity and oil pressures.

2.3.2 Measurements

Figure 2-15 and Figure 2-16 show the measurement points in the tubular tower and the transition piece during the erection process. The strain gauges (SG) locations are shown in Figure 2-15. There are strain gauges in two longitudinal levels and four circumferential locations. Red arrows with numbers show the longitudinal levels and four 'SG' signs show the circumferential locations. The longitudinal levels were assigned at top and middle of the tubular tower and under the pass in which the stabilizers' roller will pass. In order to be sure that all stress peaks are measured, four strain gauges were embedded in each location. It means 8 locations and 24 SGs on the tubular tower.

Moreover, the accelerometer and LVDT sensors are selected in order to measure the acceleration and the displacement of the tubular tower respectively. Figure 2-16 shows the location of the accelerometer, LVDT and external SGs on the transition piece.

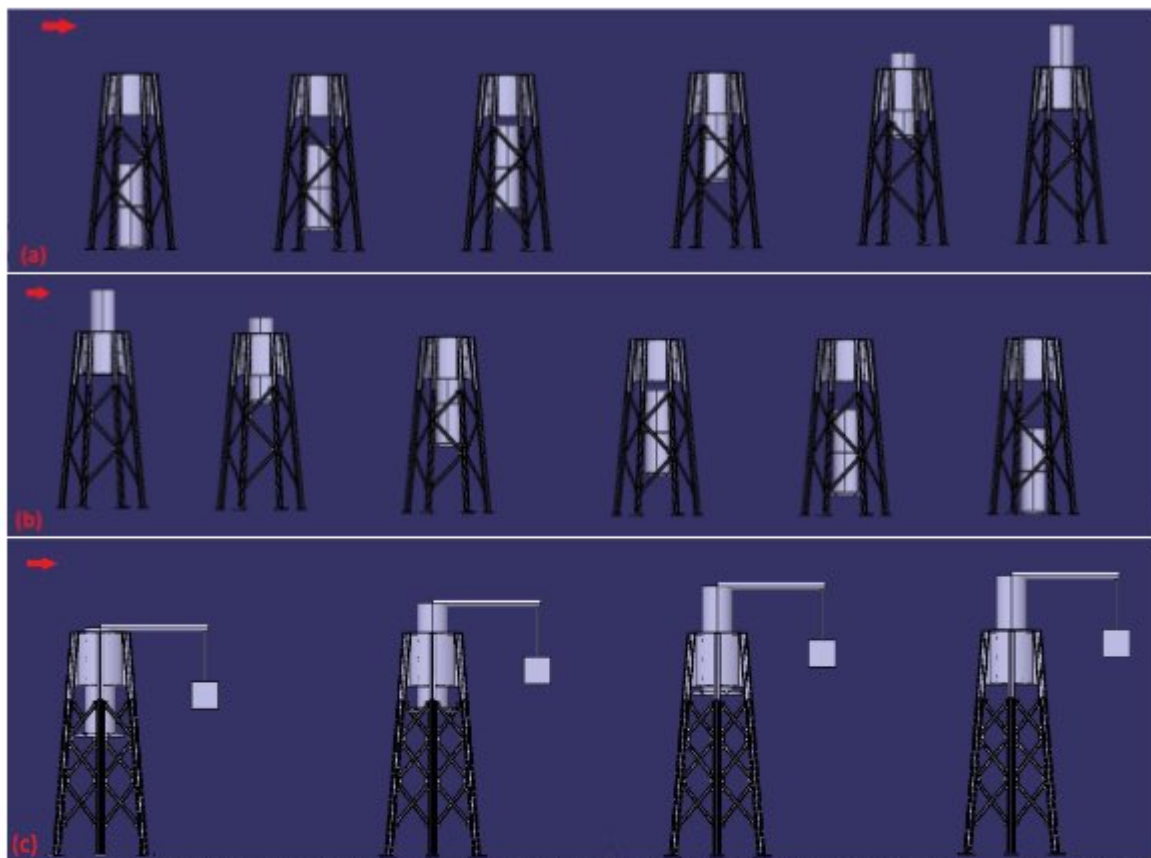


Figure 2-14: Three execution scenarios for the feasibility test, (a) simple lift up, (b) simple lift down and (c) lift up with an extra mass

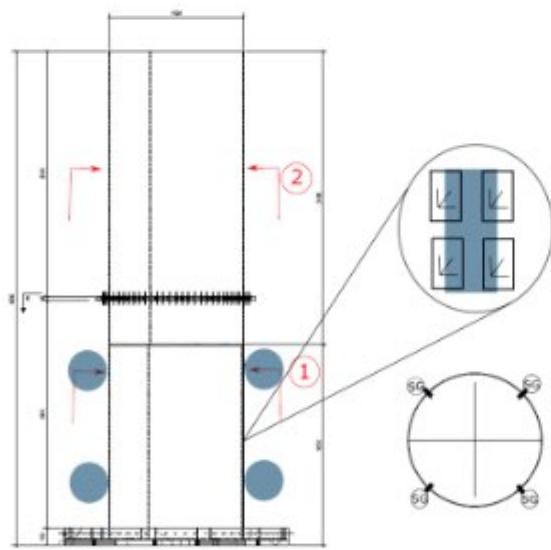


Figure 2-15: The locations for tubular tower strain gauges

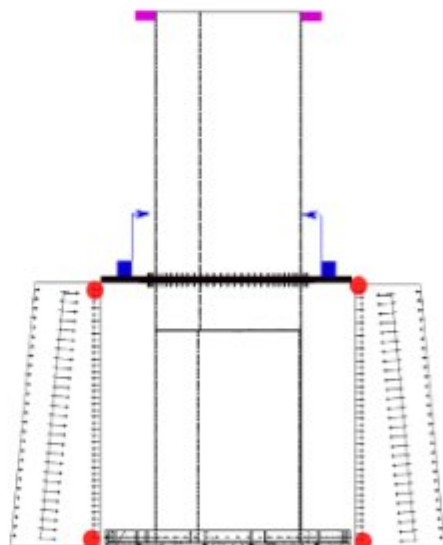


Figure 2-16: Accelerometers, LVDTs, and TP strain gauges

The purple is showing the accelerometer, the blue vectors are representative of LVDT to measure the possible displacement on the top of the transition piece and the red dots are external SGs to measure the strain on the top and bottom of the gusset plate. Only two gusset plates which are under maximum tension and compression during the 3rd feasibility scenario are instrumented.

In addition, the operators observe the strand jacks performance and the control the key parameters such as lifting speed and oil pressure to investigate and relate the erection load levels and possible faults.

The preparation of the instrumentation starts with removing the protection coating from the SG locations. Then, the four rosette SGs are fixed on the clean surface with the adhesive. In Figure 2-17 the smoothed surface and the installed SGs are illustrated.



Figure 2-17: (a) prepared surface for the SG, (b) implemented SG

The LVDTs are adjusted and mounted on the top plate to measure the prospective tilting.

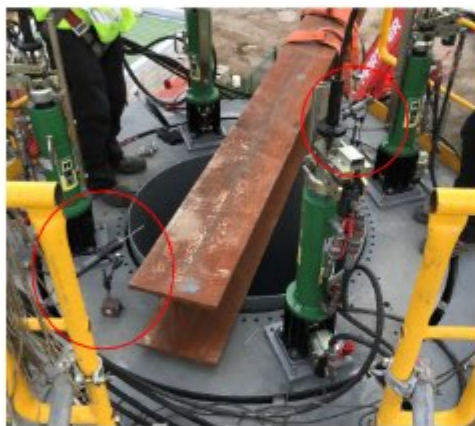


Figure 2-18: Adjusted LVDTs on the TP



Figure 2-19: HBM acquisition system

All strain gauges are soldered to the long wires to transmit the measured transient strain from the rolling of the stabilizers on the tubular segment.

The HBM data acquisition with a 32 channels switch transfer the data to a laptop. The TML strain gauges (SGs) and rosette are implemented on the prototype to capture the strains. Table 2-2 shows the properties of the strain gauge used in the experimental and Figure 2-19 shows the HBM acquisition system. The total number of required channels was 102 in which four HBM system were used.

Table 2-2: Strain gauge and rosette properties

Type	Gauge length	Gauge Resistance	Gauge Factor	Temp. Compensation for ($\times 10^{-6}/^{\circ}\text{C}$)	Transverse Sensitivity (%)
FRAB-6-11	6	120 ± 0.5	2.08 ± 1	11	0.1
FLA-3-11	3	120 ± 0.3	2.12 ± 1	11	0.3

2.3.3 Lifting Process

As it is explained in deliverables D1.2 and D2.1, the lifting procedure uses the lifting state of art using strandjacks. Four strandjacks with 10 tonnes capacity were mounted in the transition piece and the slings go through the transition piece to the bottom of the tubular tower. The controlling system and the oil pump are in the ground level and the pump sends the oil to the jacks and controller

controls the oil pressure to assure the lifting strock. Figure 2-20(a) shows the strandjacks used in the lifting process.



Figure 2-20: (a) The strandjacks arrangement, (b) attachment of slings to the bottom of the tubular segment

As this lifting process has only four strand jacks, the operator performed manual controlling of the jack systems. The controllers consist of the pressure controller and the stroke velocity.



Figure 2-21: (a) Controller unit, (b) hydraulic pump and monitoring system

While the transition piece is still on the ground, the stabilizers were attached to the shell from inside. The stabilizers are pair of the heavy-duty wheel and the elastomer mount. The elastomer is bolted to the profile that is welded to the transition piece shell. It can be seen in Figure 2-22. The location of the wheels are aligned with the rosette strain gauges on the transition piece.



Figure 2-22: The installed stabilizers on the transition piece

2.3.4 Results of testing scale prototype

The three scenarios were performed in two consecutive days. The jacks' installation and measurement initiation were done in the morning of the first day and the first scenario (simple lifting up) was performed in the afternoon. The 2nd and 3rd scenarios were performed in the second day.

Figure 2-23 shows the 1st scenario of the erection. The erection lifts the tubular tower from the ground. The erection had the maximum stroke of the jacks until the tubular tower approached the transition piece. In order to enter the transition piece and rolls on the wheels and increase the accuracy, the stroke speed slowed down. Afterwards, the erection speed was increased, and the lifting continued until the final position.

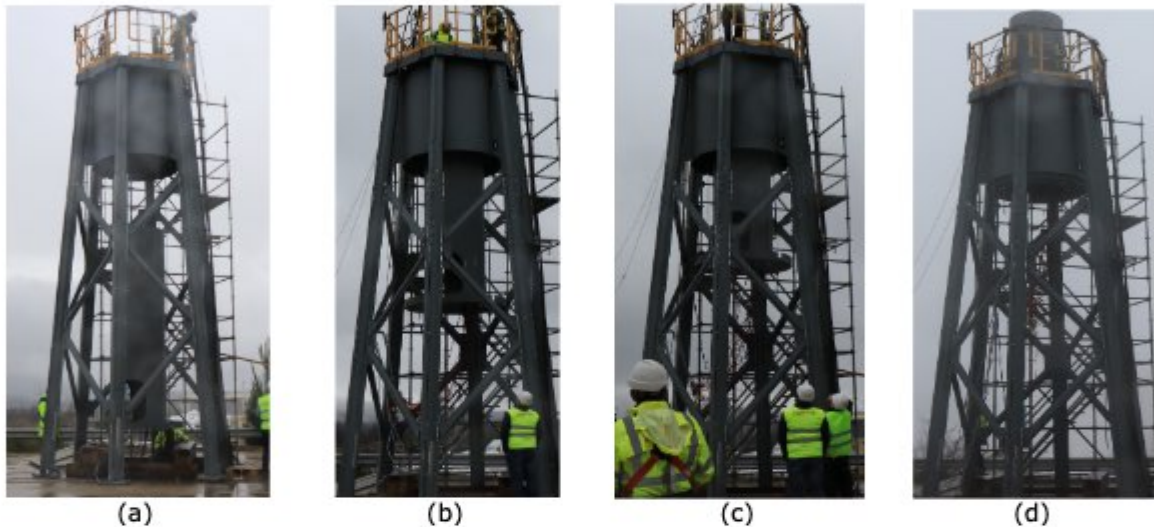


Figure 2-23: 1st scenario execution of lifting up

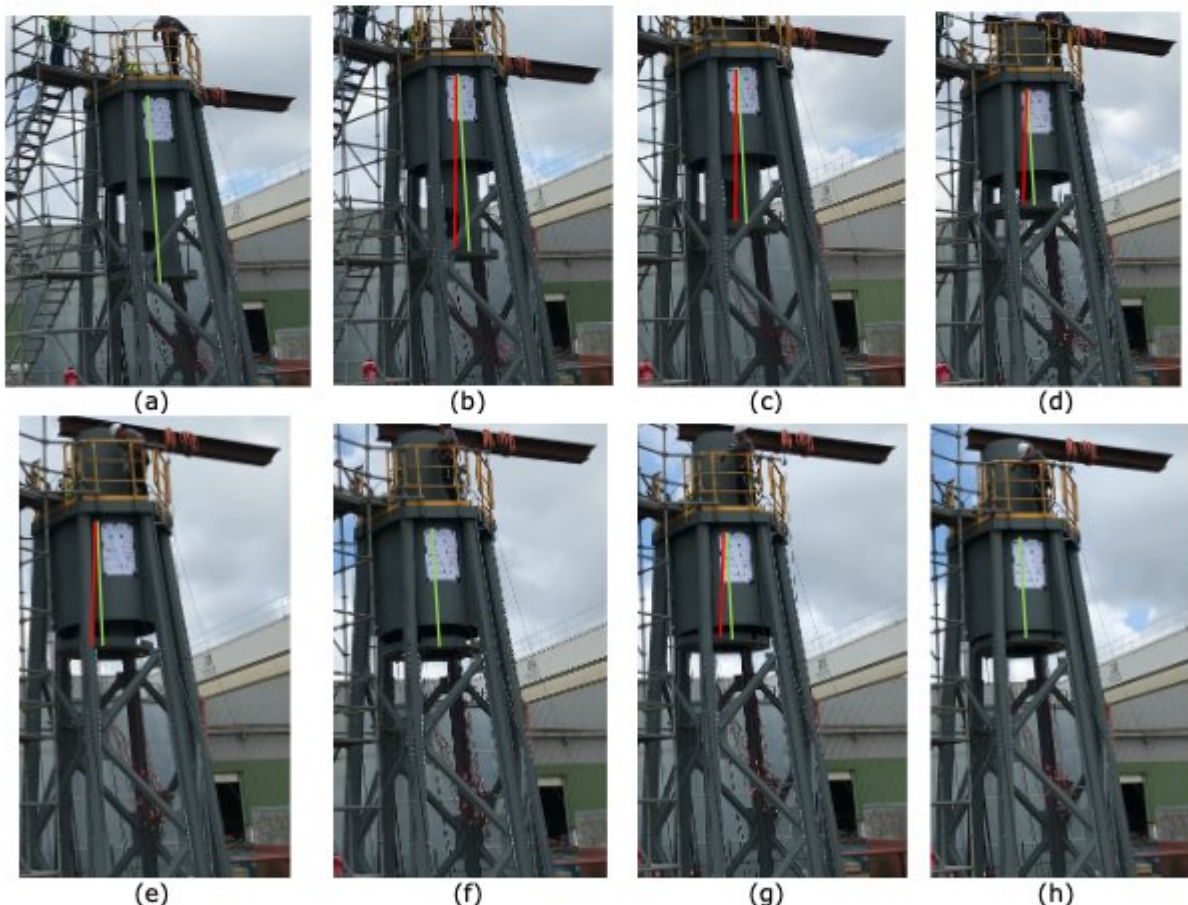


Figure 2-24: 3rd scenario execution of lifting up

The 2nd scenario was the reverse process of the lifting up and it was simply performed with no difficulties. Despite of the initial planning, the 3rd scenario (Figure 2-24) was done using two different load level. The reason was to make sure that the stabilizers could withstand the transient lateral load. Therefore, two different light (750 kg) and heavy (2000 kg) weight were mounted on top of the tubular tower with using 4 m lever arm. Several stops and tilt angle correction happened due to the extra weight on top and difficulties in controlling of the oil pressure in strand jacks simultaneously. The green line in the pictures shows the straight reference angle and red line shows the tilt angle to the reference line.

The last situation of the erection was simulated in ABAQUS software considering the appropriate loading and boundary conditions. The results show a considerable agreement with measured strain signals and the top displacement. Figure 2-25(a) shows calculated stress from the strain signal and Figure 2-25(b) shows the finite element simulation. The green signs show the reduction of the stress level due to the tilt angle correction. Moreover, the stress at the end of the measure signal that is the last stage of the erection process has almost same value as FE results.

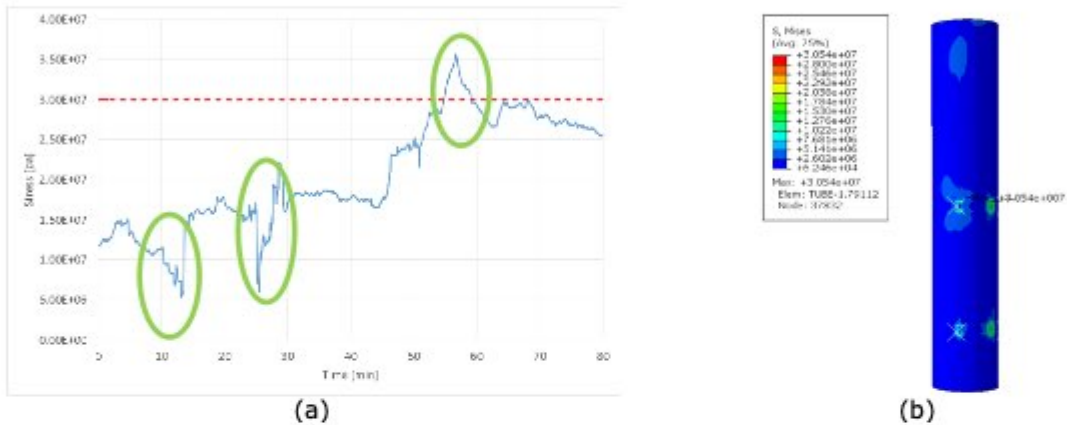


Figure 2-25: The comparison of measures stress and the finit element simulation

Moreover, Figure 2-26 shows the measured top displacement with LVDTs and top displacement from FE model. The top displacement signal also shows drop in the measurement as the tilt angle correction is performed. As it is calculated in D1.2, the nacelle assembly cause up to 2° changes in the center of gravity of the tubular tower. The tilt angle of 2.1° by the measurement and 1.5° in FE model happened which shows the similarity of the scale prototype and real scale procedures.

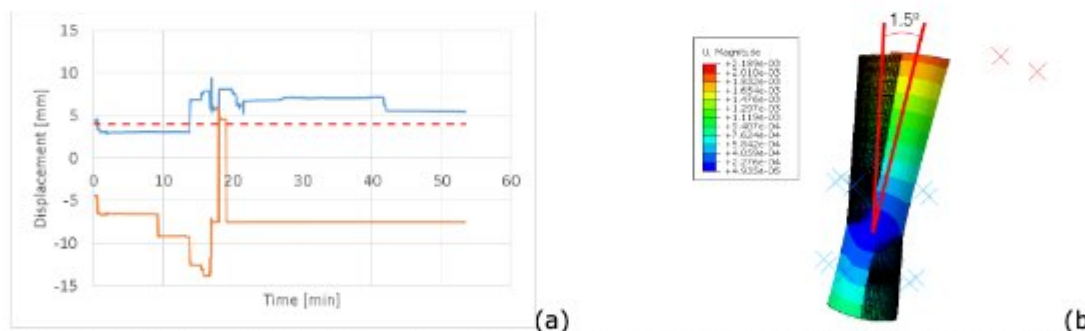


Figure 2-26: The comparison of measures top displacement and the finit element simulation



Figure 2-27: (a) tilt angle during erection with heavier burden, (b) stabilizer dislocation

The next test was increasing the top weight to 2000 kg and repeating the same process. A concrete block added to the beam. However, the moment and lateral movement of the tubular tower caused extreme load on the strand jacks and stabilizers. The elastomer form changed due to the high load. However, they did not fail and returned to the initial form after tilt angle correction with the strand jacks. The strand jacks need longer lever arm to apply the tension in order to compensate the exerted moment. Figure 2-27 shows the erection with the concrete block. The tilt angle of tubular tower and the dislocation of the stabilizer is obvious.

2.3.5 Fatigue assessment of the transition segment

The assessment of fatigue behaviour of the wind tower needs time histories of the cyclic loads at the transition piece. The 185-meters tall tower without secondary bracing equipped with the Concept 2 for the transition piece analysed in WP1 is investigated here. The forces and moments used in the analysis and given in Deliverable D2.3 are based on 600 seconds simulation of load spectra for different wind speeds performed in Task 1.1. Those are the basis for the fatigue assessment with FE-analysis using ABAQUS software to compute the stress distribution and FE-safe software to assess damage accumulation for the minimum service life of 25 years. For the calculation the forces F_x , F_y , F_z and the moments M_x , M_y , M_z are used. Decisive for the case study is the combination of moments M_x and M_y and shear forces F_x and F_y at TP level.

The fatigue assessment is performed with numerical calculations for the bolted transition piece as worked out in task 1.2. Additionally, an alternative welded solution for the same study case is also investigated. Figure 2-28 shows the two models of the transition pieces.

The fatigue behaviour of the S355 mild steel was based on experimental results from fatigue tests of smooth specimens and fatigue crack propagation tests. The fatigue tests of smooth specimens were carried out according to the ASTME606 standard under strain-controlled conditions. However, for S690 no experimental data are available. Therefore, an estimation of the cyclic and fatigue behaviour of a material was obtained from bibliography [2], [53]. The material properties used for materials in this study are summarized in Table 2-3 which gives the elastic (E : Young modulus) and monotonic strength properties (f_u : yield strength; f_u : tensile strength) as well as the cyclic elastoplastic constants (k' : cyclic strain hardening coefficient; n' : cyclic strain hardening exponent) and the strain-life and Morrow's constants (σ_f' , ε_f' , b , c). Bolts are preloaded class 10.9.

Table 2-3: Material parameters used in the FE-safe model

Steel grade	E (GPa)	f_u (MPa)	f_y (MPa)	k' (MPa)	N'	σ_f'	b	ε_f'	c
S355	211.6	745	422	595.85	0.0757	952.2	-0.089	0.7371	-0.664
(S690)	211.6	1000	770	1650	0.164	1396	-0.09	0.392	-0.56



Figure 2-28: Model of the bolted (a) and welded (b) transition segment

Due to the large number of load cycles, the WT is exposed to a multiaxial stress condition and to verify the transition piece a multiaxial-based fatigue approach is appropriate for the accurate life estimation. In this study, a multiaxial fatigue-based software package Fe-Safe [27] is used for fatigue life estimation of the transition piece. The methodology depicted in Figure 2-29: Overview of the procedure and results of the fatigue analysis for analysis can be divided in two parts: the determination of stresses under characteristic fatigue loading and determination of damage, number of cycles sustained, and total life using Fe-Safe tool. In the first step, highest loads and moments are determined from the load histories coming from aero-elastic simulation for different wind speeds and then these loads are applied on FEM to calculate the stresses on each element of the structure.

The stress data sets calculated on each element of the structure using any FEM software is imported into the Fe-Safe, loading is applied on respective stress data set, and material properties are assigned to different groups of structure to be analysed. Algorithm should be indicated for the analysis; usually for multiaxial fatigue analysis, Brown–Miller with Morrow mean stress correction and normal strain with Smith–Watson–Topper mean stress correction are used.

In this study both methods are used for the comparison perspective. The fatigue life for each node is calculated as follows:

1. The stress tensors are multiplied by the time history of the applied loading, to produce a time history of each of the six components stress tensor;
2. The time histories of the in-plane principal stresses are calculated;
3. The time histories of the three principal strains are calculated from the stresses;
4. A multiaxial cyclic plasticity model is used to convert the elastic stress-strain histories into elastic-plastic stress- strain histories;
5. A “critical plane” method is used to identify the most damaging plane by calculating the damage on planes at 10° intervals between 0° and 180° in the surface of the component;
6. For each of the critical planes, strains are resolved onto the three shear planes (1-2, 2-3, and 1-3);
7. The time history of the damage parameter (which in this case, using the Brown–Miller algorithm, is the shear and normal strain) is cycle counted;
8. Individual fatigue cycles are identified using a “Rain-flow” cycle algorithm, the fatigue damage for each cycle is calculated, and the total damage is summed;
9. The plane with the shortest life defines the plane of crack initiation, and this life is written to the output file.

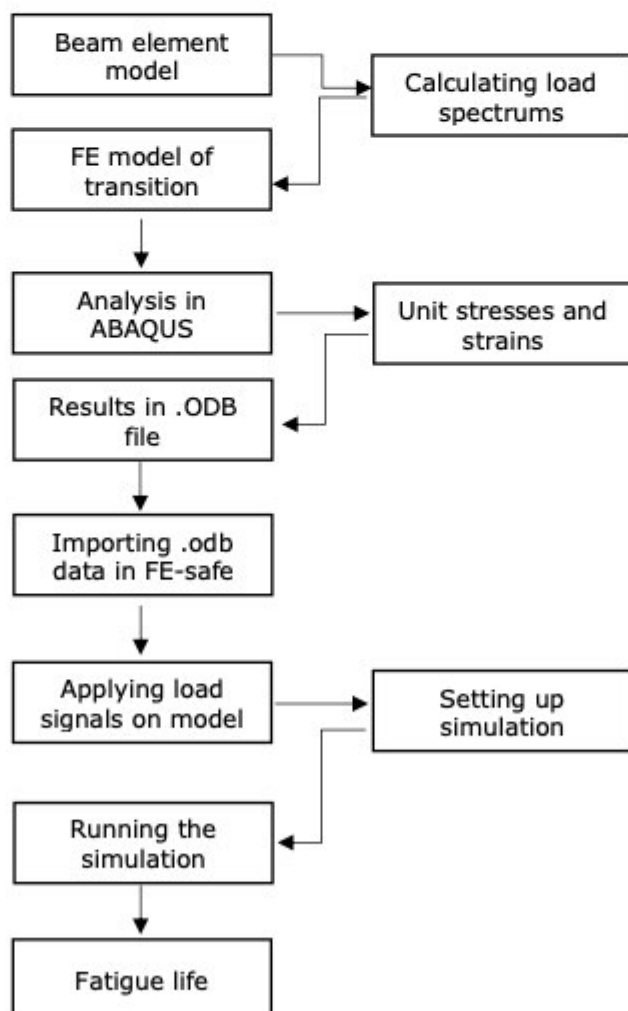


Figure 2-29: Overview of the procedure and results of the fatigue analysis

2.3.5.1 Bolted TP

Figure 2-30 (a) shows the details of the connection between tubular part and transition segment. For the flange there are two rows of bolts and for the L-flange it is necessary to put an additional row on the round plate. For the steel column it is designed to put one row of bolts in the outer area of the bolts, one row of bolts close to the tower and one row of bolts inside. Shown in the Figures is the model from ABAQUS that is used to further inspect the transition piece under cyclic loading cases using FE-Safe. It should be noted that to reduce modelling and calculation time only a segment of the transition piece was analysed as shown Figure 2-30(a), which also shows the most critical detail for stress concentration, that is the connection between the vertical tower 'legs' to the outer plate of the connection segment.

Figure 2-30(b) shows the FE mesh of the transition segment which is exclusively constituted by tri-dimensional solid elements. The element type of C3D8R was adopted, due to the high dimension of the model. In order to model accurately the transition segment, there was an effort to replicate the boundary conditions on the real structure by adding one extra level of the lattice part of wind turbine, on the model. Therefore, at the bottom end of the column a reference point (RP) was made for each support. Furthermore, coupling constraint was created in order to have a control point of that region. The surface-based coupling constraint in ABAQUS [4] provides coupling between a reference node and a group of nodes. So, all translations and rotations were restrained on the reference point. This procedure can be seen Figure 2-30(b) for the supports.

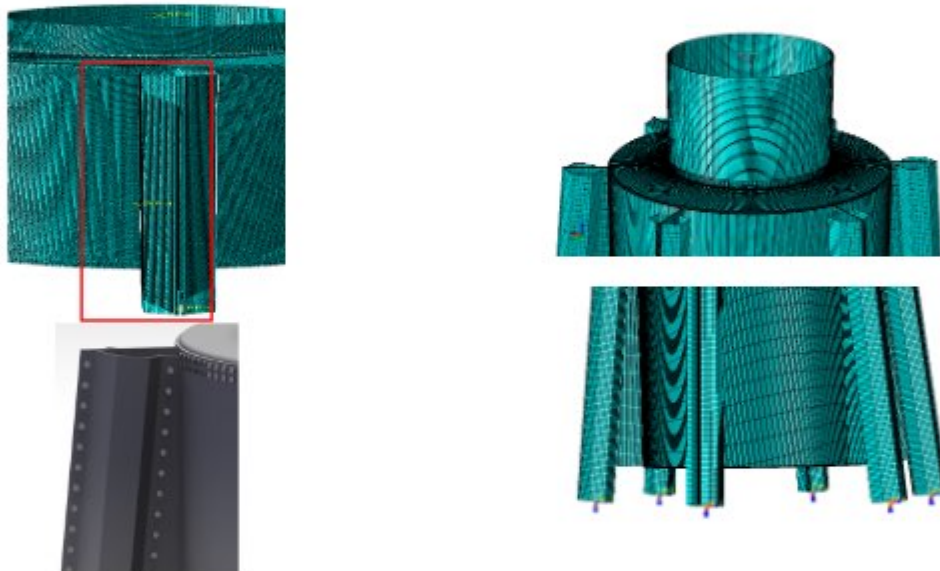


Figure 2-30: Detail for fatigue analysis (a) and FE mesh in ABAQUS

A mesh convergence study was undertaken to obtain a balance between refinement and precision in stress calculation. The results are shown in Figure 2-31. Given the results of the model analysis using ABAQUS, nodal stresses and strains were calculated and could be further used to conduct a Finite-Element analysis for fatigue calculations in FE-Safe.

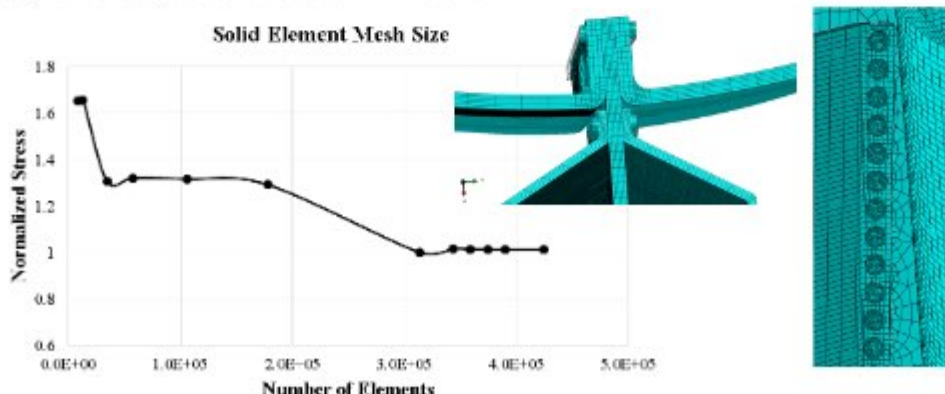


Figure 2-31: Mesh convergence study

Figure 2-32 (a) shows the results of the analysis with Fe-Safe and represents the maximum stress of the transition piece where the dark blue shows the compression and red areas show tension. An overview of the damage results is shown in Figure 2-32(b) for the outer perspective of the transition piece. Blue elements are in general not very highly loaded and grey elements show areas where higher stress is applied.

Fe-Safe gives a result-output for the overall damage analysis of the whole transition piece. The highest values for stress are at point 260 which is at the higher bolt close to the shell. From the computation it could be concluded that the fatigue life was much longer than the required service life of 25 years. Furthermore, the results of the whole calculation could be compared with the Multi-Channel Peak-Valley of the load with the same result.

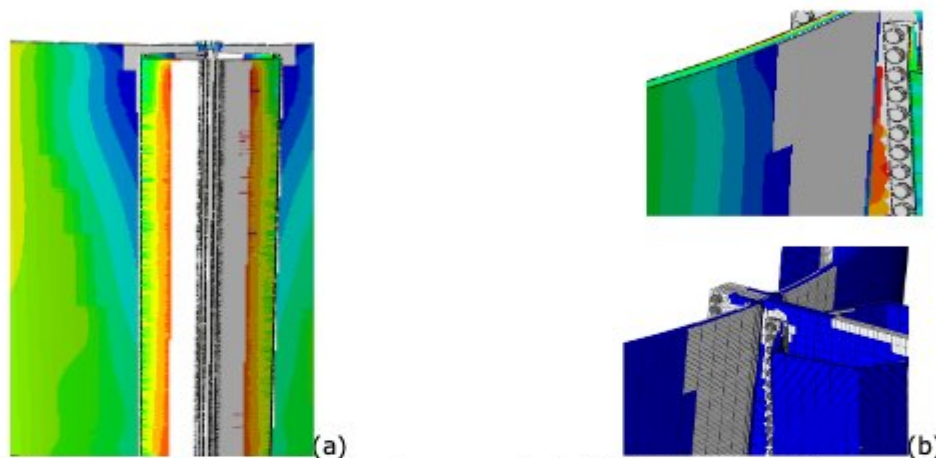


Figure 2-32: Overview of the maximum stress results (a) Detailed view of damage results in the upper part of the transition piece (b)

2.3.5.2 Welded TP

The welded transition piece is shown in Figure 2-33. Two different case studies based on different steel grade S355 and high-strength steel S690 were compared. Figure 2-33(b) shows the welded connection detail of the transition piece. The mesh density of the welded area is much higher to be able to capture the stress hot spot in the welded area.

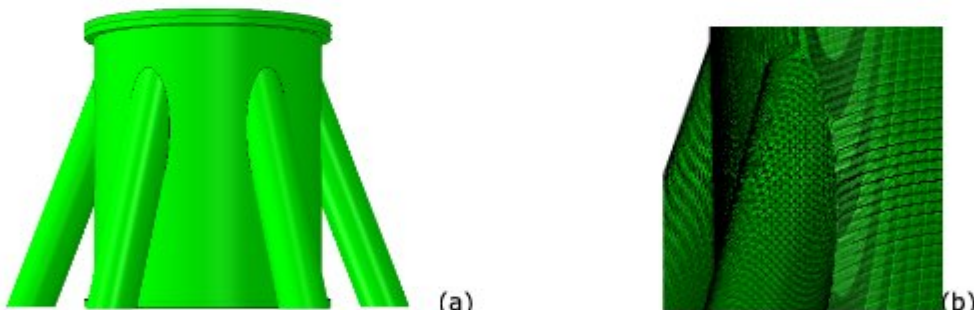


Figure 2-33: Welded transition piece (a) weld connection detail (b)

Table 2-4: Summary for fatigue life of welded transition piece using load history

Brown Miller with Morrow mean stress correction		
	Transition piece using S355	Transition piece using S690
life in years	>25	>25
Large SMAX (+ or -)	407 MPa	737 MPa
Largest damage	0	0
Normal strain with SWT correction		
	Transition piece using S355	Transition piece using S690
life in years	>25	15
Large SMAX (+ or -)	407 MPa	737 MPa
Largest damage	1.887E-6	3.541E-5

The case studies provided preliminary dimensions which are validated in the design procedure by FEM. Figure 2-34 shows the transition piece shell and the chord stress distribution using GMNA analysis for S355 steel grade. The transition piece height and thickness of 6 m and 45 mm, respectively, are suitable for the first option obtained after four design iterations. The case study that uses S690 the analysis the height is 5-m height and 35-mm thickness. Moreover, the chord dimensions were 1000 mm the diameter of and the thickness of 35 mm. As it is shown in the FEM results, the stress hot spots are located in the shell, above the welding spots and on the welding connection. Table 2-4 summarizes the results for both case studies

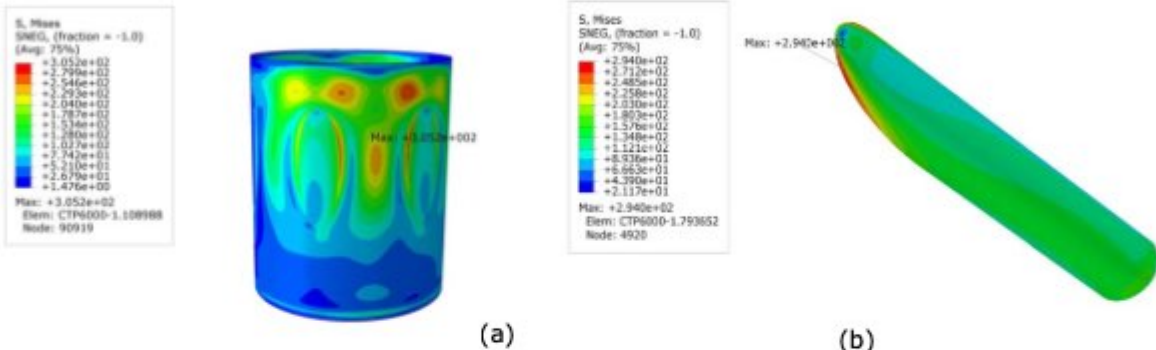


Figure 2-34: Transition piece shell and the chord stress distribution (a) shell, (b) chord

2.4 Risk assessment and analysis of construction procedure

The main novelties in the hybrid structure is the transition piece component, which concept has been developed and presents new subcomponents to facilitate the erection process. All design details are discussed in deliverables 1.2 and 1.3 and the erection mechanism is explained in deliverable 2.1. The construction and testing of the prototype has been the main concern of the involved partners concerning the assessment and control of the Technological, Manufacturing and Site Construction risks. The partner in charge of manufacturing and building the prototype has a long experience of steel manufacturing and construction and possess the staff with appropriate skills to prevent and mitigate the possible risks involved in the production assembling and testing of the prototype.

In the context of the project, the supporting structure is in its conceptual design phase. However, construction of the real scale structure with self-erection incorporated in the transition piece represents a challenge that could be only faced if a real scale prototype was built. This represents a scenario where manufacturing has entered full scale production, which does not reflect the current state of high-rise hybrid wind towers. Hence it is important to acknowledge that risk assessment of real structure would be beyond the mere up-scaling of the risks assessed during the present study.

2.5 Conclusions

The main issue within WP2 is the finding of a suitable and feasible erection process, which can be used in the hybrid tower concept. A state-of-the-art solution was found in collaboration with all partners and additional industrial experts.

The feasibility test is performed on the 1/4 scaled transition piece including the last level of the lattice and the tubular tower. The scaling was done by defining a scale policy based on the similitude law of geometry dimensionless parameter. The scale prototype design, fabrication and erection were performed, and the feasibility of scale prototype was validated. All design to execution stages considered EN 1090-2 requirements. Moreover, partners used BIM method to organize the design, fabrication and execution planning and reduce the misunderstanding and errors.

The design of the scale prototype was the most straightforward stage. Although the fabrication and lifting execution were successful, partners obtained valuable lessons. Cold form is a potential new line of business. Dedicated plant for truss legs in a process of continuous roll forming can help maturation of the market. Moreover, new machines and technologies have to appear, an evolution of the purlin fabrication to be used for thick plates. In this scale prototype, the thickness of the transition piece was 20 mm and it was difficult to keep the precision and even perform the bending on the plate. Therefore, it will be more difficult in real scale components with thickness up to 80 mm. In consequence, cold form process could not provide full accuracy for the transition piece components, which was the most complex component. Especially, the parts with consecutive rolling and bending presented lower precision. Rolling direction versus bend direction is important otherwise, it cannot meet the tolerances. Accurate methodology and control system help cold bend parts with better geometrical precision. The low precision of cold form parts causes some problems in assembly, which are problematic in the erection process. Another concern was the number and behavior of the stabilizers used to restrict the tilt angle, which was taken to the limit during the 3rd scenario conceived for the erection process feasibility test.

The several difficulties faced during assembling, mainly in the transition piece, were overcome and the erection process was successfully validated. Two main indicators were considered. First is the general behaviour, response of the lifting equipment and the feasibility of the tubular tower movement through the transition piece. The second indicator was the stresses caused by the transient forces on the stabilizers during execution.

3 Bolt material testing and selection for onshore and near-shore application

This WP dealt with the manufacturing and the complete characterization (including fatigue tests) of the steels to be used in the bolts. Two steel grades, 32CrB4 EQ and 30MnNiB4 EQ in which a new manufacturing process was applied, were chosen to evaluate the improvements they can bring.

After a complete characterization, it was seen that all the requirements established by the standard ISO 898-1:2015 were easily fulfilled. Furthermore, the grade 30MnNiB4 EQ exhibited a very high toughness at low temperatures.

Once the corresponding fatigue tests were carried out, it was observed that the fatigue limit of the conventional 32CrB4 was improved in a 13% in the case of the 32CrB4 EQ and in a 7% in the case of the 30MnNiB4 EQ. This fatigue improvement would diminish the bolt risk of failure, leading thus to a safer wind tower operation.

In order to check if this improvement of the fatigue performance could be also applicable to the whole connection, some fatigue tests were performed on double shear pre-stressed connections.

3.1 Selection and manufacturing of steels for bolts

This Task dealt with the selection and manufacturing of the steels for the bolts that were used in the connections.

3.1.1 Selection of the steels

In order to optimize the wind turbine performance, wind farms are built in the most windy regions of the World, which usually coincide with extreme weather areas (where besides the hard winds, very low temperatures and/or corrosive environments, as in the case of off-shore wind farms, are common).

That exposure to extreme weather conditions and the difficult accessibility to the places where wind towers are located increase the maintenance costs. The main way to reduce these costs is minimizing the number of interventions. In the case of wind fasteners, the three main causes of maintenance needs are: the low temperatures, the fatigue failures and the exposure to corrosive environments:

- Low temperatures: Low temperatures make the steel more brittle increasing the risk of failure caused by an impact. The standard ISO 898-1 establishes all the requirements that the steels used in wind tower fasteners and foundations must fulfill in order to assure its correct operation at low temperature. The most common steel class used in these applications is class 10.9.
- Fatigue failures: Fatigue damage is defined as a progressive damage that appears when the material is subjected to cyclic loads. The stress values that cause such damage are much lower than the material UTS or YS.
- The fatigue performance is not mentioned in the standard ISO 898-1. So, given that wind fasteners are subjected to cyclic loads, a fatigue failure could take place even having reached all the requirements established in the standard. The fatigue failure of the wind fasteners could lead to the collapse of the whole wind tower. An improvement of the steel fatigue performance would directly lead to a safer tower operation.
- Exposure to corrosive environments: The exposure of the fasteners to corrosive environments drastically decreases their in-service life.

The actual trend of building wind turbines of bigger and bigger power (> 5 MW) leads to a considerable increase of the tower dimensions. Subsequently, to ensure the correct fastening of the different parts of the tower, the fasteners diameter must be also increased. This dimensional increase makes even more difficult the attainment of the required mechanical properties.

Nowadays, to reach the previously mentioned mechanical properties with small fasteners ($\varnothing < 36$ mm) low alloyed steels (i.e. 32CrB4 or 33MnCrB6) are used. However, if bigger fasteners ($\varnothing > 36$ mm) want to be manufactured, the use of high alloyed steel grades (i.e. 30CrNiMo8) is needed in order to assure the required mechanical properties, mainly the combination of high strength and very high toughness at low temperatures. The main drawback of these alloyed grades is the high price of alloying elements (i.e. Ni, Mo...).

In this project, two steel grades manufactured with the EXTREME technology were considered. This technology recently developed by Sideror, thanks to the optimization of the steel manufacturing process, allows:

1. A maximization of the steel mechanical properties and fatigue performance.
2. To fulfill all the requirements established in the standard using low-alloyed steels in large diameter bars.

Although in this project fasteners smaller than $\varnothing < 36$ mm are expected to be used, the potential fatigue improvement achieved by the EXTREME technology would lead to a safer in-service performance of the connections exposed to very adverse climatological conditions.

The specific steel grades chosen to carry this project out were:

- 32CrB4 EQ: Given that the 32CrB4 is the most common grade used in the bolts manufacturing, the use of 32CrB4 EQ will make easier the determination of the improvements achieved with this new manufacturing technology.
- 30MnNiB4 EQ: The 30MnNiB4 is a new steel grade developed by Sidenor. It was expected that the toughness at low temperatures is improved with regards to the 32CrB4.

3.1.2 Steels manufacturing and supplying

In this project, the steel manufacturing process was divided in two parts: in the first one the steel bars were manufactured in as-rolled condition at Sidenor and, in the second one, the heat treatment was carried out on them at Friedberg.

- Manufacturing of the rolled bars: This manufacturing route (Figure 3-1) consists in the melting of scrap in the electric arc furnace (EAF), a secondary metallurgy process (performed in the ladle furnace) to improve the steel cleanliness, a continuous casting of the melted steel into billets and a hot rolling of these billets into round bars ($\varnothing 30$ mm).

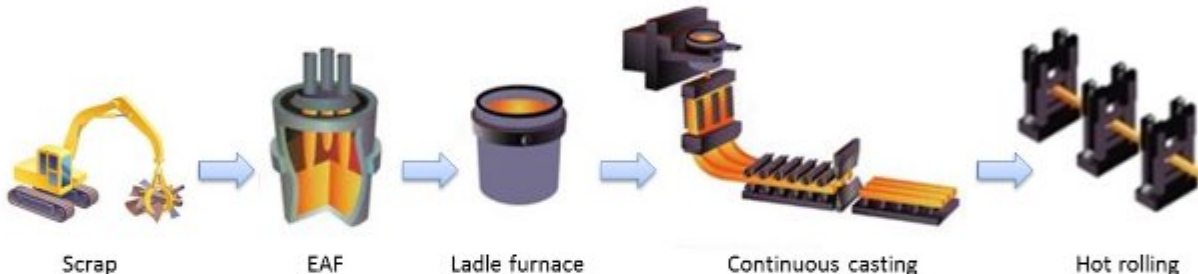


Figure 3-1. Steel manufacturing process at Sidenor.

The EXTREME technology is focused on the secondary metallurgy (the stirring and the vacuum levels are optimized), on the continuous casting (the electromagnetic stirring and the continuous casting speed are optimized in order to obtain the highest homogeneity level) and on the chemical composition (S and P are controlled to improve the steel toughness).

- Steel heat treatment: The heat treatment performed at Friedberg to obtain the required properties on the rolled bars in a quench and tempering (Q&T). The heat treatment cycles applied to each of the manufactured steels are shown in Figure 3-2.

After the heat treatment, the material needed to carry out the metallurgical characterization and the fatigue tests was sent to the corresponding partners. The remaining material was used to manufacture the bolts needed in the prototype construction (Task 2.2) and for the fatigue tests on connections (Task 3.4).

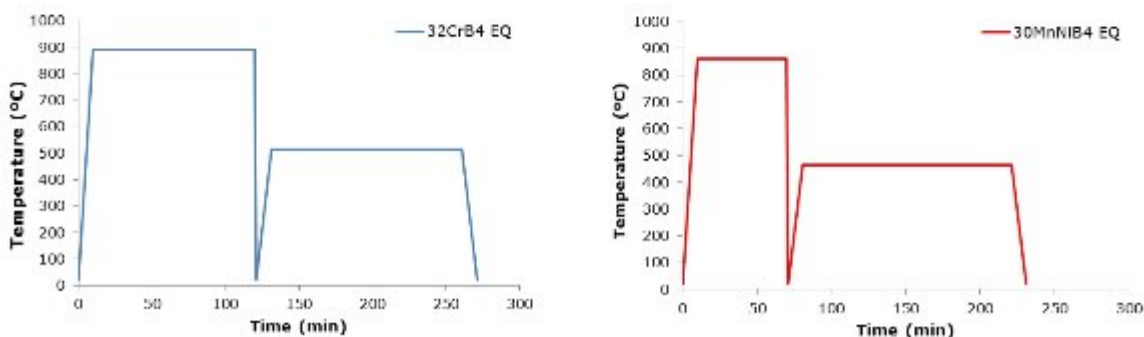


Figure 3-2: Heat treatment cycle applied to the 32CrB4 EQ (left) and 30MnNiB4 EQ (right).

3.2 Metallurgical and mechanical characterization of the chosen steels

This Task 3.2 dealt with the determination of the main metallurgical and mechanical properties of the manufactured steels. The required properties for the steels used in the bolts manufacturing are established by the standard ISO 898-1:2015. So, the obtained results were used to check if all those requirements (Table 3-1) established for the class 10.9 (the most usual one for wind fasteners) were reached.

Table 3-1. Requirements for the class 10.9 established by ISO 898-1:2015.

Min. UTS (MPa)	1.040
Min. YS _{0,2%} (MPa)	940
Min. El (%)	9
Min. RoA (%)	48
Min. KV at -40°C (J)	27
Hardness (HV)	332-394
Min. Martensite % at the bar core	90

3.2.1 Chemical and microstructural characterization

Chemical analysis: The chemical analysis was performed on the rolled bars to check if the chemical composition needed to achieve the required mechanical properties was reached. The bulk chemical composition was measured by OES. Complementary, C and S contents were also measured by LECO in order to assure the obtaining of accurate results.

The chemical composition of the manufactured steels (shown in Table 3-2) did not present any deviation with regards to the values commonly obtained for these grades.

Table 3-2. Chemical composition (all the elements in weight % except B, in ppm).

Steel	C	Mn	Si	P	S	Cr	Ni	Mo	Cu	Al	Ti	B
32CrB4 EQ	0,33	0,83	0,23	0,012	0,008	1,09	0,07	0,04	0,06	0,025	0,038	30
30MnNiB4 EQ	0,29	1,43	0,23	0,010	0,003	0,48	0,45	0,01	0,07	0,027	0,034	23

Microstructural assessment: Samples were obtained transversally to the rolling direction and, after nitral etching, the microstructures obtained in the heat treatment (quench and tempering) were evaluated using an optodigital microscope Olympus DSX-500. This equipment obtains very high definition micrographs allowing a very detailed microstructure evaluation.

The microstructure was examined in three points of the bar cross section: surface, mid-radius and core (Figure 3-3 and Figure 3-4) in order to identify potential microstructural heterogeneities or segregations.

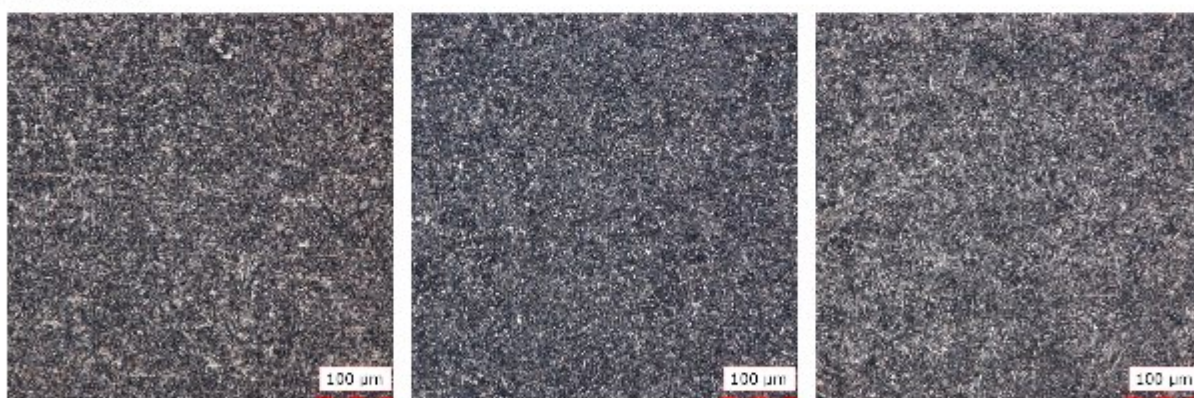


Figure 3-3: 32CrB4 EQ microstructure at 500X: Surface (left), Mid-radius (middle) and Core (right).

The microstructure obtained after the heat treatment in the 32CrB4 EQ is very homogeneous in all the cross section of the bar. Along the whole section, the microstructure is almost 100% tempered martensite, only some bainite traces are present (Figure 3-3). Anyway, the percentage of martensite at the bar core is clearly higher than the 90% required by the standard ISO 898-1:2015.



Figure 3-4: 30MnNiB4 EQ microstructure at 500X: Surface (left), Mid-radius (middle) and Core (right).

As in the case of the 32CrB4 EQ, the microstructure obtained for the 30MnNiB4 EQ is quite homogeneous along the whole cross section of the bar. Almost the 100% of the microstructure is tempered bainite, as for the 32CrB4 EQ, some bainite traces appeared (Figure 3-4). In any case, the percentage of tempered martensite at the core of the bar is clearly higher than the one required by the standard ISO 898-1:2015.

3.2.2 Hardness evaluation

A hardness profile for each of the manufactured steels was generated. The hardness measurements were carried out on the cross section of the bar (one Vickers measurement each mm from the surface to the bar core applying a load of 30 kg, with three repetitions for each measurement). The profile created with the average hardness values is shown in Figure 3-5.

As it can be shown, all the hardness values obtained across the bar section are inside the range established by the standard for the steel class 10.9.

Although the obtained values for both grades were in the hardness range accepted by the ISO 898-1:2015, the hardness of the 32CrB4 EQ was higher than the 30MnNiB4 EQ. As it will be shown in the corresponding section, this fact is related to the higher toughness of the 30MnNiB4 EQ.

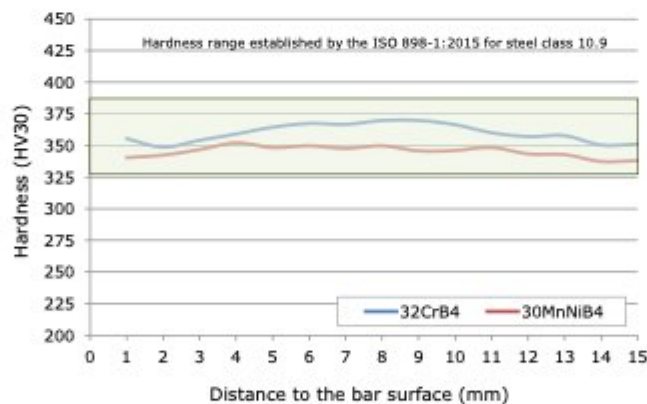


Figure 3-5: Hardness profile of the 32CrB4 EQ and 30MnNiB4 EQ steels.

3.2.3 Tensile test

Tensile tests were carried out in a hydraulic machine following the indications established in the standard ISO 6892-1:2009. All the tests were performed at room temperature. The cylindrical tensile specimens were machined at mid-radius of the bar. For each steel, three test repetitions were performed.

Conventional tensile tests: The tensile tests were performed with the test parameters commonly used at Sideror. The test was performed with two different control modes depending on the tensile curve zone:

- Control mode: STRAIN. The first part of the test was carried out at a constant strain rate of $5 \cdot 10^{-4} \text{ s}^{-1}$. This control mode was kept up to reaching a strain of 1%, when the $\text{YS}_{0,2\%}$ was already reached.
- Control mode: DISPLACEMENT. Once the 1% strain was reached, the control mode changed to displacement. Up to the specimen fracture, the displacement rate (5 mm/min) was kept constant.

As it is shown in Table 3-3 and Figure 3-6, for both steels the requirements specified in the ISO 898-1:2015 standard for tensile test (minimum values are represented by dot line in Figure 3-6) were easily reached.

Table 3-3. Results of the tensile tests performed with the conventional parameters.

Property	32CrB4 EQ		30MnNiB4 EQ	
	Average	Std deviation	Average	Std deviation
UTS (MPa)	1115	22	1072	16
$\text{YS}_{0,2\%}$ (MPa)	1066	14	1023	10
EI (%)	14,4	2,1	16,2	0,8
RoA (%)	66,1	1,0	66,1	1,0

Comparing both grades, the obtained values of the UTS and the YS of the 32CrB4 EQ were higher than the ones obtained for the 30MnNiB4 EQ. This trend is coherent with the results obtained in the hardness measurements and as it is previously mentioned, it is expected to be related with the better toughness values obtained with the 30MnNiB4 EQ.

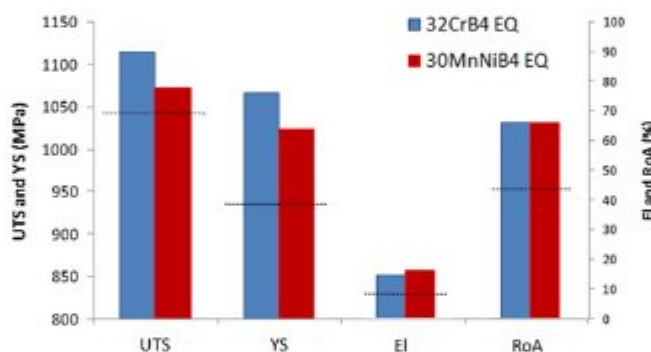


Figure 3-6. Average results of the tensile tests performed with the conventional parameters.

Tensile tests performed at constant strain rate: Some extra tensile tests were performed in order to obtain the information required in Task 4.4. In that Task, a finite element evaluation of the experimental results and the development of a new hand-calculation method considering the influence of the joint assembly tolerances was carried out. In this case, each tensile test was carried out at a constant strain rate. For each steel grade five different strain rates were considered.

As in the tests performed with the conventional parameters, the tests were performed at room temperature with cylindrical specimens machined at 12,5 mm from the bar surface. In this case, only one test per strain rate was carried out because of a limitation on the number of available specimens. The results obtained in these tests are shown in Table 3-4 and Figure 3-7.

For the 32CrB4 EQ (Figure 3-7 left) it was clearly observed that the property which is most affected by the strain rate is the YS. Its value decreases when the strain rate is decreased. The UTS is only affected when very low strain rates are used (10^{-6} s^{-1}).

The trends observed for the 30MnNiB4 EQ (Figure 3-7 right) are quite similar to those previously described for the 32CrB4 EQ: the decrease of the UTS is less pronounced than the one experimented by the YS and it is only observed for very low strain rates (lower than 10^{-5} s^{-1}).

Table 3-4. Strain rate influence on the tensile properties.

Strain rate (s ⁻¹)	32CrB4 EQ				30MnNiB4 EQ			
	UTS (MPa)	YS _{0,2%} (MPa)	EI (%)	RoA (%)	UTS (MPa)	YS _{0,2%} (MPa)	EI (%)	RoA (%)
10 ⁻²	1109	1069	20,8	66,3	1079	1029	21,2	66,2
10 ⁻³	1113	1064	20,8	68,0	1074	1017	22,3	67,6
10 ⁻⁴	1115	1058	18,6	61,7	1067	1003	20,6	66,9
10 ⁻⁵	1111	1045	19,8	60,9	1071	990	21,2	66,9
10 ⁻⁶	1095	1023	19,6	62,2	1038	960	23,1	64,7

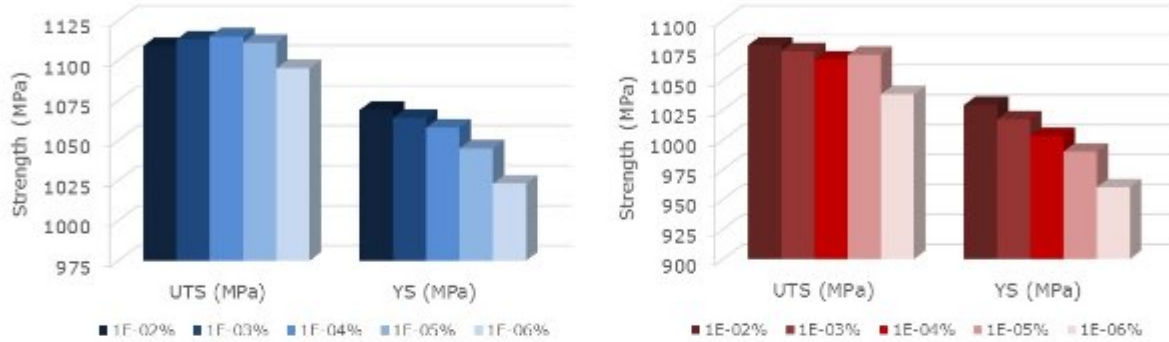


Figure 3-7. Influence of the strain ratio on the UTS and YS for the 32CrB4 EQ (left) and 30MnNiB4 EQ (right).

3.2.4 Toughness test

Toughness tests were carried out in a Charpy pendulum following the indications established in the standard ISO 148-1:2016. The tested V-notched specimens were machined at mid-radius of the bar. As in the case of the tensile tests, three repetitions for each temperatures were performed.

Although the standard ISO 898-1:2015 only establishes a minimum value for the toughness at -40 °C, different testing temperatures were also considered in order to represent the ductile-brittle transition curves and the ductile-brittle transition temperature.

Table 3-5. Results of the Charpy tests (in J)

Testing T (°C)	32CrB4 EQ		30MnNiB4 EQ	
	KV (J) Av.	Std. Dev.	KV (J) Av.	Std. Dev.
20	85	2	109	3
0	80	1	85	3
-20	53	4	70	3
-40	38	2	49	3
-60	24	1	32	1

The results of the tests, presented in Table 3-5 easily reach the requirements established by the standard ISO 898-1:2015. The toughness of the 30MnNiB4 EQ at -40 °C is about 30% higher than the one of the 32CrB4 EQ. As it is well known, hardness/UTS and toughness are properties which are inversely proportional, so the observed trend regarding toughness is coherent with what it was observed in the hardness and tensile tests, where 32CrB4 EQ was demonstrated to be harder than the 30MnNiB4 EQ.

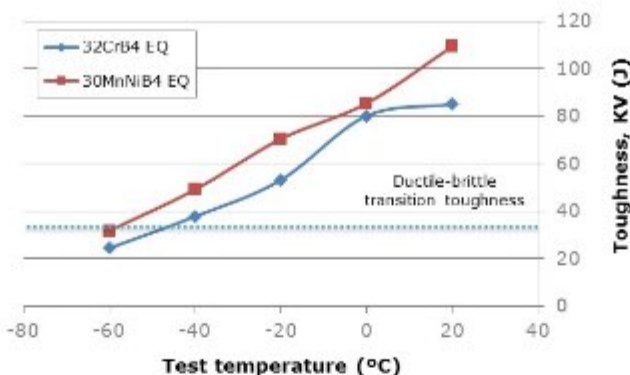


Figure 3-8. Ductile-brittle transition curve for 32CrB4 EQ and 30MnNiB4 EQ.

As shown in Figure 3-8, although the transition temperature (the one at which a toughness of 35 J is reached) is quite high for both grades, the one of the 30MnNiB4 EQ is considerably lower than the 32CrB4 EQ one (-60 °C for the 30MnNiB4 EQ vs -45 °C for the 32CrB4 EQ). This means that the performance (resistance to impacts) at low temperature of the 30MnNiB4 EQ is better than the 32CrB4 EQ one.

3.3 Testing of fatigue strength of specimens (steels for bolts)

The aim of this Task was the determination of the fatigue performance of the steels manufactured and characterized in Task 3.1 and Task 3.2. Fatigue damage is defined as a progressive damage that appears when the material is subjected to cyclic loads. The stress values that cause such damage are much lower than the material UTS or YS.

The fatigue performance is not mentioned in the standard ISO 898-1:2015. So, given that wind fasteners are subjected to cyclic loads, a fatigue failure could take place even having reached all the requirements established in the standard. Thus, this fatigue assessment would provide valuable information in order to be able to predict potential failures of the bolts during their in-service life and consequently an improvement of the steel fatigue performance would directly lead to a safer tower operation.

3.3.1 Specimens manufacturing and verification

Specimens manufacturing: The specimens were machined at mid-radius of the heat treated (Q&T) Ø 30 mm bars. Finally, given that some tests not considered in the proposal (the fatigue tests at constant strain) were included, 35 specimens of each steel grade (10 more than the initially considered for each steel) were manufactured.

Specimens verification: Once the specimens were manufactured the following characteristics were checked:

- Dimensional assessment: The dimensions of the specimens were checked in an optical profiler, being all of them in the range of the required dimensions.
- Surface roughness (Ra): Given that the surface roughness is one of the most influencing parameters on the fatigue results, the surface roughness of each specimen was measured in six different points of the testing zone with a Mitutoyo roughness tester. In all the cases the roughness (Ra) was in the range of 0,1-0,2 µm established as internal requirement for the axial fatigue tests.
- Hardness: Before the tests, a hardness measurement was carried out in one of the specimen heads. All the obtained hardness are in the range of the ones obtained in Task 4.2.

3.3.2 Test configuration and method

Axial tension-compression fatigue tests were performed with a load ratio of $R = -1$. The tests were carried out at a frequency of 25 Hz in a MTS servo-hydraulic machine (Figure 3-9). The considered run-out criteria was 10.000.000 cycles.



Figure 3-9. MTS servohydraulic machine in which the fatigue tests were conducted.

In order to carry out a complete fatigue assessment both the fatigue limit and the fatigue strength were determined. For this purpose, two different methods were used:

Fatigue limit determination: The fatigue limit is determined by the staircase method. To perform this test an initial stress and a stress increment must be defined. If the specimen subjected to the initial stress is not broken when the run-out criteria is reached, the stress is increased (in the previously fixed increment) and a new sample is tested. On the contrary, if the specimen breaks before reaching the run-out criteria, the stress is reduced (in the fixed increment) in order to carry out the following test.

The method distinguishes between two cases:

- less frequent event is failures ($C=1$) and,
- less frequent event is run-outs ($C=2$).

The method uses only the less frequent occurrence in the test results, i.e. if there are more failures than run-outs, then the number of run-outs is used, and vice versa.

The equation used to determine the fatigue limit when $C=1$ is:

$$\sigma_D = \sigma_0 + d\left(\frac{A}{N} + \frac{1}{2}\right) \quad 3.1$$

While for the case when $C=2$, the used equation is:

$$\sigma_D = \sigma_0 + d\left(\frac{A}{N} - \frac{1}{2}\right) \quad 3.2$$

The standard deviation is determined by the following equation:

$$s = 1,62d\left(\frac{N \cdot B - A^2}{N^2} - 0,029\right) \quad 3.3$$

Where:

d = stress increment; σ_0 = the lowest stress level for the less frequent occurrence; $N = \sum n_i$;

$A = \Sigma i \cdot n_i$; $B = \Sigma i^2 \cdot n_i$; i = stress level numbering; f_i = is the number of samples at stress level i .

Determination of the fatigue strength: The finite part of the Wöhler curve is obtained testing samples at higher loads until failure. Using these results together with the ones obtained during the fatigue limit determination, the Wöhler curve is generated to give a general view of the fatigue behaviour of each steel grade.

The Wöhler curve is obtained through a quadratic regression using the following equation:

$$N = N_D \left(\frac{\sigma_D}{\sigma} \right)^k$$

3.4

Where:

σ_D = the fatigue limit; N_D = the considered run-out criteria; σ = stress for a given number of cycles;

N = number of cycles for which the stress σ is reached; k = slope of the Wöhler curve.

3.3.3 Results of the fatigue test with controlled load

In Table 3-6 not only the applied stress and the number of cycles that were reached are shown, but also a brief description of the fracture origin is provided. At least two repetitions for each considered stress were carried out (if possible due to the limited number of specimens).

Results obtained for the 32CrB4 EQ: All the fatigue results obtained for the 32CrB4 EQ are shown in Table 3-6. These results are used throughout the next pages for the fatigue limit determination and the representation of the Wöhler curve.

The stress increment considered for the fatigue limit determination through the staircase method was 10 MPa.

The staircase for the 32CrB4 EQ is shown in Figure 3-10. Using these data and the Eqn. 3.1, 3.2 and 4.3 the fatigue limit and its corresponding standard deviation were calculated. The 32CrB4 EQ fatigue limit is 577 MPa with a standard deviation of 3,06 MPa.

Initial data		Results										
Minimum tension σ_0	= 540 MPa <th data-cs="2" data-kind="parent">Fatigue limit</th> <th data-kind="ghost"></th> <td data-cs="8" data-kind="parent">$\sigma_f = 577,0$ MPa</td> <td data-kind="ghost"></td>	Fatigue limit		$\sigma_f = 577,0$ MPa								
Increment	$d = 10$ MPa <th data-cs="2" data-kind="parent">Standard deviation</th> <th data-kind="ghost"></th> <td data-cs="8" data-kind="parent">$s = 3,06$ MPa</td> <td data-kind="ghost"></td>	Standard deviation		$s = 3,06$ MPa								
Failures	$x = 5$											
Non-failures	$o = 7$											
σ_{max} (MPa)	1	2	3	4	5	6	7	8	9	10	11	12
600												
590					x							
580		x		o		x		x		x		
570	o		o				o		o	o	o	
560	o											
550												

Figure 3-10. Staircase method for the fatigue limit determination of the 32CrB4 EQ.

The fatigue limit obtained for the 32CrB4 EQ improves in a 13% the fatigue limit of a conventional 32CrB4 which is about 510 MPa. With the results shown in the Table 3-6 and the Eqn. 3.4 the Wöhler curve was generated (Figure 3-12 blue).

Results obtained for the 30MnNiB4 EQ: Table 3-6 shows also all the fatigue results obtained for the 30MnNiB4 EQ. These results were used to determine the fatigue limit and to create the Wöhler curve of this steel.

In order to apply the staircase method for the fatigue limit determination, it was considered the same stress increment used for the 32CrB4 EQ (10 MPa). The staircase for the 30MnNiB4 EQ is shown in Figure 3-11. Using these data and the Eqn. 4.1, 4.2 and 4.3 the fatigue limit and its corresponding standard deviation were calculated. The 30MnNiB4 EQ fatigue limit is 545 MPa with a standard deviation of 6,95 MPa.

Table 3-6. Results obtained in the fatigue tests at constant load.

Applied stress (MPa)	32CrB4 EQ			30MnNiB4 EQ		
	Cycles	Failure/Run-out	Fracture origin	Cycles	Failure/Run-out	Fracture origin
510	-	-	-	13.610.913	Run-out	-
520	-	-	-	10.950.145	Run-out	-
530	-	-	-	10.251.872	Run-out	-
540	-	-	-	10.354.612	Run-out	-
540	-	-	-	16.059.374	Run-out	-
540	-	-	-	13.620.171	Run-out	-
540	-	-	-	8.024.715	Failure	Surface
550	-	-	-	10.248.445	Run-out	-
550	-	-	-	5.814.010	Failure	Surface
550	-	-	-	4.907.028	Failure	Surface
550	-	-	-	5.126.760	Failure	Surface
560	-	-	-	2.984.764	Failure	Surface
560	-	-	-	3.754.223	Failure	Surface
570	11.444.827	Run-out	-	1.911.959	Failure	Surface
570	10.885.223	Run-out	-	2.250.225	Failure	Surface
570	12.335.226	Run-out	-	-	-	-
570	16.357.311	Run-out	-	-	-	-
570	12.479.870	Run-out	-	-	-	-
580	10.348.813	Run-out	-	-	-	-
580	7.048.931	Failure	Surface	-	-	-
580	8.779.098	Failure	Surface	-	-	-
580	6.835.773	Failure	Surface	-	-	-
580	7.047.668	Failure	Surface	-	-	-
590	3.727.980	Failure	Surface	-	-	-
590	4.055.223	Failure	Surface	-	-	-
600	1.936.589	Failure	Surface	811.232	Failure	Surface
600	2.249.887	Failure	Surface	657.084	Failure	Surface
650	387.074	Failure	Surface	160.134	Failure	Surface
650	303.112	Failure	Surface	195.820	Failure	Surface
670	152.566	Failure	Surface	90.326	Failure	Surface
670	192.601	Failure	Surface	-	-	-
700	56.964	Failure	Surface	40.171	Failure	Surface
700	47.551	Failure	Surface	32.854	Failure	Surface
730	30.273	Failure	Surface	-	-	-
730	20.129	Failure	Surface	-	-	-

Initial data		Results											
Minimum tension $\sigma_0 = 500$ MPa		Fatigue limit $\sigma_f = 545,0$ MPa											
Increment $d = 10$ MPa		Standard deviation $s = 6,95$ MPa											
Failures $x = 5$													
Non-failures $o = 8$													
σ max (MPa)	1	2	3	4	5	6	7	8	9	10	11	12	13
560							x						
550							o	x		x		x	
540			x	o					o		o		
530		o		o									
520													
510	o												

Figure 3-11. Staircase method for the fatigue limit determination of the 30MnNiB4 EQ.

As it is normal considering the well-known direct relationship between the hardness and the fatigue limit, the fatigue limit of the 30MnNiB4 EQ is lower than the one determined for the 32CrB4 EQ. However, compared with the conventional 32CrB4 (whose fatigue limit is about 510 MPa), the fatigue limit of the 30MnNiB4 EQ is 7% higher.

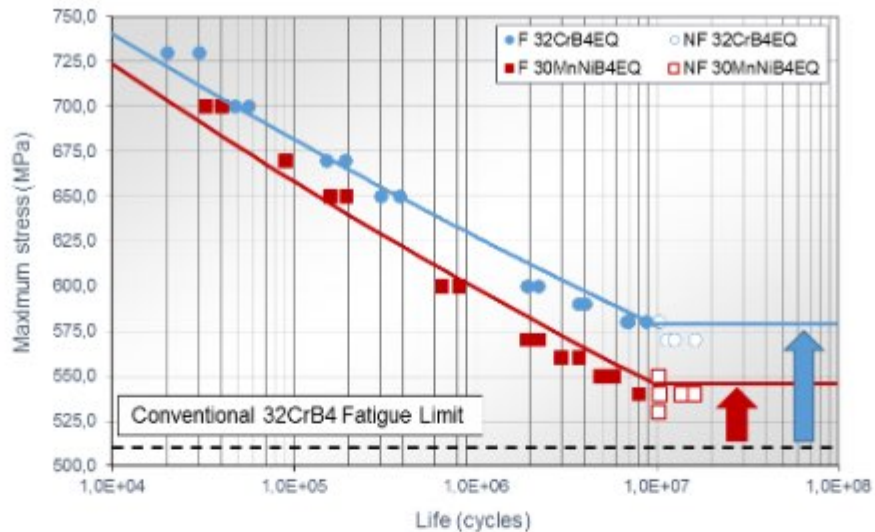


Figure 3-12. Wöhler curves obtained for 32CrB4 EQ and 30MnNiB4 EQ.

Analysis of the fatigue fractures: All the fractures generated during the previously mentioned fatigue tests were analysed by optical microscopy and by SEM.

- Analysis of the fatigue failures for the 32CrB4 EQ: Some examples of the most representative failures occurred with the 32CrB4 EQ are shown in Figure 3-13 and Figure 3-14. As shown in the images obtained by SEM, all the fractures started at surface level, this kind of fatigue failure origin is common when high stresses are applied. The lack of failures caused by the presence of inclusions indicates that the steel cleanliness level is the adequate one.

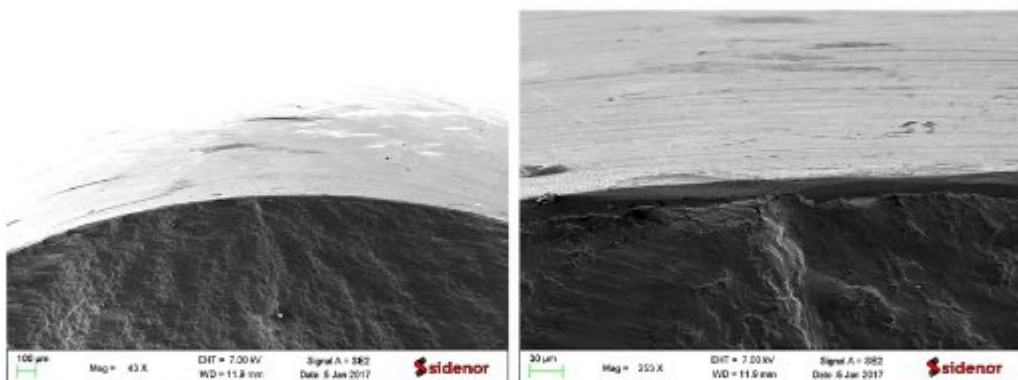


Figure 3-13. Fatigue fracture occurred in the 32CrB4 EQ after 3.727.980 cycles applying 590 MPa.

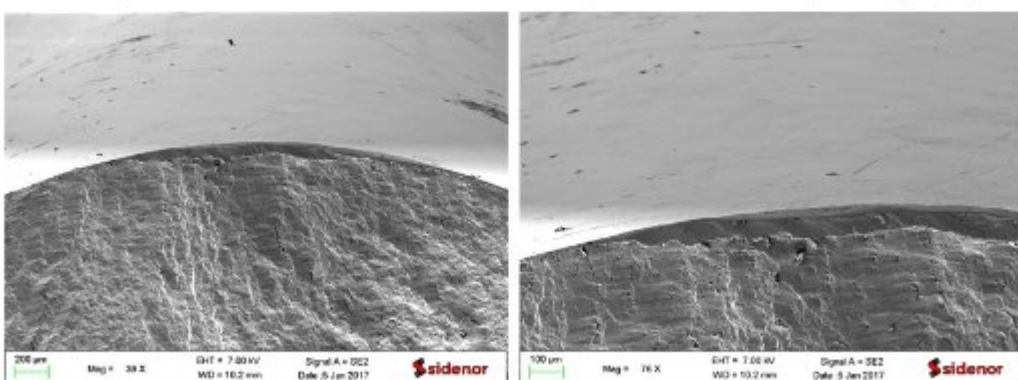


Figure 3-14. Fatigue fracture occurred in the 32CrB4 EQ after 20.129 cycles applying 730 MPa.

- Analysis of the fatigue failures for the 30MnNiB4 EQ: Some of the most representative fatigue failures which took place with the 30MnNiB4 EQ are shown in Figure 3-15 and Figure 3-16. As in the case of the 32CrB4 EQ, all the fractures started at surface level. The lack of failures

caused by the presence of inclusions indicates that the steel cleanliness level is the adequate one.

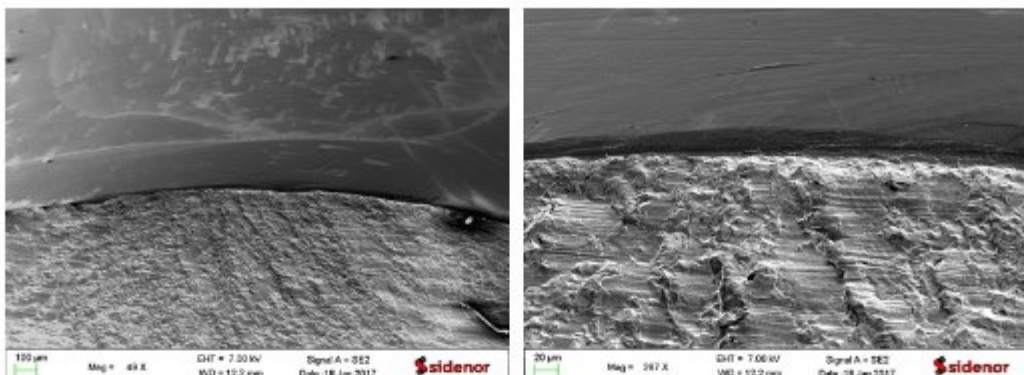


Figure 3-15. Fatigue fracture occurred in the 30MnNiB4 EQ after 2.984.764 cycles applying 560 MPa.

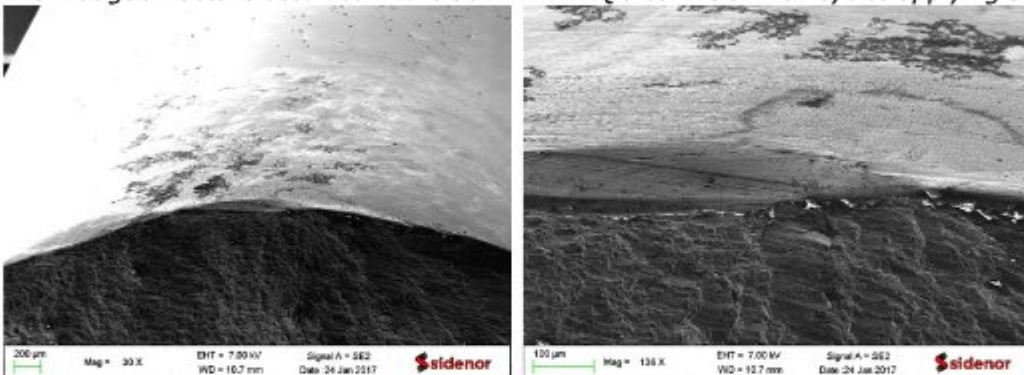


Figure 3-16. Fatigue fracture occurred in the 30MnNiB4 EQ after 657.084 cycles applying 600 MPa.

3.3.4 Results of the fatigue test at constant strain

Some extra fatigue tests were performed in order to obtain the information required in Task 4.4. In that Task, a finite element evaluation of the experimental results and the development a new hand-calculation method considering the influence of the joint assembly tolerances were carried out.

In this case, the fatigue tests were performed controlling the strain instead of controlling the applied load. As these tests were not initially expected, the run-out criteria was fixed in 5.000.000 cycles in order to reduce the testing time.

Four different strain rates were considered: 0,1%, 0,2%, 0,3% and 0,4%. Higher strain rates were not tested because the testing machine was not able to reach the required loads to produce those high deformations. Because of the lack of specimens only one repetition for each strain rate was considered.

During the test the strain and the stress for each cycle were recorded in order to generate the hysteresis loops needed to create the FEM.

Results obtained for the 32CrB4 EQ: As it is shown in Table 3-7 for the two lowest strain rates the run-out criteria was reached, while for the two highest ones the specimen was broken.

Table 3-7. Fatigue life for the tested strain rates.

	32CrB4 EQ		30MnNiB4 EQ	
Strain rate (%)	Number of cycles	Failure/Run-out	Number of cycles	Failure/Run-out
0,1	5.000.000	Run-out	5.000.000	Run-out
0,2	5.000.000	Run-out	5.000.000	Run-out
0,3	31.872	Failure	23.830	Failure
0,4	5.355	Failure	3.369	Failure

Figure 3-17 shows as an example the hysteresis loops for strain rate 0,4% where the variation of the stress-strain during the test is represented. In order to make figure more legible, only the data of a few cycles were represented. Additionally, to assure that the selected loops were adequate to see the stress-strain evolution during the test, the chosen cycles were selected from different parts of the test: the beginning, mid-test and the end of the test.

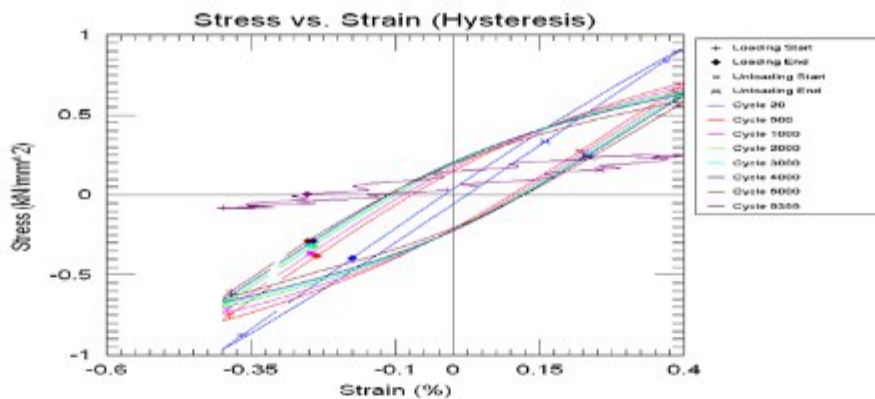


Figure 3-17. Hysteresis loops for the 32CrB4 EQ and a strain rate of 0,4%.

Results obtained for the 30MnNiB4 EQ: Similar to the shown for the 32CrB4 EQ, for the two lowest strain rates the run-out criteria was reached, while for the two highest ones the specimen was broken (Table 3-7).

The procedure followed to select the cycles represented in the Figure 3-18 was similar to the one described for the 32CrB4 EQ. The evolution of the stress-strain experimented during the tests carried out at 0,4 % strain rate with the 30MnNiB4 EQ is represented.

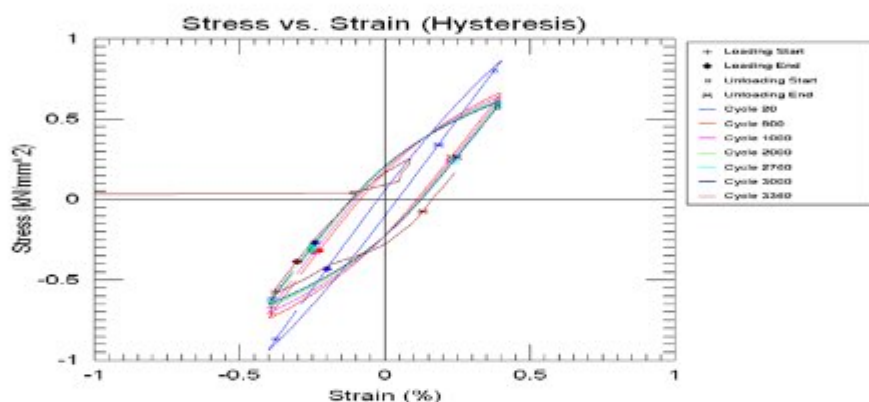


Figure 3-18. Hysteresis loops for the 30MnNiB4 EQ and a strain rate of 0,4%.

3.4 Fatigue testing of corroded double shear pre-stressed connections

The main goal of this Task was to validate the new type of steel used in the bolts (Task 4.3) of the complete connections. For that purpose, fatigue tests on corroded and non-corroded double shear pre-stressed connections were performed. More details about this test are provided in the following sections.

3.4.1 Configuration of the fatigue tests on connections

Connections geometry: The connections consisted of two pre-tensioned bolts (M12 mm) connecting three S690 steel plates (two different variants were tests with plate thickness either 3 mm or 4 mm). Imperfections in the plate surface were simulated (for instance curvature of internal plate) in order to better reproduce the real behaviour of corrosion penetration. The geometry of these connections is shown in Figure 3-19.

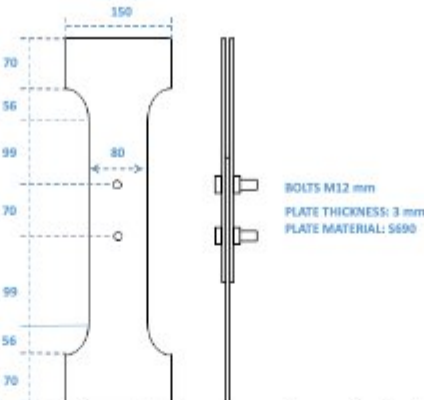


Figure 3-19. Geometry of the connections to be fatigue tested.

The following aspects were changed with respect to the initial proposal: Given the trend of using high strength steels the initially proposed steel for plates S355 was changed by S690. This change made it necessary to reduce the dimensions of the connections and the bolts because of the limitation of the testing machine to reach so high loads. The main dimensional changes were: the new connection width was 80 mm (instead of 100 mm), the plate thickness 3 or 4 mm (instead of 6 or 8 mm) and the metric of the bolts 12 mm (instead of 24 mm).

3.4.2 Connections manufacturing process

Manufacturing process: The manufacture process involved different project partners. Friedberg manufactured the bolts with the steel produced by Sidenor. Martifer manufactured and assembled the connections. The University of Coimbra performed the corrosion treatments. Finally, Sidenor carried out the fatigue tests and evaluated the obtained results. Figure 3-20 shows the whole connections manufacturing chain.



Figure 3-20. Connections manufacturing process scheme.

Verification of the chemical composition: One of the connections was analysed in order to get the chemical composition of both the bolt and plate grades used for its manufacturing. The analyses performed by Optical Emission Spectrometry are shown Table 3-8.

Table 3-8: Chemical composition (all in weight %, except * in ppm).

Component	C	Mn	Si	P	S	Cr	Ni	Mo	Cu	Al	Ti	B*
Plate	0,07	1,86	0,01	0,007	0,003	0,05	0,05	0,02	0,01	0,043	0,108	-
Bolt	0,31	1,46	0,24	0,012	0,003	0,48	0,47	0,014	0,08	0,028	0,036	23

Additionally, some tensile tests on coupons were carried out for the plate grade. These results were used for the sake of classification of the plate steel as S690 grade.

3.4.3 Test planning

In total 18 connections were manufactured with 30MnNiB4 steel grade for the bolts (see Table 3-8). 9 of them were assembled with 3 mm thickness steel plates and 9 of them with 4 mm thickness steel plates.

Of the 9 connections for each plate thickness, 3 were subjected for testing without being corroded and the other 6 being previously corroded. Each specimen was identified as C (corroded) or NC (non-corroded), follow by 3 or 4 depending on the plate thickness, and a correlative number from 1 to 6 for the replicas. The foreseen accelerated corrosion treatment for the specimens at corrosion Level was NaCl 5% at 35°C during 2 months in a Cyclic Corrosion Test Chamber (see Figure 3-21), which corresponds to extreme aggressive environment conditions (C4 environment class).



Figure 3-21. Connections in the corrosion chamber.

3.4.4 Fatigue test

Test configuration and method: The initial planning comprised axial fatigue tests, applying tension-tension loads with a load ratio $R = 0,1$ on the connections using a testing frequency of 5 Hz in a MTS servohydraulic machine (Figure 3-22). The agreed run-out criterion was 2.000.000 cycles.



Figure 3-22: MTS servohydraulic machine in which the fatigue tests were conducted

The first tested specimen corresponded to NC3, a non-corroded sample with 3 mm thickness. In this case, the specimen broke prematurely after 1.000 cycles and the fracture origin was generated on the hole. Since this failure was produced under a very low number of cycles, this specimen could not be considered as a reference for comparison of the corroded samples. Therefore, the strategy was modified, and instead of choosing a fixed constant load for all the tests, the fatigue tests for the other specimens were performed increasing the loading after an approximate number of cycles. With this test, the failure in the specimens is accumulative, and to compare non-corroded and corroded specimens it would be enough to focus on the highest level of applied stress before the rupture.

Fatigue test on NC3 (Non-corroded specimens with 3 mm thickness): Figure 3-23 displays the results for the NC3 specimens. NC3 was tested initially at 20 KN and the stress was increased after each ≈ 400.000 cycles. Both specimens broke at a load of 60 KN, with 241.415 and 439.248 cycles. Therefore, the reference level for comparison with corroded specimens was established in 60 KN.

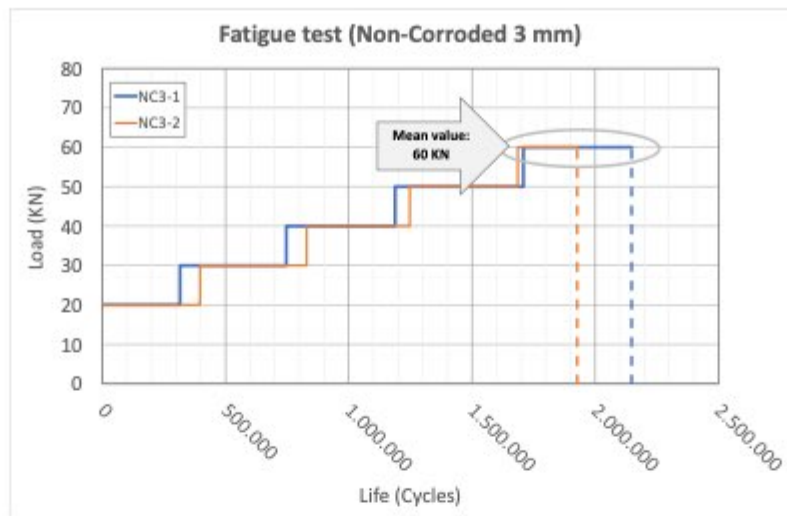


Figure 3-23. Fatigue results for NC3.

Fatigue test on NC4 (Non-corroded specimens with 4 mm thickness): Figure 3-24 displays the results for the NC4 specimens. Similarly to NC3 specimens, the starting stress level was 20 kN and after each $\approx 400,000$ cycles the load was increased in 10 kN. Following this methodology one connection reached a level of 90 kN before breaking, while the second and third ones broke at 80 kN, which means a reference load of 83,3 kN for NC4.

The reference values for comparison of fatigue performance between non-corroded and corroded connections was established in:

- 3 mm thickness reference: 60 kN.
- 4 mm thickness reference: 83,3 kN.

Fatigue test on C3 (Corroded specimens with 3 mm thickness): Corroded connections were tested according to the same procedure described for non-corroded specimens. The results for both corroded and non-corroded specimens are compiled in Table 3-10 for easier comparison, while graphical representation of corroded specimens is shown in Figure 3-25.

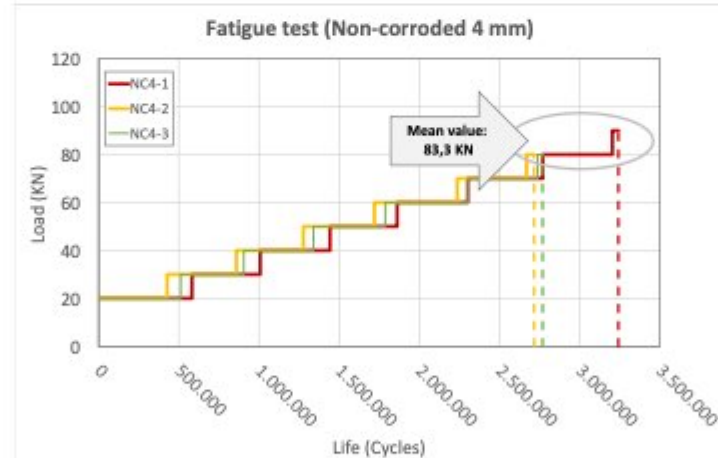
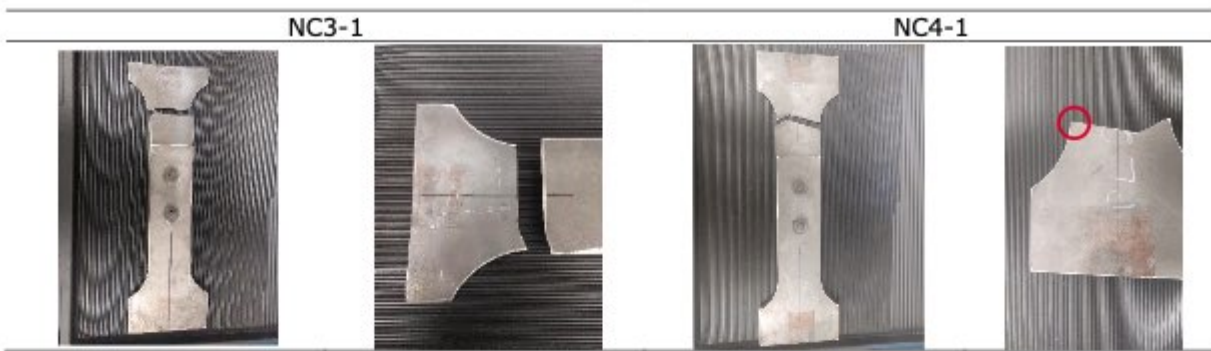


Figure 3-24: Fatigue results for NC4.

Table 3-9. Examples of failures located in the fillet radius.



One of the tests, C3-6 was not included in the evaluation due to the failure of the specimen in the clamping region, which invalids the corresponding results. Taken this into account, it is observed some dispersion among the obtained results, with highest values ranging from 50 KN to 70 KN. The mean value resulted to be 60 KN, exactly the same result registered for non-corroded connection.

Fatigue test on C4 (Corroded specimens with 4 mm thickness): The results for both corroded and non-corroded specimens are compiled in Table 3-10 for easier comparison, while graphical representation of corroded specimens is shown in Figure 3-26.

In this case, two different specimens (C4-5 and C4-6) were omitted from the results evaluation due to the failure in the clamping area. Considering the valid tests, the maximum loading reached varies between 60 KN and 100 KN, which points out the high dispersion of the test. The mean value for the acceptable specimens was established in 75 KN.

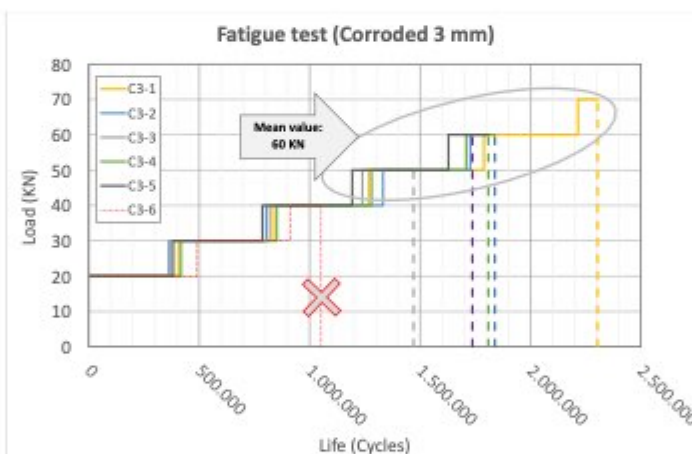


Figure 3-25. Fatigue results for C3.

Table 3-10. Results obtained in the fatigue test with incremental loading for 3 and 4 mm thickness specimens.

Maximum Load (kN)	3 mm thickness																										
	Non-corroded						Corroded																				
	NC3-1			NC3-2			-	C3-1			C3-2			C3-3			C3-4			C3-5			C3-6				
	Number of cycles	Failure		Number of cycles	Failure			Number of cycles	Failure		Number of cycles	Failure		Number of cycles	Failure		Number of cycles	Failure		Number of cycles	Failure		Number of cycles	Failure			
20	315.465	N	395.989	N	-	-	407.813	N	362.819	N	370.243	N	417.671	N	382.222	N	490.083	N									
30	431.322	N	433.722	N	-	-	428.454	N	440.818	N	449.545	N	434.031	N	403.741	N	421.420	N									
40	441.175	N	417.635	N	-	-	432.664	N	529.162	N	419.285	N	428.985	N	406.859	N	140.492	Y									
50	520.865	N	438.148	N	-	-	520.092	N	394.742	N	231.438	Y	428.896	N	435.963	N											
60	439.248	Y	241.415	Y	-	-	426.372	N	9.695	Y			129.608	Y	180.627	Y											
70			-	-	89.037	Y																					
Location	Fillet radius		Fillet radius		-		Fillet radius		Fillet radius		Fillet radius		Fillet radius		Fillet radius		Fillet radius		Clamping area								
4 mm thickness																											
Non-corroded																											
	NC4-1			NC4-2			NC4-3			C4-1			C4-2			C4-3			C4-4			C4-5			C4-6		
20	581.758	N	427.445	N	511.880	N	411.739	N	361.895	N	414.923	N	427.445	N	417.353	N	410.256	N									
30	426.133	N	431.665	N	394.266	N	430.417	N	552.773	N	393.539	N	431.665	N	427.490	N	439.512	N									
40	434.600	N	417.956	N	434.427	N	518.822	N	445.179	N	385.655	N	417.956	N	431.935	N	709.821	N									
50	419.160	N	442.560	N	446.625	N	429.699	N	513.429	N	436.431	N	442.560	N	434.993	N	516.842	N									
60	440.137	N	517.207	N	515.626	N	348.872	Y	437.891	N	186.226	Y	517.207	N	437.080	Y	97.277	Y									
70	468.031	N	432.088	N	434.776	N			422.945	N			432.088	N													
80	433.622	N	46.754	Y	30.620	Y			434.435	N			46.754	Y													
90	37.835	Y							341.977	N																	
100									23.721	Y																	
Location	Fillet radius		Fillet radius		Testing region		Fillet radius		Fillet radius		Fillet radius		Fillet radius		Fillet radius		Fillet radius		Clamping area		Clamping area		Clamping area				

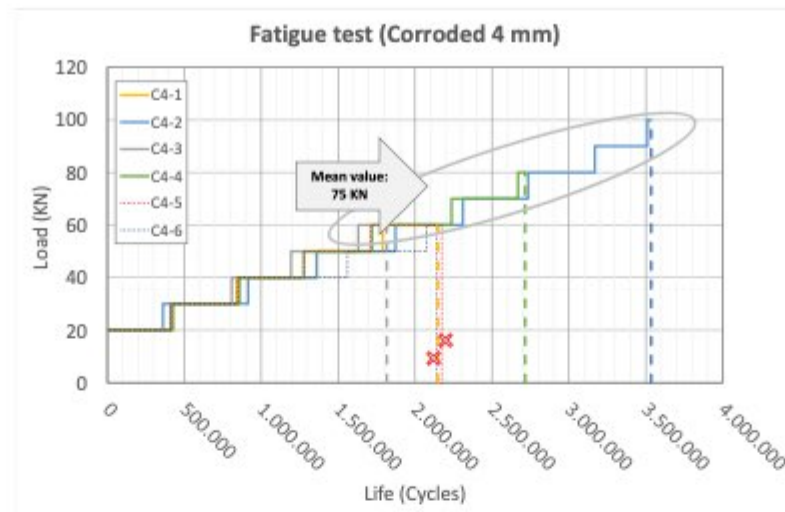


Figure 3-26. Fatigue results for C4.

Analysis of the fatigue fractures: All the fractures generated during the previously mentioned fatigue tests were analysed by optical microscopy in order to establish the fracture origin. In most of the cases, the failure was initiated in the fillet radius and not near the holes as it was expected based on numerical simulation. Some specific tests (C3-6, C4-5 and C4-6) resulted to be invalid due to failures initiated in the clamping region.

Table 3-11: Example of photos of the failures initiated in the fillet radius.

Thickness (mm)	Non-corroded	Corroded
3		
4		

From the photos in Table 3-11 it can be concluded that the failure produced in the fillet radius of the different specimens were started in the surface. All the connections with this specific kind of failure presented a ductile region starting in the surface (left side of the photos). The most probable reason for that, is the poor finishing machined surface of the connection plates.

3.4.5 Analysis of results

Figure 3-27 compares the results obtained for the 3 mm (left) and 4 mm (right) plate connections. It just can be seen that for 3 mm thickness connections no difference between non-corroded and corroded connection could be identified. In both cases, the mean highest level reached for loading have been 60 kN. Previously to the test it was expected to obtain a significant decay of the fatigue performance of the corroded connections in comparison with the non-corroded one. The main reason for these results can rely on the poor machining finishing of the plate specimens on the fillet radius.

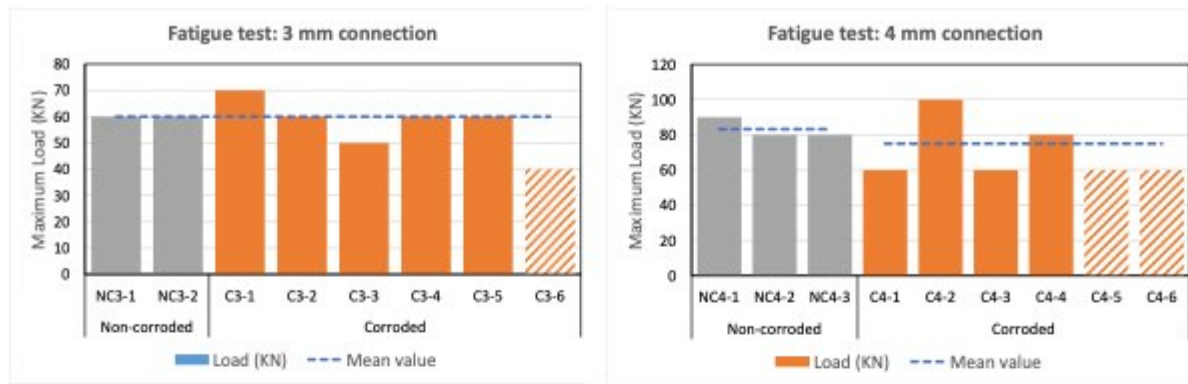


Figure 3-27. Comparison of fatigue results for 3 mm (left) and 4 mm (right) thickness connections.

Regarding the 4 mm thickness connections, a low reduction of the loading has been obtained, from 83,3 KN (reference non-corroded specimens) to 75 KN. However, due to the high dispersion on the results it cannot be concluded that this decay is significantly important.

The results seem to be coherent between the two different plate thickness evaluated. The loading ratio in KN agrees with the section ratio for both connection types.

Table 3-12: Summary of the obtained results for the fatigue test on connections.

	3 mm thickness	4 mm thickness	Ratio (4/3 mm)
Non-corroded	60	83,3	1,38
Corroded	60	75	1,25
Ratio (non-corroded/corroded)	1,00	1,11	

3.5 Selection of the most adequate steel grade for bolts manufacturing

The results on connections' fatigue testing did not give direct information of the bolts performance. Also, the obtained results did not allow to discriminate adequately between the performances of corroded or non-corroded connections. However, both steel grades considered along the project could be suitable for bolts of as small diameter as the one considered in the connections (and up to Ø<36mm). Looking at the characterization carried out in this WP it can be concluded that both grades, 32CrB4 EQ and 30MnNiB4 EQ, reach easily the required properties by class 10.9 of ISO 898-1:2005. Furthermore, both grades with EXTREME quality exceed the fatigue limit of the standard 32CrB4.

On the other hand, the current trend of increasing tower dimensions involves higher diameter bolts at the same time. In that sense, if bigger fasteners Ø>36mm want to be manufactured the use of alternative high alloyed steel grades is required. Typical grades for this kind of application could be 30CrNiMo8, 32CrNiMo6 or 40NiCrMo7 with the associated drawback of their high price due to the alloying content. In such case the 30MnNiB4 EQ represents a competitive and suitable alternative. Although the UTS and fatigue limit of 32CrB4 EQ are higher than those of 30MnNiB4 EQ, the toughness at low temperature of 30MnNiB4 EQ is higher reducing the risk of failure due to conceivable impact in aggressive environments. Moreover, the hardenability of the 30MnNiB4 EQ is higher than that of 32CrB4 EQ, so larger diameter could be manufactured assuring the martensite requirements in the core bar for class 10.9 in ISO 898-1:2005.

3.6 Conclusions

From Task 3.1 the most suitable steel grades were chosen in order to improve the mechanical properties and the fatigue performance of the steels conventionally used for the bolts manufacturing. These grades were the 32CrB4 and 30MnNiB4, both of them manufactured following the EXTREME technology developed by Sideror.

Considering all the information obtained in Task 3.2, the following main conclusions can be extracted:

- Both steel grades fulfill all the requirements specified in the standard ISO 898-1:2015.
- The microstructure obtained after the heat treatment (Q&T) for the 32CrB4 and the 30MnNiB4 is the expected one: tempered martensite, only with some traces of tempered bainite.
- The hardness and UTS values of the 32CrB4 are higher than the 30MnNiB4 ones. However, and as it is logical given the inversely proportional relationship between the UTS and the toughness, the 30MnNiB4 presents higher toughness values at low temperature.
- The ductile-brittle transition temperature is about -45 °C for the 32CrB4 and -60 °C for the 30MnNiB4.

In Task 3.3, after the performance of the fatigue tests on specimens obtained from heat treated bars of the 32CrB4 EQ and 30MnNiB4 EQ steels, it can be assured that these steels improve the fatigue performance of the conventional 32CrB4 in a considerable way.

The fatigue limit of the 32CrB4 EQ is a 13% higher than the one of the conventional 32CrB4, while in the case of the 30MnNiB4 EQ, the fatigue limit is improved in a 7% with regards to the same reference steel.

This fatigue improvement will diminish the bolt risk of failure, leading thus to a safer wind tower operation.

Considering the results obtained in the testing of the connections, the following conclusions can be extracted:

- Fatigue testing on double shear connections does not provide direct results on bolts performance since the failures are initiated in the plate fillet.
- The fracture origin in the experimental tests does not correlate with the modelling simulation. Numerical simulation predicted the failure in the hole region, however, most of the failures are produced in other region of the plates, which is probably due to imperfections not detected after cutting the plates.

4 Detailed design of in-situ bolted connections

In this WP activities have been performed in Task 4.1 to numerically investigate stability behaviour of built-up welded and bolted semi-closed cold-formed elements. The performance of the different types of cross-sections is investigated:

- Closed polygonal cross-sections built of cold formed and welded plates
- Semi-closed cross-section built of plates cold-formed into lipped polygon sectors, bolted together along the length of the member.

Task 4.2 is dedicated to test gusset plate bolted connections between braces and pylon of the lattice structure using 90° and 45° configurations. FE models have been developed in order to prepare test set-up and perform experimental testing. The experiments were performed on 12 specimens up-to-failure, that are described in Deliverable D4.2.

The subject of Task 4.3 is the experimental investigation of (a) compression behavior on pylons and (b) the behavior of 3D joints of proposed cross sections for pylons and diagonal. Three groups of experiments are aimed, where the type of cross section used is of the polygonal form: Group A – three compression tests up to failure; Group B – three tests of pylon compression up to failure, analogous to those of group A but with loaded diagonal; Group C – six tests of diagonals subjected to bending while pylon is compressed to service loads, with the objective to assess joint stiffness

A FE model was put together at LTU and several analyses were performed to assess the influence of using a plane cruciform specimen instead of the one depicted on Fig. 4.7 of Annex B of the contract. The specimens shown there are made up of a short column (in grey) connected to two horizontal arms (yellow). The arms are connected to the column by the joint that is to be investigated. The arms are shown to have an angle around 120 degrees between them. Forces are applied to the arms by means of hydraulic pistons that deliver a moment to the joint and a third piston delivers an axial load to the column. As result of this preliminary assessment two main changes were agreed for these specimens:

#1: Since the behavior of the joint may be seriously affected if placed near the end of the column due to local effects the column is extended upwards so that the joint is placed right in the middle of the column. In reality this joint appears along the length of a long column.

#2: the angle between the two arms is taken 180 degrees thus making the whole column/arms assembly a plane structure. There were serious technical difficulties with the implementation in the Lab, since the strong-floor has fixation boreholes at distances that do not comply with the arrangement of the specimen.

In Task 4.4 the numerical modeling, model calibration and parametric study of the connections is performed

4.1 Profiles with closed and semi-closed polygonal cross-section

The polygonal cross-sections are intended for the legs and the braces of the lattice structure. The interest is primarily on the legs, which are primarily members under compression. As such, the buckling behaviour of the cross-sections is of highest interest. A better understanding of the overall buckling as well as the local and distortional buckling effects on the investigated cross-sections will allow for an optimal use, minimizing the material use and the fabrication cost. Minimizing the requirements for braces and the needs of bolts can significantly reduce the erection complexity.

Current rules given in Eurocodes cannot be applied on polygonal cross-sections in a direct way. The classification methodology given in EN 3-1-1 [18] for the local buckling effects needs to be re-examined for the case of the obtuse angles of a polygonal cross-section. Moreover, the cold-formed cross-sections with many creases, especially the semi closed cross-sections need to be examined for the suitable buckling curve to accurately calculate the resistance reduction factor for overall buckling.

The semi-closed version of the polygonal cross-sections suffers from distortional buckling. Cases of distortional buckling are covered by EN 3-1-3 [20]. Distortion of the individual sectors can occur on the space between two consecutive bolts. Each sector is a lipped thin-walled channel. Distortional buckling is critical in those kinds of profiles, where the channel tends to "flatten" with the creases folding inwards or outwards. It is a rather complex buckling mode which has strong interaction with the overall buckling of the profile.

Eurocode employs an effective width method for plated class 4 cross sections. The area of the cross

section is reduced for an ineffective portion of the plate's width. Calculation of the effective width if given in part 4.4 of EN 3-1-5 [19] for internal or outstanding compression elements for simply supported plates on all four sides or on three sides respectively. A width reduction factor, ρ , is calculated based on the plate slenderness, λ_p .

Apart from plated cross-sections, tubular cross-sections are similarly classified in 4 classes based on their diameter to thickness ratio. The class limits are given in sheet 3 of Table 5.2 of EN 3-1-1[18] and class 4 tubes should be designed according to EN 3-1-6 [11] for cylindrical shell buckling.

Polygonal shaped cross-sections are fabricated by folding flat plate material. A cross-section can be described by its diameter (diameter of the circumscribed circle), the plate thickness, the number of sides and the bending radius of the corners (creases). As each side of the polygon is a flat plate, the cross-section can be classified as a plated member according to sheet 1 of Table 5.2 of EN 3-1-1 [18]. This method requires the assumption that the sides of the polygon are considered as internal compression members, in other words that the sides are effectively acting as 4-sided simply supported plates. This assumption implies that the creases are able to support the out-of-plane displacements of the sides.

The previous assumption is valid for 4 sided polygons (RHS and SHS) according the examples given in Eurocode. In this case, the out-of-plane displacements of each plate are effectively supported by the membrane reaction of the adjacent sides, providing simple support boundary conditions. As the number of sides increase, the polygon angles become obtuse and the previous assumption should be re-examined.

For an obtuse crease, the out-of-plane displacement of a given side is supported by the adjacent sides by an in-plane component (membrane action) and an out-of-plane component (plate action). As the number of sides increase and the creases become more obtuse, the in- plane component of the adjacent plates decreases, making them less capable to act as supports. It is reasonable to assume that there is an angle limit (reflected on the number of sides) where the simple support assumption is not valid. Beyond that limit, the out-of-plane deformations of one side (local buckling) crosses over the corners to the adjacent sides violating the support boundary condition.

Assuming simple support boundary conditions for the sides of a polygonal cross-section, the class can be determined by the width of each side to the plate thickness ratio for a certain yield stress. The side width for a given diameter is a function of the number of sides. By increasing the number of the polygon sides, the class 3-4 limit can be respected by using thinner plates. This thickness reduction is eventually limited by the fact that the polygon corners no longer act as supports to the sides, transforming the behaviour of the cross section from a plated one to a tubular one. This limit on the number of sides is to be investigated.

4.1.1 Member Slenderness and Distortional Buckling

The cross-sections of this task are investigated for use in lattice wind-tower legs. An important part of such lattice tower structures is the bracing system. Braces add a significant cost to the structure by the added material. Moreover, the number of connections increases both the cost and the complexity due to the detailing. It is therefore essential to optimize the requirements of primary and secondary braces.

The main purpose of the braces is to support the displacements of the tower's shortening its buckling lengths. An accurate understanding of the flexural behaviour of the polygonal profiles is required. Flexural buckling resistance of members in compression is calculated based on part 6.3 of EN 3-1-1 [18]. Cross-sections are categorised in five buckling curves which consider the geometrical imperfections and the residual stresses from the manufacturing process. The categorisation is described in Table 6.2 of EN 3-1-1. The categorisation is based on the profile shape, the manufacturing process and the steel grade.

According to Table 6.2, polygonal shaped cross section should be categorised as cold formed hollow sections. Both circular hollow sections (CHS) and rectangular hollow sections (RHS) fitin this category. Polygonal shaped hollow sections have additional cold formed folds and the adequacy of the buckling curves should be examined.

Moreover, the case of semi-closed cross-sections cannot be fitted in the given categories. The capacity of such cross-sections to operate as a uniform profile should be ensured for the current rules to be applied. In the case of densely enough bolted members for which the above requirement is fulfilled, it

is uncertain which buckling curve should be used.

Distortional buckling is a failure mode exclusive to open cross sections. As a cold-formed cross-section under compression undergoes distortional buckling the nodes (corners) of the profile are displaced leading to a transformation (distortion) of its shape. Both local and distortional buckling for cold-formed thin-walled cross-sections is covered by EN 3-1-3 [20].

Paragraph 6.1.3 of EN 3-1-3 [20] gives the resistance of cross-sections under axial compression. The effects of local and distortional buckling are being considered by means of a reduced effective area of the cross-section, A_{eff} . For the case of reduced cross-sections to A_{eff} , The cross-sectional resistance $N_{c,Rd}$ is calculated using the basic material yield stress, f_y . For sections where the gross cross-section is considered, an average cross-section yield stress is used, f_a . The cross-section average yield stress is increased for the effect of work hardening due to cold forming.

In addition to 4.4 of EN 3-1-5 [19], the effective cross-sectional area is calculated according to 5.5 of EN 3-1-3 [20]. An equivalent spring method is described for the effect of intermediate and end stiffeners.

4.1.2 Closed cross-section profiles

Several cross-sections have been investigated by altering the global and plate slenderness. The sections chosen were 9 faceted polygons. The choice was based on the hypothesis that a polygonal lattice structure will be built thus, allowing angled connections to be easily installed. Considering the transportation conditions of the profiles, a length of 12 m was considered. The joints and continuity connections are considered to reduce the effective length of the member to approximately 10m. The size of the cross-section was estimated as a polygon circumscribed in a circle with the radius, R , as seen in Table 4-1.

Table 4-1: Comparison of first buckling modes

R [mm]	b [mm]		P_{cr} [kN] Euler	FEM Plate		EC
	FEM	Euler		Global	Local	
300	205	18768	19059	57536	Global	Global
350	239	29638	30265	49317	Global	Global
400	274	42880	45176	43152	Local	Local
450	308	38270	64324	38357	Local	Local
500	342	34555	88235	34522	Local	Local

The local imperfections were first introduced by multiplying the displacement obtained from the buckling analysis by a factor function of the plate thickness, a common procedure used in shell structures. One of the main disadvantages of this procedure is that the modes have to be independently identified so that the right scaling factor is used.

A static analysis was performed to investigate the ultimate resistance of the members with imperfections. The results are summarized in Table 4-2 and compared against the design curves in Figure 4-1. When the predominant buckling mode was local (i.e. plate buckling), the strength of the member was considerably above the buckling curve.

Table 4-2: FEM analysis for t = 12 mm with buckling modes imperfection

R [mm]	Npl,S355	Npl,S460 [kN]	Nu,S355 [kN]	Nu,S460 [kN]	Nu,FEM/Npl S355	Nu,FEM/Npl S460	λ_{S355}	λ_{S460}
300	7868	10195	5650.00	7017.40	0.72	0.89	0.642511	0.731383
350	9179	11894	7061.18	8779.50	0.77	0.96	0.550725	0.626902
400	10491	13593	10052.6	13287.0	0.96	1.27	0.481886	0.548541
450	11802	15292	11626.8	14949.9	0.99	1.27	0.428337	0.487585
500	13113	16991	12850.4	16146.6	0.98	1.23	0.385505	0.438828
300	7868	10195	5650.00	7017.40	0.72	0.89	0.642511	0.731383
350	9179	11894	7061.18	8779.50	0.77	0.96	0.550725	0.626902

When high-strength steel S690 is used, the imperfection function was introduced on the cross-sections with plate thickness of 10 mm. The local imperfection was applied on the plate and on the bent corners.

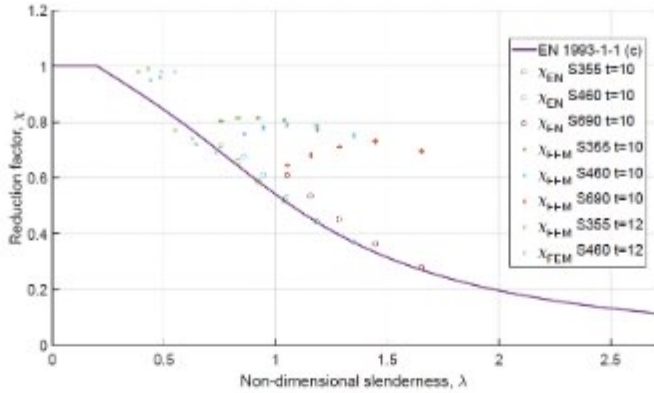


Figure 4-1: Comparison of FEM results with design curves and values

The results in Figure 4-1 show that for class 4 cross-sections a higher resistance can be achieved. More exactly an optimal cross-section would lie at the edge of class 3 to class 4. Firstly, the global imperfection has a smaller influence on the relatively stiff cross-sections. Secondly, the local imperfections do although generating higher local stresses, they have reduced influence on the plate buckling. Applying the methodology from the design codes, we can see that good agreement can be reached with the proposed buckling curves.

4.1.3 Semi-Closed Profiles – bolted cross-sections

The high number of design parameters the problem leads to a demand for a huge number of results. To fulfil this demand with FEM, an automated modelling procedure was necessary. This task was performed in ABAQUS making use of Python scripting. The resulted script is a fully automated procedure that creates and solves (pre-processing and processing) models for columns of semi-closed polygonal profiles.

A continuous column with three joints is modelled with shell elements (Figure 4-2). The two joints are on the far ends of the column while the third in the middle, providing the possibility to apply the bending moment introduced by the diagonals (Figure 4-3). The assembly consists of 3 identical sector parts and three gusset plate configurations for the three joints, all of which are constrained together on certain nodes. The column length is aligned to the global z-axis.

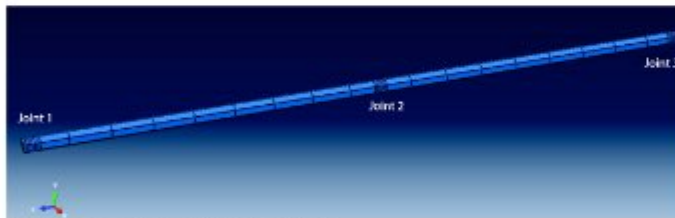


Figure 4-2: Model overview.

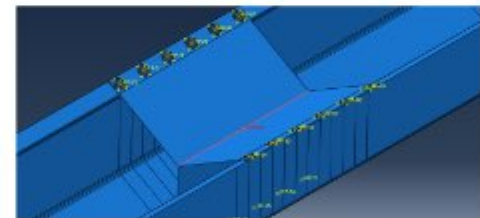


Figure 4-3: Middle joint rigid body

Hinges are considered on the two far ends of the column (joints 1 and 3). Displacements on global x, y and z are restrained on the one end which serves as the base of the column (joint 3). Lateral displacements (on x and y) are restrained on the other end where the load is applied (joint 1). Additionally, rotation around the z-axis (column torsion) is restrained on both ends for numerical stability. Only lateral displacements are restrained on the middle joint (joint 2). All boundary conditions are applied on a reference points which are coupled as rigid body to the profile edges and gusset plate configurations of each joint, see Figure 4-4.

The model is solved with RIKS analysis including non-linear geometry, effectively resulting to a geometric and material non-linearity analysis with imperfections (GMNIA). A target value calculated as $N_{pl,Rd} = f_u \cdot A$ is given to the compression load. The minimum required incrimination is varying depending on the non-linearity of each model and convergence problems are occasionally faced.

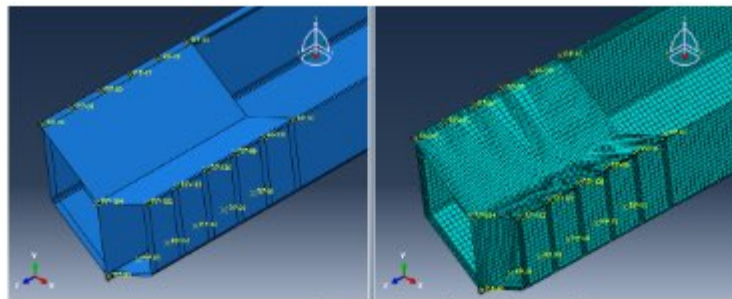


Figure 4-4: End joint detail and meshing

After the successful completion of the script execution, the user is presented with the two models (static model for imperfections and RIKS compression model) while the RIKS analysis is under process. After the solver finishes, the results contain stress and strain components for the model, von Misses stresses, nodal displacements and load-displacement curves. To this point, the post processing of the results has to be done manually.

An extra script is written to gather the maximum resistance results from a number of analyses outputs. Before it can be reliably used, it has to be made sure that the RIKS analyses is capable of increase the load at least up to the ultimate load and beyond that displacement. Currently, some cases are unable to converge when non-linearity becomes severe. Although it seems that the solver exits right before the ultimate load, this part is still in progress.

An initial study has been performed using the ABAQUS and the previously described python code. The study included analyses of 54 different models. The following parameters were varied in the parametric pre-study:

- Profile diameter (diameter of the circumcircle)
- Cross-sectional slenderness (plate thickness)
- Flexural slenderness
- Bolt spacing

All the models shared the following fixed characteristics:

- Hexagon profiles
- Imperfections introduced by the four first eigen modes of a buckling analysis
- Elastic-plastic material with $f_y = 355$ MPa

The models' parameters matrix is given in *Table 4-3*.

Table 4-3: Investigated parameters for the three frame typologies

Parameter	Range of values
Profile diameter [mm]	500-700-900
Plate thickness [mm]	7-9, 10-12, 13-15*
Flexural slenderness, λ	0.65-1.00-1.25
Bolt spacing, s/d [mm]	3, 4, 5

*One pair of thicknesses for each diameter, $t = 7-9$ mm for $d = 500$ mm, $t = 10-12$ mm for $d = 700$ mm, $t = 13-15$ mm for $d = 900$ mm.

The results of this initial study showed that the failure mode of such columns is strongly influenced by the distortional buckling of the three individual sectors. Distortion of the single sector cross section occurred between two consecutive bolts. Significant interaction with flexural overall buckling was also observed, especially for the higher slender cases.

The elastic buckling analysis of FE models showed that the studied models have predominant distortional buckling as the first buckling mode. Some of models buckled in flexural and flexural-distortional buckling mode. For this type semi-closed built-up column composed of folded plates, there is no expression in Eurocode for the critical distortional buckling load.

The RIKS analysis considering material-geometrical non-linearity and initial imperfections showed predominantly distortional buckling failure as well. Models with high global slenderness $\lambda=1.25$, experienced distortional-flexural interaction, achieving significantly lower resistance than the ones

failed in pure distortional mode. Moreover, it was noticed that members with high distortional and global slenderness appear to have higher sensitivity on the geometric parameters.

The main outcome of the short initial parametric study was that for bolt spacing between 3 and 5 times the profile diameter, distortional buckling is apparent. To examine the limits under which distortional buckling is eliminated, smaller bolt distances need to be considered (see Figure 4-5)

For that matter, second short parametric analysis consisting of 6 models was configured. The bolting distances varied between 0.8 and 2.8 times the diameter, with a step of 0.4. All 6 models were 15 m long from joint to joint and had 600 mm diameter. The plate thickness was 13 mm resulting in a class 3 profile, classified as a CHS profile.

Through this study, it was observed that for bolt distances below 1.2 times the diameter, the column failed purely under overall buckling. Above that spacing, distortional buckling of the individual sectors occurred in combination with the overall buckling.

The resistance of the examined cross-sections is calculated according to EN 3-1-1 [18] and EN 3-1-5 [19]. For the resistance calculation, classification is performed for plated cross-sections, under the assumption that the creases effectively provide simply supported boundary conditions for the faces of the polygon. As described in 2.1 above, this assumption is valid for a small number of sides but becomes invalid as the number of sides increase.

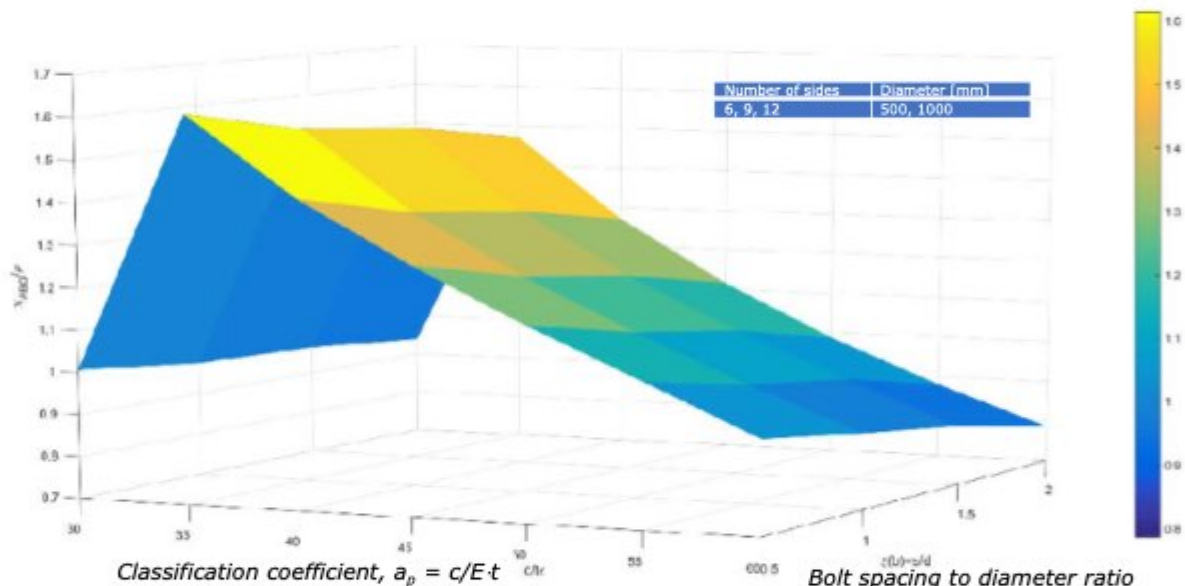


Figure 4-5: Ratio of the reduction factor based on FEM results over the effective area reduction factor from EN 3-1-5 [19] for a range of cross-sectional slenderness and bolt spacing

4.2 Experimental testing on connections

Four sets of tests on 12 specimens of gusset plate bolted connections was performed according to following parametrization with diagonal built-up from 2 sectors and connection with gusset plate and preloaded bolts (3 specimens each):

- Pylon section: nonagon welded (W)
- Pylon section: bolted built-up from 3 sectors (B),
- Pylon to diagonal angle of 90° (W90 and B90)
- Pylon to diagonal angle of 45° (W45 and B45)

4.2.1 FE modelling

A model of test specimens is built in ABAQUS software package. The finite elements type C3D8R (solid 8-node brick element with reduced integration) and SC8R (continuum shell 8-node hexahedron) are used to model structural elements. To capture accurately the stress behaviour in

the region around the bolt holes, where the higher stresses are more likely to occur, a dense mesh was made within the vicinity of the bolt holes.

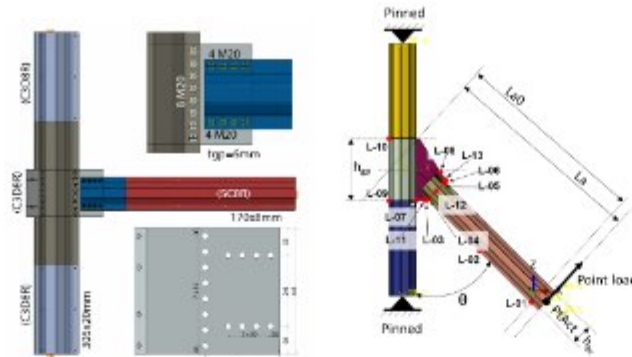


Figure 4-6: Connections' geometry

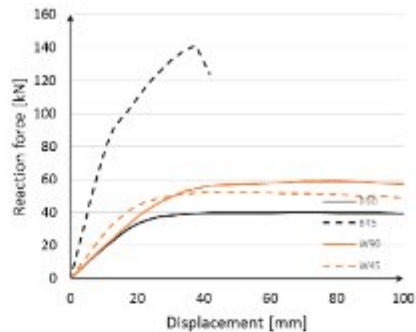


Figure 4-7: Predicted ultimate load

Three types of interaction were accounted as follows:

- *Tie constraint* that connects two surfaces so that there is no relative displacement between them, it was used to connect part with different element types
 - *Rigid body* constraint that allows simulating the planar behaviour of a cross-section and integrating the global mechanic response of the whole section (end of the members)
 - *Contact* that allows accounting for the interaction between surfaces which cannot penetrate and are characterized by friction sliding. "Coulomb friction" was used in order to describe the tangential behaviour with a friction coefficient equal to 0.4, while "Hard contact" is selected to characterize the normal behaviour

S355 steel grade with an elastic modulus of 210GPa, 355MPa yield stress and 510MPa ultimate resistance was adopted for pylon, brace and gusset plates. All bolts are high strength steel of grade 10.9 with Poisson's ratio of 0.3 and proof Young's modulus 210GP. True stress true strain material model was used, where $\varepsilon_{true} = \ln(1 + \varepsilon_{nom})$ and $\sigma_{true} = \sigma_{nom}(1 + \varepsilon_{nom})$. Bolt preload was introduced using thermal contraction of the bolt.

Four cases are analysed with the aim to have different failure modes:

- B90 with the gusset plate failure (buckling of gusset plate and net cross section failure)
 - B45 gusset plate net cross-section (brace bolts) failure
 - W90 local buckling of the pylon
 - W45 local buckling of the brace

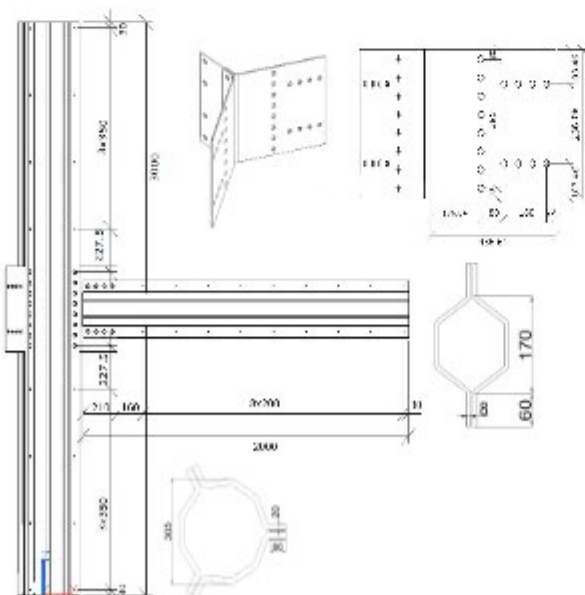


Figure 4-8: Test specimen B90

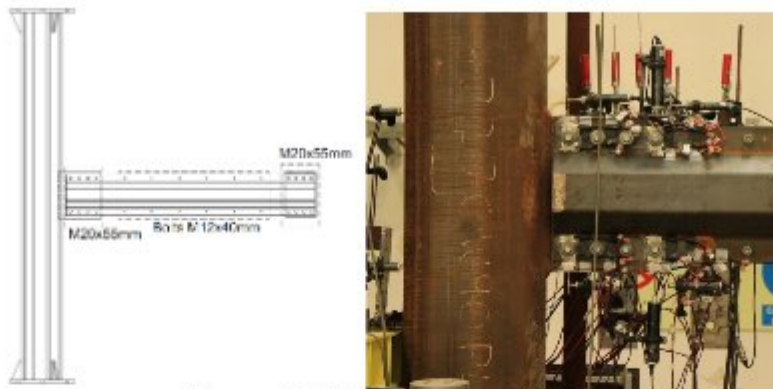


Figure 4-9: Test specimen W90

4.2.2 Pylon-Diagonal 90°

Pylon specimen is 3m long, composed of three cold formed segments and providing openings every 120°. Diagonal is 2m long, composed of 2 segments and providing openings every 180°, see *Figure 4-8* and *Figure 4-9*. Joint configuration is positioned in the middle of the pylon. It is composed of 3 gusset plates bolted together, connecting all segments of pylon and brace. Bolts used in the connection are M20 grade 10.9, while along the pylon and diagonal for connection of segments are used bolts M12. The loading is applied monotonically, in the vertical direction, at the end of brace with displacement control at constant speed of 0.02mm/s. The maximal displacement applied is 200mm.

To extract the relevant test information, assemblies are instrumented according to the scheme shown in *Figure 4-10*. The displacements are measured using displacement transducers. Strain gauges are used to measure the surface deformation.

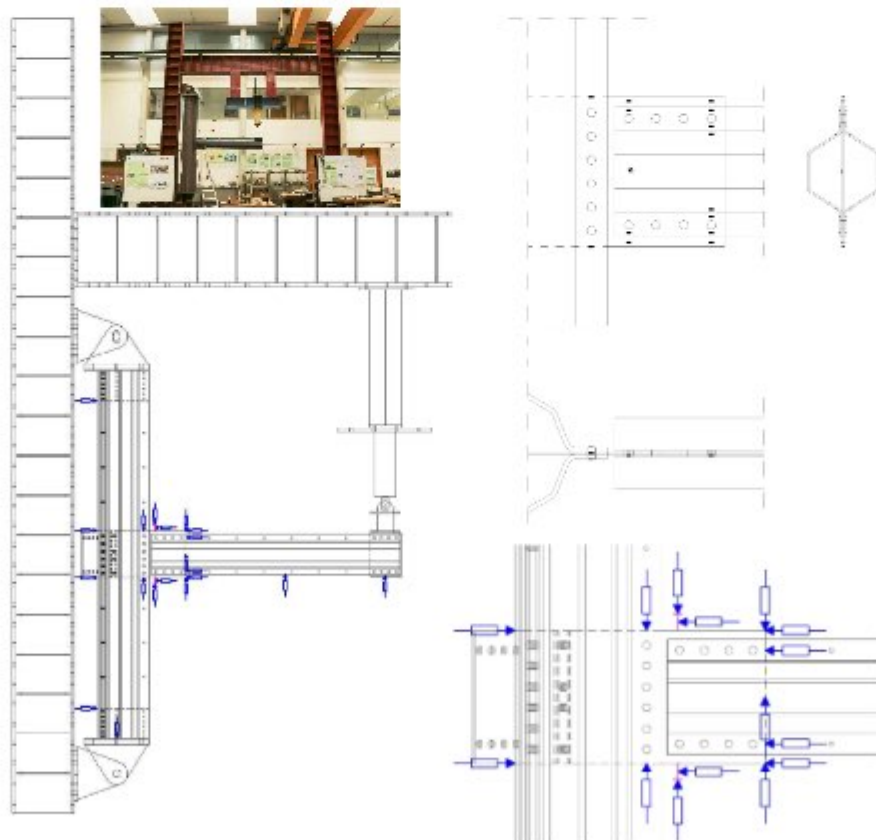


Figure 4-10: LVDTs and Strain gauges disposition

4.2.3 Pylon-Diagonal 45°

The 45° connections have the same pylon and brace configuration and length as 90° connection. The gusset plate geometry is changed in order to accommodate the different angle between the pylon and the brace, see *Figure 4-11* and *Figure 4-12*. Bolts used in the connection are M20 grade 10.9 in B45 connection, while in case of W45 connection the bolts used are M12 grade 10.9. Along the pylon and diagonal for connection of segments are used bolts M12. The loading is applied monotonically, in the vertical direction, at the end of brace with displacement control at constant speed of 0.02mm/s. The maximal displacement applied is 200mm. To extract the relevant test information, the displacement transducers are used to measure displacements and strain gauges to measure the surface deformation.

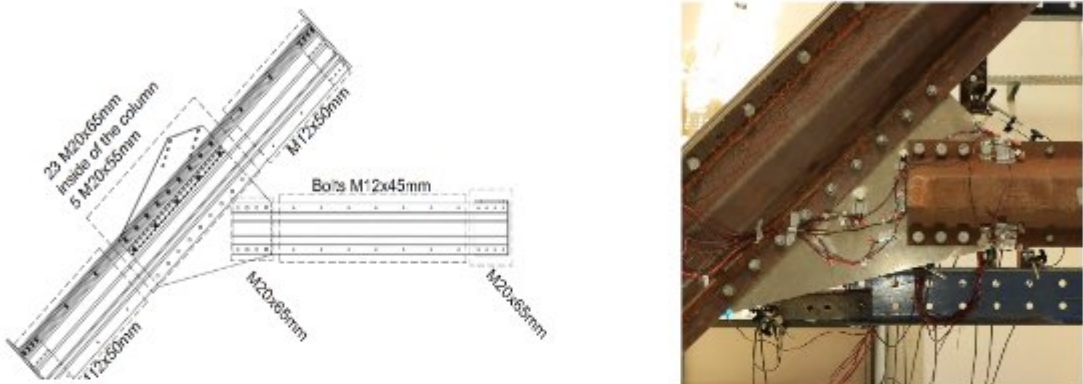


Figure 4-11: Test specimen B45

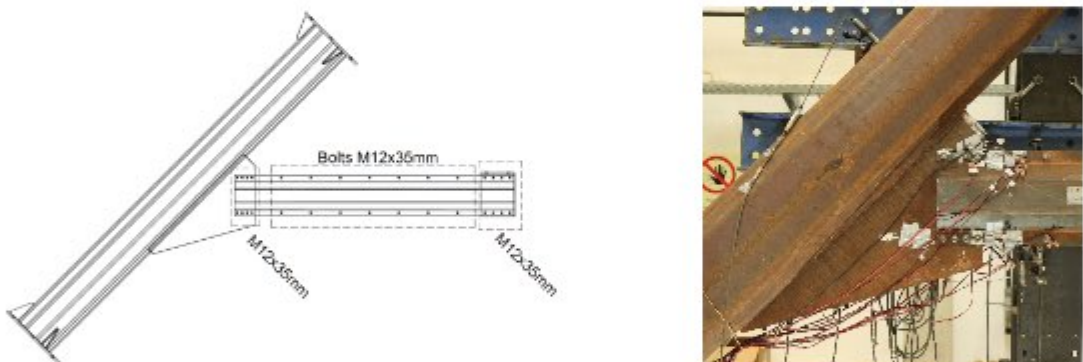


Figure 4-12: Test specimen W45

4.2.4 Results

Connection behavior is represented by the moment-rotation curve. The bending moment acting on connection corresponds to applied load (reaction force of the brace end) multiplied by the distance between the pylon axis and the point where the load is applied at the end of the brace.

Test B90 demonstrated a global and local behavior in line with the predictions. According to preliminary numerical study predicted failure mode was buckling of gusset plate in the compression zone, and gusset plate bearing in tension zone. The same failure mode was observed in the experiment (*Figure 4-13*). The maximal displacement applied was 100mm. The ultimate load observed in the tests was 48.5kN, 47.4kN and 48.0kN for T1, T2 and T3 respectively. The ultimate load achieved in the test is higher than 40.0kN, what was predicted in the preliminary numerical study. This difference is due to the material model used in the numerical study (elastic perfectly plastic material).

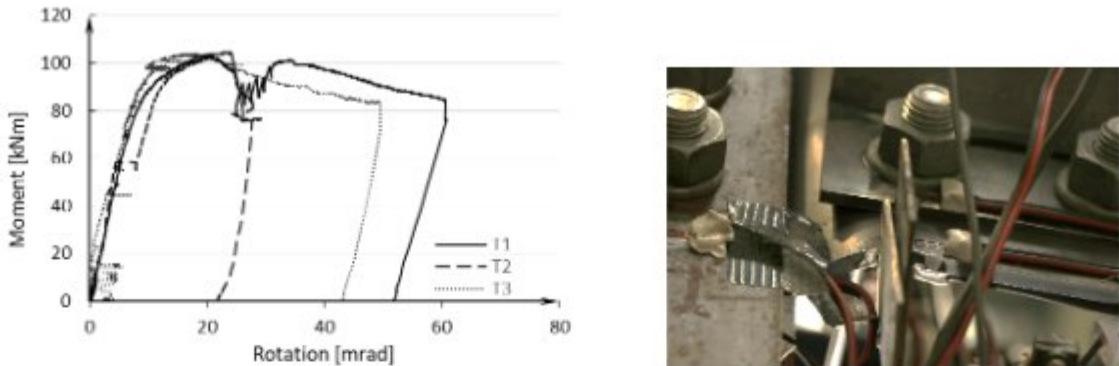


Figure 4-13: B90 moment-rotation curve (left) and failure (right)

Test W90 demonstrated a global and local behaviour in line with the predictions. According to preliminary numerical study predicted failure mode was buckling of brace in the compression zone, and brace bearing in tension zone. The same failure mode was observed in the experiment (Figure 4-14). The maximal displacement applied was 150mm. The ultimate load observed in the tests was 79.4kN, 79.0kN and 77.5kN for T4, T5 and T6 respectively. The ultimate load achieved in the test is higher than 58.9kN, what was predicted in the preliminary numerical study. This difference is due to the material model used in the numerical study (elastic perfectly plastic material).

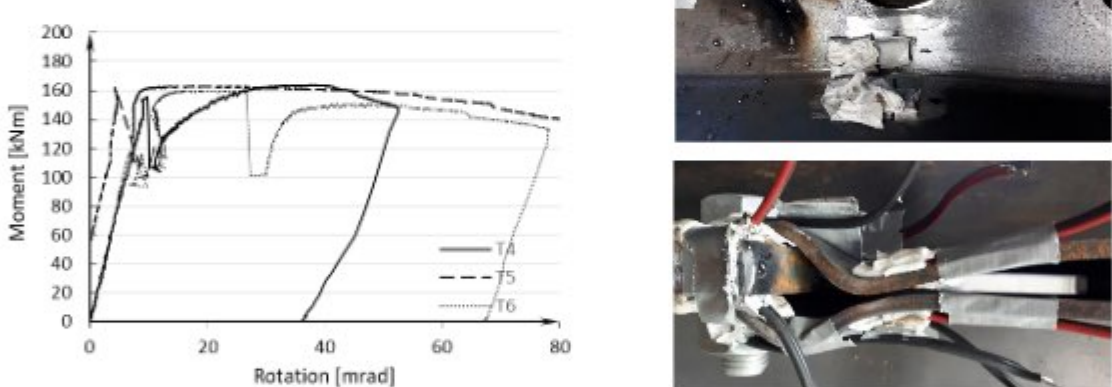


Figure 4-14: W90 moment-rotation curve (left) and failure (right)

Test B45 demonstrated a global and local behaviour in line with the predictions. According to preliminary numerical study predicted failure mode was buckling of gusset plate. The same failure mode was observed in the experiment (Figure 4-15). The maximal displacement applied was 100mm. The ultimate load observed in the tests was 125.0kN, 146.5.0kN and 127.1kN for T7, T8 and T9 respectively. The ultimate load achieved in the test is lower than 141.3kN, what was predicted in the preliminary numerical study. This difference is due to the material model used in the numerical study. The failure was due to instability which is governed by the elasticity of the material. The Young's modulus of elasticity used in the numerical study was 210GPa, while the Coupon test results have shown lower Young's modulus of the steel used for manufacturing the specimens.

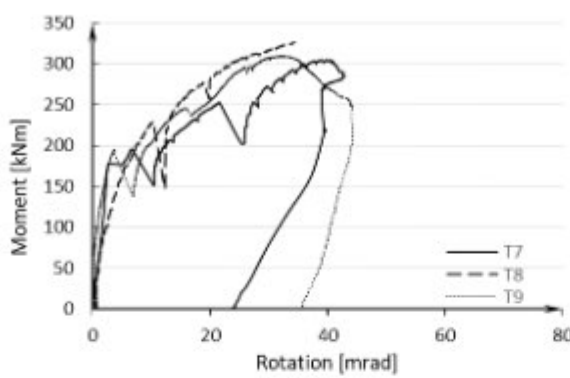


Figure 4-15: B45 moment-rotation curve (left) and failure (right)

Test W45 demonstrated a global and local behaviour different than predicted. According to preliminary numerical study predicted failure mode was buckling of brace in the compression zone, what is as it predicted in the preliminary numerical study. However, in tension zone brace block tearing was predicted and brace bearing was observed in the experimental tests (Figure 4-16). The maximal displacement applied was 150mm. The ultimate load observed in the tests was 53.0kN, 73.7kN and 58.3kN for T10, T11 and T12 respectively. The ultimate load achieved in the test is higher than 52.5kN, what was predicted in the preliminary numerical study. This difference is due to the material model used in the numerical study (elastic perfectly plastic material).

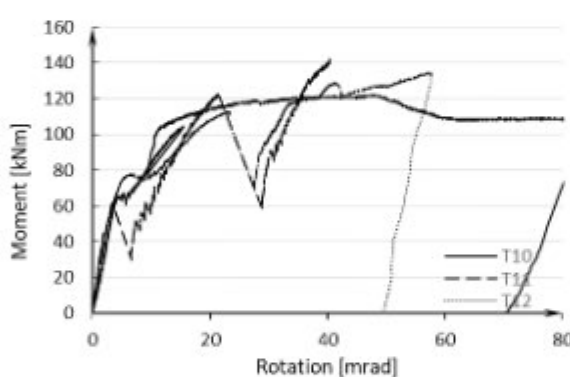


Figure 4-16: W45 moment-rotation curve (left) and failure (right)

4.3 Compression tests on pylons

4.3.1 Introduction

Polygonal cross sections constitute a separate class of cross sections. They fall into two major categories: closed (welded) and semi-closed (bolted). Extensive investigation of a number of problems associated to each of these two categories as been performed [48][51][8].

From the regulations point of view, the ultimate resistance of polygonal cross sections are not addressed in the framework of the Steel Eurocodes i.e. the General Rules EN1993-1-1 to EN1993-1-12 or the part addressing lattice towers EN1993-3-1 and EN1993-3-2. Some elements concerning the design of the welded sections, are found in a CENELEC norm (EN50341-1) intended for use by electrical / structural engineers for the design of overhead electrical energy transmission lines that dates back to 2001. In particular, polygons (welded) are used as mono-piles for the support of

electrical lines as an alternative to lattice towers. Some aspects of the ultimate resistance of the semi-closed polygons can be addressed via the provisions of EN1993-1-3 (thin walled, cold formed) but, as discovered, governing failure mechanisms are unfortunately not covered by the said standard.

On the other hand, the issue of rotational stiffness of the connections and the influence of it on the buckling length of the bracing elements of a lattice tower is already covered in EN1993-3-1 Annex G, Table G.2 for tubes and rods. As polygonal tubes ought to behave identically to their cylindrical counterparts, regulatory guidance on this subject may be considered as mature.

Therefore, the challenge of establishing the basic aspects of the resistance behavior of a type of cross sections was first faced, not as yet well-integrated into the structural engineering praxis. Subsequently, the problem of rotational connection stiffness was addressed

4.3.2 The research questions

Polygonal cross sections (PCS) come in two varieties: (a) closed (welded) and (b) semi-closed (bolted). *Table 4-4* gives the overview of the research plan:

Table 4-4: Overview of the research plan

1a	Compression resistance of welded (closed) PCS	parametric FE + tests
1b	Compression resistance of bolted (semi-closed) PCS	tests
2a	Rotational stiffness of joints of welded PCS	tests
2b	Rotational stiffness of joints of bolted (semi-closed) PCS	tests

A short discussion supporting the aforementioned choices is presented as follows.

The compression resistance of welded PCS is the first and foremost issue to start from if this type of members is to be used in structures of such size and importance as wind turbine towers. As said before, there is a standard in existence [11] covering PCS (closed) but there is a number of limitations to it:

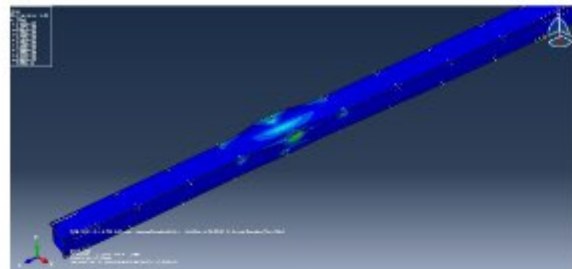
- i. only steel grades S235 and S355 are covered whereas now days grades up to S900 are potential design choices
- ii. the maximum number of polygon apexes is established to 18.

Therefore, the research questions that had to be answered concerned the validity of the failure mechanism assumed for the resistance predictions of EN50431 beyond the S355 and the 18 apex limit. This basic assumption boils down to that, the edges of the polygonal prism remain straight at failure and therefore, each facet fails as a von-Karman in-plane stressed plate according to EN1993-1-5. The LTU-team investigation found that increasing the number of vertices over 18 induces a different type of failure where edges buckle and the ultimate load approaches that of a cylindrical shell as the number of vertices increases. A limit between plate-type failure and shell-type failure was established for steel qualities up to S700 and this was verified by the Group A of experiments (9 specimens were tested).

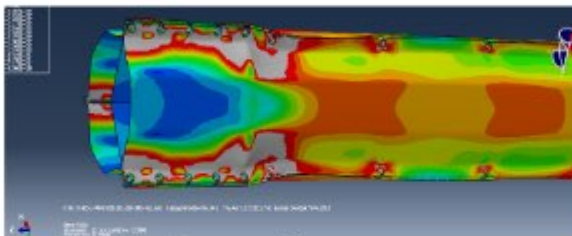
Group B of the experiments is required in order to investigate the influence of the joint detail on the ultimate resistance of welded PCS when a converging diagonal is loaded so as to cause joint rotation. Three such tests were performed.

The compression resistance of semi-closed PCS (SC-PCS) proved to be a rather more complicated subject. In the case of a hexagonal tower, these cross sections are made up of three independent 120 degree sections (sectors) bolted together over their lips (or four 90 degree sections for the square tower). Between the bolts and away from joints, each of the three 120 deg sectors of the SC-PCS, acts as an open cross section subjected to the provisions of EN1993-1-3: the expected mode of failure is a lip failure as given in Figure 4-17-a. This mode of failure always emerges when the column axial force is imparted upon the shell via boundary membrane stresses at the two ends [18][19]. However when the load is applied via the star-shaped gusset plate (as in practice) the failure mechanism is entirely different and, as evident from Figure 4-17-b is localized around the gusset plate and is due to the insertion of the axial force from the gusset plate directly to the lips (grey areas indicate yielded regions). In order to remedy this type of failure which occurs rather prematurely, a special form of gusset plate had to be used so that the gusset stiffness is gradually

reduced to match that of the columns as shown in Figure 4-18. This strong dependence of the column ultimate compression resistance to the form of the joint increases the complexity of the investigation way above what is feasible within the resources and the time frame of the project. Therefore, the issue of ultimate resistance of realistic SC-PCS was not tested within the context of sub-task 4.3



(a)



(b)

Figure 4-17: failure of SC-PCS when load is inserted smoothly (a) and when load is inserted realistically via the star-shaped gusset plate (b)

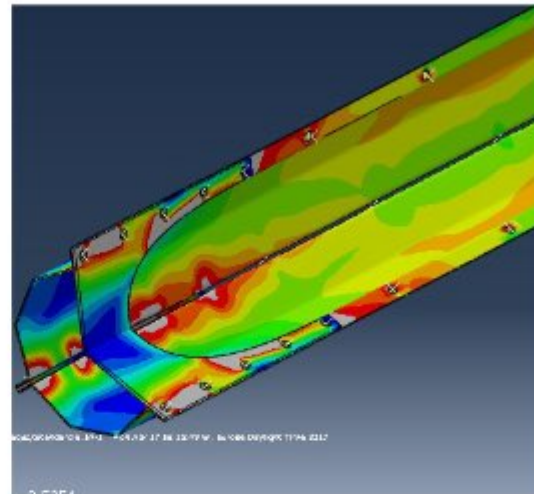


Figure 4-18: star-shaped gusset plate with varying cross section

Rotational stiffness of welded (closed) PCS (W-PCS). Two welded specimens were included in the group C of experiments (one with the gusset plate continuously welded to the pylon, another with intermittent welds between the two). Also welded specimens with a moment causing rotation to the pylon joint are included in Group B.

Rotational stiffness of bolted (semi-closed) PCS (SC-PCS). Four bolted specimens were included in the group C of experiments.

4.3.3 Experimental program for Group A

Summary: Compression tests up to failure. The tests are prescribed for welded pylons. The contract requires a joint detail along with diagonals to be included in the specimen configuration. However, the diagonals are not to be loaded but the contract is explicit in prescribing those as bolted as well as a bolted joint. Three such tests are prescribed. Nine tests were performed.

4.3.3.1 General considerations on the design of the experimental matrix

This part of the experimental aimed to the determination of the question of ultimate failure of welded PCS pylons. The currently available regulatory instrument is EN50341 [25](Annex K: Steel poles) and is based mainly on the research of Bulson [9]. The idea behind this standard is that edges between flat facets remain straight at failure. This allows each facet to be treated as a separate plate classified and resisting according to the von-Karman – Winter concepts as incorporated in EN1993-1-5.

The first issue one faces with a PCS is that of classification. The consequence of the straight edges at failure hypothesis is a pure compression Class-IV limit b/t equal to 42ϵ just like EN1993-1-1 (Table 5.2, sheet 1). However the two important questions left open by EN50341 are:

- (a) the validity of straight edges hypothesis for grades above S355
- (b) the resistance of a PCS with more than 18 vertices

The fact that such an investigation is in the interest of efficient utilization of material is shown in the example of a 5m long, S355 PCS column with a gross area of 100cm^2 :

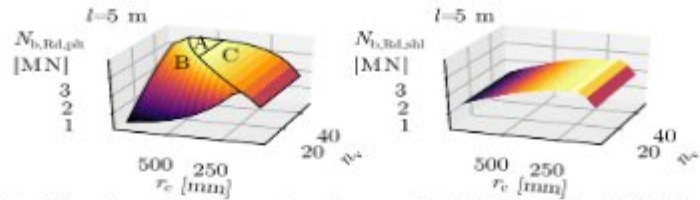


Figure 4-19: ultimate resistance of column: EN50341 (left), En1993-1-6 (right)

The independent variables here are r_c the average radius of the PCS and n_v the number of its vertices. What is depicted on left plot of Figure 4-19 is the surface of ultimate resistance of the column taken as the minimum of (A) yielding, (B) local buckling on the face plates with the rigid edges hypothesis taken as valid and (C) flexural buckling calculated with the gross cross section. On the right plot, the shell resistance according to EN1993-1-6 is given. What is evident here is that flexural buckling resistance (surface C) improves as the radius increases. On the other hand, plate buckling becomes governing for high r_c values because as c/s area A is constant, the plate width of each facet increases with r_c : this is given by surface B. Note also that plate buckling improves as n_v increases. At the point where the flexural buckling and local buckling surfaces intersect, there appears a plastic plateau (surface A).

The conclusion is that the best utilization of the material is achieved at a very narrow region of high radii and high numbers of vertices **not** covered by EN50341. Moreover one can see that, for this optimal region of (n_v , r_c) values, the *shell* resistance (i.e. the EN1993-1-6 resistance of a cylindrical shell with the same thickness and circumference as the PCS) is substantially lower. The question therefore arises what is the point when the PCS edges can no longer contain failure deformation patterns (*spillover* of buckling between adjacent facets) and whether the use of the shell buckling resistance is an appropriate methodology to follow beyond a certain number of vertices.

Extensive parametric numerical simulations (of the GMNIA type) were undertaken to determine the necessary experimental matrix. During the numerical investigation phase, it was discovered that the type of failure mechanism as well as the value of the ultimate load, is largely predetermined by the imperfection pattern introduced beforehand. Two imperfection configurations emerged as governing over two separate regions of the search space (n_v , $p_c=b/\pi t$): *plate type* imperfections contained inside each facet (straight edges hypothesis) and "distortional" imperfections (affecting straightness of edges).

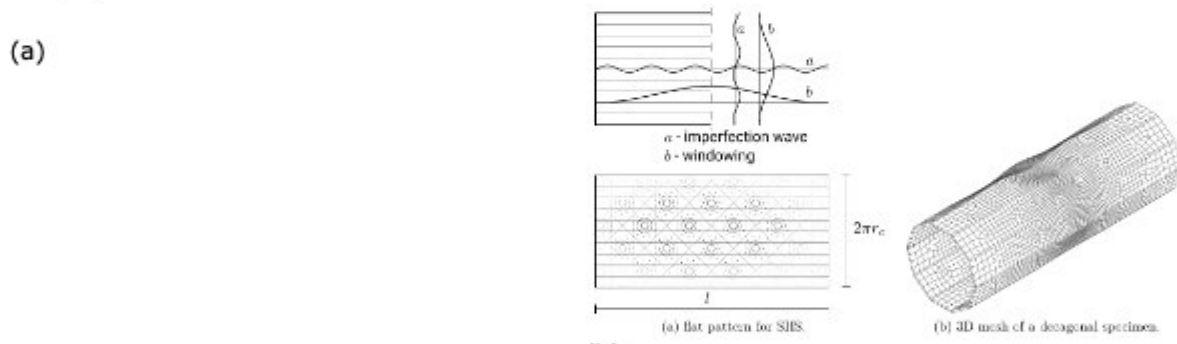


Figure 4-20: plate type imperfections (a) and "double spillover" imperfections (pairs of consecutive edges distort in the same sense) (b)

The "plate type" imperfections are depicted in Figure 4-20(a) and generally govern the relatively low plate slenderness cases; the number of circumferential waves is equal to half the number of vertices. In Figure 4-20(b) the so called "double spillover" imperfection pattern is shown: the number of circumferential waves is $\frac{1}{4}$ of the number of vertices and there is a phase offset in the circumferential wave so that there exist consecutive edges on the same imperfection half-wave, a fact that produced minimum ultimate load results.

Comparative material utilization data for various imperfection types are given in Figure 4-21.

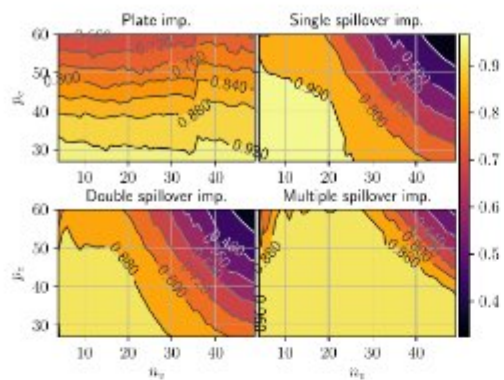


Figure 4-21: $\sigma_{\text{GMNIA}}/f_y$ for various imperfection patterns (Fabrication Class A. S355)

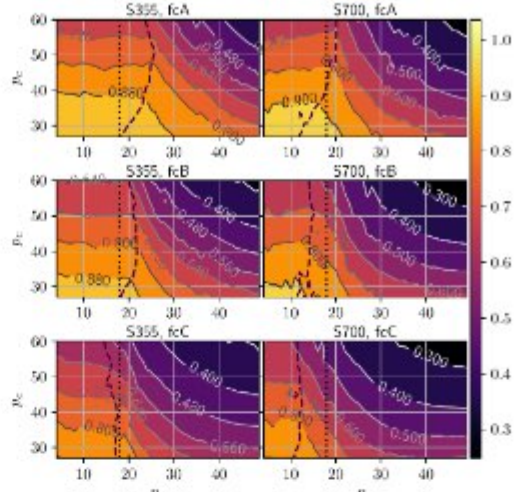


Figure 4-22: dashed line is the boundary between plate-dominated (left) and edge-distortion-dominated (right) collapse mechanism regions ($\min(\sigma_{\text{GMNIA,shl}}, \sigma_{\text{GMNIA,pit}})/f_y$).

The parametric numerical analyses were performed with the *plate* and the *double spillover* imperfection. The lower ultimate axial resistance value between the two was taken as the FE-calculated design resistance of the column. It was observed that the $(n_v, p_c = b/\xi t)$ search area is separated in two regions: one where the straight-edges-hypothesis collapse mechanism produces the lowest ultimate load and, an other, where the distortional (double spillover) mechanism emerges as governing. The results are shown in Figure 4-22.

Finally, a formula was constructed for the boundary between the two regions so that the designed may know whether to use the plate or the shell approach:

$$n_v \leq + \frac{p_c - 27}{\zeta}, \quad 27 \leq p_c \leq 60$$

where

$$\zeta = (364U_0^2 - 5U_0 + 0.021)10^{-3}$$

$$\xi = 24 - 0.02f_y$$

$$U_0 = \max[\Delta w/l_e, \Delta w/l_m]$$

Figure 4-23 failure regions boundaries

4.3.3.2 The Group A tests

The experimental program had therefore to verify the qualitative result of Figure 4-24 by way of comparing post critical responses and collapse loads. The matrix was chosen to be of S700, following the idea of investigating around the failure mechanisms boundary lines and the exact geometrical dimensions of the specimens (SP) are given in the Table (see Figure 4-24)

	SP1	SP2	SP3	SP4	SP5	SP6	SP7	SP8	SP9
n_v	16	16	16	20	20	20	24	24	24
p_c	30	40	50	30	40	50	30	40	50
r_c , [mm]	142	186	230	175	230	190	108	183	227

Figure 4-24 Matrix of specimens (S700)

All specimens were made of 3mm thick S700MC (Strenx) material only 6, 8 and 9 were made of 2mm thick plate (Salzgitter) for reasons of limiting exterior dimensions.

The specimens were laser-scanned for an estimation of the magnitude of the imperfections, in particular the deviation of edges from straightness the result is shown in Figure 4-25.

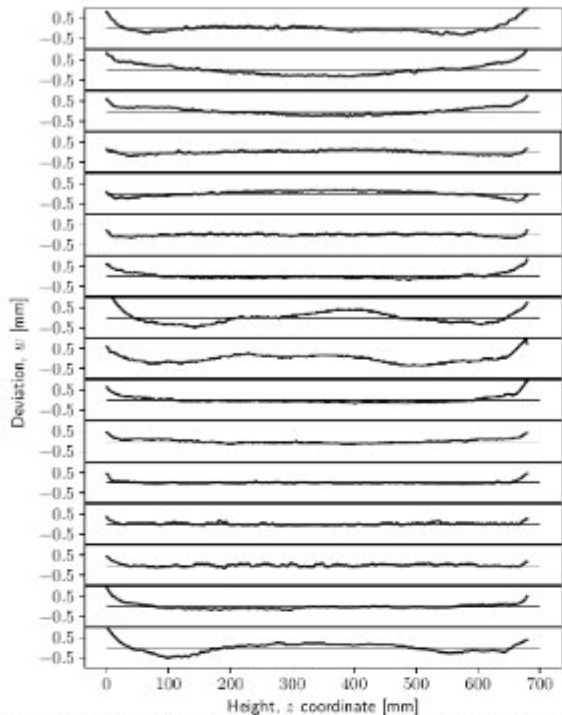


Figure 4-25: Measured edges deviation from straightness, specimen SP1 and final test set-up at COMPLAB.

The results of the experiments are summarized in Figure 4-26 in the form of stress / strain (average) diagrams. The failure patterns that emerged are shown in Figure 4-27. The qualitative conclusions can be summarized as following:

- Regular Convex Polygonal Sections (RCPSs) can be grouped in two categories based on how strongly they are attracted towards either a plate-like or a shell-like failure.
- Two regions of the search space (plate failure governed and spillover failure governed) were identified via the FEM analyses and were verified through the experiments.
- The provisions of EN 1993-1-5 and EN 1993-1-6 were checked and found to be suitable for calculating the design resistance within each of the two regions.
- An empirical formula was developed for the boundary between the two identified regions. The proposed formula returns the number of vertices, n_v , for an input of facet plate slenderness, p_c , yield strength, f_y and imperfection amplitude U_0 and suggests which of the two Eurocodes should be applied.
- By comparing between models with and without initial imperfections, RCPS were proved to be highly sensitive.
- The eigenmode-affine imperfection pattern was proved improper in certain cases, for which the double-spillover imperfection pattern yielded lower resistance.

The assessment of imperfections on nine specimens, fabricated in two different workshops with different materials, showed that they were within the tolerances of EN 1090-2 (facet flatness) and of the fabrication class A of EN 1993-1-6 (edge straightness).

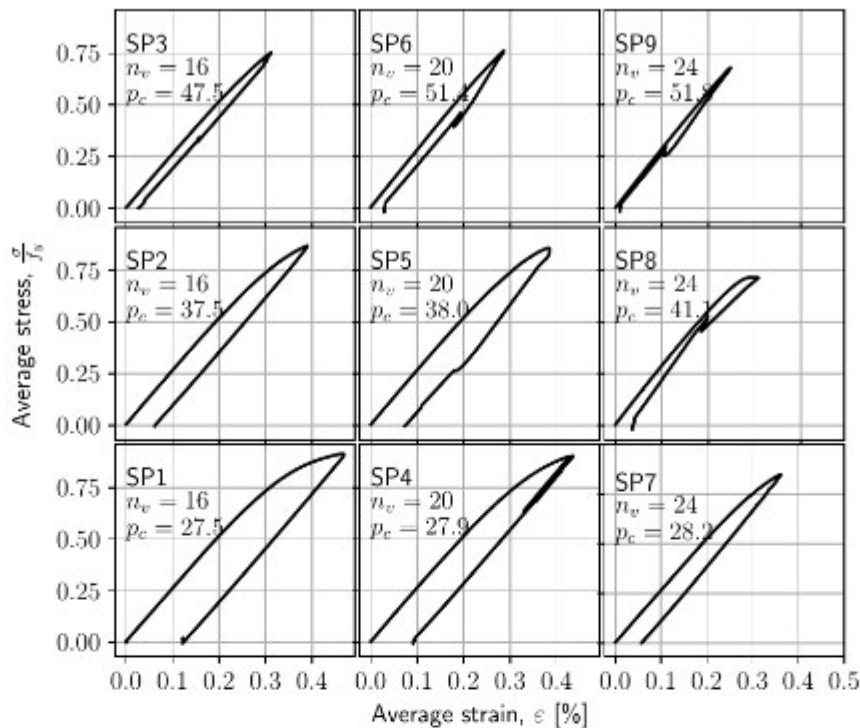


Figure 4-26: Average stress / strain date as recorder from the experiments

Figure 4-27: Laser-scanned failure patterns that developed in the specimens during testing

4.3.4 Experimental program for Group B

In this group of experiments the two branches of the cross-like specimen received opposite direction vertical forces (one upwards the other downwards).

As the objective was to measure the rotational stiffness of the joint in load levels close to the failure of the pylon (cross section area 40cm^2 , S700 steel grade therefore 2800kN squash load), a 2000kN axial force was applied. The forces at the ends of the cross branches were 10kN each (see Figure 4-28 and Figure 4-30)

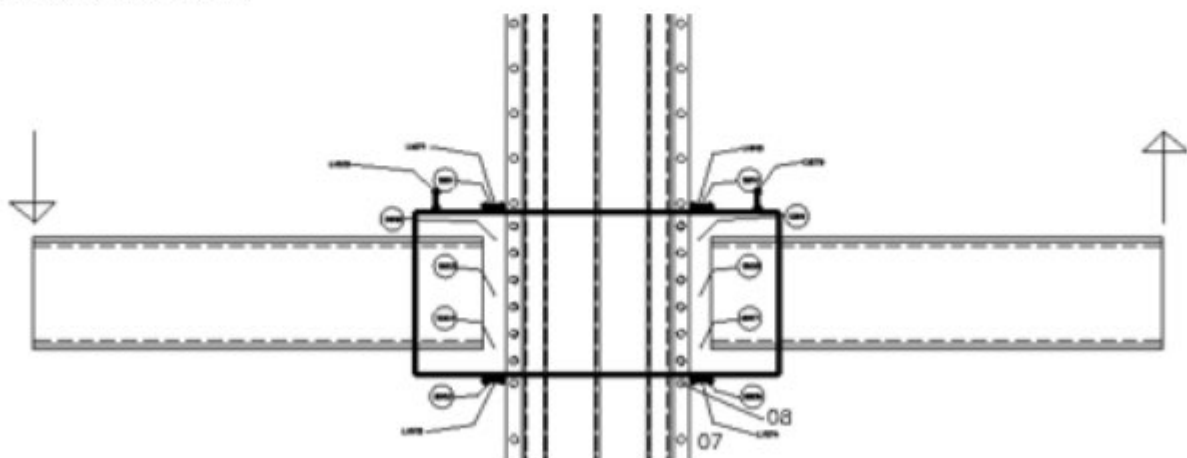


Figure 4-28: Load application pattern in group B experiments

In the case of semi-closed cross polygonal pylon sections, the factor that possibly alters the rotational stiffness of the joint as far as the pylon may affect it is the density of the bolting. In Figure 4-29 the bolts connecting the two 180deg sectors making up the cross section are numbered.

The following variations of bolting were tested:

scenario A: all bolts #1 - #8 in place

scenario B: bolts #8, #6, #4, #2 taken off

scenario C: bolts #1, #2, #4, #5, #7, #8 taken off (only #3 and #6 in place)

scenario D: all bolts except #5 are taken off

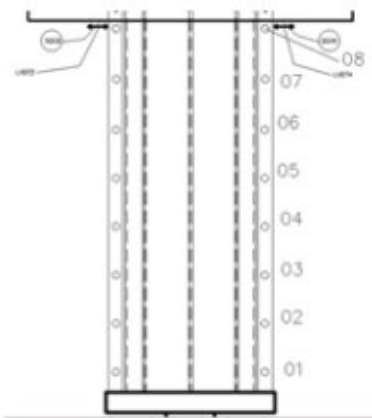
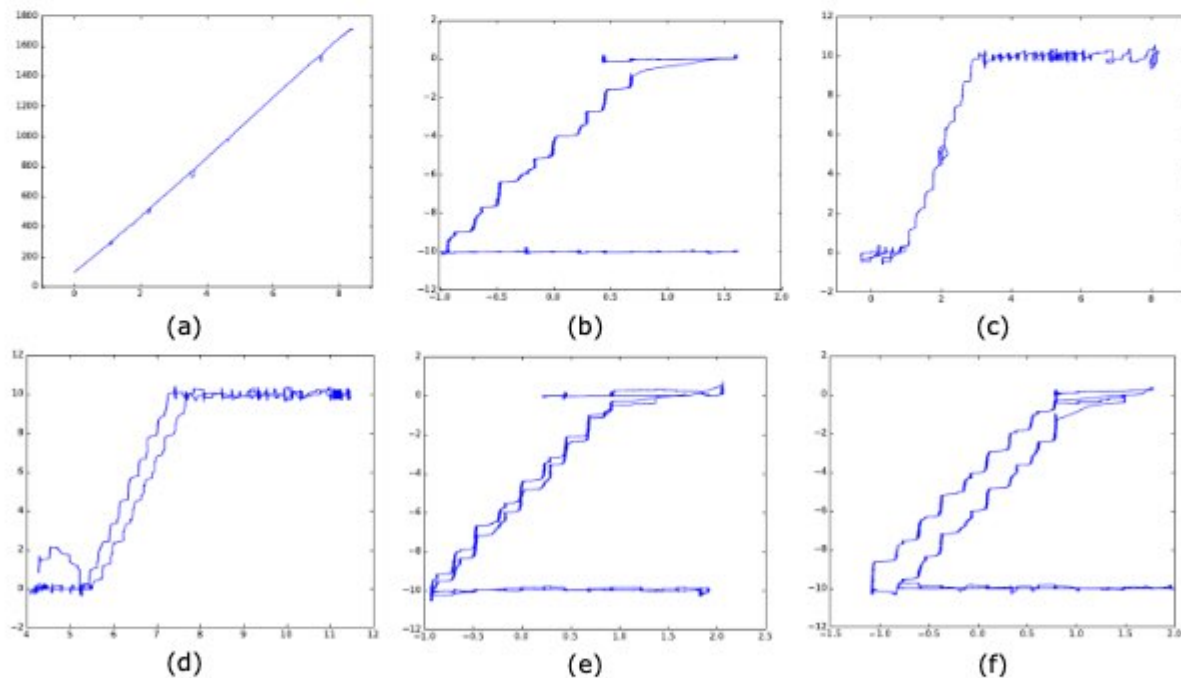


Figure 4-29: Bolts numbering in group B experiments



Figure 4-30: General setup

The results in Figure 4-31 showed that the rotational stiffness of the joint remains unaffected by the axial load in the pylon and by the bolting density at the lips of the 180 deg sector pieces.



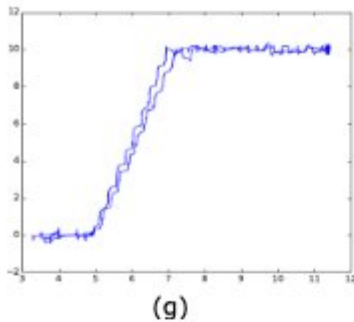


Figure 4-31: Load [kN] vs. displacements [mm] (a) scenario A pylon Axial displacement; (b) scenario A left actuator; (c) scenario A right actuator; (d) scenario B left actuator; (e) scenario B left actuator; (f) scenario D left actuator; (g) scenario D right actuator

4.3.5 Experimental program for Group C

4.3.5.1 Description of the type of specimens used - modifications

The experimental setup of this group depicted in the right part of Fig. 4.7 of Annex B of the contract had to be modified, since the pylon part of the specimen is absolutely mandatory to be of the same length above the joint as it extends below it. However, having to use a specimen being of double height required the use of a different strong frame. The problem arose with the issue of laterally stabilizing the arms (yellow horizontal) and the arm-jacks (light yellow verticals) as the mesh of attachment holes of the laboratory strong floor is too coarse.

There also exist another issue making the 120deg angle between the arms of the cruciform specimen detrimental to the validity of the results. In Figure 4-32 the FEM-generated deformed shape of such a specimen is depicted. The column (shown in light green) assumes an S-like deformed shape due to the eccentric application of the jack forces (red arrows) at the tips of the branches (shown in white).

Figure 4-32 column with arms forming a 120deg angle: deformed configuration.

The bending moment introduced in the middle of the column gives rise to shear forces. Given that, the bolts connecting the lips of the three 120degree sectors of a bolted specimen are not preloaded, shear lag in the specimen, has to be expected. In other words, it is not possible to assess the part of the force application point displacement owing to the joint deformation and that owing to the deflection of the column itself: the reason is that, the bolted column is not guaranteed to behave as a Bernoulli beam unless assembled via preloaded bolts along the 120deg sector lips. Using preloaded bolts to connect the three 120deg sectors of a PCS although easily done in the lab, would present a formidable maintenance nightmare for the end-user of such a tower. It was therefore deemed irrelevant to perform an experiment for a structural element unlikely to be found in practice.

Following these considerations a FE study was undertaken to examine differences of joint stiffness in the case of an angle-between-the-arms equal to 180° instead of 120° : the results of the analysis showed that the differences are insignificant and therefore it was decided that the experiments could be performed with specimens having the form of a planar cruciform assembly.

4.3.5.2 Description of the specimens and loading procedure

The 6 specimens with varying joint details were fabricated as shown in Figure 4-33 according to the parametrization given in Table 4-5.

Table 4-5: Specimens for testing

#	Specimen type	Characteristics
C-1	bolted (6xM16 pretensioned)	Gusset plate bolted to column at all six bolt positions
C-2	bolted (4xM16 pretensioned)	bolts #2 and #5 attaching gusset plate to column lips are removed
C-3	bolted (6xM16 bearing) over sized	bolts (non pretensioned) at all positions #1 - #6

C-4 **bolted** (4xM16 bearing) over sized

New boreholes diameter 19mm; bolts (non pretensioned M16) applied only at positions #1, #3, #4, #6

C-5 **welded**

No specimen modification

C-6 **welded (intermittent)**

fillet weld cordons exist only along the middle 50% of the gusset plate connecting the cross arms

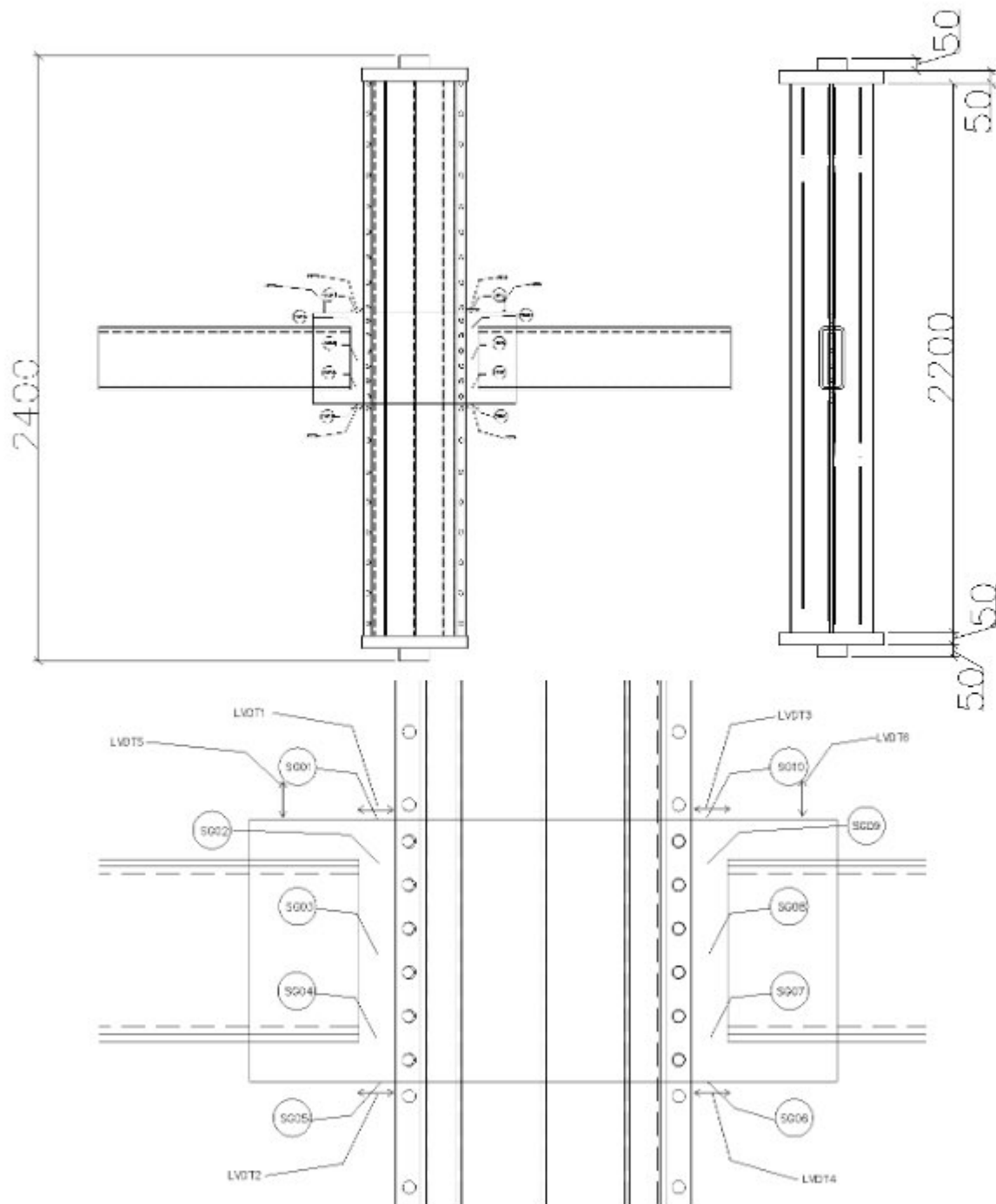
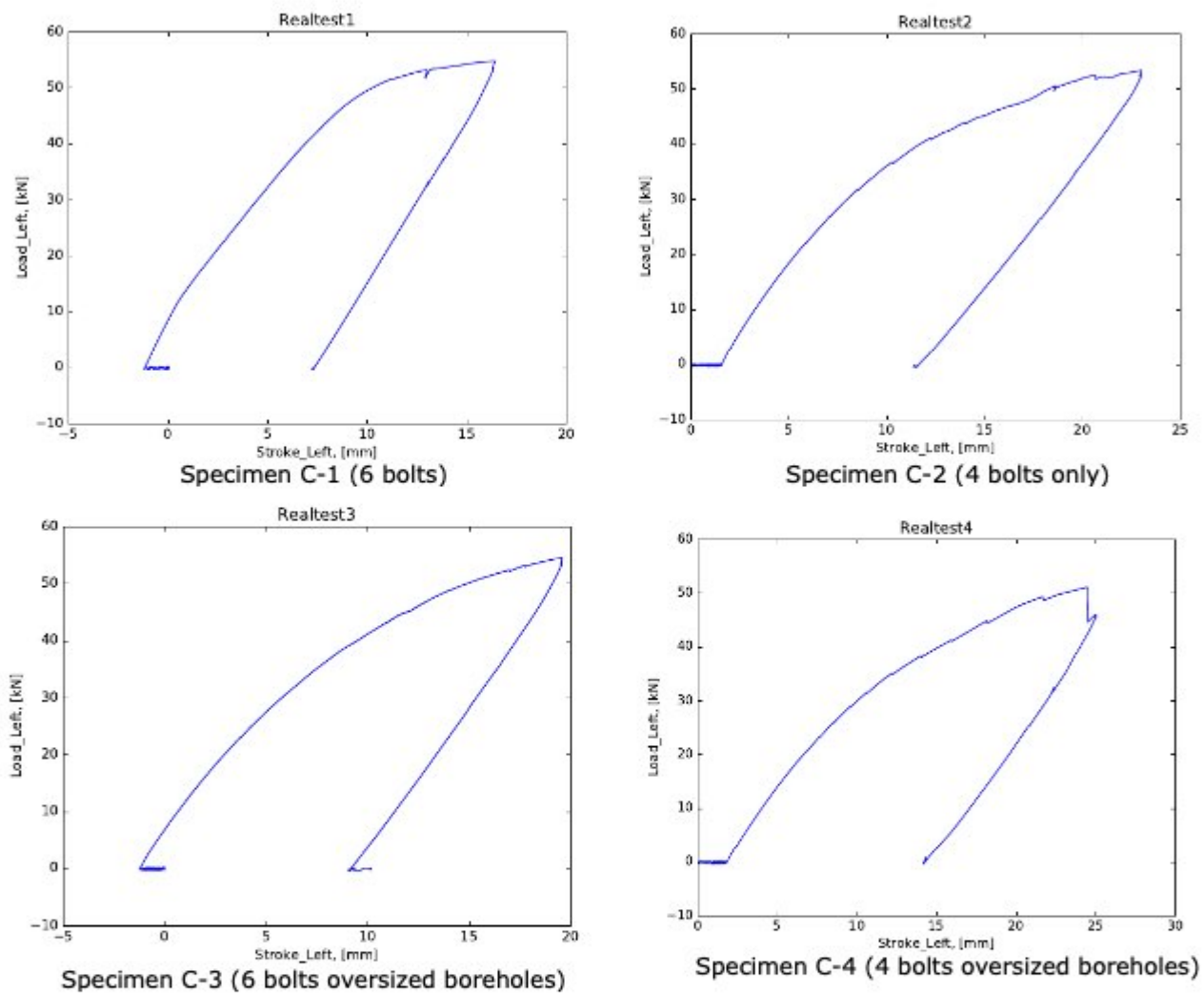


Figure 4-33: Planar cruciform specimen and Instrumentation on the gusset plate (welded specimen)

The results are briefly presented in Figure 4-34. Load application procedure was following:

- (a) increase main octagonal column axial load to approximately 20% of it's squash load (430kN) using a jack.
- (b) increase the load of the arms pistons to 100kN in 5kN steps (synchronized)
- (c) decrease the arms pistons load to zero (pistons synchronized)



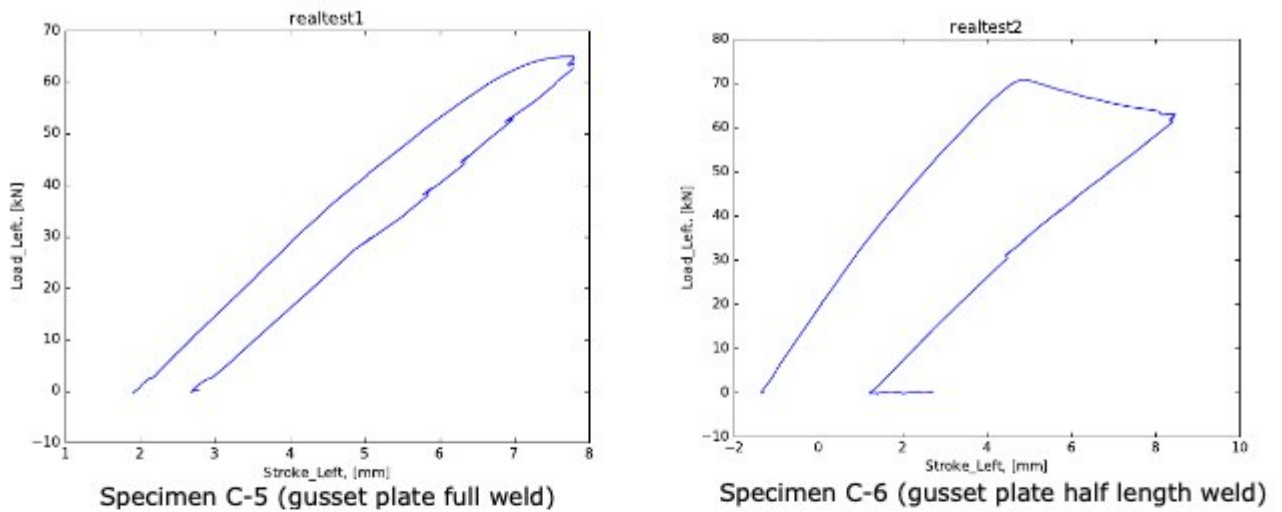


Figure 4-34: Load-displacement results od tests

4.4 FE models validation and parametric study

The behaviour of the proposed joint joints is important to the global behaviour of the tower structure and current design codes do not provide information on this type of joint. Investigation of advantages and disadvantages of welded and bolted cross-sections of profiles used in proposed connections of the lattice part was carried out in Task 4.1. Task 4.2 focuses on testing and evaluation of the behaviour of the proposed joints. As described in Task 4.2, in the test configuration the secondary member of the connection is referred as brace while the main member as pylon. Two brace-to-pylon angles are considered, i.e. 45° and 90° . The gusset plate (connecting the brace and pylon) is always bolted to the brace and either bolted or welded to the pylon.

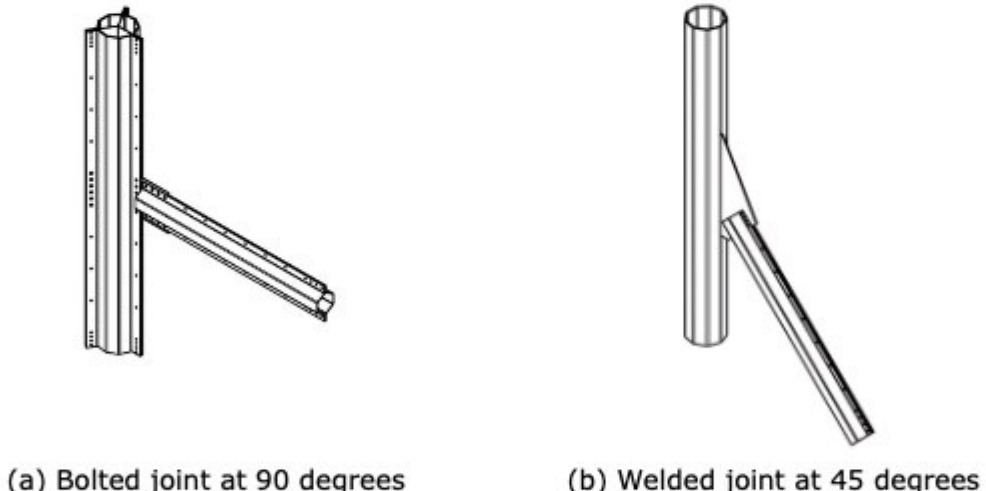


Figure 4-35: 2D joints designed for test programme in Task 4.1

The two types of joints designed and tested are shown in Figure 4-35. Important geometric dimensions of the components of the four joint specimens are summarised in Table 4-6.

Table 4-6: Key dimensions of joint specimen

	B90		B45		W90		W45	
	Pylon	Brace	Pylon	Brace	Pylon	Brace	Pylon	Brace
Inner Diameter [mm]	296	170	297	174	285	171	293	170
Thickness [mm]	12	5	12	10	20	5	12	5
Length [mm]	3000	2000	3000	2000	3000	2000	3000	2000
Bolt size	M20	M20	M20	M20	-	M20	-	M12
No. of bolts	6	4	6	4	-	4	-	4
Gusset plate thickness [mm]	6		8		15		10	

This current task focused on the development and validation of the parametric FE mode of the tested joints in the previous tasks. The validated numerical models were then used in a parametric study to examine the influence of various parameters (e.g. gusset plate thickness or brace-to-pylon angle) on the stiffness and resistance of the joints.

4.4.1.1 Finite element models of the joints

The numerical models of joints were fully parameterised using independent and dependant geometric variables based on the test specimens. Figure 4-36: Parameterisation of the brace (bolted and welded joint) presents the parameterisation of the brace. The independent variables are the total length (tLB), nominal diameter of the hexagonal section (to calculate the element length LwB and LtB and it was assumed $LwB=LtB$). Other parameters shown in the figure can be considered as dependent variables. It should be noted that the angle between the elements ($angB$) and fillet radii (rLB and rSB) are fixed to avoid over-complicating the modelling.

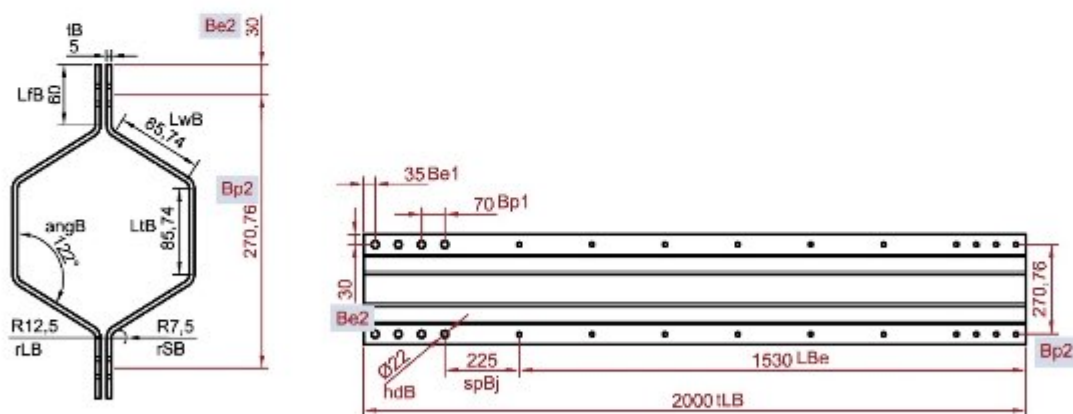


Figure 4-36: Parameterisation of the brace (bolted and welded joint)

Python and gusset plates (bolted and welded) were parametrised using the same approach. One of the key parameters in the modelling of the joints is the brace-to-pylon angle. Using the angle as an independent variable, two kinematic constraints were imposed when the angle is changed (i) the lower end of corner of the brace travels along the same vertical line and (2) the centre line of the brace always passes through the centre point the row of bolt holes of the pylon. Variation of the angle and the form of the joints are presented in Figure 4-37. The range of the angle is from 30 to 90 degrees.

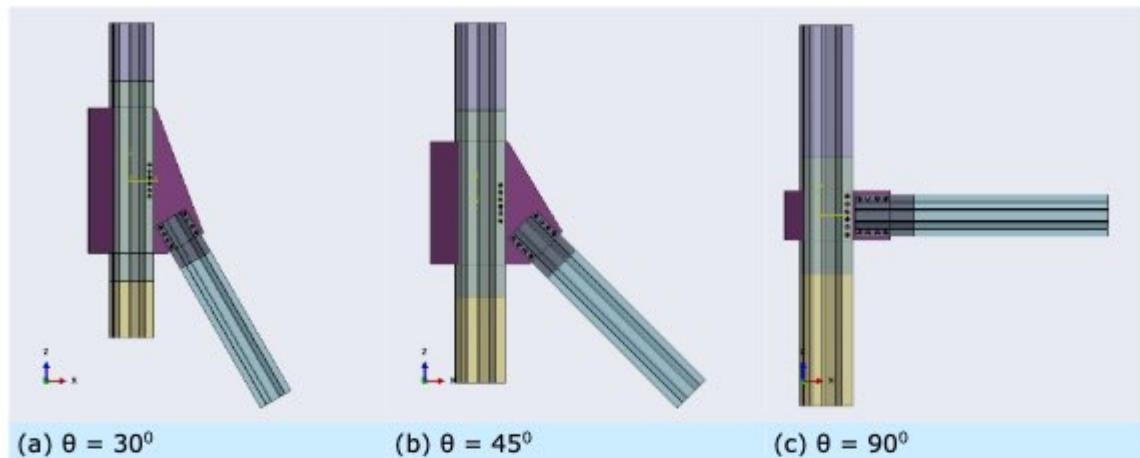


Figure 4-37: Parametric bolted joint model with various brace-to-pylon angles

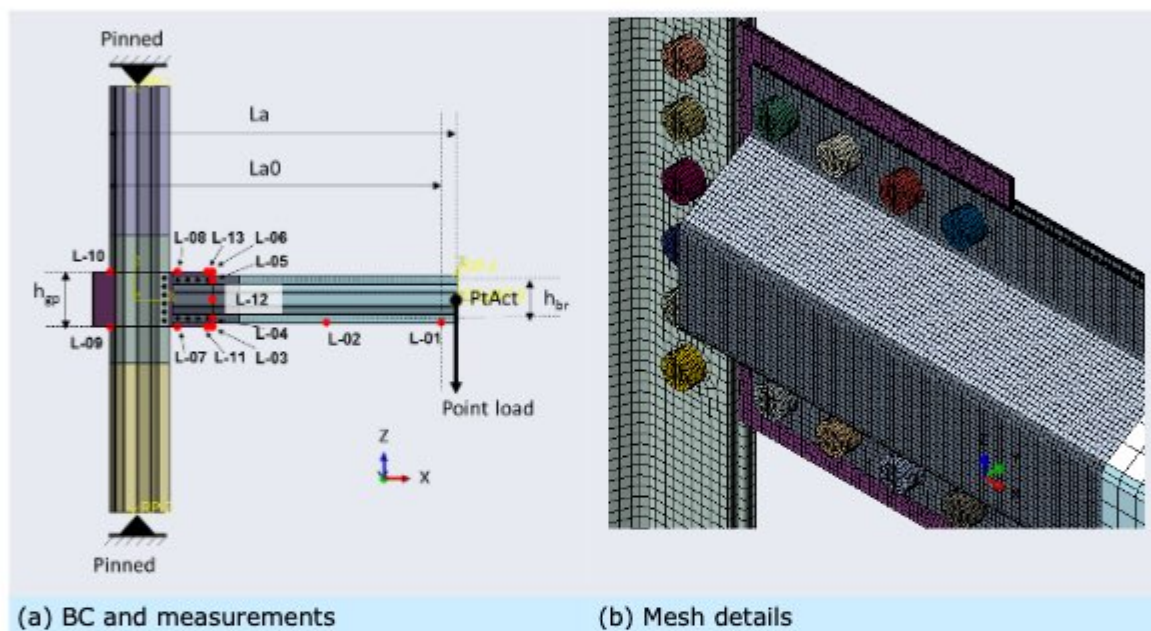


Figure 4-38: Boundary conditions, displacement outputs and mesh details (B90 joint model)

The bolted 90° joint model created in ABAQUS/CAE [1] is shown in Figure 4-38. The pylon is nominally pinned at the top and bottom. A vertical displacement controlled load (20mm) is applied at the end of the brace. No out-of-plane constraints are applied as the lateral constraints in the tests were not sufficient. The FE models are meshed using solid brick elements, even though the components fall into the category of thin objects suitable for modelling as shells. This is done to enable accurate modelling of the pre-loaded bolts and the interaction between the clamped plates. A minimum of four elements are used through the thickness of the components to accurately model the bending resistance of the plate members. In order to improve efficiency of the simulation process, fine meshes are used in the bolted region while relatively larger elements are used in other parts of the model.

Measurements are made at the same locations on the FE models and the tests. Displacement values at the reference points (L-04, L-05, L-09, L-10), shown in Figure 4-38(a), are used to calculate the rotational deformation (θ_j) of the joints according the Eq (4.1). The moment applied to the joint is calculated as the applied load multiplied by the lever arm (La).

$$\theta_j = \frac{U_{x,L-05} - U_{x,L-04}}{h_{br} \cdot \sin(\theta)} - \frac{U_{x,L-10} - U_{x,L-09}}{h_{gp}} \quad (4.1)$$

Coupon tests were carried out as part of the test programme to define the stress-strain relationship of the S355 steel used for the components. Specimens with various thicknesses were tested. Simplified tri-linear stress-strain curves are used in the model. The stress-strain curve corresponding to cold working is used to validate the model (this will be discussed later). The increase in the yield and ultimate stress due to cold working is based on EN1993-1-3 [20] for material properties of cold formed sections and sheeting.

Surface-to-surface integrations are defined for all surface pairs in the bolted region to model the friction between plates due to bolt preload. Away from the bolted joint, the remainder of the pylon and brace (mainly lips) are simply connected using tie constraints to alleviate the unnecessary demands to model bolts and holes. Bolt preload is applied using thermal contractions of the bolt shaft material. The negative temperatures needed for achieving $F_{p,c}$ were calibrated for a range of bolt diameter and clamping thickness to be used in the parametric study.

The numerical modelling consists of two steps:

- Step 1: an explicit dynamic step for bolt preload, in which an appropriate negative temperature will be applied to the bolt shank (50 sec analysis duration)
- Step 2: an explicit dynamic step for application of the displacement controlled load (200 mm) at the end of the brace (3000 sec analysis duration)

Explicit dynamic analysis is used throughout the numerical analysis, in order to avoid convergence difficulties associated with contact problems between multiple parts and potential buckling or early failure of components. The displacement load is applied slowly so that any adverse dynamic effects can be minimised.

The 2D joint models developed for Task 4.2 were extended to 3D joint models by mirroring the brace, gusset plate and bolts to the plane of the other branch 120° apart. A comparative study of the behavior of the 2D and 3D joints was carried out in the validation process.

4.4.1.2 Validation and analysis of FE models

Validation of the FE model can be carried out by comparing the moment-rotation behaviour of the B90 and W90 joints tested. The influence of the out-of-plane imperfection of the brace was also studied with the B90 joint model. It was found that an imperfection of 5mm deviation from the centre line at the end of the brace produced the most comparable results to the tests. Due to the failure mode of the W90 joints (buckling of the brace), it was necessary to consider the cold forming strain hardening for the brace material in the FE model.

The comparison of the moment-rotation behaviour of the bolted and welded 90° joints are presented in Figure 4-39 and Figure 4-40. Joint rotation is calculated according to Eq (1) and the moment by multiplying the actual load at end of the brace by the lever arm (L_a) shown in Figure 4-38(a). Relevant joint rotation parameters are also shown for reference. It can be seen that the rotational behavior of the FE model is in excellent agreement with the test specimens. Failure mode of the B90 and W90 joints were buckling of the gusset plate and brace respectively. The failure modes were reproduced by numerical models accurately. Bi-linear curve fitting is used to determine the rotational stiffness, plastic and ultimate moment resistance of the joint model.

For the bolted 90° joint model studied in Figure 4-39, due to the buckling failure of the gusset plate, the elastic moment resistance of the gusset plate is determined and compared with the model. The stiffness boundaries for joint classification calculated according to EN1993-1-8 [17] are compared with the initial stiffness of the joint. Although this type of joint is usually designed as nominally pinned, its actual stiffness indicates a semi-rigid or moment transmitting joint. The rotational stiffness of the gusset plate is also shown here and is significantly larger than the stiffness of the joint.

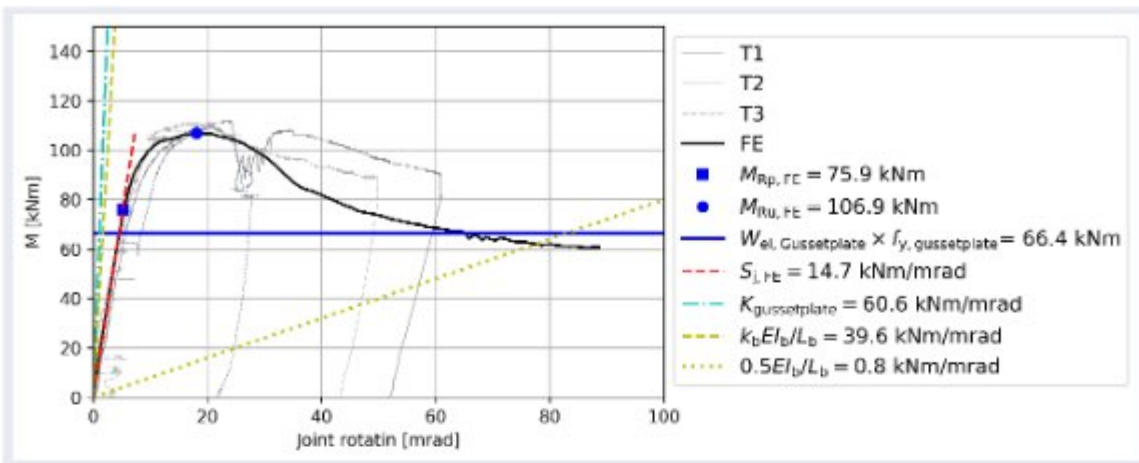


Figure 4-39: Assessment of moment – rotation behaviour (2D B90 joint with 5mm out-of-plane imperfection)

Response of the welded 90° joint is examined in Figure 4-40. Due to the failure mode of the welded joint, the elastic moment resistance of the brace cross-section is calculated and compared with the joint model. Based on the classification by stiffness, this type of joint can also be said to be capable of transmitting moment (semi-rigid).

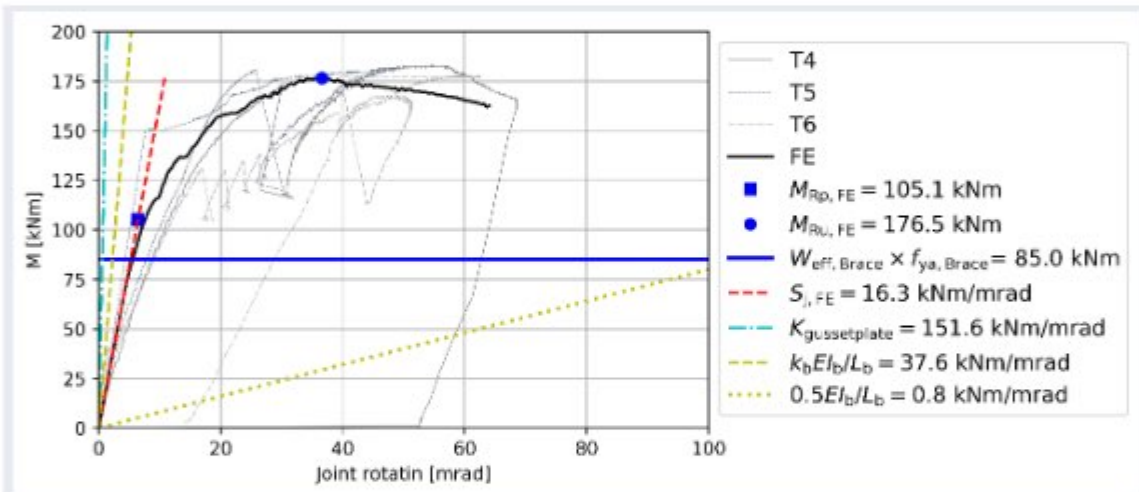


Figure 4-40. Assessment of moment – rotation behaviour (2D W90 joint)

A comparative study was carried out to examine whether the simultaneous application of load to the two brace arms of a 3D joint will introduce an adverse torsional moment on the joint leading to premature or an unintended failure mode at very low load levels.

The 90° bolted joint was considered in this study. The 3D joint model uses the same components as the 2D parametric model with additional brace at 120° to the first brace. It also has the same boundary conditions and load application. The study revealed that the effect of the torsional moment acting on the 3D joint did not lead to early failure. The failure mode and resistance of the 3D joint model is similar to the 2D joint. However, the buckling failure of the gusset plate in the 3D model occurred slightly earlier due to the resultant torsion acting on the gusset plate. In addition, the final out-of-plane deformation is greater in the 3D joint for the same reason. Nonetheless, the rotational response of the 3D joint is very similar to its 2D counterpart.

4.4.1.3 Parametric study and evaluation

Bolted and welded parametric joint models were developed and validated in the previous sections. It has been shown that the parametric joint models can accurately predict the rotational behaviour of the physical specimens. The validated FE model was subsequently used in parametric studies of the influence of brace-to-pylon angle, gusset plate thickness and bolt diameter on the response of the joints.

The range of brace-to-pylon angle was varied between 30° and 90° in the parametric study with an increment of 15° . The dimensions of components of the validated bolted 90° model were used. It should be noted that when the angle is changed the number of bolts on the pylon also changes while the bolt spacing is fixed. The initial stiffness, plastic and ultimate moment capacity as a function of the brace-to-pylon angle are shown in Figure 4-41(a). The ultimate capacity increases moderately up to 75° then reduces significantly at 90° . The initial stiffness is maximum at 45° then reduces as the angle increases to 90° . The failure modes of the five models are the same, which is the gusset plate buckling failure.

Using the validated bolted 90° model again, the gusset plate thickness was varied from 4 mm to 15 mm in this second parametric study. The influence of varying the gusset plate thickness is presented in Figure 4-41(b). When the gusset plate thickness is increased from 4 mm to 15 mm, the moment capacity increased up to a thickness of 10 mm. At this point, the failure mode transitioned from buckling of gusset plate to brace failure. Initial stiffness increased almost proportionally to the increase in thickness of gusset plate.

In the third parametric study, the influence of the bolt diameter used in the brace was examined using the validated welded 90° joint model. Four bolt diameters were considered: M12, M16, M20 and M24. The slip resistance of the preloaded bolts was kept at the same level when the bolt diameter was changed (i.e. the number of bolts was changed as well). The results of the parametric study are presented in Figure 4-41(c). It can be seen that the initial stiffness almost remained constant when the bolt diameter was varied. The moment capacities decreased when the bolt diameter was increased and less bolts were used. The same brace buckling failure can be observed in all cases.

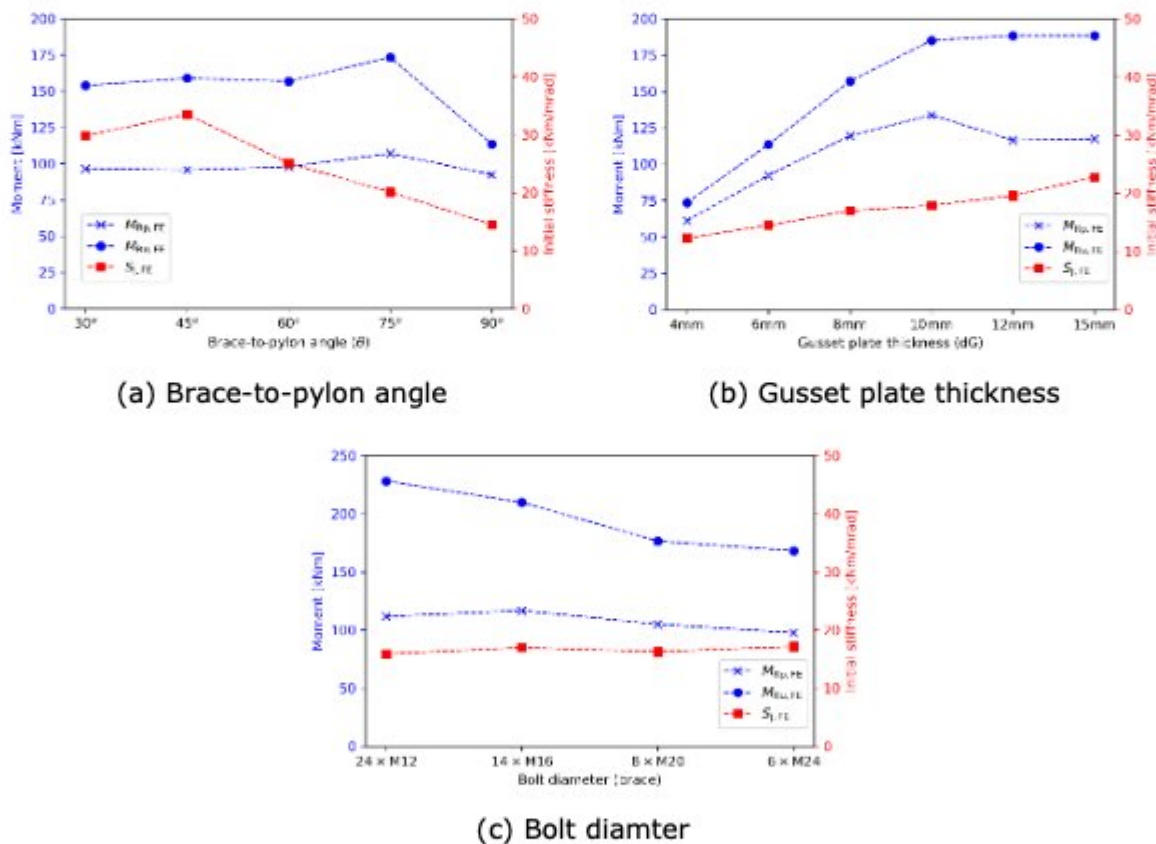


Figure 4-41: Results of parametric study

4.5 Conclusions

4.5.1 Polygonal cross-section members in compression

New type of polygonal built-up members was proposed for the lattice part of hybrid steel wind turbine tower. Cross-sections used are composed of cold formed pieces connected together with preloaded bolts creating polygonal (hexagonal and nonagonal) cross-section. The results of the initial numerical study showed that the failure mode of such columns is strongly influenced by the distortional buckling of the three individual sectors. Distortion of the single sector cross section occurred between two consecutive bolts. Significant interaction with flexural overall buckling was also observed, especially for the higher slender cases. For this type semi-closed built-up column composed of folded plates, there is no expression in Eurocode for the critical distortional buckling load. The main outcome of the initial parametric study was that for bolt spacing between 3 and 5 times the profile diameter, distortional buckling is apparent. In further analysis, it was observed that for bolt distances below 1.2 times the diameter, the column failed purely under overall buckling. Above that spacing, distortional buckling of the individual sectors occurred in combination with the overall buckling.

The resistance of the welded cross-sections is calculated according to EN 3-1-1 and EN 3- 1-5. For the resistance calculation, classification is performed for plated cross-sections, under the assumption that the creases effectively provide simply supported boundary conditions for the faces of the polygon. This assumption is valid for a small number of sides but becomes invalid as the number of sides increase.

The results of the experiments allow to draw following conclusions:

- Columns made of regular convex polygonal cross-sections can be grouped in two categories based on how strongly they are attracted towards either a plate-like or a shell-like failure.
- Two regions of the search space (plate failure governed and spillover failure governed) were identified via the FEM analyses and were verified through the experiments.
- The provisions of EN 1993-1-5 and EN 1993-1-6 were checked and found to be suitable for calculating the design resistance within each of the two regions.
- An empirical formula was developed for the boundary between the two identified regions. The proposed formula returns the number of vertices, n_v , for an input of facet plate slenderness, p_c , yield strength, f_y and imperfection amplitude U_0 and suggests which of the two Eurocodes should be applied.
- By comparing between models with and without initial imperfections, columns were proved to be highly sensitive.
- The eigenmode-affine imperfection pattern was proved improper in certain cases, for which the double-spillover imperfection pattern yielded lower resistance.

4.5.2 Single-sided brace-to-pylon connections

The joint set-up for testing was with pylon to diagonal angle of 90° and 45°. Three specimens for each parameter (B90, W90, B45 and W45) were tested (12 experiments in total). Tests B90, W90 and B45 demonstrated a global and local behavior in line with the predictions. According to preliminary numerical study predicted failure modes were: i) buckling of gusset plate in the compression zone, and gusset plate net section failure in tension zone; ii) buckling of brace in the compression zone, and brace net section failure in tension zone; iii) out of plane buckling of gusset plate; respectively. The same failure modes were observed in the experiments. Test on W45 configuration gave a failure different than predicted. According to the preliminary numerical study expected failure mode was brace block tearing. In the experiments brace bearing in tension zone was observed.

Parametric finite element models of bolted and welded joints were validated and calibrated against test results. It was shown that the response of the FE models were in excellent agreement with the test results when appropriate imperfections and material properties are used.

The parametric study using the validated FE model showed that:

- The joint used in the lattice structure can be treated as semi-rigid for moment transmission
- The largest ultimate moment capacity occurs when the brace-to-pylon angle is around 75° while the highest initial stiffness can be achieved at 45°

- Increasing the gusset plate thickness will increase the moment resistance capacity of the joint, eventually transferring the failure mode to buckling of the brace and moderately increasing the initial stiffness

The validated FE model can be used in further study to investigate the joint behaviour in various conditions and assist better design of the connections in lattice structure.

4.5.3 Double-sided brace-to-pylon connections

In this group of experiments the two branches of the cross-like specimen received opposite direction vertical forces (one upwards the other downwards).

A gusset plate failure mechanism emerged: that was buckling if the gusset plate *inside* the pylon element due, obviously to the compression stress field of the branches. Should this failure mode not be prevented (by way of appropriately reinforcing the gusset plate *inside* the pylon element), no reduction of the buckling length of the bracing trusses' bars of the tower is recommended. However, if the gusset-plate buckling issue is remedied appropriately the provisions of EN1993-3-1, Annex G.2 can be applied (see Figure 4-42).

**Table G.2 Effective slenderness factor k for bracing members
(b) Tubes and rods**

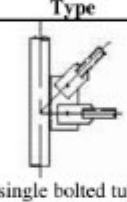
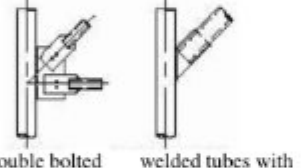
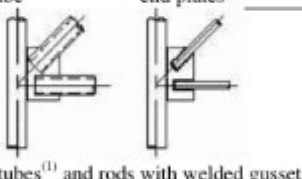
Type	Axis	$K^{(363)}$
 single bolted tube	in plane	0,95 ⁽²⁾
	out of plane	0,95 ⁽²⁾
 double bolted tube welded tubes with end plates	in plane	0,85
	out of plane	0,95 ⁽²⁾
 welded tubes ⁽¹⁾ and rods with welded gussets	in plane	0,70
	out of plane	0,85

Figure 4-42:Effective buckling lengths of bracing members in lattice towers

5 Life cycle assessment and design recommendations

This WP was focused on examining the possibilities to reduce the overall cost of the hybrid tower by optimising the production and construction process while maintaining the required level of structural reliability and sustainability. The complete design, including cost evaluation and life cycle assessment for the most promising case studies proposed, predesigned and validated in previous WPs, including construction stage and foundations, formed the basis for the optimisation process. The suitability of the investigated solutions for potential use in very aggressive environments, e.g. near-shore, were demonstrated. The results were compared with more traditional tower designs, such as tubular steel and steel-concrete hybrid towers, based on results of previous RFCS research projects.

The following specific objectives were defined:

- Cost optimization of the structural design of the hybrid lattice-tubular towers for the three most promising case studies,
- Life cycle assessment in normal and aggressive environments,
- Development of design recommendations for hybrid steel towers.

5.1 Worked design examples of hybrid steel-steel wind towers

This task was aimed at providing worked examples and cost estimates for the wind tower case studies. Deliverable D5.1 was produced in the context of this task.

5.1.1 Environmental conditions

The environmental conditions are divided into *wind conditions* and *other environmental conditions*. Only the wind conditions were considered for design load calculations as these are the primary conditions affecting structural integrity. The wind conditions include a constant mean flow (wind profile or wind shear) combined with turbulence.

5.1.1.1 Wind profile

The wind profile v represents the average wind speed as a function of height H above the ground. The commonly used profiles are the power law profile, defined as follows:

$$v = v_0 \left(\frac{H}{H_0} \right)^\alpha \quad (5.1)$$

or the logarithmic profile:

$$v = v_0 \frac{\ln\left(\frac{H}{z_0}\right)}{\ln\left(\frac{H_0}{z_0}\right)} \quad (5.2)$$

whereby v_0 : reference wind speed; z_0 : surface roughness length; H_0 : reference height; and α : power law coefficient. Figure 5-1a) compares the above equations for a mean wind speed of 10 m/s at a reference height of 10 m. Figure 5-1b) shows comparisons for a reference wind speed of 12 m/s at 80 m, which is the typical value measured in wind parks. As can be seen in this graph, the wind speed has the potential to reach up to 14 m/s or even more at high altitude (220 m).

5.1.1.2 Turbulence

The wind speed is usually expressed by a mean value. However, the wind has a turbulent nature. The expression *turbulence* denotes random variations in the wind velocity from 10 minutes. Wind turbulence models need to include the following parameters: (i) turbulence intensity I , (ii) turbulence spectra, (iii) length scale, and (iv) coherence. The wind overall turbulence intensity can be obtained from:

$$I = \frac{\sigma}{U} \quad (5.3)$$

whereby σ : standard deviation about the mean wind speed U . EN 61400-1 [40] considers three reference intensity values: 0.16, 0.14, and 0.12. Two models are given here for the calculation of

the power spectral densities of the longitudinal (along the direction of the mean wind velocity) vector component of the turbulent wind velocity: (i) von Karman model, and (ii) Kaimal model [40]:

$$\frac{nS_u(n)}{\sigma_u^2} = \frac{\frac{4nL_{2u}}{U}}{\left[1 + 70.8\left(\frac{nL_{2u}}{U}\right)^2\right]^{\frac{5}{6}}} \quad \text{von Karman model} \quad (5.4)$$

$$\frac{nS_u(n)}{\sigma_u^2} = \frac{\frac{4nL_{1u}}{U}}{\left(1 + \frac{6nL_{1u}}{U}\right)^{\frac{5}{3}}} \quad \text{Kaimal model} \quad (5.5)$$

in which $S_u(n)$: auto spectral density; L_{1u} and L_{2u} : length scales; and n : frequency in [Hz]. The two spectra functions are illustrated and compared in Figure 5-2.

The length scales are eddies length and depend on the surface roughness in the proximity of the ground surface. This relation become isotropic as the height increases from the ground.

Finally, coherence functions have to be defined. Coherence can be defined as the magnitude of the co-spectrum divided by the auto-spectrum for the longitudinal velocity components at spatially separated points in a plane normal to the longitudinal direction [40].

Having defined all the above requirements, the turbulent wind speed for a specific period of time t can be calculated using the following relationship:

$$V_m(t) = \bar{V}_0 + \sum_{i=0}^m A_i \cos(\Omega_i t + \zeta_i) \quad (5.6)$$

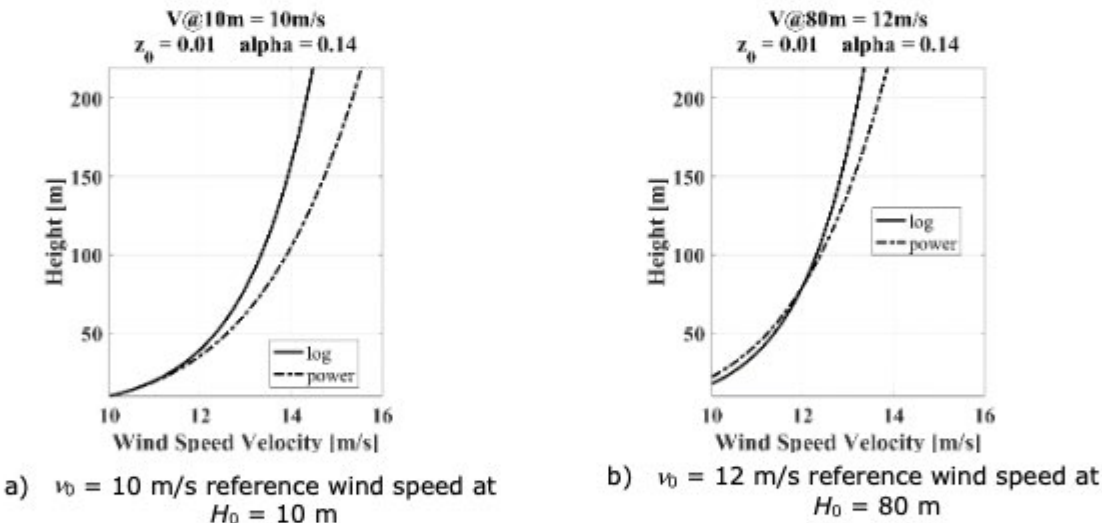


Figure 5-1: Shear profile for different reference wind speeds

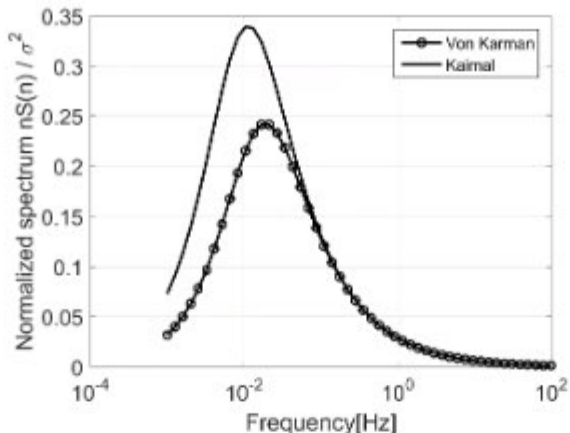


Figure 5-2: Turbulence power spectra von Karman and Kaimal mathematical functions

whereby Ω : angular velocity; ζ : stochastic variable between $[\pi, -\pi]$; \bar{V}_0 : average wind speed for a specified turbulence intensity; A_i : coefficient obtained from:

$$A_i = \frac{2}{\pi} \sqrt{\frac{1}{2} S_u(\Omega_i) + S_u(\Omega_{i+1})(\Omega_{i+1} - \Omega_i)} \quad (5.7)$$

An example of the generated turbulent wind speed is given in Figure 5-3.

5.1.1.3 Wind speed occurrence probability

Wind speed varies depending on meteorological conditions at the wind farm site. In order to estimate the total energy production of the wind turbine and to calculate the fatigue load, it is necessary to know how often wind speed changes. The Weibull distribution is the most common probability function to simulate the wind speed occurrence probability, and is obtained from:

$$f(v, c, k) = \frac{k}{c} \left(\frac{v}{c} \right)^{k-1} e^{-\left(\frac{v}{c} \right)^k} \quad (5.8)$$

in which v : wind speed; c : Weibull scale parameter; and k : non-dimensional Weibull shape parameter. The Weibull probability distribution is obtained for each site due to shape and scale properties, and it varies by the height elevation, see Figure 5-4 as an example.

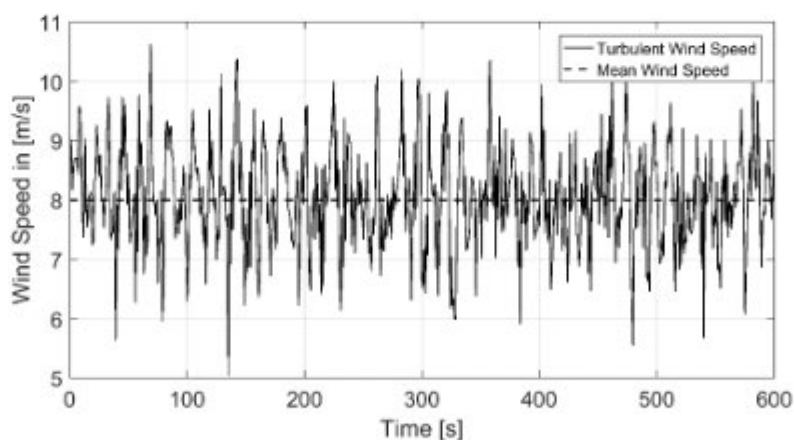


Figure 5-3: Generated turbulent wind model in 10 minutes time period

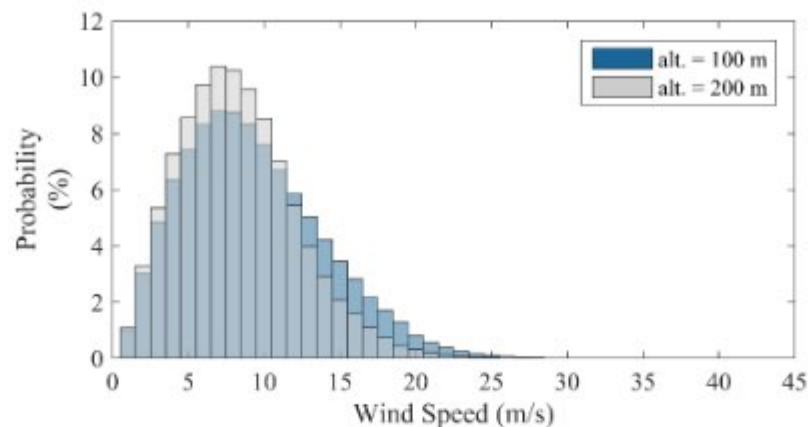


Figure 5-4: Weibull distribution comparison for 100 m and 200 m distance from the ground

5.1.2 Case studies

The case studies are shown in Figure 5-5 and Figure 5-6. The hybrid towers consist of 120 m lattice structure (bottom part) and a 65 m tubular tower (upper part). The lattice part comprises S355 cold-formed polygonal sections. The tubular part has a diameter ranging from 4500 mm at the base to 3500 mm at the top with 26 mm plate thickness. A NREL 5 MW baseline wind turbine with a total mass of 350 ton has been considered.

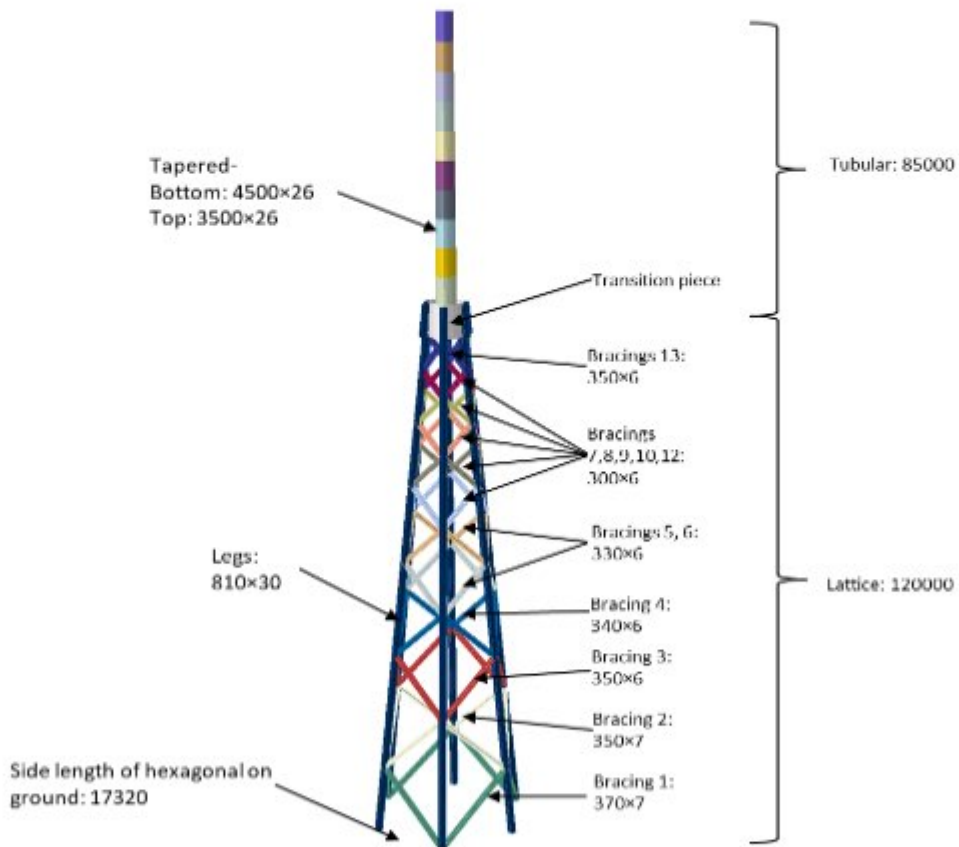


Figure 5-5: Six-legged lattice structure geometry I; dimensions in (mm)

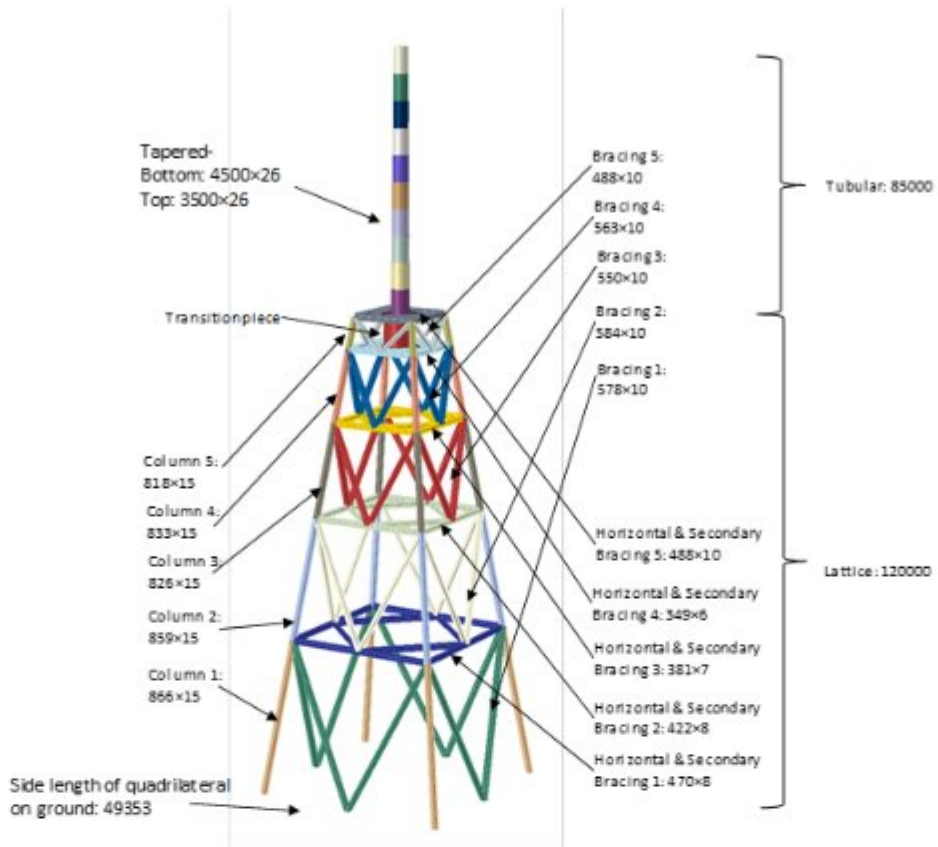


Figure 5-6: Four-legged lattice structure geometry II; dimensions in (mm)

For the 6-legged structure, different bracing configurations were considered, and the solution was optimised based on the mass and the number of connections. For the 4-legged structure, the cross-sections were chosen via an optimisation process that was verifying the capacity of the axial load, the buckling length, the slenderness ratio, the material properties and the buckling coefficient. In both cases, cold-formed polygonal sections were considered for the lattice structure.

The transition piece details for each geometry are illustrated Figure 5-7 and Figure 5-8. For the 6-legged tower, see Figure 5-5, a conical shell with an upper plate to support the lifting equipment has been considered. The columns of the lattice part are directly connected to the body of the transition piece, while the upper plate of the transition piece is connected to the lower plate of the tubular part. For the 4-legged tower, see Figure 5-6, the transition piece has been designed as a product, completely independent of the lattice part and least dependent of the tubular part. A cylinder with two rigid plates on bottom and top were applied to convert the moment into a pair of horizontal forces.

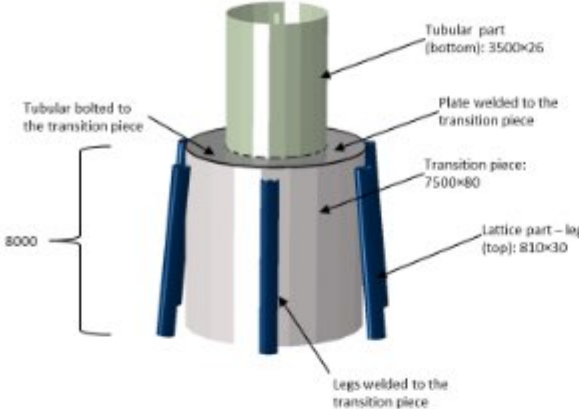


Figure 5-7: Transition piece for the six-legged lattice structure geometry I, dimensions in (mm)

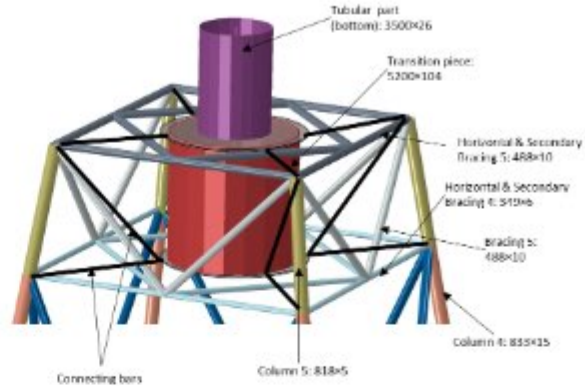


Figure 5-8: Transition piece for the four-legged lattice structure geometry I, dimensions in (mm)

5.2 Life-cycle assessment and life-cycle cost analysis of onshore installation

This task was aimed at investigating the life cycle assessment of 185 m tall hybrid wind turbine towers. Deliverable D5.2 was produced in the scope of this task.

5.2.1 Life cycle stages

The boundary system adopted in the present study is shown in Figure 5-9. The system boundary is defined as a set of criteria specifying which unit processes are part of a product system. All life stages from production of the materials to the end-of-life, i.e. (i) production, (ii) transportation, (iii) erection, (iv) operation and maintenance, and (v) disposal at end of life, have been considered. The foundations were also included in the analysis. The connection to the grid is out of scope of the present study and has been excluded. The lifetime of the turbines was taken to be 20 years. At the most crucial stage of collecting the required data, the maximum possible level of detail that would not sacrifice the accuracy of the results has been included. The Life Cycle Inventory (LCI) focused on gathering information on the primary components of a wind turbine tower.

5.2.1.1 Production stage

All materials comprising the hybrid tower are considered for this stage. Based on the calculated loads, the mass of the foundation has been estimated. The rotor consists of the blade hub which is made from cast iron, the nose cone and the three blades which are made from fiberglass reinforced polymer. The nacelle, the most complex component which is responsible for converting the kinetic energy into electricity, is composed of a group of materials including fiberglass, cast iron, copper, aluminium and steel. The percentage of the materials used in wind turbine components has been based on [5]. The largest share in the mass distribution of the whole structure belongs to the reinforced concrete foundation. The mass distribution of the structure and the mass distribution among the tower's components are shown in Figure 5-10.

In the manufacturing stage, the production of the raw materials and the energy embodied for their manufacture have been considered. In addition to the main components, the number and the mass of bolts have also been accurately evaluated. The four-legged tower design led to a larger number of bolts which is expected to affect the maintenance stage.

5.2.1.2 Transportation stage

The components were assumed to be prefabricated in the factory, wherever possible. In addition to the energy used in transport, the impact of the emissions due to the extraction and production of fuel has also been considered. The following three types of transportation have been assumed:

- 15 t trucks for general use,

- Special trucks for transfer of RNA, tubular tower and main core of crawler crane,
- 10 m³ concrete mixers.

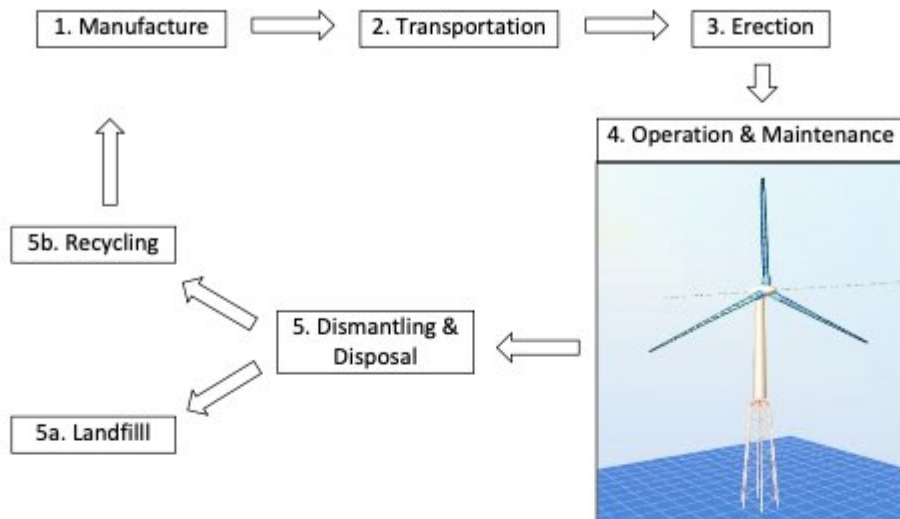
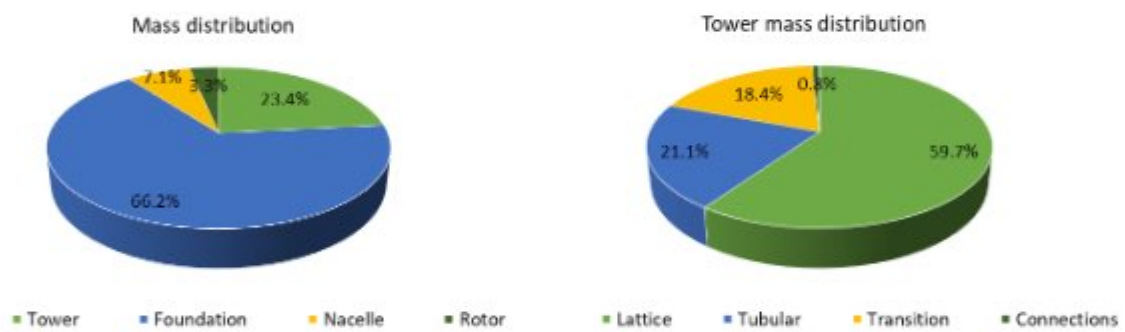
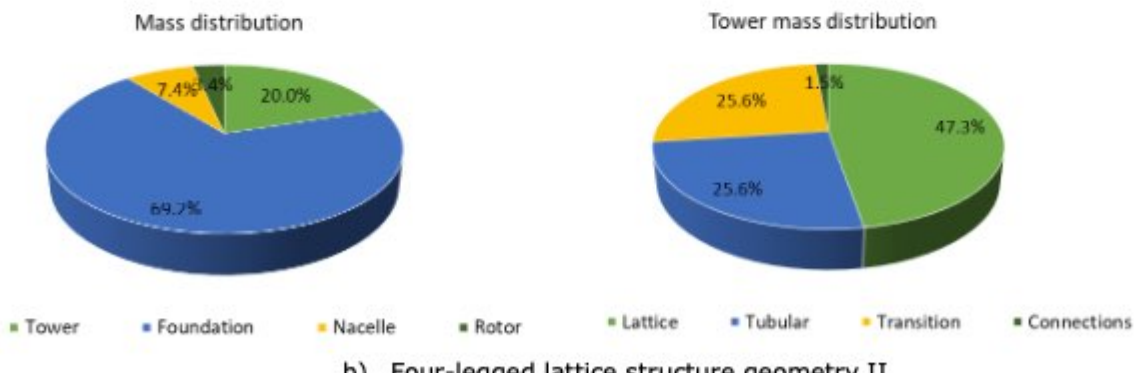


Figure 5-9: System boundary for LCA of hybrid wind turbine towers

A distance of 100 km to site has been assumed. The total number of trucks used for transportation has also been approximated, as shown in Table 5-1. The lattice tower segments would be transferred with normal trucks to site. The tubular rings are fully manufactured in factory and transported to the construction site in three pieces using a special truck, where they are assembled by bolting together the flanges. Special trucks are also needed for the RNA and the crawler crane body. The remaining materials/equipment are transported by 15 t trucks for general use, except for the concrete which arrives on site in mixers.



a) Six-legged lattice structure geometry I



b) Four-legged lattice structure geometry II

Figure 5-10: Mass distribution for the two case studies

5.2.1.3 Erection stage

Site preparation, mobile crane and strand usage have been included in the erection stage. The process has been divided in four steps, as described in Table 5-2. A total of 10 weeks has been estimated for the erection process.

5.2.1.4 Operation and maintenance stage

For the operation stage, it was considered that bolt maintenance would be undertaken twice a year by specialised personnel. As this study mainly focuses on the tower's life cycle assessment, details related to the turbine maintenance have been excluded from the analysis.

5.2.1.5 Disposal and end of life stage

In the disposal stage, the period of disassembly was roughly considered half of the erection stage (i.e. 5 weeks), during which the usage of cranes and trucks (for transfer to landfill only of the components that are not recycled) has been considered. Recycling has been considered in a closed loop approach, meaning that the recycled products have equivalent material properties to the virgin ones. Steel was assumed to be 85% recyclable, with an average material loss rate of 15%. Epoxy, fiberglass and plastic were assumed to be incinerated. Finally, the paint used in the rotor, nacelle and tower, the surface treatment in the tower as well as grid losses were excluded from the analysis.

5.2.2 LCA results for the hybrid towers

The LCA analysis was performed using the GEMIS (Global Emission Model for Integrated Systems) software [30], a freely available database and material flow analysis tool. GEMIS has been successfully applied to examine the environmental impacts of wind turbine towers [41]. A pool of 1150 products (i.e. inputs and outputs of processes), 9766 processes (i.e. activities for energy or material conversion) and 131 scenarios (i.e. selection of processes) covering data from more than 50 countries are currently available, whereas additional data can be imported by the user. Upon LCA performance, the air emissions, the greenhouse gases, the water effluents, the solid wastes and the resources used can be obtained in tabulated and graphical forms.

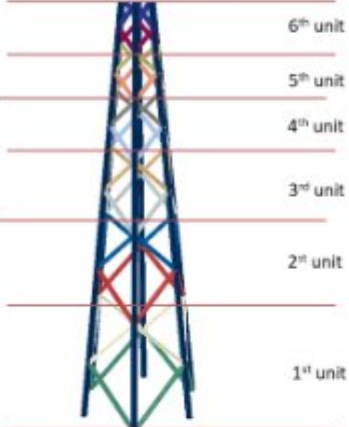
Table 5-1: Estimated number of trucks for transportation

Component	N. ^o trucks	Type of truck	
Lattice structure	33	Normal 15 t	
Tubular tower	3	Special	
Transition piece	3	Special	
Bolts	1	Normal 15 to	Normal 15 t
Concrete	90	Concrete mixer	
Reinforced bars	8	Special	
Rotor	4	Special	
Nacelle	4	Special	Special
Equipment for RNA	5	Normal 15 t	
Crawler crane - body	5	Special	
Crawler crane	15	Normal 15 t	Concrete mixer
Total n. ^o of trucks (per type)	90 65 16	Concrete mixer Normal 15 t Special	
Total n. ^o of trucks	171		

For the present study, the following data needed to be imported into the software: (i) the materials and their masses in tonnes, (ii) the transportation type and the distances in tonne-kilometre, and (iii) the residues in tonnes. The carbon emissions (in kg CO₂-equivalent), the air emissions (in kg

SO_2 -equivalent) and the energy requirements (in MJ) were subsequently exported. The collected data, categorised per life cycle stage and per structural component, are summarised in Table 5-3.

Table 5-2: Description of the erection process – time estimate

Description	Duration	Crane	Personnel
Step 1: Assembling the lattice structure			
Divide the lattice structure into units (see below) and assemble them on site, close to the erection point.			
	6 weeks	1×150 t	10 people
Step 2: Erecting the lattice structure and the tubular tower			
Assemble in turn the lattice and the tubular tower, in the following order:			
<ul style="list-style-type: none"> • unit 1 of lattice • unit 1 of tubular • unit 2 of lattice • unit 2 of tubular • unit 3 of lattice • unit 3 of tubular • unit 4 of lattice • unit 5 of lattice 	2 weeks	1×150 t 1×750 t crawler	10 people
Step 3: Lifting the tubular tower			
Install strand jacks and the last unit(s) of the lattice tower.			
Install strand carousel and lift the tubular tower.		1 week	1×150 t 1×750 t crawler
Step 4: RNA			
Install the nacelle and the rotor with blades			
1 week		1 week	1×150 t 1×750 t crawler
Total	10 weeks		

The results obtained are summarised in Table 5-4. Focus has been placed on the following four environmental impacts:

- Abiotic depletion measured in [MJ], one of the most common impact categories of LCA including the depletion of non-renewable resources, i.e. fossil fuels, metals and mineral,
- Global warming potential factor measured in CO_2 -equivalent, in which the emissions of different greenhouse gases are evaluated,
- Acidification potential measured in SO_2 -equivalent which is the result of aggregating acid air emissions,
- Energy payback time measured in months, which shows how long the wind energy system has to operate in order to generate the amount of energy that was used during its life cycle. For the calculation of the energy payback time, 2000 operational hours leading to a total annual production of 10 GWh have been assumed herein.

The contribution of each component and each stage are presented in Figure 5-11 and Figure 5-12, respectively. The main share belongs to the manufacturing stage for all LCA impact categories considered. This is followed by the erection stage, largely owing to the long duration of the erection process. As far as the share among the components is concerned, the tower, followed by the foundation are the components with the largest contribution in carbon emissions, air emissions and energy requirements.

Table 5-3: Bill of materials

Component	Stage	Comment	Unit	Quantities	
				6-leg	4-leg
Tower	Fabrication	Lattice structure	t	469.45	305.91
		Tubular tower	t	165.63	165.63
		Transition piece	t	144.81	165.64
		Connections	t	6.53	9.47
Rotor	Fabrication	Glass fibre & epoxy	t	53.22	53.22
		Cast iron	t	56.78	56.78
		Steel	t	197.60	197.60
Nacelle	Fabrication	Aluminium	t	8.00	8.00
		Copper	t	32.00	32.00
		Glass reinf. pol.	t	2.40	2.40
Foundation	Fabrication	Concrete	t	2160.00	2160.00
		Reinforc. bars	t	69.30	69.30
Tower	Transport	Truck	tkm	108641.56	64370.53
Rotor	Transport	Truck	tkm	11000.00	11000.00
Nacelle	Transport	Truck	tkm	31500.00	24000.00
Foundation	Transport	Truck	tkm	222930.00	222930.00
Tower	Erection	Crane	h	105.60	105.60
Rotor	Erection	Crane	h	7.92	7.92
Nacelle	Erection	Crane	h	7.92	7.92
Foundation	Erection	Crane	h	10.56	10.56
Tower	Operation and maintenance	Truck	tkm	652.66	946.96
Tower	Disp. & End life	Landfill	t	117.96	95.58
		Transport to	tkm	2359.25	1911.54
Rotor	Disp. & End life	Landfill	t	8.52	8.52
		Incinerator	t	26.61	26.61
		Transport to	tkm	702.54	702.54
Nacelle	Disp. & End life	Landfill	t	35.64	35.64
		Incinerator	t	1.20	1.20
		Transport to	tkm	736.80	736.80
Foundation	Disp. & End life	Landfill	t	2170.40	2170.40
		Transport to	tkm	43407.90	43407.90

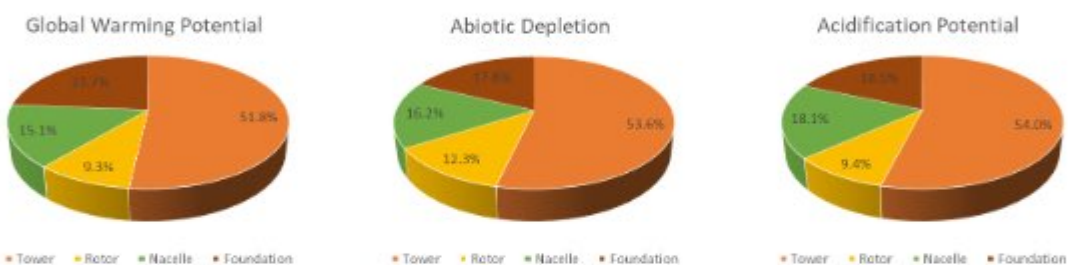
5.2.3 Comparison with tubular towers

The results are compared with those of the LCA performed for 150 m tubular towers (steel only; concrete only; steel and concrete named as hybrid) with 5 MW wind turbines presented in [31]. It should be noted that similar considerations have been made for the LCA of [31] and the study herein, thus allowing a reasonable comparison. The results are shown in Figure 5-13 and the comparison is based on the following parameters: (i) abiotic depletion, measured in MJ, (ii) global warming potential in kg CO₂-equivalent, (iii) acidification potential in kg SO₂-equivalent, and (iv) energy payback time, in months. As can be seen, the hybrid towers, even though taller, present comparable results with the conventional tubular towers. The abiotic depletion and the energy payback time are quite similar to the ones of the steel tubular tower. The acidification potential appears larger than the 150 m towers; this could be attributed to the large duration of the erection process accompanied

by long time usage of cranes and is expected to decrease as the process gets established. Given the increase in the height, the corresponding increase in the carbon emissions of 185 m towers compared to those of 150 m towers, appears reasonable.

Table 5-4: Life cycle inventory

LCA results	Unit	Quantities	
		Six-leg	Four-leg
Abiotic depletion	MJ	19445711.11	18267616.55
Acidification potential	kg CO ₂ Eq	7515.22	7445.80
Global warming potential	kg CO ₂ Eq	2065154.97	1923953.33
Energy packing time	months	6.48	6.09

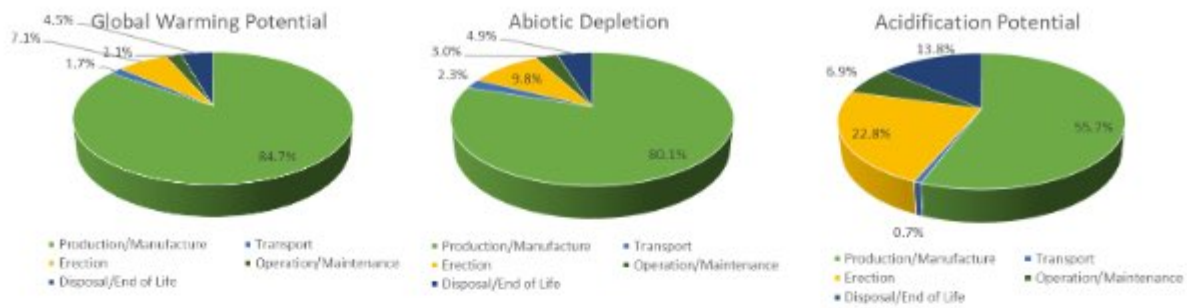


a) Six-legged lattice structure geometry I

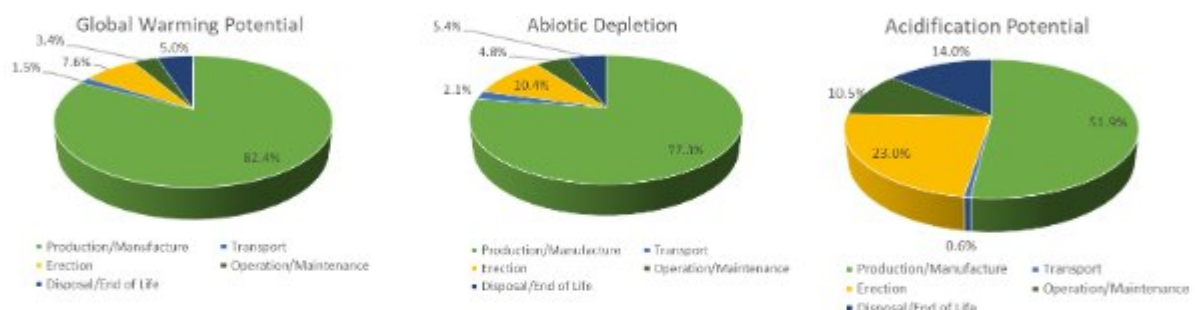


b) Four-legged lattice structure geometry II

Figure 5-11: Contribution of each component



a) Six-legged lattice structure geometry I



b) Four-legged lattice structure geometry II

Figure 5-12: Contribution of each life cycle stage

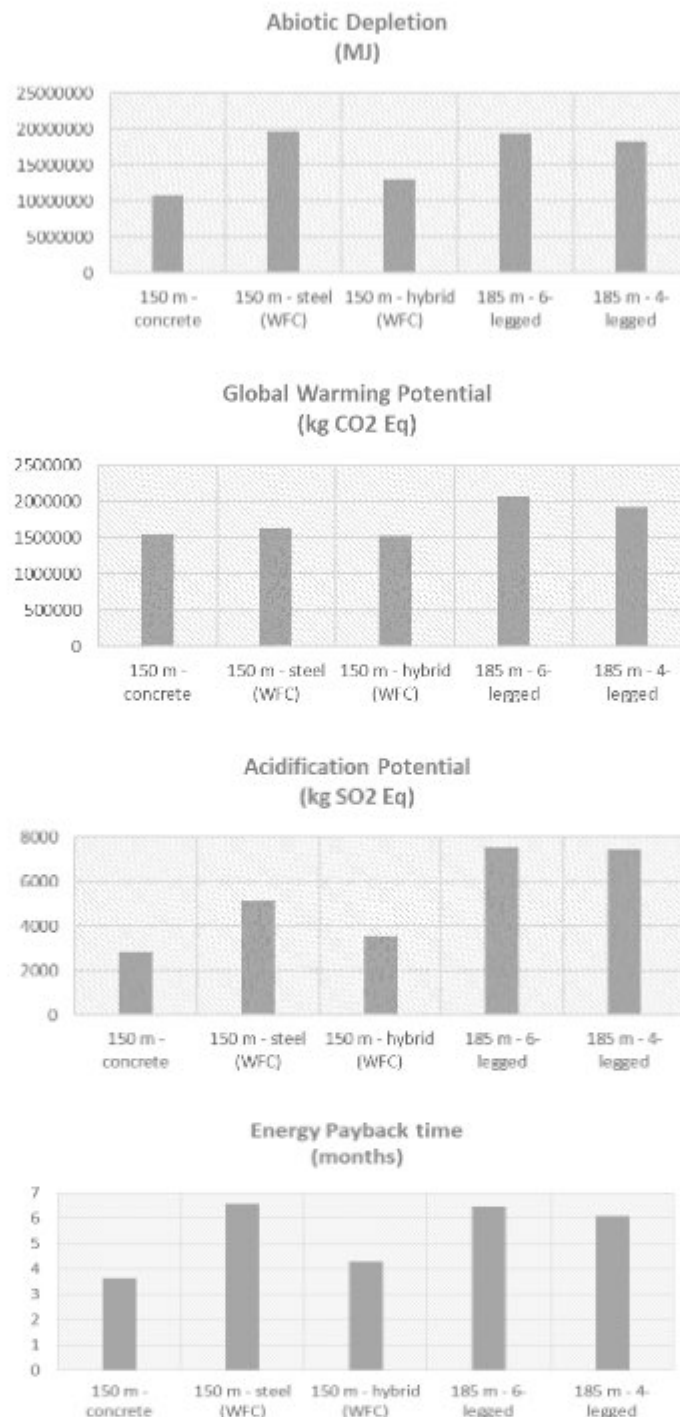


Figure 5-13: Comparison of hybrid 185 m tower with 150 m tubular towers from [31]

5.2.4 Life-cycle cost

Information collected from industrial partners has allowed an estimation of the total cost of a hybrid wind turbine tower. The following considerations were taken into account:

- For the lattice steel part: €2,000.00/ton (production and assembly),
- For the tubular steel part: € 1,800.00/ton (production and assembly),
- For the transition piece: €4,000.00/ton (production and assembly),
- For the bolts: €1,800.00/ (100 bolts) (production and assembly),
- For reinforced concrete: €250.00/m³ (production and cast in situ),

- For normal 15 ton truck: €50,00/ton (transportation),
- For special truck: €5000,00/ truck (transportation),
- For normal crane: €1000,00/day (transportation),
- For crawler crane: €5000,00/day (usage),
- For specialized personnel: €200.00 /day/person (man-hour),
- For crane mobilization: €25,000.00 / one operation,
- For crane lifting equipment: €40,000.00 / one operation,
- For RNA: €1,690.00/kW (production & maintenance).

It should be noted that the cost of RNA has been based on average values including installed, and operation & maintenance cost, whilst the total cost of the wind turbine structure will very much be affected by the aforementioned value. Moreover, this price is expected to decrease in time, as the market popularity of onshore 5 MW wind turbines increases.

The estimation of the cost for the whole tower is presented in Table 5-5. It is noteworthy that as with more conventional tubular wind turbine towers, for the presently studied structures, the tower comprises approximately 25% of the total cost.

Table 5-5: Cost estimation for hybrid wind turbine towers

Stage	Component/operation	COST	Unit	6-legged	4-legged
Manufacture	steel - lattice structure [ton]	2,000 €	Euros/ton	938,897 €	611,820 €
	steel - tubular structure [ton]	1,800 €	Euros/ton	298,131 €	298,131 €
	steel - transition pice [ton]	4,000 €	Euros/ton	579,249 €	662,562 €
	bolts [number]	1,800 €	Euros/(100×bolts M36/M42)	72,936 €	109,404 €
	Rotor Nacelle Assembly [kW]	1,690 €	Euros/kW	8,450,000 €	8,450,000 €
Transport	reinforced concrete of foundation [m3]	250 €	Euros/m3	225,000 €	225,000 €
	normal 15 ton truck [ton]	50 €	Euros/ton	27,264 €	19,087 €
	special truck [number trucks]	5,000 €	Euros/special truck	80,000 €	80,000 €
Erection	crawler crane [number days]	5,000 €	Euros/day	100,000 €	100,000 €
	crane mobilisation [number operation]	25,000 €	Euros/operation	25,000 €	25,000 €
	normal crane [number days]	1,000 €	Euros/day	50,000 €	50,000 €
Operation & maintenance	lifting equipment [number operation]	40,000 €	Euros/operation	40,000 €	40,000 €
	persons [number days*men]	200 €	Euros/day/person	100,000 €	100,000 €
	maintenance [for 20 years]	200 €	Euros/day /person	200,000 €	200,000 €
Disposal & end of life	normal crane - disassembly	50 €	Euros/ton	116,686 €	116,946 €
	persons [number days*men]	200 €	Euros/day/person	50,000 €	50,000 €
	transport (only normal crane)	50 €	Euros/ton	116,686 €	116,946 €
		TOTAL		11470 M€	11255M€
		Tower (% of total)		26.3%	24.9%

5.3 Design and installation of onshore hybrid steel wind towers: principles and details

5.3.1 General

A report that gives principles and details which address the design and installation of onshore hybrid steel wind towers was produced in the scope of this task. This was deliverable D5.3 of the project and was written with collaboration from all project partners. The report covered the following:

- Design principles for the lattice structure,
- Concept design of the transition piece,
- Fundamentals of the innovative tower erection system,
- Life cycle assessment of the resulting hybrid tower.

The report did not cover design aspects of the tubular tower.

5.3.2 Outline of the report

5.3.2.1 Section 1: Introduction

The report begins by describing the concept of onshore hybrid steel wind towers, as a combination lattice-tubular wind tower (hub height, H , 120~220 m), comprising the following three principal elements: (i) a lower lattice structure, (ii) an upper tubular component, and (iii) a transition piece connecting (i) and (ii), see Figure 5-14. This first section also lists the principal standards that served as a basis to produce design guidance.

5.3.2.2 Section 2: Materials

Section 2 covers the materials to be used in the hybrid towers, including a specially developed type of fastener (see also WP3).

5.3.2.3 Section 3: Design loads

Section 3 summarises the loads that need to be considered in design: (i) static loads, e.g. self-weight, weight of the nacelle, internal fixtures, and icing (depending on the location), (ii) dynamic loads, e.g. extreme wind, aerodynamic rotor thrust, and, if relevant, seismic loads, and (iii) fatigue loads caused by the rotor thrust, and vibration in case of resonance. More specifically, the design principles given below for the supporting structure are based on (i) wind loads acting directly on the tower, obtained from EN 1993-3-1 [13] and EN 1991-1-4 [12], and (ii) the effects of wind acting on the rotor during operation, represented by concentrated loads at the top of the tower. The load cases consist of static and dynamic loads which are caused by the airflow and its interaction with the stationary or moving parts of the wind turbine Table 5-6. Only the cases relevant to the conceptual design of the tower are summarised (the other load cases have little or no relevance or a small effect on tower loads). For each design load case, different types of loads are calculated using the relevant equations and the guidance given in EN 1991-1-4 [12]. The following abbreviations are used: ETM is the Extreme Turbulence Model, EWM is the Extreme Wind speed Model, NTM is the Normal Turbulence Model, V_{in} is the cut-in wind speed, and V_{out} is the cut-out wind speed. γ_f are partial safety factors for actions, ULS refers to Ultimate Limit States and FLS are Fatigue Limit States.

The design loads are found by aero-servo-elastic analysis under the most realistic loads acting on the tower structure's components. Such analysis accounts for the complex wind flow patterns around the wind turbine blades, and includes effects of the control and protection system of the wind turbine. For seismic analysis, the analysis determines the loads acting on the wind turbine components due to earthquake loading.

For structural modelling, the complex system of the hybrid tower is broken down into elemental components, e.g. tower, nacelle-tower connection, blades. The operational conditions of the specific wind turbine, defined in terms of wind speed and turbulence parameters, and the external loading (e.g. seismic events) need to be specified. The dynamic response can be characterised by examining the output from time domain simulations for each DLC, see Table 5-6. Load results are usually summarised in Table format that lists the extreme minimum and maximum loads.

Generalised forces at the top (index t) and base (index b) of the tubular tower component are required for the design of the three principal elements of the hybrid tower. The coordinate system adopted for these output parameters is shown in Table 5-7. The horizontal x-axis is along the wind

flow direction, the horizontal y -axis is across the wind flow direction, and the z -axis is vertical. The output parameters are summarised and defined in Figure 5-15.

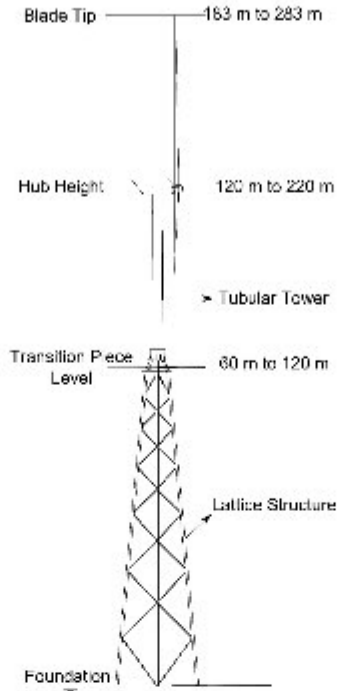


Figure 5-14: Scheme of a typical lattice-tubular hybrid wind tower

Table 5-6: Design Load Cases (DLC)

Design situation	Wind condition			Analysis	γ
1. Power production	DLC1.1	NTM	$V_{in} < V_{hub} < V_{out}$	ULS	1.25
	DLC1.2	NTM	$V_{in} < V_{hub} < V_{out}$	FLS	1.0
	DLC1.3	ETM	$V_{in} < V_{hub} < V_{out}$	ULS	1.35
6. Parked (still/idling)	DLC6.1	EWM	50-year recurrence period	ULS	1.35

Deemed-to-satisfy criteria for fatigue design are also outlined. The FLS is related to those loads associated with normal operating conditions and which occur with some frequency such that incremental contributions to fatigue damage may accumulate. In the scope of the current report, and in accordance with related design standards, see [40] and [38], the general principles given below are based on (i) the rainflow cycle counting method, which is an algorithm that identifies fatigue cycles by combining and extrapolating information from extrema (maxima and minima) in a time series,

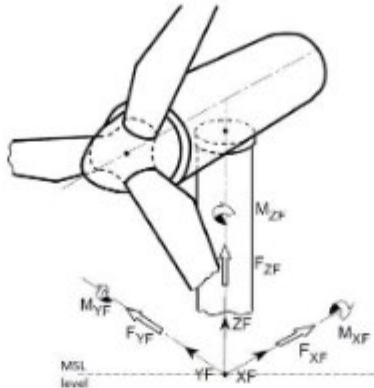


Figure 5-15: Global coordinate system

Table 5-7: Definition of output parameters (F: force, M: moment)

Generalised force	Definition
F_x	Fore-aft (wind direction) shear force
F_y	Side-side (across wind direction) shear force
F_z	Axial force
M_x	Bending in wind direction (the moment caused by side-side forces)
M_y	Bending across wind direction (the moment caused by force-aft forces)
M_z	Torsional moment

(ii) the Palmgren-Miner rule of linear damage accumulation, which calculates the total damage as a summation of increments, and (iii) the S-N curve formulation of the material fatigue characteristics. An S-N curve is a standardised plot of the stress range (S) corresponding to different number of cycles (N) resulting in fatigue failure. The Palmgren-Miner rule collates the cumulative effect of fewer number of cycles (n) at different stress levels (s). For the required service life, usually 20 years, the structure is designed such that the total damage accumulated by each cycle of incremental stress range at every critical section does not exceed the requirements for the overall damage accumulation.

5.3.2.4 Section 4: Design of the lattice structure

Presented next are the design checks and assessments to be performed in order to ensure the structural integrity of lattice towers, in accordance with Eurocode 3 for the design of steel structures. These are: (i) cross-section resistance, (ii) buckling resistance of members, (iii) resistance of connections, (iv) fatigue, and (v) constructability and transportation issues. In addition to these checks, a limit on the natural frequency of the support structure has to be imposed, in order to ensure that this remains above the largest operating frequency of the wind turbine. Example calculations are also given.

In this report, the following two different semi-closed polygonal (SCP) cross-sections are proposed:

- Nonagon, suitable for the pylons, i.e. for the leg members,
- Hexagon, suitable for the braces and the pylons (depending on the number of legs of the lattice structure).

A bolted connection assembly is provided that is particularly suited for connecting the structural members of the lattice tower, using the concept of SCP cross-sections and flat gusset plates. Two possible configurations for the cross-sections at joint locations are: the Star Form Joint (SFJ) for the nonagon SCP section, and the CruciForm Joint (CFJ) for the hexagon SCP section.

Bolted connections in this type of lattice structure have to be designed to ensure a good balance between resistance and maintenance. Resistance is naturally essential as these are the main load-transferring component in the tower system. Maintenance of the joints in this type of application can also be an issue. For example, vibration caused by wind can loosen bolted connections over time.

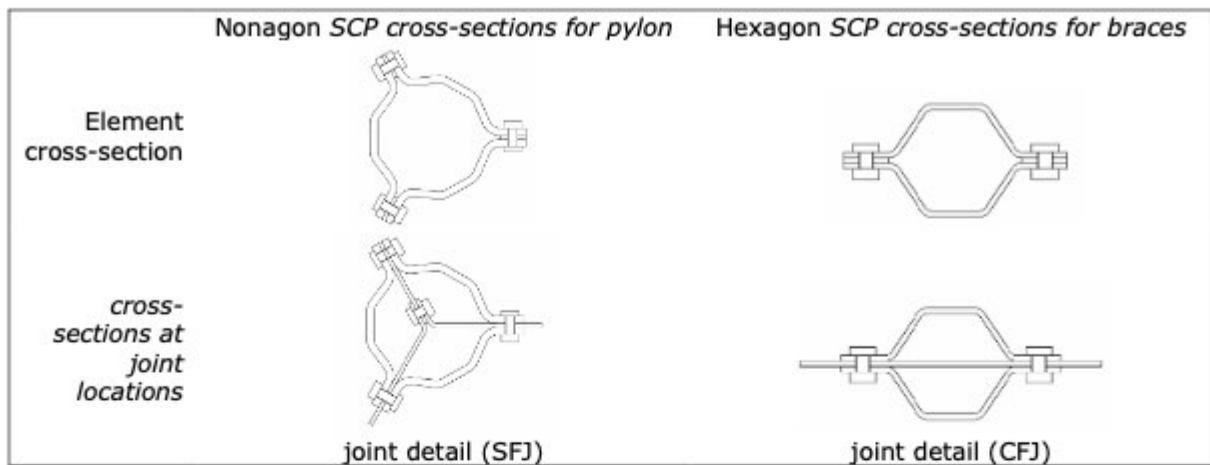


Figure 5-16: SCP cross-sections

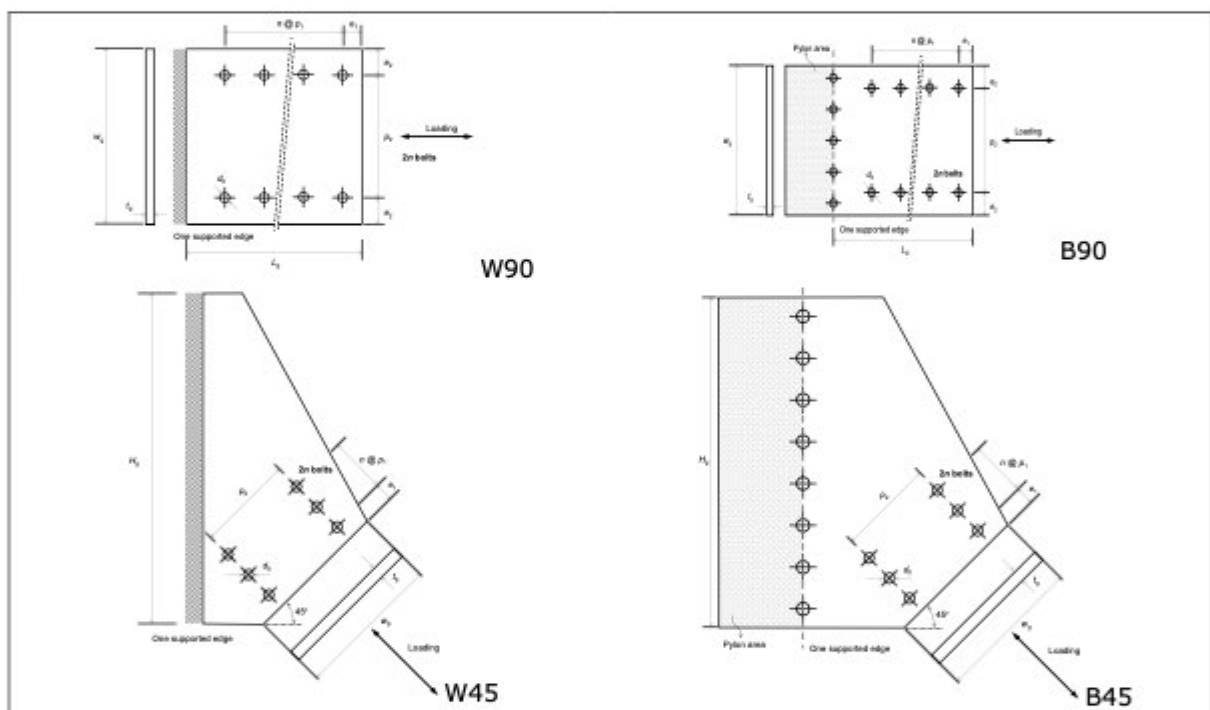


Figure 5-17: Joint configurations

For design purposes, the structural connections fall under category B, non-slip under unfactored loads, i.e. in service. The design model is fully compliant with the new revised prEN 1993-1-8 [17] design rules and assumes the traditional Truss Method to model lattice towers as space truss structures. The design procedures which follow are suitable for hand calculation or for the use of computer software.

The Whitmore section is often used to determine the peak tension or compression stress of an uneven stress distribution at the end of joints using gusset plates for truss connections. It does this by establishing an effective width l_w , which Whitmore determined could be calculated by spreading the force from the start of the joint, 30° to each side in the connecting element along the line of force. The Whitmore section can spread across the joint between connecting elements but cannot spread beyond an unconnected edge.

Gusset plate connections are neither pinned nor fixed joints, and these connections may have some effect on the stiffness, resistance and inelastic deformation capacity of the system. The gusset plate is assumed to act as a cantilever beam subjected to a point load at the free end. The length of this

cantilever is the same as for the strut for compressive resistance, L . The beam section is the Whitmore section. If we neglect the shear deformation then we obtain the following flexural beam stiffness, which is taken as the rotational spring stiffness:

$$K_\theta = \frac{EI_{\text{Whit}}}{L}$$

5.3.2.5 Section 5: Design of the transition piece

Section 5 is dedicated to the conceptual design of the transition piece, which essentially serves as an adapter of the lattice structure to the tubular tower. The basic shape of the transition piece is that of a truncated conical or cylindrical shell, made from steel grade S690 ($f_y = 690 \text{ N/mm}^2$) with top plate bolted to the bottom of the tubular tower and a bottom plate bolted to the top of the lattice structure. Two alternative structural concepts are examined:

- A custom design to connect a specific multi-legged lattice structure to a tubular tower; the underside of the bottom of the piece needs to be provided with a number of connection areas corresponding to the number of legs.
- A design that is independent of the lattice structure, but dependent on the tubular tower design, to some extent; this concept offers the advantage of industrial mass-production, which can fit each individual wind tower design on the basis of the performance needs.

Concept 1: The transition piece has the shape of (i) a truncated conical shell or (ii) a cylindrical shell, to which a number of corner posts are attached by means of gusset plates. The number of corner posts is the same as the number of legs of the lattice structure, to which they are connected to locate the transition piece in its final position. Figure 5-7**Error! Reference source not found.** illustrates this concept for a six-legged lattice supporting structure. The flange plates at the upper and lower ends of the transition piece ensure the connection between all elements. The corner posts are joined by cross struts (not shown in this scheme).

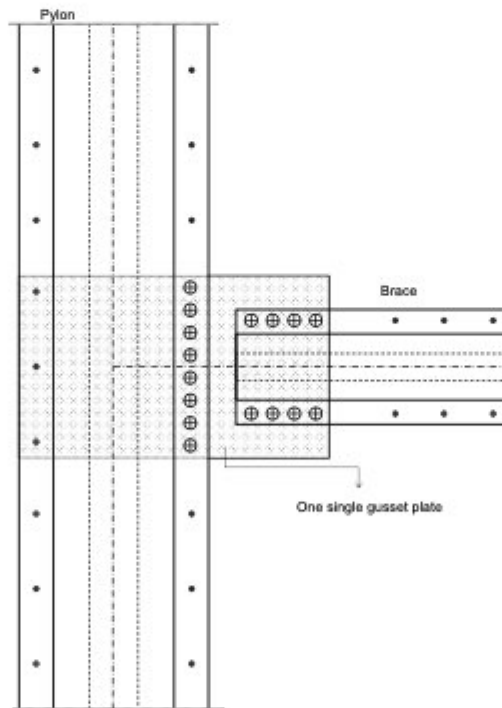


Figure 5-18: Example: joint between pylon and brace, both members using hexagonal SCP sections

Concept 2: The transition piece is a cylindrical extension of the tubular tower section and is installed inside the top level of the lattice structure, see Figure 5-8 for the case of a lattice with four-legs. The cylindrical extension is terminated by horizontal annular flanges, at the top and bottom, which are subsequently attached to the legs of the lattice structure by means of cross struts that extend

diagonally. The cylindrical extension has a slightly larger diameter to allow for the lifting of the tubular tower.

5.3.3 Section 6: Erection process

Section 6 describes the erection process, see also WP2, which is a central aspect for this hybrid concept, and defines key constraints for the design of the transition piece between the lattice structure and the tubular tower. The process for a tower that uses the first concept above for the transition piece is described by way of example.

5.3.4 Section 7: Life cycle assessment of lattice-tubular hybrid towers

The potential environmental impacts of the hybrid tower by means of a detailed life-cycle analysis are finally quantified and discussed, in section 7, see also description for Task 5.2.

5.4 Conclusions

With recent demands for taller wind turbine towers with enhanced capacities, comes a respective increase in the energy required for their manufacture and a need to investigate whether the latter can be sufficiently justified by equivalent increases in the energy yield of the system. Upon comprehensive literature review, a gap in knowledge on the life cycle analysis of tall hybrid wind turbine towers has been identified.

The life cycle performance of 185 m hybrid towers has been assessed. The component and the stage that is the most critical for the environmental impact have been presented. The LCA results were also compared with that of conventional towers, showing that the hybrid structure could be a promising solution. The abiotic depletion is quite similar to the one of the steel tubular towers. The acidification potential appears larger than the 150 m towers, which attributed to the large duration of the erection process accompanied by long time usage of cranes and is expected to decrease as the process gets established. The energy payback time is similar to the 150 meters steel tubular tower and is about 40% higher when the 150 meters steel-concrete solution is used for comparison

An estimation of the cost has been provided. Assuming average unit prices for material, transportation, cranes and lifting equipment and estimated manhours for the complete process of manufacturing, assembling and maintenance, the total cost estimates for the two different solutions were calculated and no significant difference between them was found. Considering the cost of Rotor Nacelle Assembly based on average values including installation, operation and maintenance cost the estimation of the cost for the whole tower comprises approximately 25% of the total cost. This represents about 600€/kW of a total of 2300€/kW.

6 Coordination, management and dissemination

Objective of WP6 is coordination and management of the activities performed by partners in the project, as well as planning, organization and progressive evaluation of research and dissemination of research results developed within the project. The activities have been performed as planned.

6.1 Coordination

During the project general meetings have been organized twice a year. The coordinator promoted also several restricted teleconference meetings. Mid-term report and final report (this document) have been provided. All foreseen deliverables were also prepared and provided with the reports. Publications authored by the project members related to the content and to the work developed in the project have been produced and reported in this document.

6.2 Expert's workshop

During the 3rd meeting at RWTH Aachen University in Germany an international Workshop has been organized. It was organized as a one day workshop, which was held on the first day of the meeting. The workshop objectives were to discuss the ongoing research with industrial experts and to get direct input from the experts for the project, so that the gained results are a very industry-related research. The outcome directly influenced the next work steps of the project. A publication with the presentations was issued.

The final workshop was organized on the 28th June 2018 at Broadway House in London. During the full-day workshop the most promising results of the project in view of possible practical application were presented by the project partners. Additionally, invited experts from two companies directly interested in the project outcomes presented possible future developments, i.e., Salzgitter Mannesmann Renewables, that offers lattice solutions for wind towers presented possible developments concerning the hybrid lattice-tubular concept, and HEBETEC Engineering Ltd, that was involved in the erection process presented the state-of-art solutions for computerized elevation of heavy structural parts, which can be used in real applications of the developed hybrid solution. This workshop counted on the presence of designers and a wind turbine producer. Deliverable D6.4 gives the detailed program, presentations and list of participants.

7 Impact of the results and conclusions

The technological advancements of the new wind energy converters use rotors with large diameters and long blades. This requires higher hub heights and larger support structures than currently used, to take advantage of less turbulent wind and higher wind speeds in higher altitudes. In order to make a cost-effective construction process for high rise towers new challenges are put to the well-established current technology for the support structure in steel, which is based on the tubular tower concept.

The market based on repowering of the old onshore wind parks with new wind converters is increasing rapidly. Already during 2015 German repowering share was 176 out of 1115 wind turbine generators net additions which amounts to 484.1 MW capacity. Due to the wind potential of some wind parks' locations, higher capacity of more than 5 MW is also being installed. The full repowering of the wind parks means that the whole installation is replaced with a new structure and a higher capacity converter, which requires development of new tower concepts for easier transportation and installation.

The concept of steel hybrid lattice-tubular tower is proposed in this work, to overcome known insufficient offer of steel solutions in the onshore wind energy market. A lattice structure offers several advantages: (i) it requires less material; (ii) it is easier to control dynamic characteristics by geometric changes; (iii) transportation is much more convenient when road transportation facilities present size restrictions; (iv) the wind airflow resistance is reduced, due to the 'shadow' area, compared to tubular structures; and (v) it can be used as a support structure for self-erection of tubular tower. However, the traditional lattice towers using currently available angle sections are not suitable for the use in wind towers because of the insufficient resistance and the high number of connections. The costs of lattice construction are adversely influenced by an increase in work on site due to the number of bars and connections involved and the maintenance requirements of bolted connections subjected to fatigue loading.

The solution proposed in this project uses polygonal cross-sections for the truss elements and special type of connections. The study of three cases of hybrid towers was defined as a Milestone in this project. From the several supporting structures with different heights investigated and designed, three scenarios are selected targeting 185m for the tower height. It was shown that, by controlling the members stability using hollow sections, it is possible to increase their length and reduce the number of connections. Since stability is an issue for the members with the new type of semi-closed cross sections, numerical and experimental work has been developed that show good perspectives for their application, not only in this specific area of wind energy but also in other structural applications. It also opened new research questions connected to the efficient use of high strength steel in stability governed design of truss members. On the other hand, the numerical and experimental work developed on the specific connections used for these members have shown, that designer may take advantage of the semi-rigid behaviour to increase overall stiffness and to improve tower design. In this case as well, new research questions were opened, which relate to the efficient geometry of the star-like gusset connection inside the compressed members.

Developing new type of steel for bolts with improved fatigue resistance gave answer to the research questions in this project for the use in wind towers, not overlooking other potential uses, e.g. in ring connections. The steel grades considered in this work are suitable for bolts with diameters up to $\varnothing < 36\text{mm}$. Looking at the characterization carried out, it was concluded that both grades, 32CrB4 EQ and 30MnNiB4 EQ, reach easily the required properties by class 10.9 of ISO 898-1:2005. Furthermore, both grades exceed the fatigue limit of the standard 32CrB4. The current trend of increasing tower dimensions involves higher diameter bolts at the same time. In that sense, if bigger fasteners $\varnothing > 36\text{mm}$ want to be manufactured the 30MnNiB4 EQ represents a competitive and suitable alternative. 30MnNiB4 EQ presents higher hardenability than 32CrB4 EQ so the martensite requirements are more easily achieved for large diameters. Furthermore, the price of 30MnNiB4 EQ is lower in comparison with other alternative high alloyed grades (i.e. 30CrNiMo8).

An important disadvantage of the tubular-based construction techniques, which considerably affects the competitiveness of steel solution, consequent on the weight of the tubular tower, is the need for very large concrete slab foundations, whose diameter and concrete volume increases rapidly with increasing height of the tower. The natural solution is to enlarge the tower base by using an open structure (such as a lattice), which is also a solution that has proven to be efficient in jacket foundations used in offshore installations for medium to large water depths.

Although the advantages of the proposed concept have been identified and are being explored by the industry (there are solutions in the market, for instance by Suzlon) some important

disadvantages remain: (i) the need for extremely large and expensive cranes to lift the heavy sections to extremely high levels and (ii) the difficulty of assembling the sections of tower and turbine at large heights. Solutions that can avoid these drawbacks need to allow for assembly at low level, or at least at moderate height, in order to facilitate the use of only normal height cranes. Self-erection concept is a possibility and is currently used for small wind turbines. Previous studies identified several viable self-erection techniques and pointed out two main concepts based on tower climbing devices or on secondary structures (erection tower). The main conclusion was that, from an economical point of view, the self-erection techniques compare favourably with current crane technique when the tower height and geometric complexity increase. In view of this, a state-of-the-art solution for the assembling sequence was developed in collaboration with external industrial experts. It consists in three main phases. First, the tubular parts are assembled inside the lattice structure and the transition piece is mounted on top of the lattice structure. The second phase is the erection of the tube to a position that allows the nacelle and the rotor to be mounted on top of it. Last phase uses the jackets to pull the moving part up to the final position. The feasibility test performed on a 1:4 downscaled prototype has shown the potentiality of this procedure. A full-scale test would be the natural development of this outcome.

The life cycle performance of hybrid towers has been assessed. The energy payback time is similar to the 150 meters steel tubular tower. An estimation of the cost has been provided, which assumes average unit prices for material, transportation, cranes and lifting equipment and estimated manhours for the complete process of manufacturing, assembling and maintenance. Considering the cost of Rotor Nacelle Assembly based on average values including installation, operation and maintenance cost the estimation of the cost for the whole tower comprises approximately 25% of the total cost. This represents about 600€/kW of a total of 2300€/kW. Considering 25 years and 10GWh/year, the estimated value of 0,046€/kWh compares fairly well with the cost of onshore wind energy in 2017.

During the development, the interaction with invited experts from academia and from companies external to the project team was promoted and achieved. The organization of a final full-day workshop to present the findings of the project in view of possible practical application was very successful. In this workshop, experts from companies directly interested in the project outcomes were present, e.g. Salzgitter Mannesmann Renewables, that offers lattice solutions for wind towers and HEBETEC Engineering Ltd, that offer state-of-art solutions for computerized elevation of heavy structural parts. This workshop counted also on the presence of designers and wind turbine producer.

A list of publications resulting from the work in the project follows.

Farhan M., Mohammadi M., Correia J.A., Rebelo C. (2018) Probabilistic Fatigue Analysis of a Wind Turbine Transition Piece Based on SWT Method, ICMFM XIX, Porto.

Farhan, M., Mohammadi, M.R.S., Correia, J.A., Rebelo, C. (2018). "Transition piece design for an offshore hybrid wind turbine with multiaxial fatigue life estimation". Wind Engineering, 42(4), 286-303.

Gkantou, M. and Baniotopoulos, C. (2018) Life cycle analysis of onshore wind turbine towers. In the International conference on wind energy harvesting. Catanzaro Lido, Italy. 21-23 March 2018.

Gkantou, M., and Baniotopoulos, C. (2019) Wind energy structures: Assessment from a lifecycle perspective, The 15th International Conference on Wind Engineering, Beijing, China. September 1-6, 2019.

Gkantou, M., and Baniotopoulos, C. and Rebelo, C. (To Be Submitted) Life cycle assessment of onshore hybrid wind turbine towers

Gkantou, M., Baniotopoulos, C., and Martinez-Vazquez, P., (2017) Tall hybrid wind turbine towers. Load analysis and structural response. In the international conference on wind energy harvesting 2017, 20-21 April 2017, Coimbra, Portugal.

Gkantou, M., Martinez-Vazquez, P. and Baniotopoulos, C. (2017). On the structural response of a tall hybrid onshore wind turbine tower. Procedia engineering, 199, pp.3200-3205.

Gkantou, M., Martinez-Vazquez, P. and Baniotopoulos, C., (2017) On the structural response of a tall hybrid onshore wind turbine tower. In the X International Conference on Structural Dynamics, EURODYN 2017, 10-13 September 2017, Rome, Italy.

Gkantou, M., Martinez-Vazquez, P., and Baniotopoulos, C. (2017) On the structural response of a tall hybrid onshore wind turbine tower. Procedia Engineering 199: 3200-3205.

Gkantou, M., Martinez-Vazquez, P., and Baniotopoulos, C. (2017) Tall hybrid wind turbine towers. Load analysis and structural response. In the International conference on wind energy harvesting (WINERCOST). Coimbra, Portugal. 20-21 April 2017.

Herrero D., Albarrán J.J. "EXTREME Steels: A high performance solution for wind fasteners exposed to adverse weather conditions" Book of Abstracts Winercost'17. Vol. 1. 164-170 (2017).

Jovašević S., "In-situ bolted connections in lattice towers for WEC ", Project of PhD thesis presented to the PhD program in Steel and Mixed Construction, University of Coimbra, 2016.

Jovašević S., Correia J.A.F.O., Pavlović M., Rebelo C., De Jesus A.M.P., Veljković M., Simões da Silva L. - "Global fatigue life modelling of steel half-pipes bolted connections". XVIII International Colloquium Mechanical Fatigue of Metals, Gijón (Spain), September 5-7, 2016; Procedia Engineering. {<https://doi.org/10.1016/j.proeng.2016.08.891>}

Jovašević S., Mohammadi M. Rebelo C., Pavlović M., Veljković M., "New Lattice-Tubular Tower for Onshore WEC – Part 1: Structural Optimization", X International Conference on Structural Dynamics, EURODYN 2017, September 15–17, 2017, Rome, Italy

Jovasevic S., Mohammadi M.R.S., Rebelo C., Pavlovic M., Veljkovic M., "New lattice-Tubular Tower for Onshore WEC - Part 1: Structural Oprimization", Procedia Engineering, Vol. 199. 3236-3241, 2017

Jovašević S., Rebelo C., Pavlović M. Simões da Silva L., "Steel hybrid towers for wec: geometry and connections in lattice structure", WINERCOST'17 Conference, Coimbra, 20-21 April 2017

Jovašević S., Rebelo C., Pavlović M. Correia J.A., "Finite element modelling of preloaded gusset plate connections between polygonal built-up members", CESARE'17 Conference in Dead Sea from 3-8 May 2017.

Jovasevic S., Rebelo C., Pavlovic M., Correia J.A., "Finite element modelling of preloaded gusset plate connection between polygonal built-up members", INTERNATIONAL CONFERENCE "Coordinating Engineering For Sustainability and Resilience", Vol. 1. 97-104, 2017

Jovasevic S., Rebelo C., Pavlovic M., Simoes da Silva L., "Geometry and connection in lattice towers for WEC", INTERNATIONAL CONFERENCE on Wind Energy Harvesting, Vol. 1. 317-321, 2017

Jovasevic S., Rebelo C., Pavlovic M., Veljkovic M., "Numerical investigation of preloaded gusset plate connections between polygonal built-up members", Proceedings of Eurosteel 2017, Vol. 1. Issue 2-3. 292-297, 2017

Jovašević S., Rebelo C., Pavlović M., Veljković M., "Numerical investigation of preloaded gusset plate connections between polygonal built-up members", EUROSTEEL 2017, September 13–15, 2017, Copenhagen, Denmark.

Manoleas P.s, Koltsakis E., and Lagerqvist O., 'Polygonal columns under compression', in ICTWS 2018, Lisbon.

Martinez-Vazquez, P., Gkantou, M., and Baniotopoulos, C. (2018) Assessing the impact of earthquake and wind load in the performance-based design of wind turbine towers. In the International conference on wind energy harvesting. Catanzaro Lido, Italy. 21-23 March 2018.

Matos R, Pinto P.L, Rebelo C., Veljkovic M. and Simões da Silva L. "Axial monotonic and cyclic testing of micropiles in loose sand", Geotechnical Testing Journal, Volume 41, Issue 3 (May 2018)

Matos R., Mohammadi M., Rebelo C., Veljkovic M. "A year-long monitoring of preloaded free-maintenance bolts - Estimation of preload loss on BobTail bolts", Renewable Energy - An International Journal Volume 116, Part B, February 2018, Pages 123-135

Matos R., Mohammadi M., Rebelo C., Veljkovic M., A year-long monitoring of preloaded free-maintenance bolts - Estimation of preload loss on BobTail bolts, Renewable Energy Volume 116, Part B, February 2018, Pages 123-135

Matos, R.M.M.P.; Pinto, P.M.C.M.L.; Rebelo, C.A.S.; Gervasio, H.; Veljkovic, M., "Improved design of tubular wind tower foundations using steel micropiles", Journal of Structure and Infrastructure Engineering – Maintenance, Management, Life-Cycle Design and Performance Volume 12, 2016 - Issue 9, Pages 1038-1050.

Mohammadi M. R., Farhan M., Rebelo C., Veljković M., "Preliminary Investigation on Transition Piece Design for an Onshore Wind Turbine Supporting Structure", EUROSTEEL 2017, September 13–15, 2017, Copenhagen, Denmark

Mohammadi M. R., Farhan M., Rebelo C., Veljković M., "Preliminary Investigation on Transition Piece Design for an Onshore Wind Turbine Supporting Structure", ce/papers, vol. 1, no. 2-3, pp. 4400–4409, Sep. 2017.

Mohammadi M. R., Jovašević S., Rebelo C., Pavlović M., Veljković M., "New Lattice-Tubular Tower for Onshore WEC – Part 2: Aero-Elastic Analysis and Loads Calculation", X International Conference on Structural Dynamics, ERODYN 2017, September 15–17, 2017, Rome, Italy

Mohammadi M. R., Jovašević S., Rebelo C., Veljković M., Simões da Silva L., "The hybrid highrise wind turbine tower concept", WINERCOST'17 Conference, Coimbra, 20-21 April 2017

Mohammadi M. R., Matos R., Rebelo C., "Bobtail® Bolt Preload Loss in Wind Turbine Tower Prototype – Hammerstein-Wiener Identification Model", EUROSTEEL 2017, September 13–15, 2017, Copenhagen, Denmark

Mohammadi M. R., Thomassen P., Rebelo C., "Wind turbine load simulations using two different servo-hydro-aeroelastic software codes", CESARE'17 Conference in Dead Sea from 3-8 May 2017

Mohammadi M., Jovasevic S. and Rebelo C. (To Be Submitted) Steel hybrid lattice-tubular tower for very tall wind turbines

Mohammadi M., Rebelo C., Veljković M. and Simões da Silva L. (2018) The Hybrid Highrise Wind Turbine Tower: The Transition Piece Design, WINERCOST18 - THE INTERNATIONAL CONFERENCE ON WIND ENERGY HARVESTING 2018, 21-23 March, Catanzaro Lido, Italy

Mohammadi M.R.S., Richter C., Pak D., Rebelo C., Feldmann M., "Steel hybrid onshore wind towers installed with minimal effort – development of lifting process" in Wind Energy Harvesting, 2017, pp. 188–193.

Mohammadi, M.R.S., Richter, C., Pak, D., Rebelo, C., Feldmann, M., (2018). "Steel hybrid onshore wind towers installed with minimal effort: development of lifting process". Wind Engineering, 42(4), 335-352.

Mohammadi, M.R.S., Richter, C., Pak, D., Rebelo, C., Feldmann, M., (2018). "Steel hybrid onshore wind towers installed with minimal effort: development of lifting process". Wind Engineering, 42(4), 335-352

Sabau G., Koltsakis E., Lagerqvist O., "Stability analysis of newly developed polygonal cross-sections for lattice wind towers", WINERCOST'17 Conference, Coimbra, 20-21 April 2017

Stavridou, N., Koltsakis, E., & Baniotopoulos, C. C. (2018, June). Material Optimisation use in steel lattice wind turbine towers. Paper presented at 9th GRACM International Congress on Computational Mechanics: Chania, 4-6 Chania. Greece.

Stavridou, N., Koltsakis, E., & Baniotopoulos, C. C. (2018, March). Structural Investigation of lattice and tubular steel wind turbine towers. A comparative study. In C. Baniotopoulos, C. Borri, E. Marino, B. Blocken, H. Hemida, M. Veljkovic, T. Morbiato, R. Borg & N. Hamza. Wind Energy Harvesting...(...Focusing on exploitation of the Mediterranean Area). Paper presented at Winercost'18 Conference: Catanzaro Lido, 21-23 March (pp. 291-297). Italy.

Tran, A.T., Veljkovic, R., Rebelo, C., Simões da Silva, L. "Resistance of cold-formed high strength steel circular and polygonal sections - Part 1: experimental investigations", Journal of Constructional Steel Research, 120, 245-257 (2016).

Tran, A.T., Veljkovic, R., Rebelo, C., Simões da Silva, L. "Resistance of cold-formed high strength steel circular and polygonal sections - Part 2: numerical investigations", Journal of Constructional Steel Research, 125, 227-238 (2016).

Veljkovic M., Rebelo, C., Pavlovic M. , Heistermann C. "Onshore wind towers, basics of structural design", WINERCOST Workshop 'Trends and Challenges for Wind Energy Harvesting', Coimbra, 30-31 March 2015.

List of Figures

Figure 0-1: Structure of the work-packages developed in the project	5
Figure 0-2: Schematic dimensions of hybrid supporting structure reference designs (a); overturning moment (b) and fore-aft moment on transition piece level (c).....	9
Figure 0-3: The schematic of transition piece for 6-legged (a) and 4-legged (b) tower geometries	9
Figure 0-4: Erection sequence	11
Figure 0-5: Down-scaled transition piece (a) prototype ready for erection test (b) and detail for fatigue assessment (c).	11
Figure 0-6: The 185 meters tall worked examples for 6-legs (a) and 4-legs (b) with TPs.....	14
Figure 1-1: The Global coordinate system (GL 2010)	16
Figure 1-2: Schematic dimensions of hybrid supporting structure reference designs.....	17
Figure 1-3: Sensor positions in the structure (a) and model as a beam element model.....	19
Figure 1-4: A wind step case, red line: wind speed, orange line: pitch angle, and blue line: generator power.	20
Figure 1-5: The main characteristics of the wind turbine dynamic response from DLC 1.1.....	21
Figure 1-6: The fore-aft and side-side bending moment at tower top and at transition level for (a) 120+100 m, (b) 120+65 m, and (c) 60+60 m supporting structure (lattice-tubular).....	21
Figure 1-7: The number of cycles per wind speed.....	22
Figure 1-8: Load spectra for different modes of operation.....	22
Figure 1-9: Section of the lower tubular part and TP.....	23
Figure 1-10: The diaphragms subsequently attached to the truss girders ABCD and A'B'C'D'	23
Figure 1-11: schematic representation of the Concept 1 transition piece concept	24
Figure 1-12: (a) Dimensions of the Cylindrical Shell, (b) The transition piece main components..	24
Figure 1-13: The schematic view of transition piece and the detail view of the connections	25
Figure 1-14: Schematic of 2D lattice structure	26
Figure 1-15: Wind load direction on structure	26
Figure 1-16: The steel mass against number of connections (a) and (b), and against the estimated number of bolts for (c) and (d) for 120- and 60-meters lattice structures	27
Figure 1-17: The Mode Shapes of (a) 120m, and (b) 220m tower and respective first natural frequencies	28
Figure 1-18: Weight of a strut as a function of D/t.....	30
Figure 1-19: Face brace total weight as a function of V-diagonals angle to the horizontal.....	30
Figure 2-1: Assembling sequence (a)-(n) and strands pedestal, bottom plate (0)-(p)	38
Figure 2-2: Critical stages for erection process.....	39
Figure 2-3: The schematic of tower parts for downscaling.....	40
Figure 2-4: The dimensions for TP prototype, (a) front view, (b) top view.....	41
Figure 2-5: (a) The initial 3D model, (b) Fabrication ready model in Tekkla.....	42
Figure 2-6: The fabrication details in the Tekkla model, (a) the working station space detail and (b) the connection between transition piece and the lattice structure	42
Figure 2-7: The transition piece stabilizer system	43
Figure 2-8: Schematic of cold form processes	43
Figure 2-9: The manufactured column and post treating procedure.....	43
Figure 2-10: The braces of the scaled lattice structure	44
Figure 2-11: (a) The tube segment, (b) top and lower arc plates.....	44
Figure 2-12: the tower components assembled before on site	45
Figure 2-13: The assembled scaled prototype	45
Figure 2-14: Three execution scenarios for the feasibility test, (a) simple lift up, (b) simple lift down and (c) lift up with an extra mass	47
Figure 2-15: The locations for tubular tower strain gauges	47
Figure 2-16: Accelerometers, LVDTs, and TP strain gauges.....	47
Figure 2-17: (a) prepared surface for the SG, (b) implemented SG.....	48
Figure 2-18: Adjusted LVDTs on the TP	48
Figure 2-19: HBM acquisition system.....	48

Figure 2-20: (a) The strandjacks arrangement, (b) attachment of slings to the bottom of the tubular segment	49
Figure 2-21: (a) Controller unit, (b) hydraulic pump and monitoring system	49
Figure 2-22: The installed stabilizers on the transition piece	49
Figure 2-23: 1 st scenario execution of lifting up	50
Figure 2-24: 3 rd scenario execution of lifting up	50
Figure 2-25: The comparison of measures stress and the finit element simulation.....	51
Figure 2-26: The comparison of measures top displacement and the finit element simulation	51
Figure 2-27: (a) tilt angle during erection with heavier burden, (b) stabilizer dislocation.....	51
Figure 2-28: Model of the bolted (a) and welded (b)transition segment	52
Figure 2-29: Overview of the procedure and results of the fatigue analysis	53
Figure 2-30: Detail for fatigue analysis (a) and FE mesh in ABAQUS	54
Figure 2-31: Mesh convergence study.....	54
Figure 2-32: Overview of the maximum stress results (a) Detailed view of damage results in the upper part of the transition piece (b)	55
Figure 2-33: Welded transition piece (a) weld connection detail (b)	55
Figure 2-34: Transition piece shell and the chord stress distribution (a) shell, (b) chord	56
Figure 3-1. Steel manufacturing process at Sidenor	60
Figure 3-2: Heat treatment cycle applied to the 32CrB4 EQ (left) and 30MnNiB4 EQ (right).....	60
Figure 3-3: 32CrB4 EQ microstructure at 500X: Surface (left), Mid-radius (middle) and Core (right).	61
Figure 3-4: 30MnNiB4 EQ microstructure at 500X: Surface (left), Mid-radius (middle) and Core (right).	62
Figure 3-5: Hardness profile of the 32CrB4 EQ and 30MnNiB4 EQ steels	62
Figure 3-6. Average results of the tensile tests performed with the conventional parameters.....	63
Figure 3-7. Influence of the strain ratio on the UTS and YS for the 32CrB4 EQ (left) and 30MnNiB4 EQ (right).	64
Figure 3-8. Ductile-brittle transition curve for 32CrB4 EQ and 30MnNiB4 EQ.	65
Figure 3-9. MTS servohydraulic machine in which the fatigue tests were conducted	66
Figure 3-10. Staircase method for the fatigue limit determination of the 32CrB4 EQ.....	67
Figure 3-11. Staircase method for the fatigue limit determination of the 30MnNiB4 EQ.....	68
Figure 3-12. Wöhler curves obtained for 32CrB4 EQ and 30MnNiB4 EQ.....	69
Figure 3-13. Fatigue fracture occurred in the 32CrB4 EQ after 3.727.980 cycles applying 590 MPa.	69
Figure 3-14. Fatigue fracture occurred in the 32CrB4 EQ after 20.129 cycles applying 730 MPa..	69
Figure 3-15. Fatigue fracture occurred in the 30MnNiB4 EQ after 2.984.764 cycles applying 560 MPa.	70
Figure 3-16. Fatigue fracture occurred in the 30MnNiB4 EQ after 657.084 cycles applying 600 MPa.	70
Figure 3-17. Hysteresis loops for the 32CrB4 EQ and a strain rate of 0,4%.	71
Figure 3-18. Hysteresis loops for the 30MnNiB4 EQ and a strain rate of 0,4%.	71
Figure 3-19. Geometry of the connections to be fatigue tested.....	72
Figure 3-20. Connections manufacturing process scheme.....	72
Figure 3-21. Connections in the corrosion chamber.....	73
Figure 3-22: MTS servohydraulic machine in which the fatigue tests were conducted	73
Figure 3-23. Fatigue results for NC3.	74
Figure 3-24: Fatigue results for NC4.....	74
Figure 3-25. Fatigue results for C3.	75
Figure 3-26. Fatigue results for C4.	77
Figure 3-27. Comparison of fatigue results for 3 mm (left) and 4 mm (right) thickness connections.	78
Figure 4-1: Comparison of FEM results with design curves and values	84
Figure 4-2: Model overview.	84
Figure 4-3: Middle joint rigid body.....	84

<i>Figure 4-4: End joint detail and meshing</i>	85
Figure 4-5: Ratio of the reduction factor based on FEM results over the effective area reduction factor from EN 3-1-5 [19] for a range of cross-sectional slenderness and bolt spacing.....	86
Figure 4-6: Connections' geometry.....	87
<i>Figure 4-7: Predicted ultimate load</i>	87
Figure 4-8: Test specimen B90	87
Figure 4-9: Test specimen W90	88
Figure 4-10: LVDTs and Strain gauges disposition	88
Figure 4-11: Test specimen B45	89
Figure 4-12: Test specimen W45.....	89
Figure 4-13: B90 moment-rotation curve (left) and failure (right).....	90
Figure 4-14: W90 moment-rotation curve (left) and failure (right).....	90
Figure 4-15: B45 moment-rotation curve (left) and failure (right).....	91
Figure 4-16: W45 moment-rotation curve (left) and failure (right).....	91
Figure 4-17: failure of SC-PCS when load is inserted smoothly (a) and when load is inserted realistically via the star-shaped gusset plate (b).....	93
Figure 4-18: star-shaped gusset plate with varying cross section.....	93
Figure 4-19: ultimate resistance of column: EN50341 (left), En1993-1-6 (right).....	94
Figure 4-20: plate type imperfections (a) and "double spillover" imperfections (pairs of consecutive edges distort in the same sense) (b)	94
Figure 4-21: σ_{GMNIA}/f_y for various imperfection patterns (Fabrication Class A. S355)	95
Figure 4-22: dashed line is the boundary between plate-dominated (left) and edge-distortion-dominated (right) collapse mechanism regions ($\min(\sigma_{GMNIA,shl}, \sigma_{GMNIA,plt})/f_y$).....	95
Figure 4-23 failure regions boundaries	95
Figure 4-24 Matrix of specimens (S700).....	95
Figure 4-25: Measured edges deviation from straightness, specimen SP1 and final test set-up at COMPLAB.....	96
Figure 4-26: Average stress / strain date as recorder from the experiments.....	97
Figure 4-27: Laser-scanned failure patterns that developed in the specimens during testing	97
Figure 4-28: Load application pattern in group B experiments.....	97
Figure 4-29: Bolts numbering in group B experiments.....	98
Figure 4-30: General setup	98
Figure 4-31: Load [kN] vs. displacements [mm] (a) scenario A pylon Axial displacement; (b) scenario A left actuator; (c) scenario A right actuator; (d) scenario B left actuator; (e) scenario B left actuator; (f) scenario D left actuator; (g) scenario D right actuator	99
Figure 4-32 column with arms forming a 120deg angle: deformed configuration.....	99
Figure 4-33: Planar cruciform specimen and Instrumentation on the gusset plate (welded specimen).....	100
Figure 4-34: Load-displacement results od tests	102
Figure 4-35: 2D joints designed for test programme in Task 4.1.....	102
Figure 4-36: Parameterisation of the brace (bolted and welded joint).....	103
Figure 4-37: Parametric bolted joint model with various brace-to-pylon angles.....	104
Figure 4-38: Boundary conditions, displacement outputs and mesh details (B90 joint model)	104
Figure 4-39: Assessment of moment – rotation behaviour (2D B90 joint with 5mm out-of-plane imperfection)	106
Figure 4-40. Assessment of moment – rotation behaviour (2D W90 joint).....	106
Figure 4-41: Results of parametric study.....	107
Figure 4-42:Effective buckling lengths of bracing members in lattice towers.....	109
Figure 5-1: Shear profile for different reference wind speeds	111
Figure 5-2: Turbulence power spectra von Karman and Kaimal mathematical functions	112
Figure 5-3: Generated turbulent wind model in 10 minutes time period	112
Figure 5-4: Weibull distribution comparison for 100 m and 200 m distance from the ground	113
Figure 5-5: Six-legged lattice structure geometry I; dimensions in (mm).....	113
Figure 5-6: Four-legged lattice structure geometry II; dimensions in (mm).....	114

Figure 5-7: Transition piece for the six-legged lattice structure geometry I, dimensions in (mm)	115
Figure 5-8: Transition piece for the four-legged lattice structure geometry I, dimensions in (mm)	115
Figure 5-9: System boundary for LCA of hybrid wind turbine towers	116
Figure 5-10: Mass distribution for the two case studies	116
Figure 5-11: Contribution of each component	120
Figure 5-12: Contribution of each life cycle stage	121
Figure 5-13: Comparison of hybrid 185 m tower with 150 m tubular towers from [31]	122
Figure 5-14: Scheme of a typical lattice-tubular hybrid wind tower	125
Figure 5-15: Global coordinate system	126
Figure 5-16: SCP cross-sections	127
Figure 5-17: Joint configurations	127
Figure 5-18: Example: joint between pylon and brace, both members using hexagonal SCP sections	128

List of Tables

Table 0-1: Design Load Cases for Tower Design	8
Table 1-1: NREL 5MW Gross Properties	16
Table 1-2: The dimensions of 100 m tubular tower for 220 m hybrid tower.....	16
Table 1-3: Basic parameters for wind turbine classes acc. IEC 61400-1	17
Table 1-4: Detail Load Case for Modal Analysis.	17
Table 1-5: Detail Load Case for ULS Design.....	18
Table 1-6: Detail Load Case for Fatigue state Design.	18
Table 1-7: Output parameters at wind turbine Transition piece.....	19
Table 1-8: Output parameters at wind turbine tower top.	19
Table 1-9: Case studies and the corresponding load Tables provided in D1.1.....	19
Table 1-10: Wind Turbine Mode of Operation.....	22
Table 1-11: Study cases for parametric investigation of lattice structure.....	25
Table 1-12: Maximum element length [m] of bracing system	27
Table 1-13: Geometry of Tubular part.....	27
Table 1-14: <i>120m lattice cross sections</i>	28
Table 1-15: <i>60m lattice cross sections</i>	28
Table 1-16: Maximum displacements at the top of the towers	28
Table 1-17: Maximum reaction forces in ground joints	29
Table 1-18: Ranges of independent parameters values as used in the parametric investigation... Table 1-19: Minimum and maximum total weights found.....	32
Table 1-20: Three selected solutions	33
Table 2-1: The full scale and down scaled dimensions of the transition piece.....	41
Table 2-2: Strain gauge and rosette properties	48
Table 2-3: Material parameters used in the FE-safe model.....	52
Table 2-4: Summary for fatigue life of welded transition piece using load history.....	55
Table 3-1. Requirements for the class 10.9 established by ISO 898-1:2015.	61
Table 3-2. Chemical composition (all the elements in weight % except B, in ppm).	61
Table 3-3. Results of the tensile tests performed with the conventional parameters.	63
Table 3-4. Strain rate influence on the tensile properties.	64
Table 3-5. Results of the Charpy tests (in J)	64
Table 3-6. Results obtained in the fatigue tests at constant load.....	68
Table 3-7. Fatigue life for the tested strain rates.....	70
Table 3-8: Chemical composition (all in weight %, except * in ppm).	72
Table 3-9. Examples of failures located in the fillet radius.....	75
Table 3-10. Results obtained in the fatigue test with incremental loading for 3 and 4 mm thickness specimens.	76
Table 3-11: Example of photos of the failures initiated in the fillet radius.....	77
Table 3-12: Summary of the obtained results for the fatigue test on connections.....	78
Table 4-1: Comparison of first buckling modes.....	83
Table 4-2: FEM analysis for t =12 mm with buckling modes imperfection.....	83
Table 4-3: <i>Investigated parameters for the three frame typologies</i>	85
Table 4-4: Overview of the research plan	92
Table 4-5: Specimens for testing	99
Table 4-6: Key dimensions of joint specimen	103
Table 5-1: Estimated number of trucks for transportation.....	117
Table 5-2: Description of the erection process – time estimate.....	118
Table 5-3: Bill of materials	119
Table 5-4: Life cycle inventory.....	120
Table 5-5: Cost estimation for hybrid wind turbine towers	123
Table 5-6: Design Load Cases (DLC).....	125
Table 5-7: Definition of output parameters (F: force, M: moment).....	126

List of acronyms and abbreviations

APDL	ANSYS Parametric Design Language
cFSM	Constrained Finite Strip Method
CHS	Circular hollow section
deg	Degree
DLC	Design load case
DOF	Degree of freedom
EAF	Electric Arc Furnace
EI	Elongation
EOG	Extreme Operating Gust
EQ	Extreme Quality
ETM	Extreme Turbulence Model
EWM	Extreme Wind Model
FEM	Finite Element method
FLS	Fatigue limit state
FSM	Finite Strip Method
GE	General Electric
I_{ref}	Turbulence Intensity
K_f	Stress intensity factor
$kP,1-\alpha$	Coefficient
LDST	Large Dimension Steel Tower
l_{eff}	Effective length
m	Declination
m	Meter
M	Moments
MW	Mega watt
N	Number of cycles
NREL	National Renewable Energy Laboratory
NTM	Normal Turbulence Model
NWP	Normal Wind Profile
\emptyset	Diameter
OC4	Offshore Code Comparison Collaboration
ODB	Output Data Base
PSC	polygonal semi-closed
Q&T	Quenching & Tempering
RCPS	Regular Convex Polygonal Section
RHS	Rectangular Hollow Section
RNA	Rotor Nacelle Assembly
RoA	Reduction of Area
Rpm	Revolution Per Minute
R_z	Surface finish factor
S, σ	Stress
S4R	4-node shell element
Sa	Stress amplitude
SCP	semi-closed polygonal
SEM	Scanning Electron Microscope
SLS	Service limit state
SN	Stress to number of cycles to failure
TP	Transition Piece, transition segment
ULS	Ultimate Limit State
UTS	Ultimate Tensile Strength
V_{ref}	Reference Wind Speed
WEC	Wind Energy Converter
WT	Wind Turbine
YS	Yield Strength

References

- [1] A. Fatemi and D. F. Socie, "A Critical Plane Approach To Multiaxial Fatigue Damage Including Out of Phase Loading," *Fatigue Fract. Eng. Mater. Struct.*, vol. 11, no. 3, pp. 149–165, 1988.
- [2] A. M. P. de Jesus, R. Matos, B. F. C. Fontoura, C. Rebelo, L. S. da Silva, and M. Veljkovic, "A comparison of the fatigue behavior between S355 and S690 steel grades," *J. Constr. Steel Res.*, vol. 79, no. 0, pp. 140–150, 2012.
- [3] A. Muhammad and M. Ristow, "Fatigue Life of Wind Turbine Structural Components," *NAFEMS Semin. "Simulation-based Fatigue Lifetime Predict."*, pp. 1–7, 2010.
- [4] Abaqus CAE, Version 2017: Dassault Systèmes®, 2017
- [5] Ancona D, McVeigh J (2001). Wind turbine materials and manufacturing fact sheet. Princeton Energy Resources International LLC 19
- [6] B. W. Schafer, 'Cold-formed steel structures around the world', *Steel Construction*, vol. 4, no. 3, pp. 141–149, 2011.
- [7] B. W. Schafer, 'Elastic buckling solution methods for Cold-Formed steel elements and members', in *Cold-Formed Steel Behavior and Design: Analytical and Numerical Modeling of Elements and Members with Longitudinal Stiffeners*, 1998.
- [8] Bicen, Jia, Resistance of polygonal cross sections of lattice wind towers, Luleå University of Technology, 2017
- [9] Bulson, P.S. The strength of thin-walled tubes formed from flat elements. *International Journal of Mechanical Sciences*, 11(70), pp 613-620, 1969
- [10] C. Bak et al., "The DTU 10-MW reference wind turbine," *Danish Wind power Res.*, 2013.
- [11] CEN – European Committee for Standardization "Eurocode 3 - Design of steel structures - Part 1-6: Strength and Stability of Shell Structures," 2005
- [12] CEN – European Committee for Standardization (2005). EN 1991 Eurocode 1: Actions on structures, Part 1-4: General actions – Wind actions, Brussels.
- [13] CEN – European Committee for Standardization (2006). EN 1993 Eurocode 3: Design of steel structures, Part 3-1: Towers, masts and chimneys – Towers and masts, Brussels.
- [14] CEN – European Committee for Standardization (2018). Revised EN 1993 Eurocode 3: Design of steel structures, Part 1-8: Design of joints (Final draft), Document CEN/TC 250/SC 3/WG 8 N 95.
- [15] CEN – European Committee for Standardization Eurocode 3: Design of steel structures – Part 1-1: General rules and rules for buildings. Brussels: CEN, 2005.
- [16] CEN – European Committee for Standardization, "1090-2: execution of steel structures and aluminium structures-part 2: technical requirements for steel structures," Eur. Comm. Stand. Brussels, 2008.
- [17] CEN – European Committee for Standardization, "EN 1993-1-8:2005 Eurocode 3: Design of steel structures - Part 1-8 : Design of joints," vol. 3, 2010.
- [18] CEN – European Committee for Standardization, "EN1993-1-1 Eurocode 3 : Design of steel structures -Part 1-1: General rules and rules for buildings," vol. 3, 2005.
- [19] CEN – European Committee for Standardization, "Eurocode 3 - Design of steel structures - Part 1-5: Plated structural elements," 2006.
- [20] CEN – European Committee for Standardization, EN 1993-1-3:2005 Eurocode 3: Design of steel structures – Part 1-3: General rules - Supplementary rules for cold-formed members and sheeting. Brussels: CEN, 2004.
- [21] Chu C, Conle F A, Hubner A, an Integrated Uniaxial and Multiaxial Fatigue Life Prediction Method, VDI Berichte NR 1283, 1996.
- [22] DIN EN10002-1: Metallic materials - Tensile testing, Part 1: Method of test at ambient temperature'. ECISS/TC 1, Dec-2001.
- [23] DNV, "DNV-OS-H205 Lifting Operations (VMO Standard - Part 2-5)," no. April, p. p38, 2014.

- [24] EN 14399-5. High-strength structural bolting assemblies for preloading – Part 5: Plain washers'. SIS, 2005.
- [25] EN 50341-1 Overhead electrical lines exceeding AC 45 kV – Part 1: General requirements – Common specifications, CENELEC European Committee for Electromechanical Standardization.
- [26] EN 50341-1-2. Overhead electrical lines exceeding AC 45 kV - Part 1: General requirements - Common specifications'. Oct-2001.
- [27] Fe-Safe 6 User Manual, 2014.
- [28] G. Purdy, "ISO 31000: 2009—setting a new standard for risk management," *Risk Anal.*, vol. 30, no. 6, pp. 881–886, 2010.
- [29] G. Sines, "Behaviour of metals under complex stresses," *Sines G, Waisman JL, Ed. fatigue. New York McGraw-Hill; 1959.*, pp. 145–69, 1959. (G. Sines, 1959)
- [30] GEMIS – Global Emission Model for Integrated Systems (2017). <http://iinas.org/gemis.html>, Produced by the International Institute for Sustainability Analysis and Strategy, v4.9, Darmstadt.
- [31] Gervásio H, Rebelo C, Moura A, Veljkovic M, Silva LS (2014). Comparative life cycle assessment of tubular wind towers and foundations – Part 2: Life cycle analysis. *Engineering Structures* 74, 292-299
- [32] Gurit, "Wind Turbine Blade Structural Engineering," *Wind Energy Handbook.*, p. 16, 2013.
- [33] Hau, E., *Windkraftanlagen*, Springer-Verlag Berlin Heidelberg, München, 2008.
- [34] HebeTec Engineering AG: <https://www.hebetec.com/>
- [35] Heyes P, Dakin J, St John C, the Assessment and Use of Linear Elastic FE Stress Analysis for Durability Calculations SAE Paper 951101, 1995.
- [36] Hudson C.M., Eds.E.S.D.U. Data Sheets, Engineering Sciences Data Unit, London.
- [37] I. V. Papadopoulos, "Long life fatigue under multiaxial loading," *Int J Fatigue* 2001, vol. 23, no. 839–49, 2001.
- [38] IEA – International Energy Agency (1990). Recommended practices for wind turbine testing and evaluation, 3: Fatigue loads, Report from expert group (Ed.: PH Madsen).
- [39] IEC-ISO, "ISO 31010: 2009-11," Risk Manag. Assess. Tech., 2009.
- [40] International Electrotechnical Committee, "International Electrotechnical Committee (IEC) 61400-1," 2006
- [41] IRENA – International Renewable Energy Agency. Renewable energy technologies: cost analysis series – Wind power. Technical Report.
- [42] J. Jonkman, S. Butterfield, W. Musial, and G. Scott, "Definition of a 5-MW Reference Wind Turbine for Offshore System Development," 2009
- [43] K. Miller, *Fatigue under complex stress*, vol. 11. 1977.
- [44] M. Casafont, F. Marimon, M. Pastor, and M. Ferrer, 'Linear buckling analysis of thin-walled members combining the Generalised Beam Theory and the Finite Element Method', *Computers & Structures*, vol. 89, no. 21–22, pp. 1982–2000, Nov. 2011.
- [45] M. Gargari, A. Louhghalam, and M. Tootkaboni, 'Optimal cross sections for cold formed steel members under compression', in Proceedings of 10th world congress on structural and multidisciplinary optimization, 2013.
- [46] M. Matsuishi and T. Endo, "Fatigue of metals subjected to varying stress," *Japan Soc. Mech. Eng.*, p. 37–40., 1968.
- [47] M. Pavlović, et al., Connections in towers for wind converters, part I: Evaluation of down-scaled experiments, *J ConstrSteel Res* (2015), <http://dx.doi.org/10.1016/j.jcsr.2015.09.002>
- [48] Manoleas, Panagiotis, Between square and circle. A study on the behaviour of polygonal profiles under compression, Doctoral Thesis, Luleå University of Technology, 2018.

- [49] N. D. Kelley and B. Jonkman, "Overview of the TurbSim Stochastic Inflow Turbulence Simulator - NREL/TP-500-41137," no. April, pp. 1–13, 2007.
- [50] P. H. Madsen, J. W. . Dekker, S. E. Thor, K. McAnulty, H. Matties, and R. W. Thresher, "Recommended Practices for Wind Turbine Testing and Evaluation 3. Fatigue Loads," 1990.
- [51] Ryan, Bona, Finite element modelling and parametric studies of semi-closed thin-walled steel polygonal columns, Master Thesis, Luleå University of Technology, 2017.
- [52] S. Ádány, 'Shell element for constrained finite element analysis of thin-walled structural members', *Thin-Walled Structures*, vol. 105, pp. 135–146, Aug. 2016.
- [53] S. K. Koh and R. I. Stephens, "Mean Stress Effects on Low Cycle Fatigue for a High Strength Steel," *Fatigue Fract. Engng Mafer. Strucl*, vol. 14, no. 4, 1991.
- [54] S. S. Ajeesh and S. Arul Jayachandran, 'A constrained spline finite strip method for the mode decomposition of cold-formed steel sections using GBT principles', *Thin-Walled Structures*, vol. 113, pp. 83–93, Apr. 2017.
- [55] SHOWTIME, "Deliverable 1.2: Detailing of transition segment for lattice-tubular connection," 2017
- [56] SHOWTIME, "Deliverable 1.3: Geometric definition and design methodology for hybrid towers," 2017.
- [57] SHOWTIME, Steel Hybrid Onshore Wind Towers Installed with Minimal Effort, "Deliverable 1.1: Load Analysis," 2017.
- [58] Thomassen, Paul E., Per Ivar Bruheim, Loup Suja, and Lars Frøyd. 2012. "A Novel Tool for FEM Analysis of Offshore Wind Turbines With Innovative Visualization Techniques." Pp. 374–79 in Proceedings of the Twenty-second (2012) International Offshore and Polar Engineering Conference, vol. 4. Rhodes: International Society of Offshore and Polar Engineers. Retrieved (http://www.isope.org/publications/proceedings/isope_2012/data/papers/vol1/2012-TPC-226Thoma.pdf).
- [59] W. Popko et al., "Offshore Code Comparison Collaboration Continuation (OC4), Phase I—Results of Coupled Simulations of an Offshore Wind Turbine with Jacket Support Structure," *J. Ocean Wind Energy*, vol. 1, no. 1, pp. 1–11, 2310.
- [60] Watson P, Hill S, Fatigue Life Assessments of Ground Vehicle Components, Design of Fatigue and Fracture Resistant Structures, ASTM STP 761, 1982, pp. 5-27 Abelkis P.R.
- [61] Z. Li and B. W. Schafer, 'Buckling analysis of cold-formed steel members with general boundary conditions using CUFSM conventional and constrained finite strip methods', 2010.
- [62] Z. Li, J. C. Batista Abreu, J. Leng, S. Ádány, and B. W. Schafer, 'Review: Constrained finite strip method developments and applications in cold-formed steel design', *Thin-Walled Structures*, vol. 81, pp. 2–18, Aug. 2014.

Getting in touch with the EU

In person

All over the European Union there are hundreds of Europe Direct information centres. You can find the address of the centre nearest you at:
https://europa.eu/european-union/contact_en

On the phone or by email

Europe Direct is a service that answers your questions about the European Union. You can contact this service:

- by freephone: 00 800 6 7 8 9 10 11 (certain operators may charge for these calls),
- at the following standard number: +32 22999696 or
- by email via: https://europa.eu/european-union/contact_en

Finding information about the EU

Online

Information about the European Union in all the official languages of the EU is available on the Europa website at: https://europa.eu/european-union/index_en

EU publications

You can download or order free and priced EU publications at: <https://publications.europa.eu/en/publications>. Multiple copies of free publications may be obtained by contacting Europe Direct or your local information centre (see https://europa.eu/european-union/contact_en).

EU law and related documents

For access to legal information from the EU, including all EU law since 1952 in all the official language versions, go to EUR-Lex at: <https://eur-lex.europa.eu>

Open data from the EU

The EU Open Data Portal (<https://data.europa.eu/euodp/en/home>) provides access to datasets from the EU. Data can be downloaded and reused for free, for both commercial and non-commercial purposes.

The SHOWTIME research project aimed to develop a steel hybrid solution for onshore wind turbine towers using a lattice structure for the lower portion of the tower and a tubular upper portion. The solution is targeted at tall onshore applications (hub height 120 – 220 meters). The objectives and outcomes of the research focused on:

- optimal proportions and geometry of lattice and tubular parts of the hybrid structure, considering transport and crane size constraints; conceptual design of several case studies was performed including the load calculation;
- the erection process, in which the lattice portion of the tower is used as support for the installation of the upper tubular part of the tower and the turbine; the construction of a small-scale prototype and the preparation of the load and feasibility tests were performed. The practicality of the erection process was evidenced by field tests on the prototype.
- the development of new type of steel for bolts with focus on the fatigue behaviour of bolts manufactured with new type of steel and the fatigue tests of corroded and non-corroded bolted connections using the same type of bolts; considerable improvements of the fatigue behaviour were achieved.
- tests and numerical assessment of the performance of a new type of built-up cold form mild and HS steel members and respective connections. Conclusions were obtained on suitable design buckling curve and bolt spacing, stiffness of connections and effectiveness of the gusset plate internal to the pylon.
- life-cycle environmental impact and cost assessment, as well as design recommendations based on case studies highlighting the advantages of the proposed tower concepts.

